A sobering view of our energy future *p. 1322*

Maternal care alters newborn mouse genomes *pp. 1330 & 1296*

Wet route to phosphorus fine chemicals *pp. 1333 & 1303*

Science

$15
23 MARCH 2018
sciencemag.org
AAAS

SPECIAL ISSUE

CANCER IMMUNOTHERAPY

Engineered & personalized

CONTENTS

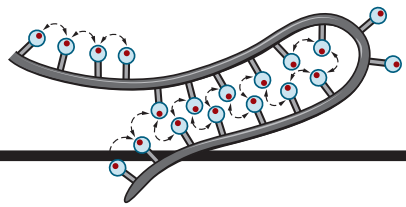

1334 & 1391
Electron transport in radical polymers

23 MARCH 2018 • VOLUME 359 • ISSUE 6382

NEWS

IN BRIEF

IN DEPTH

FEATURES

INSIGHTS

PERSPECTIVES

POLICY FORUM

SPECIAL SECTION

Cancer immunotherapy

ON THE COVER

Artist's rendering of a patient receiving personalized treatment for cancer. With the help of newly developed immunotherapies, a growing number of patients are partners in their own treatment. For more on techniques and strategies for cancer immunotherapy, see page 1344.
Illustration: Daniel Hertzberg

GRAPHIC (TOP): A. KITTERMAN/*SCIENCE*; ILLUSTRATION: DANIEL HERTZBERG

CONTENTS

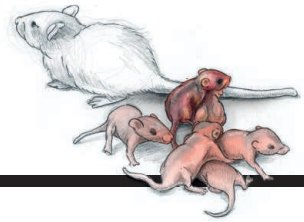

1330 & 1395
Maternal care and genome plasticity

23 MARCH 2018 • VOLUME 359 • ISSUE 6382

PHOTO: REZUS/ISTOCKPHOTO.COM ; GRAPHIC: V. ALTOUNIAN/*SCIENCE*

BOOKS *ET AL.*

LETTERS

RESEARCH

IN BRIEF

RESEARCH ARTICLES

REPORTS

DEPARTMENTS

SCIENCE (ISSN 0036-8075) is published weekly on Friday, except last week in December, by the American Association for the Advancement of Science, 1200 New York Avenue, NW, Washington, DC 20005. Periodicals mail postage (publication No. 484460) paid at Washington, DC, and additional mailing offices. The title SCIENCE is a registered trademark of the AAAS. Domestic individual membership, including subscription (12 months): $165 ($74 allocated to subscription). Domestic institutional subscription (51 issues): $1808; Foreign postage extra: Mexico, Caribbean (surface mail) $55; other countries (air assist delivery): $89. First class, airmail, student, and emeritus rates on request. Canadian rates with GST available upon request, GST #125488122. Publications Mail Agreement Number 1069624. **Printed in the U.S.A.**
Change of address: Allow 4 weeks, giving old and new addresses and 8-digit account number. **Postmaster:** Send change of address to AAAS, P.O. Box 96178, Washington, DC 20090–6178. **Single-copy sales:** $15 each plus shipping and handling; bulk rate on request. *Science* is indexed in the *Reader's Guide to Periodical Literature* and in several specialized indexes.

Published by AAAS

Science
AAAS
1200 New York Avenue, NW, Washington, DC 20005
Clarendon House, Clarendon Road, Cambridge, UK CB2 8FH

SUBSCRIPTION SERVICES For change of address, missing issues, new orders and renewals, and payment questions: 866-434-AAAS (2227) or 202-326-6417, FAX 202-842-1065. Mailing addresses: AAAS, P.O. Box 96178, Washington, DC 20090-6178 or AAAS Member Services, 1200 New York Avenue, NW, Washington, DC 20005

INSTITUTIONAL SITE LICENSES 202-326-6730 **REPRINTS:** Author Inquiries 800-635-7181 **COMMERCIAL INQUIRIES** 803-359-4578 **PERMISSIONS** 202-326-6765, permissions@aaas.org **AAAS Member Central Support** 866-434-2227 www.aaas.org/membercentral.

INFORMATION FOR AUTHORS See www.sciencemag.org/authors/science-information-authors

EDITORIAL

Lumping and splitting

Editor-in-Chief, Science *Journals.*
jberg@aaas.org

Next month, the National Postdoctoral Association will convene its annual meeting in Cleveland, Ohio, where, among many topics, the matter of how data can inform policies to improve post-Ph.D. career pathways will be discussed. Many such data are indeed "out there," but a major question is whether they are accessible and usable—which brings me to the value of taxonomies.

In 1758, Carl Linnaeus provided a systematic framework for the classification of animals and plants based on detailed visual observations of many organisms. This taxonomy captured important relationships between different groups of organisms and provided a systematic method for naming organisms, including those yet to be discovered. Moreover, the taxonomy was refined over time as more information became available.

The organization of information in this way has turned out to be enormously useful in data analysis across many different enterprises. Taxonomies allow classification of items based on their characteristics so that closely related items are grouped together and given the same name. They are hierarchical so that items that share many but not all characteristics are associated. For characteristics that vary continuously rather than in a discrete fashion, taxonomies can include cut-off points to allow binning of items for subsequent analysis. A key factor in developing taxonomies involves the preference for "lumping" versus "splitting," terms that evolved early in discussions of biological taxonomies. Lumpers prefer broader categories that include items that share important features despite some differences; splitters prefer narrower categories, emphasizing variations rather than common features.

What happens when there is too much lumping or too much splitting? Consider the classification of cancer cells. Too much lumping, such as defining cancer cells only by their tissue of origin, will obscure biologically and clinically important differences, whereas too much splitting will yield too many categories with insufficient information available about any given one. We are rapidly accumulating data about cancer cells—genomic, proteomic, metabolomic—which may be combined with other data, such as sensitivity to therapeutic agents, to enhance the richness and value of such taxonomies.

"Creating useful taxonomies requires careful analysis..."

During my time as a director at the U.S. National Institutes of Health, I sought to answer a seemingly simple question regarding a pool of individuals who had recently received their first major grant funding: How many postdoctoral fellowships did these early-career scientists complete? Examining individual biographical sketches, I found that the job titles for many scientists changed multiple times during the period between completion of his/her doctorate training and initiation of his/her independent position. A 2014 analysis* by the National Postdoctoral Association revealed that 37 different job titles had been used to describe positions that appear, to a reasonable observer, to be postdoctoral fellowships. The excessive splitting here sometimes is related to differences in sources of funding or other factors but, in many cases, is simply due to lack of an agreed taxonomy. This has inhibited many analyses of this important component of many scientific training paths. The development of a proposed taxonomy for career paths for those with Ph.D. degrees in biomedical sciences (see peerj.com/preprints/3370/) represents an important step in facilitating the compilation of career outcomes data in a manner suitable for detailed analysis, particularly when coupled with recent commitments for transparency from leading institutions (see science.sciencemag.org/content/358/6369/1388.full). This taxonomy includes classification by sector, career type, and job function and can help illustrate the many post-Ph.D. career alternatives and the frequencies of their use.

Creating useful taxonomies requires careful analysis about underlying data and the intended uses, as well as engagement with the communities that may be affected by their use. The development of detailed taxonomies for post-Ph.D. career alternatives and commitments to collect and share the underlying data lays the foundation for much important analysis in the near future.

–Jeremy Berg

*http://c.ymcdn.com/sites/www.nationalpostdoc.org/resource/resmgr/docs/npa_policyreport2014_final.pdf

10.1126/science.aat5956

> "My job there wasn't to raise money. It was to educate."
>
> **Epidemiologist Kenneth Mukamal**, responding to a 17 March story in *The New York Times* that suggested he and the U.S. National Institutes of Health lobbied the alcohol industry to fund a study of the benefits of moderate alcohol consumption.

IN BRIEF

Edited by **Jeffrey Brainard**

CLIMATE SCIENCE

A warming trend brought ice to Canada

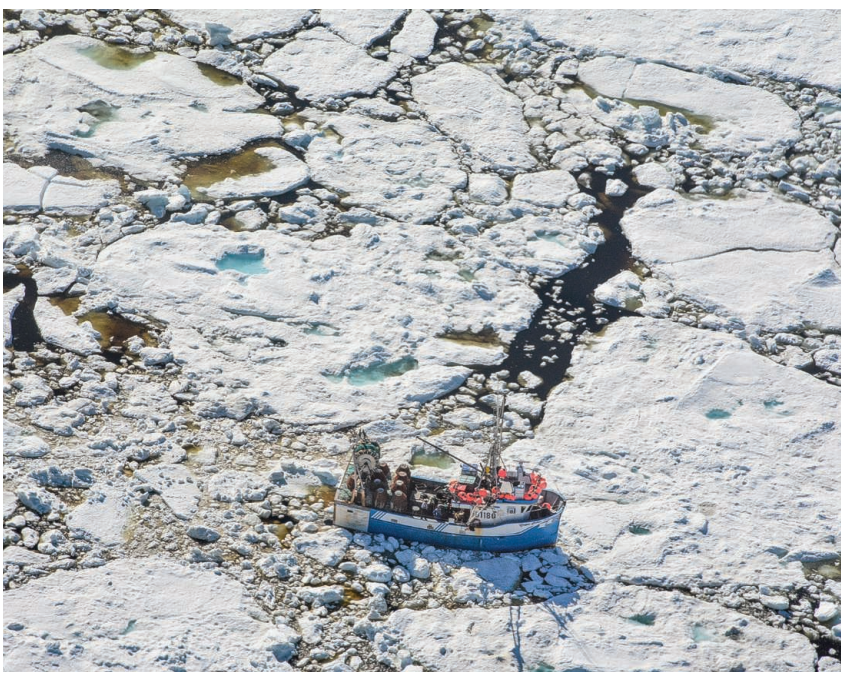

The melting of ice dams allowed sea ice from the Arctic Ocean to float south.

It might be counterintuitive, but a warming planet means more Arctic sea ice is showing up in busy North Atlantic shipping lanes. Typically, winter temperatures cause dams called ice arches to form across channels joining the Arctic and North Atlantic oceans, preventing ice from drifting south. But last year, the arches failed to form for the second time in a decade, data collected by a Canadian icebreaker revealed. Chunks of ice up to 8 meters thick surged south, clogging shipping lanes off the province of Newfoundland and Labrador in Canada well into June 2017, researchers reported in the 15 March issue of *Geophysical Research Letters*. Some vessels became trapped, others sank after their hulls were punctured, and ferries and fishing were delayed. "This is something we need to better prepare for in the future," said climate scientist David Barber of the University of Manitoba in Winnipeg, Canada, who is a lead author of the study. "We expect this phenomenon to go on for at least a couple more decades as we transition to an ice-free Arctic in the summer."

Fatality halts AV research

TRANSPORTATION | Both supporters and critics of autonomous vehicles (AVs) knew that the first pedestrian fatality tied to this technology would generate headlines and on 18 March, the inevitable happened: An Uber Volvo hit and fatally injured a woman walking her bicycle across a busy, multilane road in Tempe, Arizona. A person was sitting behind the AV's steering wheel, but the car was said to be in self-driving mode. Uber immediately suspended its AV testing program in three states and Canada, and the U.S. government has begun an investigation. Opponents of a pending Senate bill allowing greater freedom for states to set rules governing AVs say the accident demonstrates the need for greater caution, while advocates say that testing under controlled conditions will improve a technology that they maintain is already safer than the use of human drivers.

More kids sketch female scientists

SCIENCE CAREERS | When asked to draw a scientist, school-age children in the United States are increasingly sketching women, researchers report in *Child Development*. They studied 20,860 pictures drawn by students aged 5 to 18 over 5 decades. In the 1960s and 1970s, less than 1% of students depicted scientists as female, but that rose to an estimated 34% by 2016. Among only girls, the figure grew from about 1% to more than 50%. The trends parallel an uptick in the number of actual female

A third grade girl in Texas drew this scientist.

IMAGES: (LEFT TO RIGHT) EMILIE GOULET; COURTESY OF LEON WALLS, UNIVERSITY OF VERMONT

Published by AAAS

PHOTO: REBIKOFF-NIGGELER FOUNDATION

MARINE BIOLOGY

The anglerfish's deep-sea light show is revealed

Deep-sea explorers diving off Portugal's Azores islands have captured rare images in the wild of a female deep-sea anglerfish. Like most other members of its order, the species, *Caulophryne jordani*, is known for the bioluminescent, lurelike appendage that drifts in front of its mouth to attract prey. In addition, as this photo shows, these female anglerfish are resplendent with apparently bioluminescent, elongated filaments projecting from their fist-size bodies. The photo and an accompanying video are the first to show a small male of this species fused to a female's underside, essentially acting as a permanent sperm provider. Most of what scientists know of deep-sea anglerfish comes from dead animals pulled up by trawls, which have lost their bioluminescence. The images were captured at a depth of 800 meters by wildlife filmmakers Kirsten and Joachim Jakobsen using the Rebikoff-Niggeler Foundation's manned LULA1000 submersible. To see the video, visit http://scim.ag/anglerfish.

scientists. From 1960 to 2013, the percentage of biological scientists who were women rose from 28% to 49%, for example.

IPCC forms gender task force

CLIMATE SCIENCE | The Intergovernmental Panel on Climate Change (IPCC) last week established a task force to consider ways to improve gender equity within the organization, such as recruiting more female scientists to serve as authors of its authoritative reports on climate science. The move comes on the heels of a recent study evaluating gender disparity within the group. It found that although IPCC has increased the proportion of women who serve as report authors—to 23% in 2013, as IPCC worked on its fifth report, up from just 2% on its first report, in 1990—barriers to participation remain. At a meeting in Paris, IPCC decided that one of the task force's two co-chairs should be female; they and the rest of the committee's members have yet to be named. The gender panel is expected to issue a report at an IPCC meeting next year.

Fungus threatens NASA samples

SPACE EXPLORATION | An abundance of fungus has been found growing in what is supposed to be a clean laboratory at the Johnson Space Center (JSC) in Houston, Texas, that stores NASA's only collection of extraterrestrial meteorites. The discovery of the fungi, mostly of the common genus *Penicilium*, raises questions about the accuracy of analyses conducted there. Aaron Regberg, a geomicrobiologist at JSC, reported the surprising finding this week at the 2018 Lunar and Planetary Science Conference in The Woodlands, Texas. It's worrying, he said, because some fungal species produce rare amino acids that, when found in meteorite samples, are usually considered to be extraterrestrial in origin. Regberg says knowing background sources of potential contaminants such as fungi will be important when JSC uses clean rooms in the coming years to analyze rocks returned by future missions to Mars or other destinations.

Using DNA to track snakes

CONSERVATION | Florida researchers for the first time used DNA traces left by snakes in soil to detect them on land. Scientists studied the environmental DNA (eDNA) in cells shed by Burmese pythons, an invasive species that has wreaked havoc in southern Florida. The researchers, from Florida Gulf Coast University in Fort Myers, reported this month in *Herpetologica* that they monitored burrows with cameras and found DNA in those that snakes had recently vacated. Tests suggested that eDNA can identify the reptiles' presence for up to a week afterward. The new technique could help conservationists and land managers protect Florida's native animals by revealing where the pythons are hiding and which way they are spreading.

Crowd funds younger scientists

RESEARCH FUNDING | Crowdsourced funding campaigns are helping some scientists, especially students and women, raise small amounts of seed money to jump-start research projects, a study has found. Students landed the majority of funds raised on Experiment.com, the largest online platform that coordinates such donations, and women had higher success rates than men. Experiment.com allows each project leader to propose a target dollar amount, but a project receives funds only if the target is met. Scholars affiliated with the National Bureau of Economic Research in Cambridge, Massachusetts, examined more than 700 such campaigns. The median amount raised was $3100, and the money typically went to equipment and travel. Donors may have been motivated by a desire to help younger applicants who were seeking amounts too small to be funded by traditional grant programs or were not experienced enough to compete successfully for those, the authors wrote.

South Sudan stops Guinea worm

PUBLIC HEALTH | South Sudan, which long had the highest prevalence of Guinea worm infections in the world, has eliminated the disease despite the civil war that is ravaging the country. At a 21 March press conference in Atlanta—after *Science* went to press—South Sudan Health Minister Riek Gai Kok was

THREE QS

Brazilian astronomy 'strangled'

A plan for Brazil to join the 15-nation European Southern Observatory (ESO) astronomical research consortium was canceled last week. Brazil's president, Michel Temer, never ratified the arrangement, nor did the country make any payments to the consortium, which some critics said the country could not afford during its current fiscal crisis. ESO had been treating Brazil as an interim member.

Reinaldo de Carvalho, president of the Brazilian Astronomical Society in São Paulo and an astronomer at the Brazilian National Institute for Space Research in São José dos Campos, discussed the breakup with *Science*. This interview has been edited for brevity and clarity. (For more, see http://scim.ag/Brazilastron.)

Q: What was missing for Brazil to ratify the agreement?

A: The financial crisis was clearly a problem, in addition to a lack of political will. This goes to show, once again, the need for a long-term state policy on science and technology, instead of just government policies that change all the time.

Q: How will this departure from ESO impact the development of Brazilian astronomy?

A: We will be strangled, limited by our current facilities, and will have a very difficult time competing in the "first world" of astronomy. ESO represents the only path for a sustainable, significant growth of Brazilian astronomy. ... It will be very difficult for us to be principal investigators when requesting observing time in the telescopes. We will have to tag along with our European partners for that, like we used to do before the agreement was signed, 7 years ago. It's like going back in time.

Q: Brazil is a member in other observatories, such as the Gemini and Southern Astrophysical Research (SOAR) telescopes. To what degree do they compensate for the loss of Brazil's participation in ESO?

A: It's something, but very far from fulfilling the needs of our research community. We have much more human resources than Gemini and SOAR are able to accommodate, and small participations in a few telescopes will not put us in the frontier of science.

PHOTO: WELLCOME TRUST

NEUROSCIENCE

A wearable scanner makes brain studies easier

Magnetoencephalography (MEG), which detects the weak magnetic fields emitted by communicating neurons, is a powerful tool for capturing brain activity in real time, but it comes with a huge caveat: Participants must keep their heads absolutely still inside a large, bulky scanner to get accurate readings. Now, a U.K. research team has developed the first wearable MEG device, replacing the liquid-helium cooled superconductors normally used to detect magnetic fields with small glass cubes containing vaporized rubidium atoms whose reaction to magnetic fields is monitored by a laser. It returns a map of brain activity just like conventional MEG technology, and because the magnetic sensors move with the masklike instrument, a wearer's brain signals are recorded clearly even when they are in motion, the group reports this week in *Nature*. "This is remarkable work," says MEG researcher Matti Hamalainen of Massachusetts General Hospital in Boston. "It really indicates that MEG is moving forward conceptually into a new era."

scheduled to announce that health workers have detected no new cases in the country during the past 15 months. Guinea worm disease, also known as dracunculiasis, is caused by a roundworm that develops inside the human body and emerges from the skin causing an intense burning sensation. It affected millions in Africa and Asia 3 decades ago, but an eradication campaign is now very close to finishing: Only 30 cases were reported from Chad and Ethiopia in 2017.

Science draws Facebook posts

SOCIAL MEDIA | Posts about science on Facebook have drawn millions of followers, but less than a third of these items offer news about new scientific discoveries, according to an analysis of the social media platform released this week by the Pew Research Center in Washington, D.C. The next most common categories were "news you can use" (21% of posts) and promotions (16%). Pew studied more than 6000 posts by 30 of Facebook's most popular science-related pages during the first half of 2017. Most of the 30 focused on only one or two topics, such as health and medicine or astronomy and physics. Pew also found that the volume of posts about science on 15 "multiplatform" pages—maintained by organizations such as *National Geographic* and *Science* that publish magazines—more than doubled from 2014 to 2017.

SCIENCEMAG.ORG/NEWS
Read more news from *Science* online.

PHOTO: CHRIS J. RATCLIFFE/STRINGER/GETTY IMAGES

CHEMICAL WEAPONS

U.K. attack puts nerve agent in the spotlight

Researchers race to understand deadly compound developed by Soviet scientists

By **Richard Stone**

One of the world's deadliest poisons has emerged from the shadows after the audacious attempt earlier this month to murder a former Russian spy on U.K. soil. Scientists are racing to unravel why the mysterious nerve agent, concocted by Soviet chemists in the 1970s, is so potent. They fear its chemical structure will make finding an antidote unusually difficult, and that the compound could cause long-lasting health effects in those who survive exposure.

The drama began on 4 March, when Sergei Skripal and his daughter Yulia were discovered gravely ill on a park bench in Salisbury, U.K. In 2006, a Russian military tribunal had convicted Skripal, a former colonel in Russia's foreign intelligence service, of treason. He settled in Salisbury after a spy swap in 2010.

U.K. investigators say they recovered residue of a nerve agent on clothing and belongings in Skripal's home and at a pizzeria in which he and Yulia dined just before taking ill. U.K. officials accused Russia of perpetrating the crime, sparking a diplomatic row in which the United Kingdom expelled 23 Russian diplomats, drawing a reciprocal response from Russia. Meanwhile, as *Science* went to press, the Skripals remained in critical condition, and a responding police officer who was exposed was in serious condition.

The poison, U.K. investigators have revealed, is one of the Novichok, or "newcomer," class of nerve agents the Soviet Union began developing nearly 50 years ago. In 1992, a former Soviet military chemist, Vil Mirzayanov, blew the lid off the clandestine program, claiming that the hitherto-unknown chemicals are several times more toxic than VX—until then, the deadliest known nerve agent. Even for an experienced chemist, "it would be extremely dangerous to try to make these compounds. You could easily get yourself killed," says Mohamed Abou-Donia, a neurobiologist at Duke University in Durham, North Carolina.

> ***"It would be extremely dangerous to try to make these compounds. You could easily get yourself killed."***
> **Mohamed Abou-Donia**, Duke University

The assassination attempt has thrust the Novichok agents back into the spotlight, but few experts in the rarefied area of chemical weapons defense are willing—or able—to shed further light on them. Information about the Novichok nerve agents is classified, says one U.S. military scientist who, like other U.S. government scientists, declined to speak with *Science*.

Mirzayanov's 2008 memoir, *State Secrets: An Insider's Chronicle of the Russian Chemical Weapons Program*, still gives the fullest picture of the Novichok agents. He writes that the compounds—perhaps five in all, in the family of phosphoramidates, he told *Science* in an interview last week—are similar in structure to other nerve agents such as sarin, soman, and tabun. Like their cousins, they bind to acetylcholinesterase (AChE), an enzyme that dismantles the neurotransmitter acetylcholine when it is released into synapses. Without medical intervention, acetylcholine builds up in synapses, eroding muscle function and preventing signals from the brain from reaching the muscles that control respiration and maintain blood pressure (*Science*, 5 January, p. 23).

Using data in the open literature, Zoran Radić, a chemist at the University of California, San Diego (UCSD), in recent days

Investigators, cloaked in protective suits, gathered evidence in the suspected assassination attempt.

has explored how a Novichok named A-232, which is similar in structure to tabun and soman, forms a conjugate with AChE. (Some news reports have speculated that A-232 was used in the Skripal attack.) His modeling found that A-232 would nestle snugly in AChE's active center, a narrow gorge in the enzyme (see image, below). Like other nerve agents, it would form a stable covalent bond with a serine group in the cleft. All of the Novichok compounds would likely bind to AChE "in a very similar way," based on structural information in Mirzayanov's book, Radić says.

But, he notes, the compound has a structural feature that traditional nerve agents lack: an amine group studded with an extra proton. That's bad news in two respects. For one, it could make it harder to identify the right antidote. All nerve agent victims are given atropine, which blocks muscarinic acetylcholine receptors. They are also given an oxime, a compound that can pry an agent out of AChE's active center before the agent has "aged," or bound irreversibly to the enzyme. An oxime's effectiveness depends on a nerve agent's structure and how it sits in the gorge. The exact configuration of the bond between

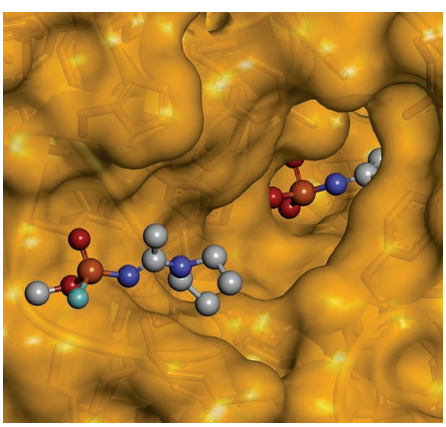

New modeling studies of the nerve agent A-232 (balls and sticks) depict its descent from acetylcholinesterase's gorge opening (left) to a tight fit in the enzyme's deep active center (right).

IMAGE: Z. RADIĆ, USING NANOPRO.VR BY NANOME, INC.

A-232 and AChE might "compromise" oximes now approved for use in Europe and the United States, Radić says. Experimental oximes might be more effective, he says.

The second concern, Radić says, is that A-232's alkyl amine group could enable it to target other enzymes in addition to AChE—and that raises the specter of severe symptoms arising months or years after exposure. Even sarin and some organophosphate pesticides that lack A-232's structural quirk can trigger a lasting neurotoxic syndrome with symptoms such as nightmares, memory deficits, muscle weakness, and depression.

An observation in Mirzayanov's memoir supports the possibility of lasting effects. He worked for 26 years in the Soviet Union's premier chemical weapons lab, the State Scientific Research Institute for Organic Chemistry and Technology in Moscow. One day, he recounts, a rubber tube that piped A-232 into a spectrometer ruptured, exposing his colleague, Andrei Zheleznyakov, to minute amounts. Zheleznyakov felt dizzy and his vision blurred, and he collapsed on the way home that day—but survived. Months later, Mirzayanov says, Zheleznyakov developed difficulties concentrating and became withdrawn.

The amine group could also explain an intriguing detail about the Novichok compounds, says UCSD pharmacologist Palmer Taylor. Whereas other nerve agents are manufactured as liquids and dispersed as aerosols or vapors, these compounds are thought to form a fine powder, a picture supported by reports of a powdery residue on personal belongings of Skripal and his daughter.

For terrorists, sarin would be the nerve agent of choice to inflict mass casualties because of its high volatility and rapid uptake in the body. But the Novichok compounds would be a formidable weapon for an assassin. Given their reported toxicity, ingesting or inhaling minuscule amounts could be fatal. On 18 March, U.K. foreign secretary Boris Johnson alleged that Russia has stockpiled Novichok agents precisely for use in assassinations.

If that's true, whoever made the attempt on Skripal's life botched the job. Investigators have hypothesized that the nerve agent was either introduced into Yulia's suitcase before she boarded a flight from Moscow to London on 3 March, or blown into the air vents of Skripal's BMW. Either way, the Skripals "were accumulating a very low dose," presumably through the skin, Taylor says. "Not much blood is coming from the skin back to the heart." The Skripals and the ill police officer may have survived thus far because they didn't inhale or ingest larger doses of the agent.

Taylor says "it would be far too dangerous" for UCSD and other academic labs to make Novichok compounds. But they could safely study the nerve agent–AChE conjugate—if military labs were willing to share samples. Until that happens, any further insights into the Novichok compounds are likely to remain a secret guarded closely by both the Russian weaponeers and the Western military chemists seeking to counter them. ■

FUNDING

Accounting rules hobble Spanish institutes

Staff at centers for solar energy research and oceanography raise alarm

By **Tania Rabesandratana**, *in Reus, Spain*

Stifling government accounting rules are threatening scientific projects and jobs at several Spanish research bodies. Scientists at both the Spanish Oceanography Institute (IEO), headquartered in Madrid, and the Solar Platform of Almería (PSA), a large solar research center in the Tabernas Desert, have expressed concern about what they see as senseless red tape that holds up spending.

Some 340 staff at IEO—60% of the total—sent a manifesto to the press last week to warn that the center is "collapsing." The problems compound the plight of Spanish science, which suffered from budget cuts during the country's recent economic woes and faces a proliferating bureaucracy aimed at controlling spending.

IEO's troubles stem partly from rules that apply to five public research bodies, known as OPIs in Spanish, with a total of 1700 researchers. Under accounting regulations introduced by the current conservative government in 2014, a team of six state auditors must preapprove every purchase at IEO, which has nine research centers across the country and five research ships. As a result, projects and recruitment have been severely delayed and IEO spent only half of its budget last year, down from 90% in 2013, according to the manifesto.

Researchers have trouble recruiting staff or buying equipment even if they receive funding from outside Spain, says Manuel Ruiz Villarreal, a physicist at IEO's A Coruña branch and the principal investigator of four projects funded by the European Union, including an effort to predict the health risks of toxic algal blooms. Ruiz Villarreal says the auditing system, known as "prior intervention," should be lifted for projects that receive external funding

and are already subject to checks after the money is spent.

Other OPIs must adhere to similar rules, but the manifesto says the situation is worst at IEO, which signatories say reveals a "structural problem" in the institute's management. "We've been raising the alarm for several years," Ruiz Villarreal says. "As a researcher, I can't go to the minister of the treasury myself. Our management has to tackle this."

"It's true we are having difficulties," admits IEO Director Eduardo Balguerías Guerra, who says the institute needs time to adapt to the rules but denies that its activities are paralyzed. "All the OPIs and the secretary of state are working very hard to solve these problems," he says. Until Spain's 2018 budgets are approved, additional restrictions will continue to exacerbate the difficulties, Balguerías Guerra says. But after that, he thinks the situation will improve.

Carmen Vela, state secretary in charge of research, development, and innovation, has admitted that IEO had "problems in its day-to-day management" and "had a bad [budget] execution." Vela told members of the Spanish congress's economy, industry, and competitiveness committee on 14 March that the institute's low spending was due to a large building project that did not get approval last year. She also conceded that the "prior intervention" system has created difficulties for the OPIs and said she is taking steps to minimize damage. But some observers say a patchwork of emergency measures won't provide a lasting solution.

PSA, the solar energy center, is part of an OPI called the Center for Energy, Environment, and Technology, which has also suffered from a 2016 regulation stipulating that funds received before September must be spent before the end of that same year. PSA scientists say this rule makes no sense when a grant is meant to be spread across several years, as many EU grants are. In the first 6 weeks of this year, PSA lost 14 research jobs out of a total of 40 because funds received earlier were blocked and the center couldn't advertise the posts, says Sixto Malato, a scientist in PSA's research unit for the solar treatment of water. He stepped down from his role as PSA director last November to protest the rules.

A total of €6 million, the entirety of PSA's research budget, is blocked and will have to be gradually returned to the European Commission with interest if the rules are not reversed, Malato says. "The government has to recognize their mistake," he says. "We're not asking for funds, we're asking [the treasury] to let us use external funds that will be spent in Spain and create jobs in Spain." ■

ASTROPHYSICS

Hawking's bid to save quantum theory from black holes

He struggled to explain why black holes don't destroy information, a puzzle that may be his greatest legacy

By **Adrian Cho**

When Albert Einstein died in 1955, he had spent decades on a lonely, quixotic quest: to derive a theory of everything that would unify gravity and electromagnetism—even though physicists discovered new nuclear forces as he worked. Stephen Hawking, the great British physicist who died last week at age 76, also worked until the end. But he focused on perhaps the most important problem in his area of physics, one his own work had posed: How do black holes preserve information encoded in the material that falls into them?

"He was clearly working on this big loose end, which really represents a profound crisis for physics," says Steven Giddings, a quantum physicist at the University of California, Santa Barbara. In a final bid to solve it, Hawking and two colleagues proposed a way for information to end up scribbled on a black hole's inscrutable verge, although others are skeptical.

A black hole is the gravitational field that remains when a star collapses under its own gravity to an infinitesimal point. Within a certain distance from the point—at the black hole's event horizon—gravity grows so strong that not even light can escape. Or so theorists once assumed. Thanks to quantum uncertainty, the vacuum roils with particle-antiparticle pairs flitting in and out of existence too fast to detect directly. At the event horizon, Hawking realized in 1974, one particle in a pair can fall into the black hole while the other escapes. As the black hole radiates such particles, it loses energy and mass until it evaporates completely. Such "Hawking radiation" is too feeble to observe, but few scientists doubt its existence.

But Hawking's signature insight led to a troubling conclusion. Imagine throwing a dictionary into a black hole that then evaporates. Because the emerging Hawking radiation is presumably random, the information in the dictionary shouldn't come back out with it. Such information loss would wreck quantum mechanics, which requires that the "wave function" that describes any system—be it the dictionary or the universe—evolve in a predictable way. That can't happen if information is lost. If allowed for black holes, such information loss would spread through quantum phys-

With John Preskill (left) and Kip Thorne (middle), Stephen Hawking (right) wrestled with a black hole paradox.

PHOTO: CALTECH ARVHICES

ics like a cancer, researchers say, spoiling things like energy conservation.

Hawking thought at first that the problem would be solved by changing quantum theory. In 1997, he and Kip Thorne, a gravitational theorist at the California Institute of Technology (Caltech) in Pasadena, entered a wager with John Preskill, also a Caltech theorist. Hawking and Thorne stuck to their position that black holes destroy information. By 2004, however, Hawking changed his mind and conceded the bet. He gave Preskill a baseball encyclopedia—from which arcane information could be recovered at will.

Hawking spent much of his later years trying to figure out how a black hole could regurgitate information—although he also worked on theories of what triggered the big bang. Three years ago he began his last work on black holes with Malcolm Perry, a theoretical physicist and Hawking's colleague at the University of Cambridge in the United Kingdom, and Andrew Strominger, a theorist at Harvard University. "It was only 2 weeks ago that I saw him," Perry says. "He certainly wasn't in the best shape, but his mind was clearly focused on the problem."

In a pair of recent papers, the scientists attack a pillar of black hole theory called the no-hair theorem. It is widely interpreted to mean that just three parameters—mass, spin, and electric charge, the last presumably zero—suffice to describe a black hole. Like bald pates, black holes of similar masses and spins then have no details—no "hair"—to distinguish them, as American theorist John Archibald Wheeler quipped. That sameness implies a black hole keeps no record of whether, say, it swallowed the play *King Lear* or the movie *King Kong*.

But strictly speaking, Strominger says, the theorem states only that two similar black holes can be "transformed" into each other by a handful of mathematical relations called diffeomorphisms, which relabel the coordinates of space-time. An infinite family of other diffeomorphisms has been neglected for decades, he says. They imply that a black hole's event horizon might be bedecked with an infinity of charges, a bit like electric charges. The charges could distinguish one black hole from another and encode in-falling information, Strominger says. "We're cautiously optimistic about this idea," he says. "Stephen was very optimistic."

However, the charges may not encode enough information or may not do so in a unique way, Giddings cautions. One theorist who requested anonymity out of respect for Hawking says his various solutions for the black hole information problem pale next to his best work. Hawking's latest work also misses a bigger issue, the theorist says. If a black hole preserves information, he argues, then an unavoidable conclusion of Einstein's theory of gravity—that there's no way to tell if you're falling into a huge black hole—must be wrong.

Others credit Hawking for working on important problems in spite of the degenerative nerve disease, amyotrophic lateral sclerosis, that led to his use of a wheelchair and eventually rendered him able to speak only through a computerized voice synthesizer. Ironically, Hawking's disability may have helped him avoid the isolation that enveloped Einstein, says Marika Taylor, a theoretical physicist at the University of Southampton in the United Kingdom, who from 1995 to 1998 was Hawking's graduate student. Hawking had to rely on collaborators to flesh out his ideas, she says, and so remained deeply connected to his peers. "Without stepping on the toes of his actual family," Taylor says, "his physics family was incredibly important to him." ■

Stephen Hawking, betting man

By **Daniel Clery**

Famously playful, Stephen Hawking left a trail of light-hearted bets about serious scientific questions. In the best known, he wagered that information falling into a black hole is lost forever; he later changed his mind and conceded the bet (see main story, p. 1316). That wasn't his first loss. In a high-profile bet in the early 1970s, he claimed that black holes themselves—the subject of so much of his life's work—did not exist.

At the time, the best candidate for a black hole was Cygnus X-1, one of the strongest x-ray sources in the sky, centered on a supergiant star. Theorists suspected an unseen orbiting companion was sucking in material from the star, creating a superhot accretion disk blazing with x-rays. Astronomers could calculate the companion's orbit and infer its minimum mass: six times that of our sun. Theory suggested it had to be a black hole, but other, remote possibilities remained.

Hawking bet another theorist, Kip Thorne of the California Institute of Technology (Caltech) in Pasadena, that Cygnus X-1 was not a black hole, with the prize being a magazine subscription. Hawking explained in his 1988 bestseller *A Brief History of Time: From the Big Bang to Black Holes* that the bet was a sort of "insurance policy" for him. "I have done a lot of work on black holes, and it would all be wasted if it turned out that black holes do not exist. But in that case, I would have the consolation of winning my bet, which would bring me 4 years of the magazine *Private Eye*," he wrote.

But a few years later, even though astronomers were still not certain that Cygnus X-1 was a black hole, Hawking conceded. Thorne wrote in his 1994 book *Black Holes and Time Warps: Einstein's Outrageous Legacy*, "Late one night in June 1990 ... Stephen and an entourage of family, nurses, and friends broke into my office at Caltech, found the framed bet, and wrote a concessionary note on it with validation by Stephen's thumbprint."

That loss did little to dent Hawking's enthusiasm for a wager. Just a year later, he bet that a theoretical object called a naked singularity can't exist. A singularity is a point where the gravitational field becomes infinite. Every black hole should contain one, hiding behind its event horizon. Thorne and his Caltech colleague John Preskill believed an exposed singularity, without an event horizon, could also exist; Hawking considered that "an anathema ... prohibited by the laws of classical physics." The loser would pay up in clothing, to cover nakedness.

In 1997, Hawking conceded the bet "on a technicality," Preskill says. The same day he framed a new version: that a naked singularity can never form under "generic" conditions. That bet remains unresolved.

A few years later, Hawking entered the game again with a contrarian bet. The long-sought Higgs boson was hailed as the last missing piece of the Standard Model of particle physics. Hawking was not keen to see it discovered. He worried that it would simply cement the Standard Model without pointing the way to a more coherent theory. As a result, in the early 2000s he bet Gordon Kane, a particle physicist at the University of Michigan in Ann Arbor, that the particle would not be found.

When the Higgs was confirmed in July 2012, Hawking hailed it as an "important result" and said Peter Higgs, who had proposed the particle 48 years earlier, should receive a Nobel Prize (as he did, the next year). But, Hawking said, "It's a pity in a way because the greatest advances in physics have come from experiments that gave results we didn't expect." He then added, "It seems I have just lost $100." ■

Extreme nausea and relentless vomiting strike many pregnant women, endangering them and their babies.

PHOTO: VESNA ANDJIC/ISTOCKPHOTO.COM

BIOMEDICINE

Protein may explain morning sickness, and worse

Two groups point to a possible trigger for vomiting, nausea

By **Roni Dengler**

After paralyzing nausea and intractable vomiting caused her to lose the baby she was carrying in 1999, Marlena Fejzo decided to use her professional skills to understand her personal tragedy. A geneticist at the University of California, Los Angeles, Fejzo began to research hyperemesis gravidarum (HG), an extreme form of the "morning sickness" that afflicts most pregnant women. Jeopardizing the health of mother and fetus with dehydration and malnourishment, the little-studied condition hospitalizes at least 60,000 U.S. women a year.

Now, two studies, one led by Fejzo, suggest that an excess of a blood-borne protein, growth differentiation factor 15 (GDF15), is a cause of HG, and perhaps other cases of nausea and vomiting in pregnancy. The finding "finally gives some answers … and validates what women have been experiencing," says Caitlin Dean, a U.K. nurse who became chair of a patient advocacy group after enduring unrelenting vomiting and nausea when pregnant multiple times. In the past, some doctors asserted that women exaggerated their symptoms, and even today, women with hyperemesis report that medical staff brush off the severity of their symptoms as a routine part of pregnancy.

Dean, who now studies HG as part of a Ph.D. program at the University of Plymouth in the United Kingdom, calls the GDF15 discovery "an incredibly exciting breakthrough" that proves HG is a physical, not a psychological, condition. The finding "also points to potential therapeutic intervention," says biochemist Stephen O'Rahilly of the University of Cambridge in the United Kingdom, who led the second study, which independently highlighted GDF15.

Unable to keep food and liquids down as early as 4 weeks into a pregnancy, women with HG can lose more than 5% of their normal body weight. They suffer electrolyte imbalances, vitamin deficiencies, and other symptoms of starvation that can lead to blood clotting dysfunction and brain atrophy. Violent vomiting can produce complications such as esophageal rupture and retinal detachment. Symptoms peak around 9 weeks' gestation, but can persist until birth. The traumatic experience can lead women to end a pregnancy or decide not to have more children.

Some studies have implicated estrogen and pregnancy hormones in HG. Fejzo, whose initial research focused on cancer genetics, has slowly built a case that genes play a role in the condition. In 2007, she persuaded the consumer genetic testing company 23andMe to incorporate questions about pregnancy sickness into its surveys, enabling her and her colleagues to scan the genomes of thousands of the company's customers for DNA variations associated with hyperemesis.

That partnership paid off. In *Nature Communications* this week, Fejzo's team reports two genome-wide association scans. One compares the genomes of 1306 women who received intravenous (IV) fluid therapy for nausea and vomiting during pregnancy—a proxy for HG—to those of 15,756 who did not report any nausea or vomiting while expecting. Two variants stood out, the most significant associated with the gene for GDF15 and the second with a gene for a protein called IGFBP7. Previous animal studies suggest that both molecules influence placenta development and appetite.

In the second analysis, the team scrutinized the genomes of pregnant women reporting a gradient of nausea and vomiting symptoms, from none to very severe. The same DNA variants stood out. Finally, Fejzo confirmed the results in a non-23andMe cohort of hundreds of women with hyperemesis who required IV fluid therapy or a feeding tube. The genome scans didn't implicate estrogen or other hormones. Fejzo's study shows "very clearly that genetic variation close to GDF15 is the single, strongest genetic signal for hyperemesis," O'Rahilly says.

Last year, O'Rahilly's team reported in a preprint that women who said they had vomiting during the second trimester had more GDF15 in their blood at 12 to 18 weeks of gestation than those who reported no nausea and vomiting or only feeling nauseated. That finding, he suggests, connects GDF15 to more typical pregnancy sickness, and perhaps to HG as well.

The molecular link makes sense to Samuel Breit, an immunologist and physician at St. Vincent's Hospital in Sydney, Australia. His team has previously found cancer patients with an anorexic and muscle-wasting syndrome called cachexia also have high blood levels of GDF15. Such patients experience persistent nausea and extreme vomiting as well. Last year, another group found that knocking out GDF15's receptor in the brain made mice resistant to chemotherapy-induced nausea.

These clues have sparked interest in blocking the actions of GDF15 for therapy, O'Rahilly says. Fejzo and other researchers caution that it's too soon to consider testing such a strategy in expectant women, given how little is known about the protein's role in pregnancy. Reduced serum levels of GDF15 are associated with miscarriage, so the molecule may confer some protective effect—perhaps by keeping the mother from consuming potentially toxic foods. But Dean is optimistic. "At least there is hope now for the future," she says. ■

FUNDING

A research behemoth is born in Britain

Expectations are high for the new £6 billion funder, UK Research and Innovation

By **Erik Stokstad**, *in Cambridge, U.K.*

Combine U.S. agencies akin to the National Institutes of Health, National Science Foundation, and National Endowment for the Humanities. Toss in some energy and innovation research and fuel it all with the largest boost in R&D spending in recent history. Then put one person in charge.

That's what the United Kingdom has done in a major reorganization of research funding that unites all the research councils that support U.K. science. The intent is to provide a strategic vision and voice for science, boost efficiency, foster interdisciplinary research, and—fingers crossed—kick-start an economy jeopardized by Brexit. "There is a lot to be hopeful for," says Sarah Main, executive director of the Campaign for Science and Engineering in London.

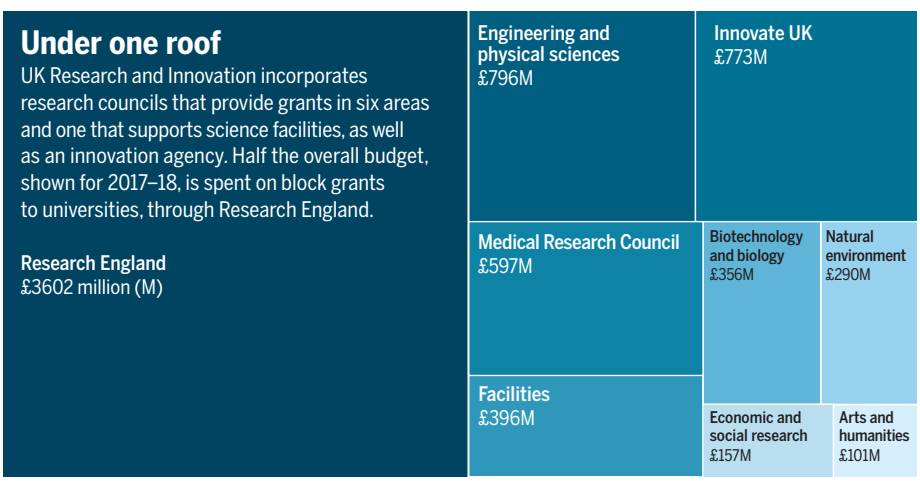

CREDITS: (GRAPHIC) V. ALTOUNIAN/*SCIENCE*; (DATA) DEPARTMENT FOR BUSINESS INNOVATION & SKILLS; HIGHER EDUCATION FUNDING COUNCIL FOR ENGLAND; INNOVATE UK

The new organization, UK Research and Innovation (UKRI), officially opens 1 April. It is headed by Mark Walport, who led the Wellcome Trust research charity from 2003 to 2013 and then served as the government chief science adviser. John Kingman, a former senior civil servant at the treasury department who is experienced in research and innovation policy, is UKRI board chair. "It's a very powerful top team," says Kieron Flanagan, a science policy expert at The University of Manchester who spoke in a personal capacity because he is participating in a country-wide university strike over pension benefits.

One big question is to what extent UKRI leadership can help bring about a science-friendly outcome for Brexit negotiations, preserving collaborations and funding from Europe. Also unclear is how much autonomy the research councils will keep and whether UKRI will emphasize biomedical research and favor the "golden triangle" of London, Oxford, and Cambridge. The choice of immunologist Walport, 65, as the new CEO in February 2017 was well-received, but he is not commenting before the release of a general strategy, expected in May.

The reorganization has its roots in a 2015 review of the funding councils by biologist Paul Nurse, now head of The Francis Crick Institute in London, who argued that a unified organization with a high-profile leader could help win greater government support for science. His recommendations were included in a higher education reform law passed in May 2017. Lawmakers also placed Innovate UK, a government-funded organization designed to help business generate new technology, within UKRI.

The seven disciplinary councils (see graphic, above) will together continue to give out about £3 billion annually, mostly as peer-reviewed grants, while part of another council—now renamed Research England—will keep providing £3 billion in unrestricted grants to English universities. The latter funding, mostly awarded in proportion to universities' productivity and impact, can be used for infrastructure or operations in any field. (Northern Ireland, Scotland, and Wales will keep their separate, smaller funding councils, independent of UKRI, as part of their devolved governments.) A new central fund outside the councils is intended to stimulate interdisciplinary research.

In a January lecture, Walport said early priorities include boosting international collaborations and stimulating growth in places that are lagging economically. Some observers hope he will also promote gender equality and diversity in the research community, and open-access publishing. "There is an opportunity to reset the agenda," says Stephen Curry, a structural biologist at Imperial College London. Walport launched an innovative open-access policy at the Wellcome Trust, and UKRI will soon review the councils' policies—which encourage and pay for open access immediately upon publication—including their cost-effectiveness.

UKRI starts with well-filled coffers. The government is giving it most of £4.7 billion in new science funding, ramping up over 4 years, as part of a new industrial strategy. In return, UKRI needs to generate economic benefits fast. "The organization will have to devise robust ways to get that money out the door in quite tight time scales," says physicist Richard Jones of The University of Sheffield. "I think that's going to be a real challenge."

Critics of the reform that led to UKRI didn't see the need for a new agency and worry about a loss of independence for the research councils. With so much power being concentrated, scientists could be left with little political recourse if they disagree with a major funding decision, Flanagan says. "UKRI will have a huge amount of freedom and autonomy with little oversight," he says.

The large proportion of life scientists and representatives of the research-rich southeast United Kingdom on the UKRI board also raises concerns. UKRI "has to convince the community that they represent all parts of our country and all parts of the scientific community," says Athene Donald, a physicist here at the University of Cambridge.

Ottoline Leyser, a plant scientist at the University of Cambridge, is optimistic that UKRI will listen to the research community. "We need to say what we want and say it in a positive way. The doors are open for that kind of input." Indeed, UKRI can only win over skeptics if it makes decisions transparently and with broad input from stakeholders, says James Wilsdon, a science policy expert at The University of Sheffield. "Until it's operational for a year or two," he says, "we won't really know how it's going to all work." ■

FEATURES

THE REALIST

Vaclav Smil looks to history for the future of energy. What he sees is sobering

By **Paul Voosen**

As a teenager in the 1950s, Vaclav Smil spent a lot of time chopping wood. He lived with his family in a remote town in what was then Czechoslovakia, nestled in the mountainous Bohemian Forest. On walks he could see the Hohenbogen, a high ridge in neighboring West Germany; less visible was the minefield designed to prevent Czechs from escaping across the border. Then it was back home, splitting logs every 4 hours to stoke the three stoves in his home, one downstairs and two up. Thunk. With each stroke his body, fueled by goulash and grain, helped free the sun's energy, transiently captured in the logs. Thunk. It was repetitive and tough work. Thunk. It was clear to Smil that this was hardly an efficient way to live.

Throughout his career, Smil, perhaps the world's foremost thinker on energy of all kinds, has sought clarity. From his home office near the University of Manitoba (UM) in Winnipeg, Canada, the 74-year-old academic has churned out dozens of books over the past 4 decades. They work through a host of topics, including China's environmental problems and Japan's dietary transition from plants to meat. The prose is dry, and they rarely sell more than a few thousand copies. But that has not prevented some of the books—particularly those exploring how societies have transitioned from relying on one source of energy, such as wood, to another, such as coal—from profoundly influencing generations of scientists, policymakers, executives, and philanthropists. One ardent fan, Microsoft co-founder Bill Gates in Redmond, Washington, claims to have read nearly all of Smil's work. "I wait for new Smil books," Gates wrote last December, "the way some people wait for the next *Star Wars* movie."

Now, as the world faces the daunting challenge of trying to curb climate change by weaning itself from fossil fuels, Smil's work on energy transitions is getting more attention than ever. But his message is not necessarily one of hope. Smil has forced climate advocates to reckon with the vast inertia sustaining the modern world's dependence on fossil fuels, and to question many of the rosy assumptions underlying scenarios for a rapid shift to alternatives. "He's a slayer of bullshit," says David Keith, an energy and climate scientist at Harvard University.

Give Smil 5 minutes and he'll pick apart one cherished scenario after another. Germany's solar revolution as an example for the world to follow? An extraordinarily inefficient approach, given how little sunlight the country receives, that hasn't reduced that nation's reliance on fossil fuels. Electric semitrailers? Good for little more than hauling the weight of their own batteries. Wind turbines as the embodiment of a low-carbon future? Heavy equipment powered by oil had to dig their foundations, Smil notes, and kilns fired with natural gas baked the concrete. And their steel towers, gleaming in the sun? Forged with coal.

"There's a lot of hopey-feely going on in the energy policy community," says David Victor, an expert on international climate policy at the University of California, San Diego. And Smil "revels in the capability to show those falsehoods."

But Smil is not simply a naysayer. He accepts the sobering reality of climate change—though he is dubious of much climate modeling—and believes we need to reduce our reliance on fossil fuels. He has tried to reduce his own carbon footprint, building an energy-efficient home and adopting a mostly vegetarian diet. He sees his academic work as offering a clear-eyed, realistic assessment of the challenges ahead—not as a justification for inaction. And he says he has no ax to grind. "I have never been wrong on these major energy and environmental issues," he says, "because I have nothing to sell."

Despite Smil's reach—some of the world's most powerful banks and bureaucrats routinely ask for his advice—he has remained intensely private. Other experts tap dance for attention and pursue TED talks. But Smil is a throwback, largely letting his books speak for themselves. He loathes speaking to the press (and opened up to *Science* only out of a sense of duty to The MIT Press, his

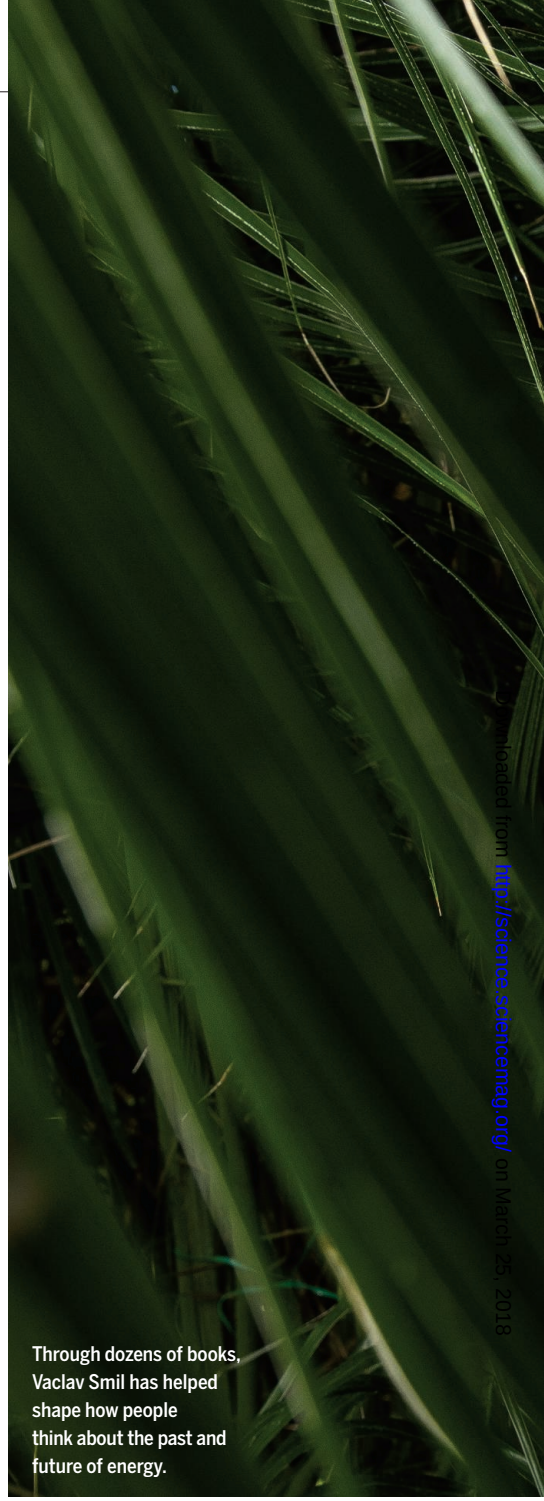

Through dozens of books, Vaclav Smil has helped shape how people think about the past and future of energy.

PHOTO: DAVID LIPNOWSKI

longtime publisher). "I really don't think I have anything special to say," he says. "It's out there if you want to know it."

THIS PAST DECEMBER, Smil stepped out of a hotel in Washington, D.C., and pulled on a knit cap—he'd allow no wasted heat, especially given a persistent head cold. He had given a lecture the previous day and now was making a beeline for a favorite spot: the National Gallery of Art. He was a regular in the nation's capital during the 1980s and '90s, consulting with the World Bank, the Central Intelligence Agency, and other government agencies. But the United States's security clampdown after 9/11—its the increasing political dysfunction—soured him on the country's leaders. "This government is so inept," he said. "It cannot even run itself in the most basic way."

Still, Smil can't shake his affection for the United States. It goes back to his childhood: During World War II, U.S. soldiers—not Soviet troops—liberated his region from the Nazis. And it was to the United States that Smil and his wife, Eva, fled in 1969, after the Soviets invaded Czechoslovakia to stymie a political uprising.

Nothing was exceptional about his childhood, Smil says. His father was a police officer and then worked in manufacturing; his mother kept the books for a psychiatric hospital's kitchen. But even as a boy, he was aware of the miasma of falsehood that surrounded him in Cold War Czechoslovakia, and it spurred his respect for facts. "I'm the creation of the communist state," he says, recalling how, as a child, he heard that the Soviet Union had increased production of passenger cars by 1000% in a single year. "I looked at it and said, 'Yeah, but you started from nothing.'" Officials

Energy inertia

The transition from wood ("traditional biofuels") to fossil fuels—first coal, then oil and natural gas—took more than a century. Today, fossil energy is dominant, with wind and solar making up a mere sliver of the mix. The pace of past energy transitions suggests that a full-scale shift to renewables will be slow.

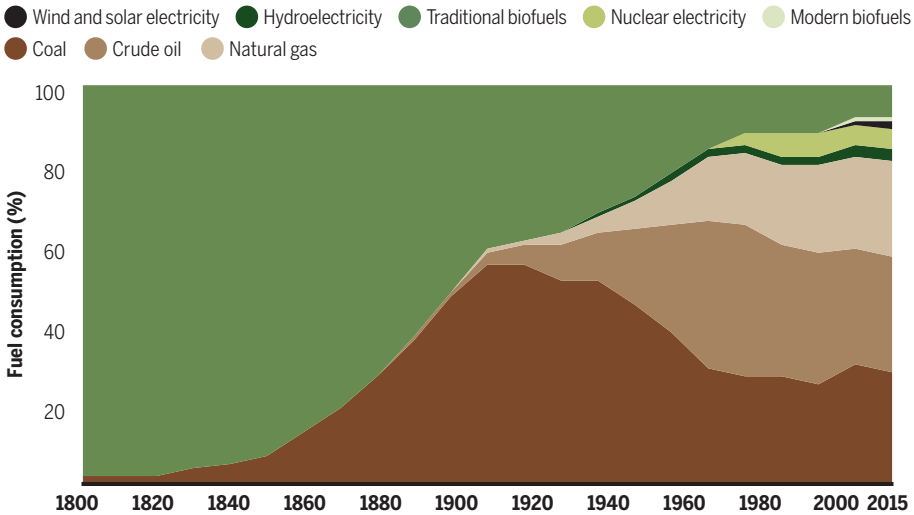

Down the density ladder

In the past, humanity has typically adopted energy sources that have greater "power density," packing more punch per gram and requiring less land to produce. Renewables (green), however, are lower in density than fossil fuels (brown). That means a move to renewables could vastly increase the world's energy production footprint, barring a vast expansion of nuclear power.

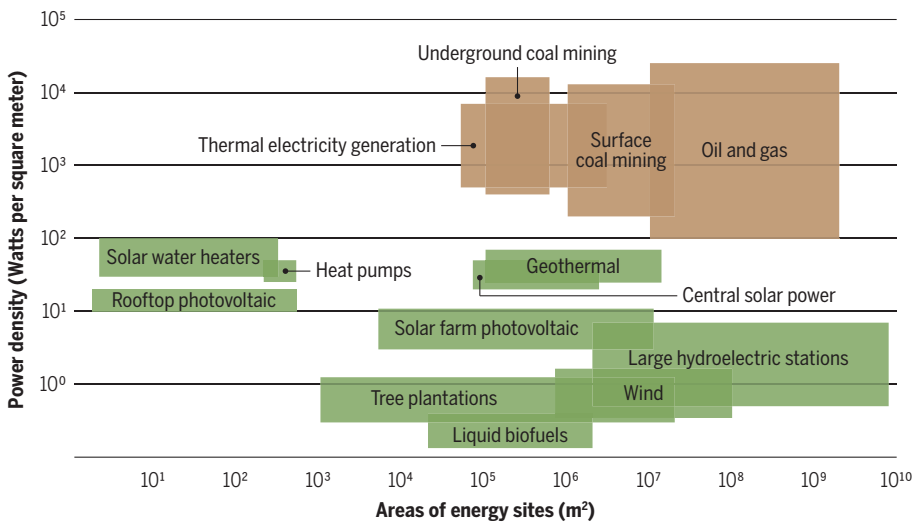

would claim they had exceeded their food plan, yet oranges were never available. "It was so unreal and fake," Smil says. "They taught me to respect reality. I just don't stand for any nonsense."

As an undergraduate, Smil studied the natural sciences at Charles University in Prague. He lived in an old converted cloister. Its thick stone walls kept it chilly, summer and winter. And in the first of Smil's personal energy transitions, heat came not from wood, but from coal—hard black anthracite from Kladno or dirty brown lignite from North Bohemia.

He got to indulge his curiosity, taking 35 classes a week, 10 months a year, for 5 years. "They taught me nature, from geology to clouds," he says. But Smil decided that a traditional scientific career was not for him. No lab bench called: He was after the big picture.

After graduation, he also realized that his future would not be in his homeland: He refused to join the Communist Party, undermining his job prospects. He worked in a regional planning office while Eva pursued her medical degree. After Soviet troops invaded, many friends and neighbors panicked and left. But the couple waited for Eva's graduation, dreading a travel ban. They finally departed in 1969, just months before the government imposed a travel blockade that would last for decades. "That was not a minor sacrifice, you know?" Smil says. "After doing that, I'm not going to sell myself for photovoltaics or fusion or whatever and start waving banners. Your past always leads to who you are."

The Smils ended up at Pennsylvania State University in State College, where Vaclav completed a doctorate in geography in 2 years. With little money, they rented rooms from a professor's widow, and Smil made another energy transition: Periodically, an oil truck arrived to refuel the basement furnace. Smil then took the first job offer he received, from UM. He's been there ever since.

For decades until his retirement, Smil taught introductory environmental science courses. Each year ended with a 10-question, multiple choice final exam, with a twist: "There could be no right answer, or every answer was correct, and every combination in between," says Rick Baydack, chair of the environmental science department at UM, who was once Smil's student.

Otherwise, Smil was a ghost in his department, taking on only a few graduate students. Since the 1980s, he has shown up at just one faculty meeting. But as long as he kept teaching and turning out highly rated books, that was fine for the school. "He's a bit of a recluse and likes to work on his own," Baydack says. "He's continued down a path he set for himself. What's happening around him doesn't really matter."

TODAY, SMIL STRADDLES the line between scientist and intellectual, flashing the tastes of a "rootless bohemian cosmopolitan," as his old communist masters used to call him. He's fluent in a flurry of languages. He's a tea snob and foodie who is reluctant to eat out because so much restaurant food is now premade. Stand in a garden and he can tell you the Latin names of many of the plants. He's an art lover: Mention the Prado Museum in Madrid and he might tell you the secret of finding 5 minutes without crowds to appreciate Diego Velázquez's *Las Meninas*, his favorite painting, which depicts a Spanish princess encircled by her retinue. And then he'll say, "I appreciate and love blue-green algae," which helped kick off Earth's oxygen age. "They are the foundation."

Smil's breadth feels anachronistic. In modern academic science, all the incentives push to narrow specialization, and Smil believes his eclectic interests have complicated his career. But his ability to synthe-

CREDITS: (GRAPHIC) J. YOU/*SCIENCE*; (DATA) V. SMIL, *ENERGY TRANSITIONS*. PRAEGER, 2017; V. SMIL, *POWER DENSITY*. MIT PRESS, 2015

size across disparate fields also has proved a strength, enabling him to trace how energy courses through every capillary of the world's economy.

Smil's writing career kicked off in the mid-1970s, just as an embargo on oil sales by Middle Eastern nations woke up developed nations to just how hooked they were on petroleum, for transportation, heating, farming, chemicals, even electricity. The jolt came just after the publication of *The Limits to Growth*, an influential study that, using a simple computer model, warned of a pending depletion of the planet's resources.

Smil was intrigued and taught himself programming to re-create the model for himself. "I saw it was utter nonsense," he recalls; the model was far too simple and easily skewed by initial assumptions. He constructed a similar model of how carbon dioxide emissions affect climate and found it similarly wanting. He understood the physics of the greenhouse effect and the potential for a carbon dioxide buildup to warm Earth, but models seemed too dependent on assumptions about things like clouds. Ever since, he's held models of all kinds in contempt. "I have too much respect for reality," he says.

Instead, he scoured the scientific literature and obscure government documents for data, seeking the big picture of how humanity generates and deploys energy. What ultimately emerged in several blandly titled books—including *General Energetics: Energy in the Biosphere and Civilization* (1991), *Energy in World History* (1994), and *Energy Transitions: History, Requirements, Prospects* (2010)—is an epic tale of innovation and transformation, worked through one calculation at a time.

That work has guided a generation to think about energy in the broadest sense, from antiquity to today, says Elizabeth Wilson, director of the Institute for Energy and Society at Dartmouth College. "You could take a paragraph from one of his books and make a whole career out of it," she says. And yet Smil has avoided mental traps that could come with his energy-oriented view, she adds. "[He] does a really good job of being nuanced."

In essence, Smil says, humanity has experienced three major energy transitions and is now struggling to kick off a fourth. First was the mastery of fire, which allowed us to liberate energy from the sun by burning plants. Second came farming, which converted and concentrated solar energy into food, freeing people for pursuits other than sustenance. During that second era, which ended just a few centuries ago, farm animals and larger human populations also supplied energy, in the form of muscle power. Third came industrialization and, with it, the rise of fossil fuels. Coal, oil, and natural gas each, in turn, rose to prominence, and energy production became the domain of machines, as such coal-fired power plants.

Now, Smil says, the world faces its fourth energy transition: a move to energy sources that do not emit carbon dioxide, and a return to relying on the sun's current energy flows, instead of those trapped millions of years ago in deposits of coal, oil, and natural gas.

The fourth transition is unlike the first three, however. Historically, Smil notes, humans have typically traded relatively weak, unwieldy energy sources for those that pack a more concentrated punch. The wood he cut to heat his boyhood home, for example, took a lot of land area to grow, and a single log produced relatively little energy when burned. Wood and other biomass fuels have relatively low "power density," Smil says. In contrast, the coal and oil that heated his later dwellings have higher power densities, because they produce more energy per gram and are extracted from relatively compact deposits. But now, the world is seeking to climb back down the power density ladder, from highly concentrated fossil fuels to more dispersed renewable sources, such as biofuel crops, solar parks, and wind farms. (Smil notes that nuclear power, which he deems a "successful failure" after its rushed, and now stalled, deployment, is the exception walking down the density ladder: It is dense in power, yet often deemed too costly or risky in its current form.)

One troubling implication of that density reversal, Smil notes, is that in a future powered by renewable energy, society might have to devote 100 or even 1000 times more land area to energy production than today. That shift, he says, could have enormous negative impacts on agriculture, biodiversity, and environmental quality.

To see other difficulties associated with that transition, Smil says, look no further than Germany. In 2000, fossil fuels provided 84% of Germany's energy. Then the country embarked on a historic campaign, building 90 gigawatts of renewable power capacity, enough to match its existing electricity generation. But because Germany sees the sun only 10% of the time, the country is as hooked as ever on fossil fuels: In 2017, they still supplied 80% of its energy. "True German engineering," Smil says dryly. The nation doubled its hypothetical capacity to create electricity but has gotten minimal environmental benefit. Solar can work great, Smil says, but is best where the sun shines a great deal.

Perhaps the most depressing implication of Smil's work, however, is how long making the fourth transition might take. Time and again he points back to history to note that energy transitions are slow, painstaking, and hard to predict. And existing technologies have a lot of inertia. The first tractor appeared in the late 1800s, he might say, but the use of horses in U.S. farming didn't peak until 1915—and continued into the 1960s.

Fossil fuels have similar inertia, he argues. Today, coal, oil, and natural gas still supply 90% of the world's primary energy (a measure that includes electricity and other types of energy used in industry, transportation, farming, and much else). Smil notes that the share was actually lower in 2000, when hydropower and nuclear energy made up more of the mix. Since then, "we have been increasing our global dependence on fossil fuels. Not decreasing," he says.

A key factor has been the economic boom in China, a nation Smil has studied since the 1970s, and its burgeoning appetite for coal. Smil was among the first Western academics invited to study the Chinese energy system. He sounded early warnings about the nation's cooked farm statistics and perilous environmental state. Now, Smil is disheartened by China's consumer culture: Instead of aiming to live more modestly, he says the Chinese are "trying to out-America America."

Meanwhile, despite years of promotion and hope, wind and solar account for just about 1% of the world's primary energy mix. In part, he notes, that's because some of the key technologies needed to deploy renewable energy on a massive scale—such as higher-capacity batteries and more efficient solar cells—have seen only slow improvements. The bottom line, he says, is that the world could take many decades to wean itself from fossil fuels.

"You could take a paragraph from one of his books and make a whole career out of it. [He] does a really good job of being nuanced."

Elizabeth Wilson, Dartmouth College

SMIL SEES FEW OPTIONS for hastening the transition. And that is where he and some of his biggest fans—including Gates—diverge. Smil's realism appeals to Gates, who first mentioned Smil on his blog in 2010. Like many tech tycoons, Gates had made

failed investments over the previous decade in biofuels, a technology Smil has scorned because it is so land-hungry. Over the next year, Gates, who declined to be interviewed for this story, publicly detailed his conversion to Smilism. It was not an easy one: After reading his first Smil book, Gates "felt a little beat up. … Am I ever going to be able to understand all of this?" But he ultimately concluded that "I learn more by reading Vaclav Smil than just about anyone else." That enthusiasm has written Smil's epitaph: "I'll forever be Bill Gates's scientist," Smil says.

The two have met just a few times, but they email regularly. And Gates has opened doors for Smil: Swiss banks weren't calling for his advice before. But they keep the relationship pure. "I would never ask him for any favor—never ever," Smil says. "As simple as that."

Microsoft co-founder Bill Gates is an avid reader of Vaclav Smil's books, including *Energy and Civilization*, at the bottom of this stack. "I learn more by reading [him] than just about anyone else," Gates has written.

But when it comes to the future of energy, they make an odd couple. In 2016, Gates helped start Breakthrough Energy Ventures, a billion-dollar fund to speed clean energy innovations from the lab to market. "I am more optimistic than [Smil] is about the prospects of speeding up the process when it comes to clean energy," Gates has written. Smil puts it another way: "He's a techno-optimist, I'm a European pessimist."

Smil says that pessimism is rooted in his understanding of history. But even some of his fans say he puts too much stock in the lessons of the past. "Sometimes I've heard him speak too confidently" about how slowly technology transitions occur, says Keith, another Gates adviser. History, Keith notes, offers a small sample size.

Smil says he would be delighted to be proved wrong—as he has been, twice, in the past. In particular, a breakthrough in cheap energy storage would change the game. "Give me mass-scale storage and I don't worry at all. With my wind and photovoltaics I can take care of everything." But "we are nowhere close to it," he says.

WHEN NOT ON THE ROAD, Smil lives a quiet life in Winnipeg. He cultivates hot peppers, tomatoes, and basil in containers. (Deer would eat a traditional garden.) He cooks meals in Indian or Chinese styles, eating meat maybe once a week. He drives a Honda Civic, "the most reliable, most efficient, most miraculously designed car." He built his current home in 1989, a modest house of about 200 square meters. He used thicker-than-standard studs and joists, so he could stuff 50% more insulation into the walls, and all of the windows are triple-paned. There's a 97% efficient natural gas furnace. "My house," he says, is "a very efficient machine for living."

Despite those choices—and all that can be learned from his work—Smil is not comfortable offering solutions. Any he suggests typically come down to encouraging individual action, not sweeping government policies or investment strategies. If we all cut consumption, lived more efficiently, and ate less meat, he suggested at one recent lecture, the biosphere would do fine. Fewer livestock, for instance, might mean farmers would stop overfertilizing soybeans to feed to animals. Less fertilizer, in turn, would drastically cut emissions of nitrous oxide, a powerful greenhouse gas, from the soil. "Less pork and less beef, right? That's it," Smil says. "Nobody is really talking about it."

Such statements can make Smil sound as though he were an author of *The Limits to Growth*—not a critic. And the reality is that "there are many Vaclavs," says Ted Nordhaus, an environmentalist and executive director of The Breakthrough Institute, an environmental think tank in Oakland, California. There is the hard-edged skeptic, and then "there are times where Vaclav will be an old-fashioned conservationist. We could all be perfectly happy living at the level of consumption and income as Frenchmen in 1959."

Smil doesn't apologize for his contradictions. And for all his insistence on documenting reality, he accepts that many concepts cannot be defined. What does a healthy society look like, and how do you measure it? He abhors gross domestic product, the traditional measure used by economists, because even horrendous events—natural disasters and shootings, for example—can prompt spending that makes it grow. But the alternatives don't look great, either. Happiness indexes? Some of "the happiest nations on the planet are Colombia and the Philippines," Smil says. "What does that tell you?"

Lately, he's been thinking about growth, the obsession of modern, fossil-fueled economies and the antithesis of Smil's lifestyle of efficient, modest living. How do children grow? Energy systems? Cyanobacteria? Empires? His next book, in 195,000 words, will examine growth in all forms. "I'm trying to find the patterns and the rules," he says. "Everything ends. There is no hyperbolic growth."

Still, although Smil can see the present better than most, he is loath to predict the future. Those two times he was wrong? He could not have imagined, he says, how soon the Soviet Union would fall. Or how fast China would grow. And he is not about to say that a collapse is inevitable now—not even with humanity on a problematic course and unlikely to change direction soon. "You ask me, 'When will the collapse come?'" Smil says. "Constantly we are collapsing. Constantly we are fixing." ■

PHOTO: THE GATES NOTES, LLC

CLIMATE

Are wood pellets a green fuel?

A return to firewood is bad for forests and for the climate

By **William H. Schlesinger**

James Watt's steam engine vaulted coal to its major role as a fuel for the Industrial Revolution. Today, about 40% of the world's electricity is generated in coal-fired power plants, consuming more than 80% of the coal mined each year. Because combustion of coal produces carbon dioxide (CO_2) and other air pollutants, efforts to combat climate change have now turned to seeking alternatives to coal. Natural gas is cleaner and less expensive but, like coal, returns fossil carbon to the atmosphere. Recently, attention has focused on woody biomass—a return to firewood—to generate electricity. Trees remove CO_2 from the atmosphere, and burning wood returns it. But recent evidence shows that the use of wood as fuel is likely to result in net CO_2 emissions and may endanger forest biodiversity.

In recent years, ~7 million metric tons of wood pellets per year have been shipped from the United States to the European Union (EU), where biomass fuels have been declared carbon neutral and are thus considered to count toward fulfilling the commitments of the Paris Agreement. The EU aims to generate 20% of its electricity by 2020 using renewable sources, including burning woody biomass. In part to revive a languishing forest products industry, the U.S. Congress may also declare wood a carbon-neutral fuel. Despite its withdrawal from the Paris Agreement, the United States may see a few utilities switch from coal to wood, which costs roughly the same as natural gas. The switch could be further incentivized with a carbon tax on fossil carbon (*1*).

Cutting trees for fuel is antithetical to the important role that forests play as a sink for CO_2 that might otherwise accumulate in the atmosphere. Each year, an estimated 31% of the CO_2 emitted from human activities is stored in forests (*2*). However, managed forests store less carbon than their

Cary Institute of Ecosystem Studies, Post Office Box AB, Millbrook, NY 12545, USA. Email: schlesingerw@caryinstitute.org

PHOTO: OFFICE OF THE DUKE FOREST/DUKE UNIVERSITY

Young loblolly pines are harvested in the southeastern United States.

native counterparts (*3*), and harvesting of native forests will therefore be a source of, not a sink for, atmospheric CO_2. Furthermore, wood contains less energy than coal, and wood burning thus generates higher CO_2 emissions per kilowatt of electricity. The CO_2 emissions from burning wood offset CO_2 that might otherwise be emitted from fossil-fuel combustion (*4*, *5*), but full carbon accounting must also consider how long it takes to restore the carbon pool of forested land that has been converted to atmospheric CO_2 (*6*).

The large-scale abandonment of agricultural activities during the Great Depression (1929 to 1939) led to a rapid expansion of mostly natural forests across the southeastern United States. Later, these natural stands were replaced by plantations of loblolly and slash pine, which were the favorites of the forest products industry because they grow well in the warm, wet climate of the Southeast (see the photo). Loblolly pine plantations achieve a maximum biomass of 125 metric tons per hectare in about 40 years (*7*). But because this species achieves its maximum rate of biomass accrual in about 20 years, rotations are usually kept short to maintain the fastest carbon uptake possible. Thirty-four operating and proposed wood-pellet plants dot the landscape of the Southeast, each anticipated to receive logs from the region within an 80-km radius. Maine and the Canadian Maritime provinces also eye the potential for wood pellets to revitalize their forest products industries; most of this wood would derive from natural forests and not plantations.

It is not only the burning of wood that adds CO_2 to the atmosphere. Making wood pellets and shipping them to Europe can account for about 25% of the total carbon emitted to the atmosphere from the use of wood pellets in European power plants (*8*). Carbon neutrality for wood is only achieved if the areas that are harvested are allowed to regrow such that they store more than their original biomass. Furthermore, the benefits of wood power must be discounted by the loss of the carbon sequestration that would have occurred in the original forests if they had not been harvested (*6*).

Although the carbon uptake by southeastern forests is greatest at about 20 years, regrowing stands continue to have lower biomass than unharvested stands for 40 to 100 years (*9*, *10*). Rotation lengths of less than 40 years seem certain to transfer carbon from biomass to CO_2 in the atmosphere. By contrast, nonwoody biomass fuels such as switchgrass or silvergrass (*Miscanthus*) regrow within a year, balancing the emissions from their combustion to their subsequent uptake of CO_2 through photosynthesis. With wood, there is the assumption—but no guarantee—that new trees will be planted and will persist long enough to pay back the carbon debt created by burning the previous stands. If that carbon stock is not restored, burning wood may actually emit more CO_2 to the atmosphere than burning coal (*10*).

Much of the argument about the carbon neutrality of wood power centers on the time frame of analysis. Because CO_2 persists for many decades in the atmosphere, some scientists argue that CO_2 emitted to the atmosphere does not contribute substantially to global warming in intervals less than a century (*11*). Others hold that all CO_2 molecules in the atmosphere exert the same effect and that plantation rotations of less than 20 years make a substantial net contribution to global warming. Ocko *et al.* (*12*) argue that the impacts on warming should always be reported for both 20- and 100-year periods, so that policy-makers can understand the net CO_2 emissions that are associated with the time horizon of different policy options. Full international participation is paramount; it makes no sense to have Europeans embracing wood pellets as carbon neutral, thereby overlooking the CO_2 emitted during shipment and the losses of carbon stock from forests harvested outside Europe. This is another example of exporting CO_2 emissions beyond the border (*13*).

Many environmental economists believe that the increased value of forests for wood-pellet production will ensure that more forests are planted (*14*); when trees have little or no value, the landscape is more likely to succumb to commercial or residential development. But in the southeastern United States, these forests are most likely to be pine plantations, which are of limited value for the preservation of its rich regional biodiversity. Furthermore, increased demand for wood pellets can raise the price of raw wood, diverting harvest to old-growth forests, which are important areas for biodiversity.

Biodiversity losses in the southeastern United States mostly result from land clearing (*15*), and agricultural clearing during the past two centuries likely already had great impacts on biodiversity. Following agricultural abandonment in the early 20th century, forests are now more widespread but are mostly pine plantations with low biomass and low diversity. Ultimately, the question is what kinds of forests are most desirable for the future. Unless forests are guaranteed to regrow to carbon parity, production of wood pellets for fuel is likely to result in more CO_2 in the atmosphere and fewer species than there are today. ■

REFERENCES

1. P. Dwivedi, M. Khanna, *Glob. Change Biol. Bioenergy* **7**, 945 (2015).
2. W. H. Schlesinger, E. S. Bernhardt, *Biogeochemistry: An Analysis of Global Change* (Elsevier, ed. 3, 2013).
3. K.-H. Erb *et al.*, *Nature* **553**, 73 (2018).
4. K. C. Kelsey *et al.*, *Carbon Balance Manag.* **9**, 6 (2014).
5. S. V. Hanssen *et al.*, *Glob. Change Biol. Bioenergy* **9**, 1406 (2017).
6. M. T. Ter-Mikaelian *et al.*, *J. Forestry* **113**, 57 (2015).
7. P. M. Schiffman, W. C. Johnson, *Can. J. For. Res.* **19**, 69 (1989).
8. A. L. Stephenson, D. J. C. Mackay, *Life Cycle Impacts of Biomass Electricity in 2020* (U.K. Department of Energy and Climate Change, London, 2014).
9. J. G. G. Jonker *et al.*, *Glob. Change Biol. Bioenergy* **6**, 371 (2014).
10. J. D. Sterman *et al.*, *Environ. Res. Lett.* **13**, 015007 (2018).
11. J. K. Shoemaker *et al.*, *Science* **342**, 1323 (2013).
12. I. B. Ocko *et al.*, *Science* **356**, 492 (2017).
13. K. Kanemoto *et al.*, *Environ. Sci. Technol.* **50**, 10512 (2016).
14. C. S. Galik, R. C. Abt, *Glob. Change Biol. Bioenergy* **8**, 658 (2016).
15. S. Martinuzzi *et al.*, *Ecol. Appl.* **25**, 160 (2015).

10.1126/science.aat2305

NEUROSCIENCE

Early life experience shapes neural genome

Transposons accumulate in neurons of pups with lack of maternal care in mice

By **Saera Song**[1] and **Joseph G. Gleeson**[2]

The brain is constantly changing in response to environmental experiences throughout life. Mounting evidence from animal and human studies suggests that brain development and behavior are influenced by early life experiences. Several compelling experimental models have been developed to study the effect of early life experiences on the brain, such as stress, exposure to toxins, availability of nutrients, adversity, and quality of maternal care (*1*). The relationship between genes and environment on the brain and how they affect behavior has been a long-standing issue. Can the genome of individual brain cells be changed by environmental factors? If so, which types of genetic changes can result? What is the molecular basis of this genetic diversity? What are the physiological implications? On page 1395 of this issue, Bedrosian *et al.* (*2*) explore one possibility for how neuronal genomes can exhibit plasticity in response to environmental factors during early life, providing integrative evidence for the effect of early maternal care on the genomes of neurons.

Somatic mosaicism is the phenomenon by which cells within an organism can have different genetic sequences. The brain exhibits extensive somatic mosaicism, and this is of particular interest because it can contribute to neuronal diversity and potentially expand the range of behavior of the individual (*3*). Mobile elements are DNA sequences that can change their position within the genome, either by a DNA-based (transposition) or RNA-based (retrotransposition) mechanism (*4*). Retrotransposition is one of the main forms of somatic mosaicism in the brain (*5*). Dividing cells, such as neural progenitor cells, may tolerate or even support increased levels of retrotransposition relative to other cells, resulting in neurons with unique genomes (*6*–*8*). Long interspersed element-1 (L1, also known as LINE-1) is the most abundant class of retrotransposon, comprising about 17% of the mammalian genome. L1 elements remain mobile in both human and mouse genomes throughout life. L1 elements are ~6 kb long, and the insertion of L1 into DNA during retrotransposition results in the generation of variably sized target site duplications, which flank the new insertion. It can be challenging to detect neuronal L1 retrotransposition events because individual events can be specific to a particular cell and can vary in frequency based on the brain region and/or cell type being assayed and the method of detection (*9*–*11*). Despite such challenges, it is now understood that somatic retrotransposition occurs in neurons of both humans and mice and can influence neural disease. These advances were achieved through the development of new experimental tools such as copy number quantitative polymerase chain reaction (PCR) assays, L1 reporter assays, and next-generation sequencing of bulk and single cells. Building on this previous work, Bedrosian *et al.* hypothesize that neuronal genomes can be influenced by environmental factors such as early life experiences.

Rodent pups receive maternal care as one of the first biological embedding experiences. Natural variations of maternal care can be assessed by monitoring licking and grooming behaviors, nesting patterns, contact time, and the type of posture in rodents (*12*). Bedrosian *et al.* developed a droplet digital PCR (ddPCR) assay to detect copy number of L1 retrotransposons in neuronal cell genomes. They demonstrated that pups reared under conditions of low maternal care for the first 2 weeks after parturition accumulate L1 retrotransposons. This L1 accumulation was observed in the hippocampus but not in the frontal cortex or heart, suggesting that they represent somatic mosaic events. The hippocampus exhibits plasticity, and it is highly sensitive to environmental stimuli, making it more likely to foster retrotransposition during early life (*7*). To further support the apparent inverse correlation of increased L1 copy number and decreased maternal care, the authors manipulated the effect of maternal care by separation, resulting in a compensatory increase in care that dams (female parents) provide to pups upon reunification. Maternal separation attenuated accumulation of L1 copies of pups reared with low-maternal-care dams. Moreover, a cross-fostering experiment showed better correlation of L1 copy number with the maternal care of the dam that reared the pups rather than the biological dam. As a potential mechanism, Bedrosian *et al.* also report that neuronal cells from pups that experienced low maternal care had reduced L1 promoter methylation on the binding sites of the transcriptional repressor protein, Yin Yang 1 (YY1), which correlated with reduced expression of DNA methyltransferase 3A (DNMT3A). Thus, the changes in retrotransposition may be regulated at the epigenetic level (see the figure). It will be interesting to measure the effect of these events on neuronal cell phenotypes and on the behavior of the offspring.

It is well established that maternal care can affect epigenetic control and changes in gene expression in the brain (*13*). The study

Maternal care alters genomic structure

Early life experiences such as maternal care affect DNA sequence in neurons of the hippocampus via L1 retrotransposition. The accumulation of L1 retrotransposons in the hippocampus of rodent pups reared with low maternal care might contribute to higher anxiety-like behavior in adulthood.

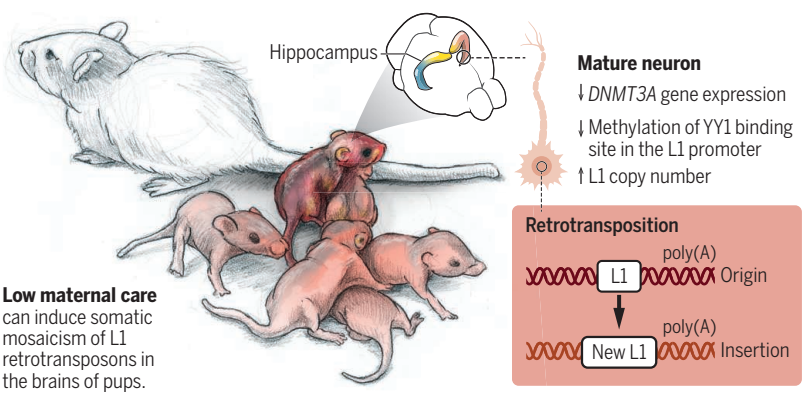

Low maternal care can induce somatic mosaicism of L1 retrotransposons in the brains of pups.

[1]*Institute for Genomic Medicine, Columbia University Medical Center, New York, NY 10032, USA.* [2]*Laboratory for Pediatric Brain Disease, Howard Hughes Medical Institute, Rady Children's Institute for Genomic Medicine, University of California, San Diego, San Diego, CA 92093, USA. Email: jogleeson@ucsd.edu*

by Bedrosian *et al.* brings new insight into this concept, demonstrating that plasticity in DNA sequences can change in response to environmental cues. More detailed analysis, including mapping of L1 insertion sites to demonstrate their integration into genomic DNA by single-cell genomic analysis from hippocampal neurons, is necessary to critically test this hypothesis. In addition, it will be interesting to examine the effect of other environmental challenges on L1 retrotransposition in the brain or to identify other types of somatic genomic variations in the brain that can result from environmental factors. However, caution is warranted in extrapolating these findings to humans. L1 is much more active in mouse than human brain, and there are higher numbers of active L1s in the average mouse genome (3000 to 4000) compared with human (~80 to 100) (*14*, *15*). Additionally, we still do not completely understand the biological and physiological consequences of L1 retrotransposition events. As in previous reports, higher anxiety-like behavior was observed in adult mice that were reared with low maternal care (*12*), and thus it would be interesting to investigate whether increased L1 copy number contributes to these behaviors. It is believed that mosaic DNA mutations can potentially alter the physiological properties of individual neurons, contributing to overall brain function, neural circuits, and behavior, although such changes could just as easily be maladaptive. Somatic mosaicism resulting from retrotransposition or other types of mutations may represent a bridge between environmental and genetic factors that create functional diversity among brain cells or the predisposition to brain disorders. With a further understanding of how environmental factors contribute to somatic mutations in the human brain, it may become possible to better predict risk and develop new treatments for neuropsychiatric disease. ■

REFERENCES

1. M. Di Segni, D. Andolina, R. Ventura, *Semin. Cell Dev. Biol.* (2017); https://doi.org/10.1016/j.semcdb.2017.09.039.
2. T. A. Bedrosian *et al.*, *Science* **359**, 1395 (2018).
3. M. J. McConnell *et al.*, *Science* **356**, eaal1641 (2017).
4. C. R. Beck *et al.*, *Annu. Rev. Genomics Hum. Genet.* **12**, 187 (2011).
5. S. R. Richardson, S. Morell, G. J. Faulkner, *Annu. Rev. Genet.* **48**, 1 (2014).
6. A. R. Muotri *et al.*, *Nature* **435**, 903 (2005).
7. N. G. Coufal *et al.*, *Nature* **460**, 1127 (2009).
8. J. K. Baillie *et al.*, *Nature* **479**, 534 (2011).
9. G. D. Evrony *et al.*, *Cell* **151**, 483 (2012).
10. K. R. Upton *et al.*, *Cell* **161**, 228 (2015).
11. G. D. Evrony *et al.*, *eLife* **5**, e12966 (2016).
12. I. C. Weaver, M. J. Meaney, M. Szyf, *Proc. Natl. Acad. Sci. U.S.A.* **103**, 3480 (2006).
13. M. Kundakovic, F. A. Champagne, *Neuropsychopharmacology* **40**, 141 (2015).
14. J. L. Goodier *et al.*, *Genome Res.* **11**, 1677 (2001).
15. B. Brouha *et al.*, *Proc. Natl. Acad. Sci. U.S.A.* **100**, 5280 (2003).

10.1126/science.aat3977

NEUROBIOLOGY

RNA targeting and translation in axons

Local translation of transcripts takes center stage in neuron growth and regeneration

By **Antonella Riccio**

Neurons are among the largest and most complex cells in nature, often extending very long axons, which in adult mammals, including humans, can reach up to one meter in length. These extraordinary morphological features pose a challenging problem as to how information codified in the nucleus can reach the periphery of the cell in a timely manner to respond to extrinsic stimuli. Similar to virtually all eukaryotic cells, neurons have adopted the strategy of localizing RNA asymmetrically. The nature of the transcripts targeted to dendrites and axons have been extensively studied, and they encode synaptic proteins, cytoskeleton components, ion channels, mitochondrial and ribosomal proteins, and proteins required for plasma membrane biogenesis. However, the mechanism underlying local translation has remained elusive. On page 1416 of this issue, Terenzio *et al.* (*1*) add a new piece to the puzzle and show that local translation to produce the protein mammalian target of rapamycin (mTOR) precedes the burst of protein synthesis associated with the regeneration of injured axons. mTOR is a serine/threonine kinase that plays a central role in regulating protein synthesis (*2*).

Peripheral localization of transcripts is a widespread phenomenon that mediates many cellular processes. In neurons, coding and noncoding RNAs are targeted to dendrites and axons, where messenger RNAs (mRNAs) are rapidly translated in response to extrinsic stimuli. Local protein synthesis has been shown to mediate synaptic development and plasticity in dendrites, whereas in axons, it is necessary for axon extension and steering in response to guidance cues (*3*). Although polyribosomes were visualized at the base of dendritic spines more than 30 years ago, the presence of the translational machinery in axons has been hotly debated. This was mostly because in axons, ribosomes are found close to the plasma membrane, which makes visualization by using classical microscopy techniques difficult. Because of their localization, it has even been proposed that axons may "borrow" ribosomes from surrounding cells, such as Schwann cells that produce the myelin sheath that coats axons (*4*).

Comparative analyses of RNAs localized in either dendrites, axons, or cell bodies showed expression patterns that only partially overlap and differ depending on cell type and developmental stage (*5*–*7*). Interestingly, transcripts that are highly expressed in cell bodies are not necessarily enriched in axons or dendrites, indicating that RNAs do not reach the peripheral compartments by passive transport but are sorted and delivered with an active mechanism. How are transcripts selected to be transported to axons? At least two mechanisms must be taken into account, one intrinsic to the RNA and dependent on its structure and a second related to the extrinsic signals that trigger transcript localization. Although the information necessary for RNA transport can be stored anywhere along the transcript, most elements that regulate mRNA targeting are found within the 3′ untranslated regions (UTRs). The first localization element of a neuronal transcript was identified in the 3′UTR of the mRNA encoding β-actin and was named "zipcode" because it was necessary for delivering the mRNA to axons in response to neurotrophins (*8*). A number of localization elements have since been found in the 3′UTRs of transported transcripts (*5*, *9*). Although the ribonucleotide sequences of localization elements described so far show little resemblance, it is possible that the folding of the RNA may form common secondary structures.

"Further understanding of the basic mechanisms underlying mRNA localization...will lay the foundations for developing new therapeutic approaches for many neural disorders."

MRC Laboratory for Molecular Cell Biology, University College London, London, UK. Email: a.riccio@ucl.ac.uk

RNA transport and translation in regenerating axons

In developing neurons, mRNA localization and translation mediate axon growth. Although adult neurons are less dependent on this mechanism to maintain nerve homeostasis, after injury many transcripts, including *mTOR*, are transported to axons and translated at the lesion site. Local translation of *mTOR* increases protein synthesis in a positive loop that supports nerve growth and regeneration.

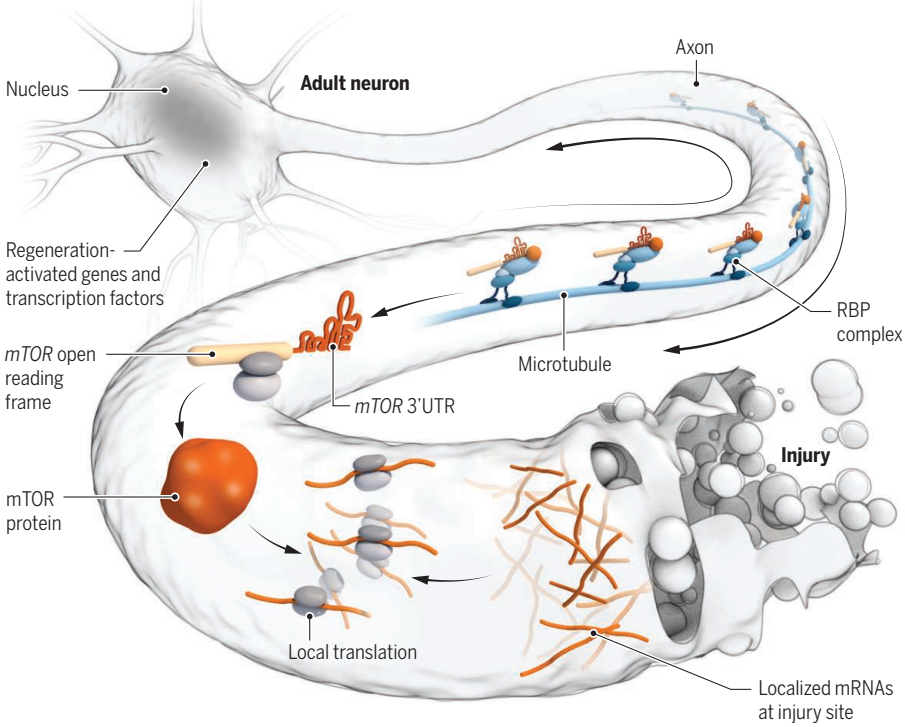

The main aim of asymmetric distribution of mRNA is to compartmentalize signaling. For example, the guidance cue netrin-1 induces localized synthesis of β-actin in growth cones, which mediates the steering of retinal axons toward the guidance cue (*10*). Interestingly, RNA localization and local protein synthesis is regulated with a high degree of signal specification. In developing sensory neurons, for example, distinct transcripts are targeted to axons in response to different neurotrophins (*11*). A potential mechanism entails that each extrinsic signal activates specific RNA-binding proteins (RBPs) that act as a hub to recruit and transport different sets of transcripts. This has been demonstrated for splicing factor glutamine-rich (SFPQ), an RBP that regulates the transport of functionally related transcripts in response to neurotrophins (*12*).

A prototypical example of the advantages brought about by signal compartmentalization in neurons is provided by the regenerative response that follows nerve injury. Compared with developing neurons, adult neurons have fewer ribosomes in axons, and lower levels of local protein synthesis are required for their maintenance. However, a sudden change of circumstances, such as traumatic injury, has a profound impact on gene expression and dramatically increases RNA localization to axons (*9*), ensuring that regenerating axons receive a constant supply of newly synthesized proteins. The initial response to axon damage requires the activation of the signaling protein extracellular signal–regulated kinase (ERK) and an increase of intracellular calcium at the site of the lesion. These events are necessary for membrane resealing, and although short-lived, they can also influence gene expression. After this acute response, Terenzio *et al.* found that a sustained retrograde propagation of the injury signal to the nucleus induces the targeting of newly synthesized transcripts, including those encoding mTOR to the lesion site of the axons. The combination of increased transport of mRNAs and high local translation of mTOR results in the synthesis of proteins necessary for nerve regeneration (see the figure).

A number of fundamental questions remain unanswered. It is still unknown how RNAs are sorted in the nucleus and "tagged" for transport to dendrites and axons. A potential mechanism may involve small noncoding RNAs and/or the UTRs of targeted transcripts that in combination with specific RBPs, such as SFPQ, could act as a scaffold to tag mRNA for transport. Indeed, the 3′UTR of the transcript interacts with the encoded cell surface protein CD47, driving localization to the plasma membrane (*13*). Genome-wide analyses of 3′UTR expression, such as poly(A)-seq and 3′end-seq, will help to obtain a comprehensive picture of the features shared among 3′UTRs of peripherally localized transcripts.

Noncoding RNAs, including microRNAs, are also present in both dendrites and axons. It is not known whether their role is confined to regulating mRNA stability and translation of localized transcripts or whether they represent the missing link between extrinsic signals applied at the periphery of the cell and nuclear functions. mRNAs encoding transcription factors are known to be transported and translated in both axons and dendrites (*6*, *14*, *15*). However, their biological importance is uncertain, mostly because it is difficult to understand how they could elicit a transcriptional response that is distinct from the one induced by the much larger fraction of the same transcription factors residing in the nucleus. It is possible that noncoding RNAs, and perhaps UTRs, form a tag that determines the binding of axon-derived transcription factors to specific promoters in a manner akin to many enhancer RNAs, which interact with transcription factors and RNA polymerase II on the promoters of regulated genes.

The mechanistic links between extrinsic signals and translational activation in developing and regenerating axons are still largely unknown. Although Terenzio *et al.* made the important discovery that local translation of mTOR regulates protein synthesis in response to injury in adult axons, whether this is a mechanism shared with other neurons and at different developmental stages remains unclear. It should also be noted that the incorrect processing and delivering of mRNA has been linked to the pathogenesis of many human neurological disorders, to the point that it has been proposed that most, if not all, neurodegenerative diseases fundamentally are disorders of RNA metabolism (*15*). Further understanding of the basic mechanisms underlying mRNA localization in dendrites and axons will lay the foundations for developing new therapeutic approaches for many neural disorders. ■

REFERENCES

1. M. Terenzio *et al.*, *Science* **359**, 1416 (2018).
2. R. A. Saxton *et al.*, *Cell* **169**, 361 (2017).
3. C. E. Holt *et al.*, *Neuron* **80**, 648 (2013).
4. F. A. Court *et al.*, *J. Neurosci.* **28**, 11024 (2008).
5. C. Andreassi *et al.*, *Nat. Neurosci.* **13**, 291 (2010).
6. I. J. Cajigas *et al.*, *Neuron* **74**, 453 (2012).
7. L. F. Gumy *et al.*, *RNA* **17**, 85 (2011).
8. H. L. Zhang *et al.*, *Neuron* **31**, 261 (2001).
9. I. Rishal *et al.*, *Nat. Rev. Neurosci.* **15**, 32 (2014).
10. K. M. Leung *et al.*, *Nat. Neurosci.* **9**, 1247 (2006).
11. D. E. Willis *et al.*, *J. Cell Biol.* **178**, 965 (2007).
12. K. E. Kosker *et al.*, *Nat. Neurosci.* **19**, 690 (2016).
13. B. D. Berkovits *et al.*, *Nature* **522**, 363 (2015).
14. K. Ben-Yaakov *et al.*, *EMBO J.* **31**, 1350 (2012).
15. L. C. J. Costa *et al.*, *Dev. Neurobiol.* **78**, 209 (2018).

10.1126/science.aat1498

GRAPHIC: C. BICKEL/*SCIENCE*

From rock-stable to reactive phosphorus

A low-temperature route converts phosphate into an anion useful in chemical synthesis

By **John D. Protasiewicz**

The main use of phosphate minerals is as fertilizer, but phosphorus is used in herbicides, flame retardants, drugs, battery electrolytes, and other materials. To date, the key feedstock for these materials is elemental phosphorus, particularly white phosphorus (P_4). Reduction of phosphate to P_4 is energy intensive, and it must be converted into other intermediates, such as PCl_3, through reaction with chlorine gas (all of which are highly reactive and toxic). On page 1383 of this issue, Geeson and Cummins (*1*) report a set of simple transformations that afford a less energy-intensive strategy for converting phosphate into the bis(trichlorosilyl)phosphide anion **1**. Anion **1** serves as a P_4 surrogate useful for the synthesis of a number of important organophosphorus compounds, including an organophosphorus-based drug.

Phosphorus is too reactive to be found in nature in its elemental state. In particular, white phosphorus is reactive with oxygen, and phosphorus is most commonly found in its highest formal oxidation state (+5), as in phosphate (PO_4^{3-}) salts or in organophosphorus compounds. Phosphate is concentrated in phosphate-containing rock and the mineral apatite (*2*). In the 17th century, Brand, in his pursuit of the philosopher's stone, isolated this element as an eerie glowing substance from human urine (*3*). The awareness that supplies of readily collected phosphate are limited has led to greater interest in its recovery and avoiding its environmental discharge (*4*).

The industrial reduction of phosphate requires high temperatures (1400° to 1600°C) and addition of other materials, such as silica and coke (a carbon source), to create strong new element-oxygen bonds that offset the energy costs associated with removing P–O bonds (*5*). Geeson and Cummins's approach begins with phosphoric acid, which is widely available from phosphate rock and used in fertilizer manufacture. Phosphoric acid can be readily transformed into trimetaphosphate in the form of a tetrabutylammonium salt. Remarkably, the reaction of trimetaphosphate with excess trichlorosilane ($HSiCl_3$) under mild heating (110°C) provides a previously unknown anion, **1**, in 65% yield. Anion **1** was unambiguously characterized by a series of spectroscopic techniques and single-crystal x-ray diffraction studies.

This transformation of phosphorus in phosphate that was "rock stable" and in its highest oxidation state has three remarkable features. It cleanly reduced phosphorus to a lower formal oxidation state that is better suited for chemical elaboration. It also created a phosphorus center with a formal negative charge that is better able to participate in nucleophilic reactions (i.e., make new phosphorus-element bonds). Further, phosphorus was functionalized with two trichlorosilyl units that serve as additional sites for possible differential reactivity. The use of the reagent $HSiCl_3$ (available in quantity because it is a key precursor to pure silicon for the electronics industry) is important, because the reaction that removes oxygen atoms from phosphorus is facilitated by formation of strong Si–O bonds.

Anion **1** thus represents a versatile synthon for a variety of interesting materials (see the figure). Consistent with the anionic phosphorus center and oxophilic silicon centers, addition of water protonates the phosphorus center and exchanges the silyl groups for hydrogen atoms to form the phosphorus analog of ammonia, phosphine (PH_3). Oxidative fluorination of **1** with xenon difluoride removes the silyl groups to afford the hexafluorophosphate anion $[PF_6]^-$, which is an anionic component critical to the function of most lithium-ion batteries. The nucleophilic character of the phosphorus atom in **1** allows direct alkylation (formation of P–C bonds). Addition of excess (4-chlorobutyl)benzene (an alkyl halide) to anion **1** produced the dialkylated phosphine (a secondary phosphine) of the form R_2PH (R = $CH_2CH_2CH_2CH_2Ph$).

Even more interesting was the discovery that anion **1** need not be isolated to create useful organophosphorus compounds from inorganic phosphate. Specifically, starting with the trimetaphosphate anion, addition of both (4-chlorobutyl)benzene and $HSiCl_3$ followed by heating led to the direct formation of the intermediate secondary phosphine $RP(SiCl_3)H$, which reacts with water to afford the primary phosphine RPH_2. Secondary and primary phosphines are important ligands, as well as precursors to ligands, for binding to transition metals and forming catalysts that carry out many important industrial processes. Geeson and Cummins also demonstrated successful transformation of RPH_2 to fosinopril, a drug used to treat hypertension and to ward off stroke and heart attacks (*6*), highlighting that their process can afford fine organophosphorus chemicals and avoid use of P_4 as a phosphorus source. ■

From rock to drugs

Geeson and Cummins harvested phosphorus from unreactive phosphate sources (such as phosphoric acid produced from apatite rock) by reduction with trichlorosilane. Anion **1** can be used to synthesize many compounds, including the drug fosinopril.

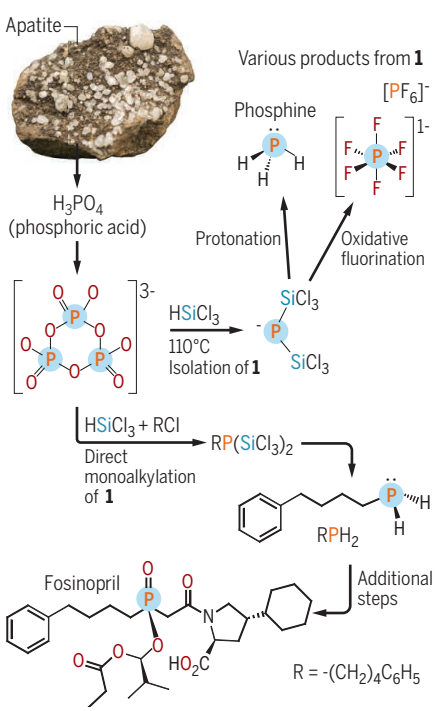

Department of Chemistry, Case Western Reserve University, Cleveland, OH 44106, USA. Email: protasiewicz@case.edu

REFERENCES

1. M. B. Geeson, C. C. Cummins, *Science* **359**, 1383 (2018).
2. https://en.wikipedia.org/wiki/Apatite
3. J. Emsley, *The Shocking History of Phosphorus: A Biography of the Devil's Element* (Macmillan, 2001).
4. http://blogs.discovermagazine.com/crux/2017/03/15/phosphorus-supply-low/
5. J. R. Brummer, J. A. Keely, T. F. Munday, *Phosphorus. Kirk-Othmer Encyclopedia of Chemical Technology*; http://onlinelibrary.wiley.com/book/10.1002/0471238961.
6. www.webmd.com/drugs/2/drug-6036/fosinopril-oral/details

10.1126/science.aat1206

POLYMER CHEMISTRY

A radical advance for conducting polymers

Organic radical polymers can have much higher electrical conductivities than anticipated

By **Jodie Lutkenhaus**

Organic radical polymers have unusual electronic properties, with potential applications in batteries, electronics, and memory storage (*1*–*3*). The first nitroxide-based organic radical polymer, reported by Okawara and co-workers in 1972 (*4*), has since been used as an electroactive material in battery electrodes (*5*). With recent explorations into organic radical polymers for thermoelectrics and electronics (*2*, *6*), the electrical conductivity of these materials has become a center of interest. On page 1391 of this issue, Joo *et al.* (*7*) add an important facet to this discussion by demonstrating the highest reported conductivity for an organic radical polymer.

Organic radical polymers consist of a polymeric hydrocarbon backbone and pendant radical functional groups (see the figure). This results in an electronic structure that is neither like an aliphatic polymer nor like a conjugated polymer. Conjugated polymers accommodate charges through electronic delocalization along the backbone. By contrast, organic radical polymers bear charge at highly localized radical sites. This subtle difference results in extremely fast charging kinetics and battery-like behavior for radical polymers, whereas conjugated polymers have more sluggish kinetics and behave more like capacitors.

Electrons are thought to move in organic radical polymers by hopping from radical to radical and through segmental motion of the polymer chain (*8*, *9*). Therefore, electron transport is a function of many factors, including the distance between radicals, radical concentration, and diffusion of the radical site or polymer backbone. In an earlier experimental study, Rostro *et al.* found that a model organic radical polymer, poly(2,2,6,6-tetramethylpiperidinyloxy methacrylate) (PTMA), has a conductivity of ~1×10^{-4} S m^{-1} and that this conductivity could be enhanced by adding the radical small molecule 2,2,6,6-tetramethylpiperidine 1-oxyl (TEMPO) (*10*). On the other hand, Zhang *et al.* carefully studied the conductivity of the same polymer and found it to be completely insulating, regardless of how it was synthesized (*6*). These studies used different measurement techniques and different length scales of observation.

Joo *et al.* now report that conductivity increases dramatically up to 20 S m^{-1} for an ether-oxygen–based organic radical polymer when observed over a distance of 600 nm or less. This value is on par with that of some conjugated polymers. The authors conclude that the observations are likely a result of local organization of percolating radical sites at or below that length scale. This local organization is similar to the manner in which charged polymers self-organize (*11*). It increases the local concentration of radical sites and thereby raises the probability of radical-to-radical electron hopping. This benefit is lost at larger length scales, and conductivity declines dramatically. The length scale of Zhang *et al.*'s measurement was on the order of micrometers (*6*).

Another important factor that enhances conductivity is the flexibility of the polymer backbone and linker group. Sato *et al.* have shown that electron self-exchange among radical sites correlates to the diffusion of the polymer (*9*). A more flexible backbone and linker group should thus enhance the diffusion of the polymer and the pendant radical site. This will enhance the frequency at which radical sites will come sufficiently close to each other to transfer an electron. Joo *et al.* chose an ether-oxygen–containing backbone and linker group, which is exceptionally flexible; ether-oxygen groups are commonly used to facilitate ion diffusion in solid polymer electrolytes. The polymer has a glass transition temperature below room temperature, which facilitated thermal annealing to promote the local organization of radical sites. Most other organic radical polymers studied for their conductivity have glass transition temperatures above room temperature, making them difficult to thermally anneal without decomposition, and have low polymer mobility.

Comparison of organic radical and conjugated polymers shows that the governing factors to achieving high conductivity are very different. Diffusion and proximity of radical sites are important to electron transport in organic radical polymers, which tend to be amorphous in nature. By contrast, electron transport in conjugated polymers benefits from controlled crystallization and extended conjugation lengths along the backbone. Yet in both classes of polymer, conductivity is improved via local structural organization upon annealing.

How an organic radical polymer conducts

The organic radical polymer PTEO [poly(4-glycidyloxy-2,2,6,6-tetramethylpiperidine-1-oxyl)] has a flexible structure that helps to increase the polymer's conductivity at length scales of 600 nm or less.

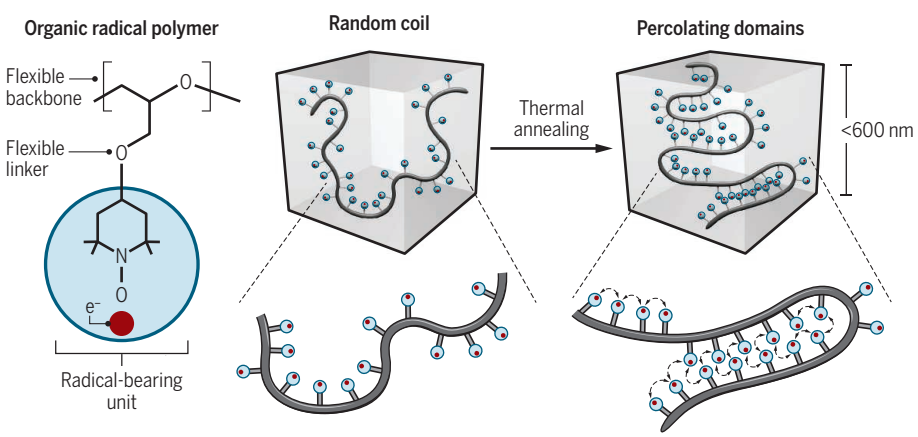

Pendant radical groups on the polymer backbone bear highly localized electrons.

Unannealed, these radical groups are too far apart to transport electrons over large distances.

Annealed, the radical groups organize into percolating domains that facilitate electron transport.

GRAPHIC: A. KITTERMAN/*SCIENCE*

Artie McFerrin Department of Chemical Engineering and Department of Materials Science and Engineering, Texas A&M University, College Station, TX 77843, USA. Email: jodie.lutkenhaus@tamu.edu

Organic radical and conjugated polymers have been proposed as transparent conductors, but conjugated radical polymers have a characteristic color because of their intrinsic band gap. Organic radical polymers show little absorption in the visible range, which is seen as an added advantage.

Joo *et al.*'s work raises many important questions and indicates future areas of study. The authors claim that enhanced conductivity arises from percolating or self-organized regions, but there is no definitive structural evidence to confirm this concept. Experimental neutron scattering studies and simulations are needed, among other approaches, to explore this further. Besides structural evidence, there is a need for understanding the dynamics of the system, particularly the diffusion of the polymer backbone and the radical site. Once structure and dynamics are understood, these may be correlated to electronic conductivity and may even be manipulated to enhance the conductivity even further.

Although the conductivity is exceptionally high for this polymer type, wider application will require this conductivity to be sustained over a larger length scale (>600 nm). This might be accomplished through annealing or through synthetic design to increase the length scale of the percolating regions. Another pertinent question is how partial doping affects conductivity. Doping converts the neutral nitroxide radical to oxoammonium cations, which may adjust the mobility of the polymer and the concentration of radical sites. Last, organic radical polymers are important components in organic radical batteries and redox flow batteries, in which the polymer–electrolyte interface becomes important. Understanding solvent–polymer interactions and their relationships to conductivity could benefit these applications. Given that Joo *et al.*'s report presents such a large leap for electrical conductivity in organic radical polymers, many more exciting findings for this interesting class of polymer are likely to follow. ■

REFERENCES

1. S. Muench *et al.*, *Chem. Rev.* **116**, 9438 (2016).
2. E. P. Tomlinson, M. E. Hay, B. W. Boudouris, *Macromolecules* **47**, 6145 (2014).
3. K. Nakahara, K. Oyaizu, H. Nishide, *Chem. Lett.* **40**, 222 (2011).
4. T. Kurosaki, K. W. Lee, M. Okawara, *J. Polym. Sci. A* **10**, 3295 (1972).
5. H. Nishide *et al.*, *Electrochim. Acta* **50**, 827 (2004).
6. Y. Zhang *et al.*, *J. Mat. Chem. C* **6**, 111 (2018).
7. Y. Joo *et al.*, *Science* **359**, 1391 (2018).
8. T. W. Kemper, R. E. Larsen, T. Gennett, *J. Phys. Chem. C* **118**, 17213 (2014).
9. K. Sato *et al.*, *J. Am. Chem. Soc.* **140**, 1049 (2018).
10. L. Rostro, A. G. Baradwaj, B. W. Boudouris, *ACS Appl. Mat. Interf.* **5**, 9896 (2013).
11. L. M. Hall *et al.*, *J. Am. Chem. Soc.* **134**, 574 (2012).

10.1126/science.aat1298

METABOLISM

Targeting angiogenic metabolism in disease

Targeting endothelial cell metabolism offers new therapeutic opportunities for various conditions

By **Xuri Li**[1] *and* **Peter Carmeliet**[1,2,3]

Blood vessels, which are lined by endothelial cells (ECs), supply oxygen and nutrients to every cell in the body. When tissues (or tumors) grow, they stimulate ECs to form new blood vessels (angiogenesis), so that they become better nourished. Hence, inhibiting angiogenesis to starve tumors has become a clinically approved therapy. For more than 40 years, antiangiogenic medicine has focused on targeting angiogenic signaling proteins, such as vascular endothelial growth factor (VEGF). However, the success of VEGF-targeted therapy for cancer and neovascular ocular diseases is limited by insufficient efficacy and/or drug resistance, necessitating a fundamentally different approach. Targeting EC metabolism is gaining increasing attention as a possible alternative for inhibiting angiogenesis.

Blood vessels are lined by quiescent (nondividing) phalanx ECs, so-called because of their cobblestone morphology and role in barrier formation. For vessels to sprout during angiogenesis, phalanx ECs must undergo phenotypic changes. Angiogenic signals such as VEGF induce the formation of a migratory tip EC and proliferative stalk ECs that elongate the sprout (*1*) (see the figure). A tip cell can be overtaken by a more competitive stalk cell, so that the fittest cell always leads the way.

Cellular metabolism, the process that converts nutrients to energy and biomass, is essential for ECs to survive, migrate, and grow, hence its importance in forming new blood vessels. It was postulated that ECs can only execute the orders of growth factors if they accordingly adapt their metabolism, suggesting that EC metabolism could regulate angiogenesis (*2*). Several metabolic pathways in ECs have been characterized, yielding new therapeutic targets. A pioneering observation in the EC metabolism field was that ECs are addicted to anaerobic glycolysis (that is, glucose metabolism not requiring oxygen), even though they are exposed to high blood oxygen concentrations, which would be expected to favor oxidative glucose metabolism (requiring oxygen) (*3*). Indeed, ECs rely on glycolysis to generate >85% of their energy source, adenosine triphosphate (ATP), much more than most other quiescent cells. Tip cells use glycolysis to provide energy for migration, whereas stalk cells use glycolysis to generate energy and divert glycolytic intermediates to other pathways for biomass synthesis in order to proliferate. There are several advantages of such glycolytic reliance: If ECs rely solely on oxidative metabolism, they would not be able to revascularize ischemic tissues, which are deprived of oxygen; distantly removed from blood vessels, oxygen concentrations drop faster than those of glucose, enabling ECs to rely on anaerobic glycolysis for continued growth in hypoxia; and even though the ATP yield from glucose is higher for oxidative metabolism, glycolysis generates ATP more rapidly, thereby allowing ECs to quickly revascularize ischemic tissues.

The key role of glycolysis for ECs explains why mice lacking the glycolytic activator 6-phosphofructo-2-kinase/fructose-2,6-biphosphatase 3 (PFKFB3) in ECs suffer impaired (retinal) vessel sprouting because of decreased EC proliferation and migration (*3*). Also, fibroblast growth factor 2 (FGF2) stimulates vessel growth through up-regulation of hexokinase 2 (HK2), another glycolytic enzyme (*4*).

EC metabolism differs from that of other cell types. Most other cell types use glucose and glutamine for nucleotide synthesis, whereas ECs additionally use fatty acid oxidation (FAO), in conjunction with substrates replenishing the Krebs cycle (*5*). As a result, in mice lacking the FAO-regulator carnitine palmitoyltransferase 1A (CPT1A) in ECs, blood vessel expansion is impaired because of decreased EC proliferation, suggesting CPT1 blockade for antiangiogenic targeting.

Amino acids, such as glutamine and asparagine, are another important source of nutrients for ECs. Glutamine is used for biomass

[1]*State Key Laboratory of Ophthalmology, Zhongshan Ophthalmic Center, Sun Yat-Sen University, 54 South Xianlie Road, Guangzhou 510060, People's Republic of China.* [2]*Department of Oncology, Laboratory of Angiogenesis and Vascular Metabolism, Katholieke Universiteit (KU) Leuven, Leuven, B-3000, Belgium.* [3]*Laboratory of Angiogenesis and Vascular Metabolism, Center for Cancer Biology, Vlaams Instituut voor Biotechnologie (VIB), B-3000 Leuven, Belgium. Email: peter.carmeliet@kuleuven.vib.be; lixr6@mail.sysu.edu.cn*

synthesis, redox homeostasis (to prevent oxidative stress), and other processes. Glutamine deprivation or inhibition of glutaminase 1 (GLS1), the enzyme that converts glutamine to glutamate, impairs replenishment of carbons into the Krebs cycle, macromolecule production, and redox homeostasis in ECs (*6, 7*). Inhibition of glutamine metabolism impairs tip-cell migration and stalk-cell proliferation, causing vessel sprouting defects in vivo (*6, 7*). Notably, silencing of GLS1 in ECs reduces their competitiveness to obtain the tip position in vascular sprouts in vitro (*6*). Blocking GLS1 might thus therapeutically inhibit tumor and ocular angiogenesis.

Glutamine metabolism is linked to asparagine metabolism. It provides nitrogen for asparagine synthesis to sustain cellular homeostasis. Hence, silencing asparagine synthetase (ASNS), which converts glutamine-derived nitrogen and aspartate to asparagine, impairs EC sprouting (*6*), thus identifying ASNS blockade as an antiangiogenic approach. In contrast to cancer cells, the proliferation defect of glutamine-starved ECs cannot be rescued by antioxidant supplements or replenishment of the Krebs cycle alone (*6*), again illustrating the distinct nature of EC metabolism and also the attractive potential to target EC metabolism for antiangiogenic therapy of tumors and eye diseases.

An outstanding issue is which signaling molecules regulate EC metabolism. Insights into such molecular signals may offer therapeutic opportunities. In ECs, tip cell–inducing VEGF and FGF signaling stimulates glycolysis by up-regulating the expression of PFKFB3 and HK2, respectively, whereas stalk-cell Notch signaling lowers glycolysis by down-regulating PFKFB3 expression (*3*). The transcription factor forkhead box O1 (FOXO1) acts as a gatekeeper of phalanx EC quiescence, by reducing glycolysis and mitochondrial respiration (*8*). Another proquiescence signal, Kruppel-like factor 2 (KLF2), induces similar effects. Possibly, inhibitors of FOXO1 or KLF2 might thus be useful to revascularize ischemic or engineered tissues.

How does EC metabolism mechanistically affect EC functions? Glycolytic enzymes in cell protrusions interact with the actin cytoskeleton to generate high amounts of ATP locally for cytoskeleton remodeling during EC migration (*3*). Moreover, by providing energy for endocytosis (cellular ingestion) of cell-cell junction proteins, glycolysis makes tumor vessels leaky (*9*). Also, through enhancing nuclear factor-κB (NF-κB) signaling, glycolysis makes tumor ECs adhesive for cancer cells. These phenotypic changes facilitate entry of cancer cells into the blood and metastasis to distant tissues (*9*). Understanding how metabolism controls EC biology will increase its value for drug targeting of vascular defects.

Abnormal tumor vessels facilitate cancer cell metastasis and impair chemotherapy and immunotherapy. Hence, reducing these abnormalities (called tumor vessel normalization) offers therapeutic opportunities to reduce metastasis and improve other therapies (*10*). Compared to healthy ECs, tumor ECs have higher glycolysis levels (*9*), offering the opportunity to selectively target them without causing systemic toxicity in other cell types, which do not rely as prominently on glycolysis and can compensate by switching to other metabolic pathways. Blockade of PFKFB3, decreasing EC glycolysis rate by only 20 to 35%, sufficed to inhibit pathological angiogenesis in mouse models of ocular neovascularization and inflammatory bowel disease and to induce tumor vessel normalization, thereby suppressing metastasis and improving chemotherapy responses (*9, 11, 12*). Development of small-molecule PFKFB3 blockers is under way.

To avoid systemic effects, the goal should be to cool down the overheated metabolic (glycolytic) engine of tumor ECs, rather than to shut it down completely, as this will cause toxicity. Indeed, a small-molecule PFKFB3 blocker induces beneficial tumor vessel normalization at a low dose, but causes tumor vessel disintegration at a high dose, which allows cancer cells to escape and disperse throughout the body more easily, arguing against maximally tolerable antiglycolytic therapy (*9, 13*). Pharmacological blockade of CPT1 or GLS1 also reduces ocular neovascularization in mice (*5, 6*), illustrating the potential of targeting these metabolic enzymes for antiangiogenic therapy. Profiling of tumor and ocular EC metabolism at the single-cell level promises to yield additional metabolic targets. Besides tumor and ocular angiogenesis, other hypervascular diseases—for example, vascular malformations and pulmonary hypertension—might also benefit from anti–EC metabolic therapies.

Notably, EC metabolism can also be manipulated to promote blood vessel growth. This can be beneficial to reoxygenate ischemic tissues. Indeed, acetate supplementation stimulates blood vessel growth in mice treated with a CPT1 blocker without systemic effects (*14*). Transplantation of tissue organoids (engineered tissues in a dish) may offer an alternative to donor organ usage. Stimulating vascularization of tissue organoids by modulating EC metabolism or delivering metabolites would benefit this regenerative medicine approach. It remains to be assessed if EC metabolism can be targeted to regenerate dysfunctional endothelium, which causes cardiovascular complications in diabetes, atherosclerosis, aging, and others. Emerging evidence implies perturbations of EC metabolism underlying EC dysfunction in such patients (*15*). Correcting these perturbations, for instance, by delivering metabolites that drive EC metabolism, could offer new therapeutic opportunities. Finally, when lymphatics (EC-lined vessels that drain fluid) are dysfunctional, lymphedema develops, for which no cure exists. The potential of FAO and acetate to modify EC metabolism so as to stimulate lymphatic EC differentiation (through epigenetic regulation) and growth to improve fluid drainage may offer new therapeutic opportunities for this disease (*14*). EC metabolism studies are in their infancy, yet their future promise is exciting. ■

Metabolic pathways in angiogenesis

During angiogenesis, endothelial cells undergo metabolic changes that facilitate the formation of a sprout by stalk cells, which is directed by the tip cell. Key regulators of endothelial cell metabolism, PFKFB3, CPT1A, and GLS1, might be new therapeutic targets for various conditions.

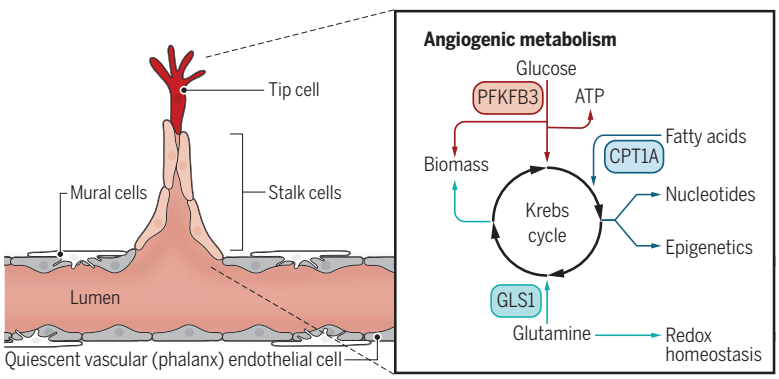

REFERENCES

1. P. Carmeliet *et al.*, *Nature* **473**, 298 (2011).
2. P. Fraisl *et al.*, *Dev. Cell* **16**, 167 (2009).
3. K. De Bock *et al.*, *Cell* **154**, 651 (2013).
4. P. Yu *et al.*, *Nature* **545**, 224 (2017).
5. S. Schoors *et al.*, *Nature* **520**, 192 (2015).
6. H. Huang *et al.*, *EMBO J.* **36**, 2334 (2017).
7. B. Kim *et al.*, *EMBO J.* **36**, 2321 (2017).
8. K. Wilhelm *et al.*, *Nature* **529**, 216 (2016).
9. A. R. Cantelmo *et al.*, *Cancer Cell* **30**, 968 (2016).
10. S. Goel *et al.*, *Physiol. Rev.* **91**, 1071 (2011).
11. S. Schoors *et al.*, *Cell Metab.* **19**, 37 (2014).
12. S. Schoors *et al.*, *Cell Cycle* **13**, 16 (2014).
13. L. C. Conradi *et al.*, *Angiogenesis* **20**, 599 (2017).
14. B. W. Wong *et al.*, *Nature* **542**, 49 (2016).
15. G. Eelen *et al.*, *Circ. Res.* **116**, 1231 (2015).

10.1126/science.aar5557

GRAPHIC: N. DESAI/*SCIENCE*

POLICY FORUM

Efforts to address environmental pollution, such as in this waterway in Wuzhen, China, can bring many cobenefits for human health.

PHOTO: NATIONAL GEOGRAPHIC CREATIVE/ALAMY STOCK PHOTO

HEALTH AND ECONOMIC DEVELOPMENT

Expanded health systems for sustainable development

Advance transformative research for the 2030 agenda

By **Christopher Dye**

Since the United Nations (UN) launched the 2030 Agenda for Sustainable Development in 2015, the global health community has grown accustomed to the new catalog of 17 Sustainable Development Goals (SDGs, 2016–2030), and even to the criticism that has been leveled at numerous imprecise targets. SDG 3 makes universal health coverage (UHC, Target 3.8) central to achieving the principal health goal of healthy lives and well-being for all at all ages, and sets targets for reducing the burden of noncommunicable diseases and injuries, a conspicuous omission from the Millennium Development Goals (MDGs, 2000–2015) which focused on maternal and child health and major communicable diseases. But the greater ambition of the 2030 Agenda is to anchor health in development, recognizing that good health depends on and contributes to other development goals, underpinning social justice, economic prosperity, and environmental protection. These aspirations have been frequently voiced but scarcely pursued, and the SDGs are often treated simply as a checklist of new goals and targets. Yet their potential is far greater—collectively they should be a force for discovery of new ways to achieve better health and well-being. To this end, the legacy of the MDGs, and the structure of the SDGs, lead to a testable proposition for research: Advance health and development by expanding the scope and enhancing the effectiveness of the systems and services that prevent and treat illness. At stake is the question of how to accelerate gains in health through broad-based sustainable development, building on successes and compensating for weaknesses of targeted, time-limited health programs.

That question is not new, and neither is the view that systems analysis can help answer it. The idea of strengthening health systems has been pursued for years in some segments of the global research and development community, but has usually been tackled within separate compartments of the health sector. The SDGs can promote a more expansive and interrogative approach to creating systems for better health—pushing politicians to seek ways of collaborating across multiple sectors of government; urging businesses and citizens to reconsider their roles, responsibilities, and reasons for contributing to public health; stimluating funders to support research across traditional disciplines; inspiring scientists to step beyond the security of familiar methods and procedures; and encouraging ethicists to consider which arguments for equity, rights, and fairness do and do not work in different settings.

World Health Organization, Geneva, Switzerland.
Email: chrisdye56@gmail.com

LEGACY OF THE MDGs

The MDGs were conceived as a partnership between richer and poorer countries to end extreme poverty. Interventions targeted low-income countries with high burdens of disease. Despite early aspirations to achieving broad-based development, these interventions were generally top-down (vertical) rather than systemic (horizontal); focused more on technologies and less on the means of using them; were driven by foreign aid rather than domestic finance; measured progress in terms of national averages concealing inequalities among individuals; and set short-term deadlines rather than promoting long-term development. Even so, substantial health gains were made in the MDG era: The number of people living in extreme poverty; the malaria, tuberculosis (TB), and under-five mortality rates; and the maternal mortality ratio all fell by about one-half or more between 1990 and 2015.

Analyses of progress toward the MDGs [such as (*1*, *2*)] have exposed strengths and weaknesses of such targeted health programs, making at least two often-forgotten points. First, although medical technologies such as vaccines and drugs can be linked to better health, these interventions rely on functioning health services, run by skilled health workers with health information systems, supply chains, and financing and governance mechanisms. In some settings, vertical programs targeting selected diseases may have damaged the health systems that they needed to succeed, by attracting resources disproportionately, or simply through neglect (*3*). Reintegrating disease-control programs into general health services now poses operational challenges (*4*).

Second, these studies reaffirm the indirect health risks (and potential benefits) of social, economic, and environmental factors that lie outside the control of the health sector, such as female education and fertility, family income, and access to safe water and sanitation. The idea of modifying these factors by working across disciplines and sectors has a long history, but multidisciplinary research and intersectoral action are still exceptional rather than routine. For example, cross-disciplinary initiatives from the human ("Health in All Policies," HiAP) and veterinary health ("One Health") communities have common aims but remain largely separate enterprises. One challenge of working across sectors is to balance the control of selected diseases of high importance (such as HIV/AIDS, TB, malaria) with

the management of systemic risks to health (e.g., provision of safe water, sanitation, and housing, or mechanisms for finance, governance, monitoring, and planning). Both are important, but the MDGs emphasized the former, whereas the SDGs stress the latter.

The choice between the two should encourage, in the SDG era, a more open-minded approach to investigating causes and risks of ill health, unconstrained by specific methods or disciplines. The ideal response to any risk would consider interventions across the whole chain of events from primary (upstream) causes to ultimate (downstream) effects on health. But assessment of risk is typically partial, rarely comprehensive. Thus, if a study focuses, for example, on selected social determinants of TB (e.g., income, employment, housing), then the proposed solutions will likely address only these determinants, missing other possible behavioral (tobacco smoking), environmental (air pollution), medical (HIV coinfection), metabolic (diabetes), and occupational (mining) risks and, critically, the interactions between them. Furthermore, the failure to implement proven interventions (e.g., early diagnosis and treatment for TB) is rarely considered to be a "risk factor," but could be the largest modifiable cause of illness or death in any given setting (*5*). There is not yet a standard, comprehensive approach to evaluating preventable risks to health.

"...failure to implement proven interventions...is rarely considered to be a 'risk factor'..."

The MDGs became the world's principal framework for international cooperation in development. Now that the SDGs have inherited that role, advertising the interlinkages between health and all other goals, the debate about how to improve health is taking place not just among health ministers but also among heads of state, private businesses, nongovernmental organizations, and civil society. That national and international debate should be informed by a research agenda that is equally broad and actively promoted among all players.

SDGs AS A HEALTH SYSTEM

A health system, broadly conceived, provides essential medical and public health services (centered on SDG 3) but also links health with agriculture, education, employment, energy, environment, finance, trade, transport, and urban planning (embraced by the other 16 Goals), potentially with mutual benefits. Whether an intervention affects health directly or indirectly, the properties of an effective system are the same. A skilled workforce, medical technologies, infrastructure, and finance and governance mechanisms are all needed to deliver services that should be affordable, efficient, equitable, ethical, measurable, responsive, resilient, sustainable, and testable. The importance of understanding how to instill these properties was neglected in the MDG era, even though they are a precondition to achieving high population coverage of technologies including diagnostics, drugs, vaccines, and insecticides. Some examples of the opportunities and challenges in strengthening health systems are given below.

Affordable

Providing full coverage of health services while avoiding financial hardship for patients is a major test for UHC (*6*). The first international conference on financing in the SDG era, held in Addis Ababa in 2015, concluded that each country should take primary responsibility for its own economic and social development, including measures to increase domestic public finance for health, principally through progressive taxation that favors the poorest (a task for HiAP), and decrease reliance on foreign aid (*7*). Given the scale of the task—for example, to avoid out-of-pocket payments for health services that drive more than 100 million people into poverty every year—the costs are expected to be substantial. By one estimate, the governments of 67 low- and middle-income countries would need to nearly triple current spending on health between 2014 and 2030 (*8*).

The immediate financial challenge to poorer countries is enormous but, subject to evaluation, could bring benefits in the long run. One is to reduce dependency on unpredictable and earmarked foreign aid, thereby stimulating self-sufficiency. Another is the incentive to improve efficiency, given limited resources, by streamlining financial flows, cutting wasteful spending, pooling health revenues to maximize options for redistribution, and matching funds to priority health services and populations. In addition, tackling the causes of illness upstream could deliver a double benefit: Costs can in principle be shared across sectors to achieve compatible objectives—for example, through joint policies on energy use, climate change, air quality, and health, while saving on the costs of treating illnesses that have been avoided. In this domain, the question of how best to translate theory into practice is itself a topic for research.

The age-old adage that prevention is better than cure is not yet backed by a satisfactory case for investment. One alluring reason to revisit the options for prevention is that health risks from avoidable exposures explain a large fraction of deaths worldwide (environment >28%, behavioral >67%) (*9*) and yet, according to national health accounts, preventive and public health services command only 4% of around US$8 trillion spent on global health annually (*10*). The question of how much to spend on prevention remains unresolved, in part because investments that bring health benefits, but where health is not the primary purpose (in other sectors such as agriculture, education, and transport), have not been systematically quantified and so remain invisible.

Studies of disease burden have ranked causes of illness and death both in terms of health outcomes (ischemic heart disease, cerebrovascular disease, lower respiratory infections) and preventable risks (high blood pressure, tobacco smoking, air pollution). Which list should be used to set priorities for intervention? What economic methods are preferred when comparing the returns on direct (health sector) and indirect (other sectors) investments in health, among other desirable outcomes of development?

Equitable

Inequity is not merely a numerical impediment to achieving high levels of service coverage, "leaving no one behind," but also denies individuals the right to health by compromising their freedoms and entitlements, which are goals in their own right. In the 2030 Agenda, goals for health and equity stand on common ground, and there is mutual support for approaches that foster better health among the disadvantaged (SDG 3); gender equality (SDG 5); equality within countries in general (SDG 10); and transparency, accountability, and nondiscriminatory laws (SDG 16). Deeper investigations of how to exploit these linkages could accelerate recent positive trends: For example, despite rising income inequality within countries, there is growing evidence that inequalities in access to health services are falling, and they appear to be falling more (immunization) or less (antenatal care) quickly depending on the service provided (*11*). This points to the research needed to identify the financial and economic determinants of health service provision, for poorer or richer members of each population.

Although some of the barriers to health care, and therefore ways to overcome them, are unique to specific settings, there

Child growth monitoring, such as at this clinic in Kilifi, Kenya, is integral to strategies to promote health, whether within or beyond the health sector.

PHOTO: JOSEPH OKANGA/REUTERS

are some generalities. One is that equity and prevention often go hand in hand: For example, policies for universal education and the reduction of outdoor air pollution have widespread benefits for health (*12*).

Measurable

The list of 230 agreed indicators that track progress toward the SDGs emphasizes the outcomes for development (what is to be achieved), rather than the "means of implementation" (how it will be achieved). These include financing mechanisms; the development and application of technologies; capacity building; and global and national partnerships, policies, and institutions. WHO analysis of a subset of 42 health-related indicators across 11 SDGs shows that 26 measure health outcomes and 12 report on the coverage of health services, but only four deal with factors and functions that contribute to better outcomes (employment of health workers, foreign funding for research, domestic funding for essential health services, and emergency preparedness) (*13*). Moreover, the underlying causes of ill health, to which interventions must respond, are no more than implicit.

Whether the agreed indicators are precisely or appropriately defined, and whether they can be serviced by data, have been much discussed. But the SDG framework presents a larger challenge to measurement and evaluation: Where there is no information on the underlying causes of illness and death, or on the components of the response, it will be harder to explain and modify health trends. Although the number of SDG indicators is already daunting, still more data will be needed, at least to resolve selected questions. The emphasis on measurement was a success of the MDG era; the SDGs have that data-analytical heritage to build on.

Sustainable

Thirty years ago, the World Commission on Environment and Development defined development as sustainable when it "meets the needs of the present without compromising the ability of future generations to meet their own needs" (*14*). In general, the case for long-term investment must counter the disinclination to pay now for benefits gained in future, which are perceived to have lower value because of discounted economic returns on investment, or short political time scales. One approach, crucial to mitigating the dangers of climate change, is to blend strategies that have both short- and long-term benefits, such as cutting atmospheric pollutants that are produced jointly with greenhouse gases (*15*).

Testable

The case for developing and testing new technologies has been abundantly made, but given the need to forge new links within and across disciplines and sectors, health systems research, in the broadest sense, is a potential source of new means of prevention and treatment. Whereas the efficacy of drugs, vaccines, and diagnostics determined by clinical trials is usually applicable in a wide range of settings, the "means of implementation" commonly depend on local circumstances. Finding the best way to implement technologies presents a wide variety of research questions demanding imaginative study designs: to test new legal and financial instruments, to explore ways of expanding the health workforce beyond the medical profession, to create common platforms for health delivery, among many others. Now is the time to present compelling arguments for carrying out such studies, as research funding agencies become more receptive to supporting multidisciplinary and operational research.

BETTER SYSTEMS, BETTER HEALTH?

Critics who have argued that the 2030 Agenda embraces everything in general and nothing in particular are at risk of missing a huge opportunity. The SDGs are not merely an inventory of new goals and targets, drawn up to satisfy every constituency; together, they are a stimulus to find new ways of advancing health and well-being. The idea of improving health systems to achieve UHC is at the forefront of SDG 3, but the logic of creating better systems for health applies more widely, potentially, although not necessarily, with mutual benefits between the health goal and all other goals. The notion that the SDGs are "integrated and indivisible" has been frequently articulated but the means of capturing the benefits have not yet been fully exploited, across the spectrum of activities from research and development to policy and practice. The few examples given here focus on questions about the opportunities for primary prevention, for achieving health equity, for sharing financial investment across sectors to reach common goals, and for devising long-term solutions. Where there are answers, action can be taken now. But the 2030 Agenda is also an expanded agenda for systems research. The working hypothesis is that better systems can indeed deliver substantially better health. ■

REFERENCES AND NOTES

1. S. Kuruvilla *et al.*, *Bull. World Health Org.* **92**, 533 (2014).
2. J. Ruducha *et al.*, *Lancet Global Health* **5**, e1142 (2017).
3. T. Hafner, J. Shiffman, *Health Policy and Plan.* **28**, 41 (2013).
4. V. Haldane *et al.*, *AIDS Care* **30**, 103 (2018).
5. C. Dye, M. Raviglione, *Nature* **502**, S13 (2013).
6. A. Sen, *Harvard Public Health Rev.* **4**, 1 (2015).
7. World Health Organization, *New Perspectives on Global Health Spending for Universal Health Coverage* (World Health Organization, Geneva, 2017).
8. K. Stenberg *et al.*, *Lancet Global Health* **5**, e875 (2017).
9. GBD 2016 Risk Factors Collaborators, *Lancet* **390**, 1345 (2017).
10. Organisation for Economic Cooperation and Development, *Health Expenditure and Financing* (Organisation for Economic Cooperation and Development, Paris, 2016).
11. World Health Organization, *State of Inequality: Childhood Immunization* (World Health Organization, Geneva, 2016).
12. M. Tobias, *Lancet* **389**, 1172 (2017).
13. World Health Organization, *World Health Statistics* (World Health Organization, Geneva, 2017).
14. World Commission on Environment and Development, *Our Common Future* (United Nations World Commission on Environment and Development, Oxford, 1987).
15. D. Shindell *et al.*, *Science* **356**, 493 (2017).

ACKNOWLEDGMENTS

I thank B. Aylward, J. Kutzin, T. S. Koller, S. Kuruvilla, A. Monnot, P. Rosenberg, A. Soucat, K. Stenberg, N. Valentine, and B. Williams for helpful comments and sources. The author is solely responsible for the views expressed in this paper, which do not necessarily represent the decisions, policy, or views of the World Health Organization.

10.1126/science.aaq1081

The Jökulsárlón lake emerged when the Breiðamerkurjökull glacier started to recede from the edge of the Atlantic Ocean.

POLAR STUDIES

Before we called it "climate change"

A researcher collects accounts of scientists' first inklings that the Arctic was in trouble

By **Sarah Boon**

We often think of the Arctic as a cold landscape of sea ice, permafrost, glaciers, and snow. But it's also a canary in a coal mine: It's warming faster than the rest of Earth because of positive feedback cycles built into its interlinked climate-ice-ocean systems. This rapid change has global implications, some of which we are already seeing, including melting permafrost and declining sea ice. That the Arctic is changing in response to climate change is now common knowledge, but it wasn't always so.

Brave New Arctic, by Arctic scientist Mark Serreze, delves into the recent history of Arctic research, following a trail of scientific breadcrumbs from the late 1970s to the present day to show how our understanding of the region's response to climate and climate change has evolved over time.

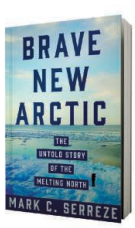

Brave New Arctic
The Untold Story of the Melting North
Mark C. Serreze
Princeton University Press, 2018. 269 pp.

Early suggestions that something unusual might be happening in the Arctic were dismissed due to a lack of data, resulting in the dominance of theories that attributed signs of warming to regular variability in large-scale atmospheric circulation patterns such as the Arctic Oscillation (AO) and the North Atlantic Oscillation (NAO). In recent years, however, data sets were finally long enough (and shocking enough) for researchers to dismiss the AO/NAO paradigm and declare global warming a key culprit.

But Serreze doesn't just describe what we now know about the Arctic; he talks about how we know it. From modeling studies that project future climates to field studies that measure permafrost temperature, he shows how research changes as technology advances (for example, when remote-sensing tools became available to measure the mass balance of Arctic glaciers, researchers no longer had to use time-consuming manual measurements). In doing so, he gives readers insight into the scientific process.

For those who call climate researchers alarmist, Serreze shows how cautious they actually were in interpreting early study results. They hedged their bets by noting that seemingly alarming results might change once more comprehensive data sets became available. They stuck with the AO/NAO paradigm until it no longer made sense to do so, resisting the urge to implicate climate change in Arctic changes when the data showed only short-term variability. But they also recognized when the data began to clearly show a climate change connection: when the NAO and AO regressed from their high positive phases but Arctic sea ice continued to decline.

Serreze is obviously an expert on Arctic science, and he sometimes struggles to translate complex scientific concepts into plain language. In attempting to describe the Arctic Ocean pycnocline, for example, he writes "[T]he warmer water at the top is … the lighter (that is, less dense) water, which maintains a stable vertical profile, thus inhibiting vertical mixing. … the *decrease* in temperature with depth, known as a thermocline, represents an *increase* in density with depth, known as a pycnocline." And, in many cases, the scientific detail he provides isn't required, as in chapter 7, where he describes atmospheric dynamics and geostrophic balance over the course of two pages. He should be summarizing key points here, not introducing complicated new concepts.

Despite these shortcomings, Serreze succeeds on one important front: humanizing Arctic science. He tells anecdotes about his research and the people he's worked with. He portrays scientists whose work he discusses as regular people. Although some quoted passages are clumsy and jargon-filled (e.g., "'Bruce Peterson [Woods Hole Marine Biological Laboratory], who was on the ARCSS committee, approached me and Larry Hinzman [UAF] about organizing a workshop on designing an integrated study of Arctic hydrology. … The workshop resulted in the Arctic CHAMP report [Community-wide Hydrologic Analysis and Monitoring Program]'"), they show how researchers think and how they make decisions about what to research.

Perhaps most important, Serreze is humble enough to recognize the limits of science. "[T]he scientific process is prone to human frailties, including vanity, envy, competition, greed, and narcissism," he writes. "Anyone who claims that these things don't exist in science is either lying or willfully ignorant." ■

The reviewer is a freelance science writer and editor and cofounder of Science Borealis, Canada's science blog aggregator. Email: snowhydro1@gmail.com

10.1126/science.aas9815

HEALTH AND MEDICINE

Knowledge, wisdom, and the brain

A neuroscientist's battle with brain cancer prompts a personal reflection on identity and the disease process

By **Adam Hayden**

The Neuroscientist Who Lost Her Mind
My Tale of Madness and Recovery
Barbara K. Lipska with Elaine McArdle
Houghton Mifflin Harcourt, 2018. 208 pp.

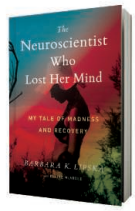

In *The Neuroscientist Who Lost Her Mind*, Barbara Lipska shares the story of her firsthand experience with metastatic brain cancer. In doing so, she provides readers the opportunity to foster a "sense of connection with others who suffer" and to combat continued stigmatizing of mental illness. Lipska's evolution as scientist, patient, and person explores the physiological basis of mental illness, while uplifting the importance of personal identity. True as it is that "[w]e *are* our brains," her story is evidence that rich personal narratives offer value to an empirical pursuit of neuroscientific investigation.

Throughout the book, Lipska leverages her explicit understanding of the brain's complex connections and the relationships between functional areas to weave together tactile and real scenes and characters from her life. Her project succeeds across a range of criteria. She is adept at employing her vast technical knowledge as a neuroscientist, combining discussions of her own basic research, conducted at the National Institute of Mental Health (NIMH), with human research in clinical settings. She also provides a rich sensory experience by translating her ordeal into experiences the reader might feel, taste, and smell.

The book begins with a description of the functional areas of the brain, highlighting their responsibilities, tasks, and anatomical locations. It does so by referencing the reader's own external anatomical features, including the forehead, hairline, and top of the skull: visible landmarks set atop hidden, complex systems. The neuroanatomical survey continues with a description of spatial tasks performed by the parietal lobe that "tells us where we are in relation to things around us, and where our bodies start and end." Passages like these highlight Lipska's ability to fit complicated ideas into modes amenable to a lay audience.

She does well to introduce these systems to make the point that mental illness is "abnormal brain structure and function," yet she learns that knowledge of the anatomy is no replacement for experience. "[I]t is my own suffering that truly taught me how the brain works," she ultimately concludes.

Lipska's prose soars when narrating her experiences, as in a scene in which she describes an exam she underwent to troubleshoot a blind spot in her field of vision—an early sign of neurological trouble to come. To illustrate the division of labor between our sensory inputs and the processing of our brains, she vividly describes her ophthalmologist, "her pretty young face," she continues, "her glittering earrings almost touching my ears and cheeks." Recalling this mundane experience, now cast in a new light, Lipska tacitly invites the reader to imagine herself or himself in the examination room.

Lipska's neurological symptoms were not only sensory; her personality changed as well. Her assertiveness became more direct, her skepticism was more pronounced, and her instruction demanded more urgency: traits of a scientist, amplified by illness. We, the reader, experience her slow departure from reality alongside her, never realizing the moment her account of events becomes unreliable. While reading one of these scenes in the familiar setting of my local coffee shop, I was forced to withdraw from the book and give pause, before returning, with enthusiasm. The eerie similarity between the reader's experience and Lipska's cannot be overstated.

Throughout the book, Lipska compares her experience to that of her research animals. "It's likely that communication between my prefrontal cortex and my hippocampus is failing, which is unpleasantly reminiscent of the prefrontal cortical connections I disrupted in rats to study schizophrenia," she writes at one point. Eventually, she determines that her best chance at survival is an unproven immunotherapy treatment still in the early stages of testing. She has become, she notes with irony, "*an experimental rat*."

Her neurological symptoms, we learn, were caused by inflammation, a side effect of the experimental immunotherapy. Once the swelling was treated with steroids, her symptoms abated, returning Lipska from the brink of madness. With the hope of total remission and the anxiety of recurrence, she accepted a new label to incorporate into her identity: survivor.

This grappling with identity—and Lipska's gradual acceptance that the sense of self is both the outcome of, and the struggle with, our own physiology—may be the book's greatest contribution. Through this realization, we may connect with our own suffering to more firmly grasp our sense of identity. ■

Lipska (center left) skis with family one month after undergoing surgery to remove a tumor from her brain.

PHOTO: COURTESY OF BARBARA K. LIPSKA

The reviewer is a philosopher of science, a freelance writer, and an individual living with glioblastoma based in Indianapolis, IN, USA. Email: adammarchayden@gmail.com

10.1126/science.aas9782

LETTERS

Shortfin mako shark (*Isurus oxyrinchus*)

Edited by **Jennifer Sills**

Shortfin mako sharks threatened by inaction

Oceanic shark populations are declining as a result of high fishing pressure and lack of international catch quotas (*1*, *2*). There has been management inaction for decades partly because species data is poorly recorded (*1*–*4*). However, despite improvements in data quality and models underpinning more accurate scientific stock assessments (*5*), regulators are not abiding by scientists' advice, as exemplified by the lack of action after the recommendations made at the November 2017 meeting of the International Commission for the Conservation of Atlantic Tunas (ICCAT).

The tunalike shortfin mako shark *Isurus oxyrinchus* is one of the fastest sharks, clocking speeds of up to 70 km/h (*6*). Yet, it is the second-most common oceanic shark caught by high-seas longline and net fisheries, principally for high-value fins (*2*–*4*). Although grossly underestimated (*2*), North Atlantic reported catches currently exceed 3300 tons annually—about 130,000 individuals (*5*). The 2017 ICCAT stock assessment confirmed that the North Atlantic is overfished (*5*) and recommended reducing the annual mako shark catch to 500 tons or less to prevent further declines (*7*).

ICCAT member nations did not agree to a quota to limit North Atlantic mako catches. Instead, ICCAT recommended (but did not require) a compromise in which sharks brought alongside vessels alive should be released (*8*). Research [e.g., (*2*, *3*, *9*)] indicates that 60 to 80% of longline-hooked makos reach vessels alive. Accordingly, considering longline-only catches for 2016 [3146 tons (*7*)], let us assume that vessels adhere to recommendations and promptly release all live sharks (optimistically, 80% of 3146 tons caught, or 2517 tons released). About 30% (755 tons) are likely to die after release (*9*). The retained catch (20% of 3146 tons, or 629 tons) added to the sharks that die post-release still total about 1400 tons annually, nearly three times the upper limit of scientific advice.

Action taken so far by ICCAT will not halt the decline. Even if total catches decrease to 500 tons, probability of stock rebuilding by 2040 is only 35%, rising to 54% for zero catch (*5*). Thus, recovery will be very slow even if prohibition can be agreed upon and, importantly, is enforced.

David W. Sims,[1,2]* Gonzalo Mucientes,[3] Nuno Queiroz[3]

[1]Marine Biological Association of the UK, Plymouth PL1 2PB, UK. [2]University of Southampton, Southampton SO14 3ZH, UK. [3]CIBIO/InBIO–Universidade do Porto, 4485-668 Vairão, Portugal. *Corresponding author. Email: dws@mba.ac.uk

REFERENCES

1. B. Worm *et al.*, *Mar. Pol.* **40**, 194 (2013).
2. S. E. Campana, *Can. J. Fish. Aquat. Sci.* **73**, 1599 (2016).
3. N. Queiroz *et al.*, *Proc. Natl. Acad. Sci. U.S.A.* **113**, 1582 (2016).
4. M. D. Camhi, E. K. Pikitch, E. A. Babcock, Eds., *Sharks of the Open Ocean: Biology, Fisheries and Conservation* (Blackwell, Oxford, 2008).
5. International Commission for the Conservation of Atlantic Tunas, "Report of the 2017 ICCAT Shortfin Mako Assessment Meeting" (Madrid, Spain, 2017); www.iccat.int/Documents/Meetings/Docs/2017_SMA_ASS_REP_ENG.pdf.
6. G. Diez, M. Soto, J. M. Blanco, *J. Fish Biol.* **87**, 123 (2015).
7. International Commission for the Conservation of Atlantic Tunas, "Report of the Standing Committee on Research and Statistics (SCRS)" (Doc. No. PLE 104/2017, Madrid, Spain, 2017); www.iccat.int/Documents/Meetings/Docs/2017_SCRS_REP_ENG.pdf.
8. International Commission for the Conservation of Atlantic Tunas, "Draft Recommendation by ICCAT on the Conservation of North Atlantic Stock of Shortfin Mako Caught in Association with ICCAT Fisheries" (Doc. No. PA4-812B/2017, 2017); www.iccat.int/com2017/DocENG/PA4_812B_ENG.pdf.
9. S.E. Campana, W. Joyce, M. Fowler, M. Showell, *ICES J. Mar. Sci.* **73**, 520 (2016).

10.1126/science.aat0315

Mitigate risk for Malaysia's mangroves

Malaysia is the third largest mangrove-holding nation, with 4691 km^2 of mangroves (*1*), despite the reported losses including 278 km^2 between 2000 and 2014 (*1*). Mangrove habitat loss in Malaysia is mainly attributed to land conversion for agriculture, aquaculture, and urban development (*2*). Malaysia's mangroves are also affected by severe erosion, aggravated by anthropogenic disturbances along with the rising sea level (*3*). The combined effect from these disturbances jeopardizes the role of mangroves as a functional habitat that provides vital ecosystem services and connectivity and secures the livelihoods of Malaysia's coastal communities (*4*). The remaining mangroves are now fragmented and are susceptible to further disturbances, putting the ecosystems at a greater risk of collapsing (*5*).

To mitigate the risk, a comprehensive governance framework for resource management and habitat conservation should control anthropogenic influences (*6*). An intertidal habitat, mangroves lie between terrestrial and marine ecosystems. Land and natural resources are protected by a variety of state by-laws and inconsistent implementation and enforcement of national policies by the states (*7*). Meanwhile, the primary law pertaining to Malaysia's marine biotic resources—Fisheries Act 1985—focuses largely on the management of fisheries, aquaculture, and marine parks and provides no protection for intertidal habitats (*8*). As a result, mangroves fall into administrative loopholes; they are partially conserved and governed through various federal laws and policies, which are being enforced at the state level by multiple agencies with differing interests and priorities (*9*). With such piecemeal protection efforts, mangroves continue to be indirectly disturbed or directly exploited regardless of whether they are deemed a legally protected site.

To ensure the sustainability of Malaysia's mangroves, state authorities—with scientists' input (*10*)—must streamline their priorities. Flaws in the planning, approval, and project implementation processes must be minimized. Environmental impact assessments must be improved to prevent setbacks such as insufficient data and inadequate baseline studies, poor reporting by incompetent personnel, and the lack of public participation in the review process (*11*). Existing laws must be strictly enforced. Given the increasing threats from global climate

change, and considering mangroves' outstanding ability to efficiently fix and store atmospheric carbon (*12*), Malaysia must waste no time in making plans to fully conserve all remaining mangroves.

A. Aldrie Amir
Institute for Environment and Development (LESTARI), Universiti Kebangsaan Malaysia, 43600 Bangi, Selangor, Malaysia.
Email: aldrie@ukm.edu.my

REFERENCES

1. S. Hamilton, D. Casey, *Glob. Ecol. Biogeogr.* **25**, 729 (2016).
2. D. Richards, D. Friess, *Proc. Natl. Acad. Sci. U.S.A.* **113**, 344 (2016).
3. N. A. Awang, W. H. Jusoh, M. R. A. Hamid, *J. Coastal Res.* **71**, 122 (2014).
4. V. C. Chong, *Aquat. Ecosyst. Health* **9**, 249 (2006).
5. N. Duke *et al.*, *Science* **317**, 41 (2007).
6. M. M. Foley *et al.*, *Mar. Pol.* **34**, 955 (2010).
7. W. Talaat, N. M. Tahir, M. L. Husain, *J. Polit. Law* **5**, 180 (2012).
8. Government of Malaysia, *Laws of Malaysia: Fisheries Act 1985 (Act 317)*, Second reprint (2006); www.agc.gov.my/agcportal/uploads/files/Publications/LOM/EN/Act%20317%20-%20Fisheries%20Act%201985.pdf.
9. D. Friess *et al.*, *Conserv. Biol.* **30**, 933 (2016).
10. D. A. Friess, E. L. Webb, *Environ. Conserv.* **38**, 1 (2011).
11. O. A. Lee, *Ocean Coast. Manage.* **53**, 439 (2010).
12. D. C. Donato *et al.*, *Nat. Geosci.* **4**, 293 (2011).

10.1126/science.aas9139

India's Ph.D. scholar outreach requirement

As demand increases for scientists and researchers to take part in public engagement and outreach (*1*–*3*), the Government of India's Department of Science and Technology plans to require Ph.D. scholars to write a popular science article on their research before completing their degree (*4*). The Department's National Council of Science and Technology Communication has launched a related program that will select the best entries from such articles by Ph.D. scholars and postdoctoral fellows each year. Winners will receive a monetary reward and a certificate of appreciation, and their work will be published in a mass media outlet (*5*). These ideas are part of the government's larger plan to push science and technology organizations to embrace "scientific social responsibility" and to encourage scientists to popularize science among the public (*4*, *6*, *7*). Dialogue with nonspecialist audiences builds support for science and makes clear its relevance in society (*8*). If implemented properly, the proposed degree requirement can boost science communication while serving as a global trendsetter in the field.

However, this policy will not be effective unless appropriate provisions are made to train the scholars in science communication and equip them with writing skills. Integrating science communication training into science curricula is imperative to nurture a future generation of scientists who can explain their research to the public (*8*, *9*). During such training, Ph.D. scholars should be taught to communicate their research with not only peers, but the public, the media, and other stakeholders. In addition to teaching scholars to write research papers, reports, and grant proposals, courses should cover how to translate research into accessible language appropriate for popular science articles and press releases, how to engage with nonscientist audiences, how to dejargonize public speaking scripts, how to give media interviews and handle media queries, and how to document (film) their research for public consumption. Activities such as learning by doing, role playing, and real-life engagements can further hone writing and communication skills. Efforts should also be made to inculcate a sense of responsibility and passion for communicating research to society among Ph.D. scholars. Without such comprehensive communication support, the government's plan to improve scientific outreach would become just another numeric parameter.

Abhay S. D. Rajput
Indian Institute of Tropical Meteorology, Pune, India and Department of Humanities and Social Sciences, BITS Pilani, Pilani, India. Email: abhaysdr@gmail.com

REFERENCES

1. "Survey of factors affecting science communication by scientists and engineers" (The Royal Society, UK, 2006).
2. A. Dudo, J. C. Besley, *PLOS One* **11**, e0148867 (2016).
3. H.P. Peters, *Proc. Natl. Acad. Sci.* **110** (suppl. 3), 14102 (2013).
4. J. Koshy, "Aspirant scientists may first need to tell a story," *The Hindu* (2017); www.thehindu.com/news/national/aspirant-scientists-may-first-need-to-tell-a-story/article19835061.ece.
5. Government of India, Ministry of Science and Technology, Department of Science and Technology (2018); http://dst.gov.in/republic-day-2018.
6. Press Information Bureau, Government of India, Ministry of Science and Technology (2017); http://pib.nic.in/newsite/PrintRelease.aspx?relid=169646.
7. Press Information Bureau (2017); http://pib.nic.in/newsite/PrintRelease.aspx?relid=167194.
8. A. S. D. Rajput, *Curr. Sci.* **113**, 2262 (2017).
9. S. E. Brownell, J. V. Price, L. Steinman, *J. Undergrad. Neurosci. Educ.* **12**, E6 (2013).

10.1126/science.aat0303

Editor's Note

Last week's Working Life (http://scim.ag/instainequality) drew heated criticism. We will run a selection of reader responses in an upcoming issue.
Tim Appenzeller, News Editor

SPECIAL SECTION

The new generation of cancer immunotherapies includes ways to engineer patients' own immune cells to kill their cancer and patient-specific neoantigen vaccines. This image alludes to the hope of personalized therapy tailored to each patient.

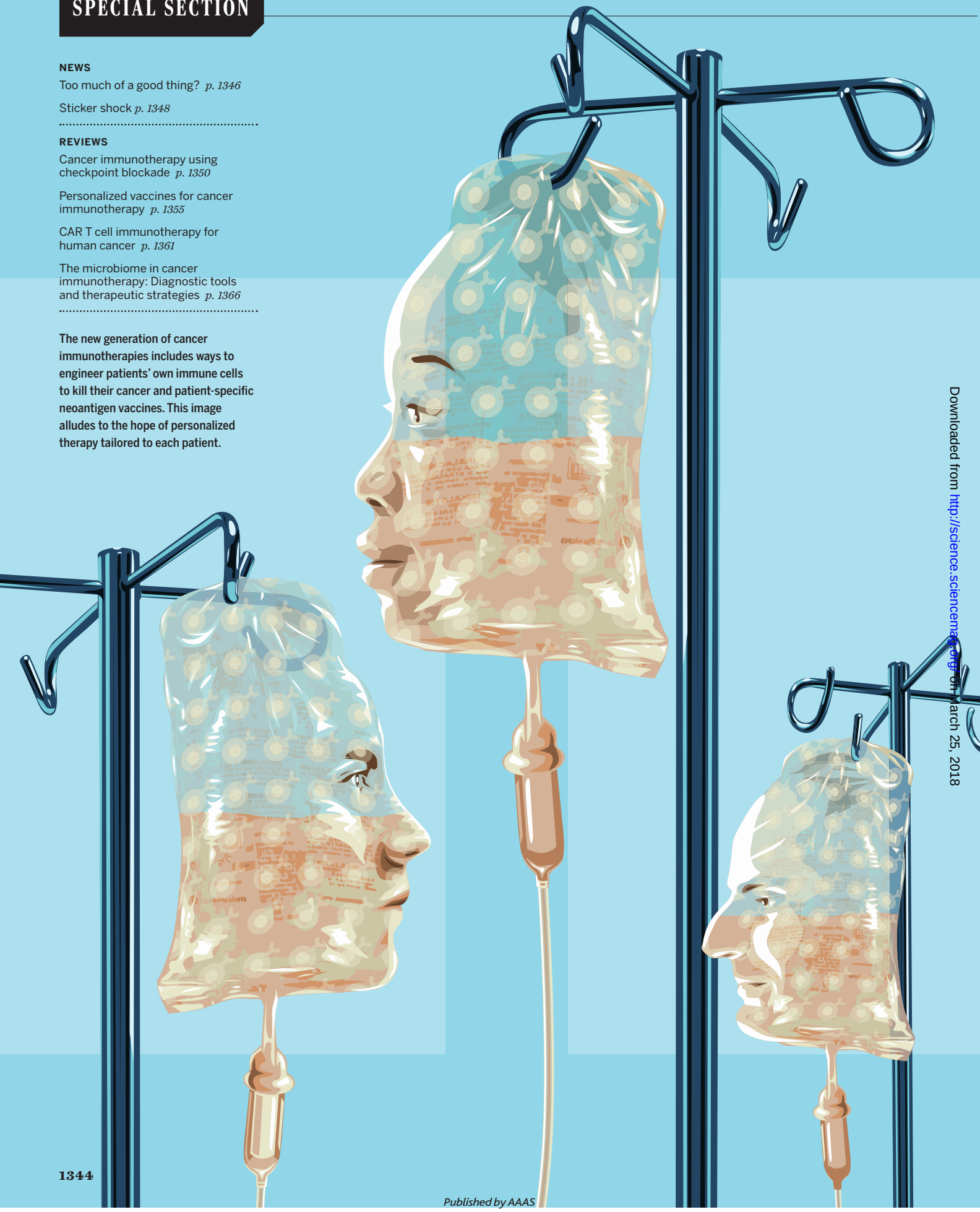

THE CANCER IMMUNOTHERAPY REVOLUTION

By **Priscilla N. Kelly**

Cancer immunotherapy—the science of mobilizing the immune system to kill cancer—has been pursued for more than a century. Yet only recently has this powerful strategy finally taken center stage in mainstream oncology. The past few years have seen unprecedented clinical responses, rapid drug development, and first-in-kind approvals from the U.S. Food and Drug Administration. Reports of terminal cancer patients defying the odds and achieving complete remissions are accumulating. These success stories are the culmination of decades of painstaking research by pioneering scientists and physicians. Newly approved immunotherapies include drugs that can manipulate components of the immune system and methods to genetically engineer patients' own T lymphocytes to recognize and attack their tumors.

Researchers are racing to expand the use of immunotherapy to benefit more cancer patients. But it remains unclear why only a subset of individuals respond to treatment and how to better achieve sustained remissions. Hundreds of clinical trials are under way to see whether improved responses can be attained by combination therapy approaches. Unraveling the cellular and molecular basis of treatment resistance should facilitate rational design of new mechanism-based studies. Advances in genome sequencing are identifying predictive biomarkers and facilitating the design of personalized vaccines that target patient-specific tumor neoantigens. These lines of research, along with growing evidence that the gut microbiome plays a defining role in immunotherapy response, are charting innovative paths toward truly personalized medicine.

ILLUSTRATION: DANIEL HERTZBERG

Published by AAAS

TOO MUCH OF A GOOD THING?

Cancer experts debate whether there's a glut of immunotherapy trials

By **Jocelyn Kaiser**

As the growing wave of excitement over immunotherapies has swept through the cancer field, a concern has followed in its wake: Are there now too many clinical trials for these novel treatments, which enlist the immune system to battle tumors? One recent tally found more than 1100 studies combining a popular new class called checkpoint inhibitor drugs, which unleash suppressed immune cells, with other treatments. That's up from about 100 trials testing these combos through 2014.

Some academic researchers, pharma executives, and other cancer experts have decried this explosion of trials as a counterproductive glut motivated more by the race for money than by good science. They worry that many of these efforts may not finish because of a lack of participants. Even if these trials do meet enrollment targets, many duplicate other trials and are diverting resources that could go to novel drugs, Richard Pazdur, director of the U.S. Food and Drug Administration's (FDA's) Oncology Center of Excellence in Silver Spring, Maryland, has warned.

"The trials have to be smarter," says Yale University lung cancer researcher Roy Herbst.

One influential patient advocacy group, although eager to see preclinical research translated into treatments, is also concerned about the skyrocketing number of combination trials. "It's very exciting to have options, but we're somewhat worried that it will take too long to find these patients and get answers," says Ellen Sigal, chairperson of Friends of Cancer Research in Washington, D.C.

Some cancer researchers, however, think the competition is healthy—and the best studies and combos will prevail. "It's not surprising to me that there are more and more trials," says David Feltquate, head of oncology early clinical development at Bristol-Myers Squibb (BMS) in Princeton, New Jersey, which markets two checkpoint inhibitor drugs and is developing others. "We are in what I would call the golden age of oncology drug development." Antoni Ribas, a melanoma immunotherapy researcher at the University of California, Los Angeles, also sees no reason to worry. "I basically disagree with the common notion that we have too many trials open."

Checkpoint inhibitors, which block cell-surface proteins that enable a cancer to hide from the immune system's T cells, have become big business thanks to the impressive medical outcomes they sometimes produce. In patients with metastatic disease, the drugs have wiped out tumors for years. Since 2011, six checkpoint inhibitors have been approved for melanoma, lung cancer, and some other cancers—all targeting a protein called CTLA-4 or PD-1 on immune cells or PD-1's binding partner, PD-L1, on cancer cells. But only about 20% of patients overall respond to these drugs, and the race is on to learn whether combining them with other treatments can push that figure higher.

That excitement and the commercial potential of checkpoint inhibitors—a year's

In a trial at MD Anderson Cancer Center in Houston, Texas, bladder cancer patient David Wight received two immunotherapy drugs known as checkpoint inhibitors.

PHOTO: ILANA PANICH-LINSMAN/*THE NEW YORK TIMES*/REDUX

course of the approved PD-1 inhibitors sold by Merck and BMS costs about $150,000—explains the unprecedented growth in trials. At least 1105 combination studies are now testing drugs targeting PD-1 or PD-L1, according to the Cancer Research Institute (CRI), a nonprofit in New York City, which reported its findings online in December 2017 in the *Annals of Oncology*. That is out of a larger universe of 3042 active trials testing immunotherapy treatments. The PD-1/PD-L1 inhibitor combination trials alone started in the past 3 years are seeking more than 138,000 patients, including 52,539 for trials launched in 2017.

Feltquate says BMS, which has about 225 trials underway globally with its two approved checkpoint inhibitors, has not noticed a lag in patient recruitment. "If anything, enrollment is actually faster than we had seen historically."

Indeed, it's hard to find checkpoint inhibitor trials that have been stymied by competition, partly because the U.S. database ClinicalTrials.gov doesn't include patient accrual data. But by examining a database of National Cancer Institute (NCI)-sponsored trials, which posts enrollment data, *Science* identified a few examples of trials that may be having trouble recruiting subjects within the planned time frame. (NCI-funded trials sometimes struggle more than company-led efforts because the firms pay more to participating institutions per patient and can recruit patients globally.)

Yet the principal investigators of those trials often expressed no concerns about patient accrual when contacted. Jonathan Schoenfeld of the Dana-Farber Cancer Institute in Boston, for example, says his trial of a checkpoint inhibitor–radiation combo for lung cancer initially attracted few patients because of competing trials, but is picking up steam.

One leader of an NCI trial at a major cancer center did attribute slow enrollment to competition, but asked that the trial details not be identified because its funding is coming up for renewal. The trial combines a drug that targets a specific flaw in the cells of some cancer patients with a checkpoint inhibitor. The investigators will extensively analyze tumor biopsies to see whether the added drug helps T cells recognize cancer cells.

But 16 months after the trial was launched, only eight people have enrolled, far fewer than the four per month projected. Elad Sharon, a senior investigator with NCI's Cancer Therapy Evaluation Program in Bethesda, Maryland, which oversees the trial, blames other studies seeking the same small pool of patients with the rare cancer type targeted. "It's a little frustrating. A better designed trial is getting crowded out by less well-designed trials," Sharon says. NCI plans to make changes to boost enrollment and finish the trial, he adds.

In the worst case, lagging enrollment might force investigators to cancel a trial, says Richard Schilsky, chief medical officer of the American Society of Clinical Oncology in Alexandria, Virginia. "If the trials don't complete, there really is a rift of the ethical obligation that we have with patients who are willing to participate as research subjects," he says.

The rush to test combination therapies may also have taken a toll on rigor. As a cost-saving measure, many trials don't contain control, or comparator, arms, Schoenfeld notes. Others are launched despite a lack of a hypothesis or animal data providing a mechanistic rationale, says Ira Mellman, Genentech's vice president for cancer immunology in San Francisco, California. "Many seem to be tried simply because they are possible to do or the agents are available," he says.

Even those who lament the proliferation of trials note that taming it won't be easy. FDA has no authority to rein in immunotherapy trials as long as they pass certain standards. "Everybody does the study they want to do as long as they can get it funded and get it through the system … there's no oversight," Schilsky says.

As a first step, some are calling for better coordination. Groups like CRI, the Parker Institute for Cancer Immunotherapy set up by tech billionaire Sean Parker, NCI, Friends of Cancer Research, and FDA are encouraging companies to share their drugs as part of multicenter, innovative clinical trial designs that have several treatment arms and a single control group. "We cannot do one-off [single site] trials anymore. It will take too long and will ravage the patient population," Sigal says.

And the NCI-managed cancer moonshot started by former Vice President Joe Biden has launched a 5-year effort in which academics and 11 companies are working together to find biomarkers revealing why some patients respond better to immunotherapies than others do. "There's no doubt we could focus more if people got together in a precompetitive way," Herbst says. "It is happening. We just need more of it." ■

Trial explosion

More than 1000 clinical trials are combining other cancer treatments with immunotherapy drugs, called checkpoint inhibitors, that target the proteins PD-1 or PD-L1 (bottom bars). The number of subjects needed for those trials has skyrocketed (below), and some trials may not find enough patients.*

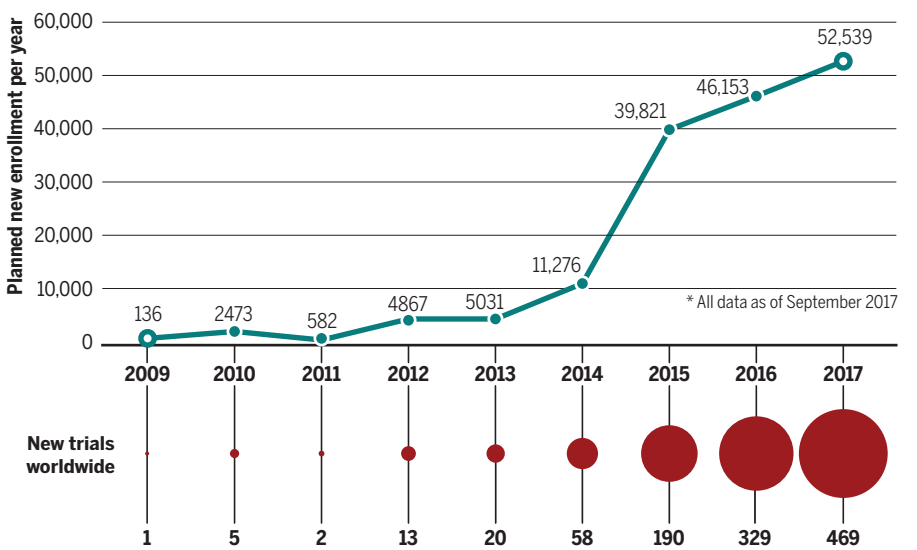

Combination trials with PD-1/PD-L1 inhibitors

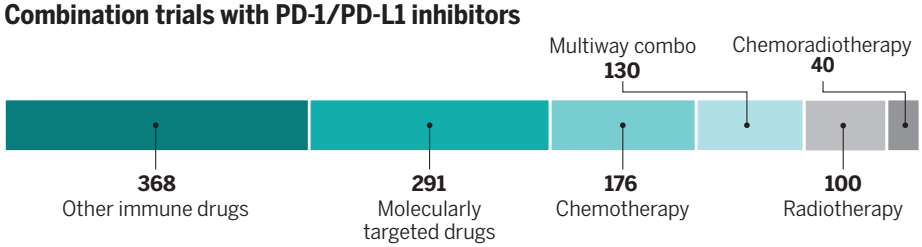

GRAPHIC: N. DESAI/*SCIENCE*

STICKER SHOCK

A data-savvy doctor speaks out about cancer drug costs

By **Jennifer Couzin-Frankel**

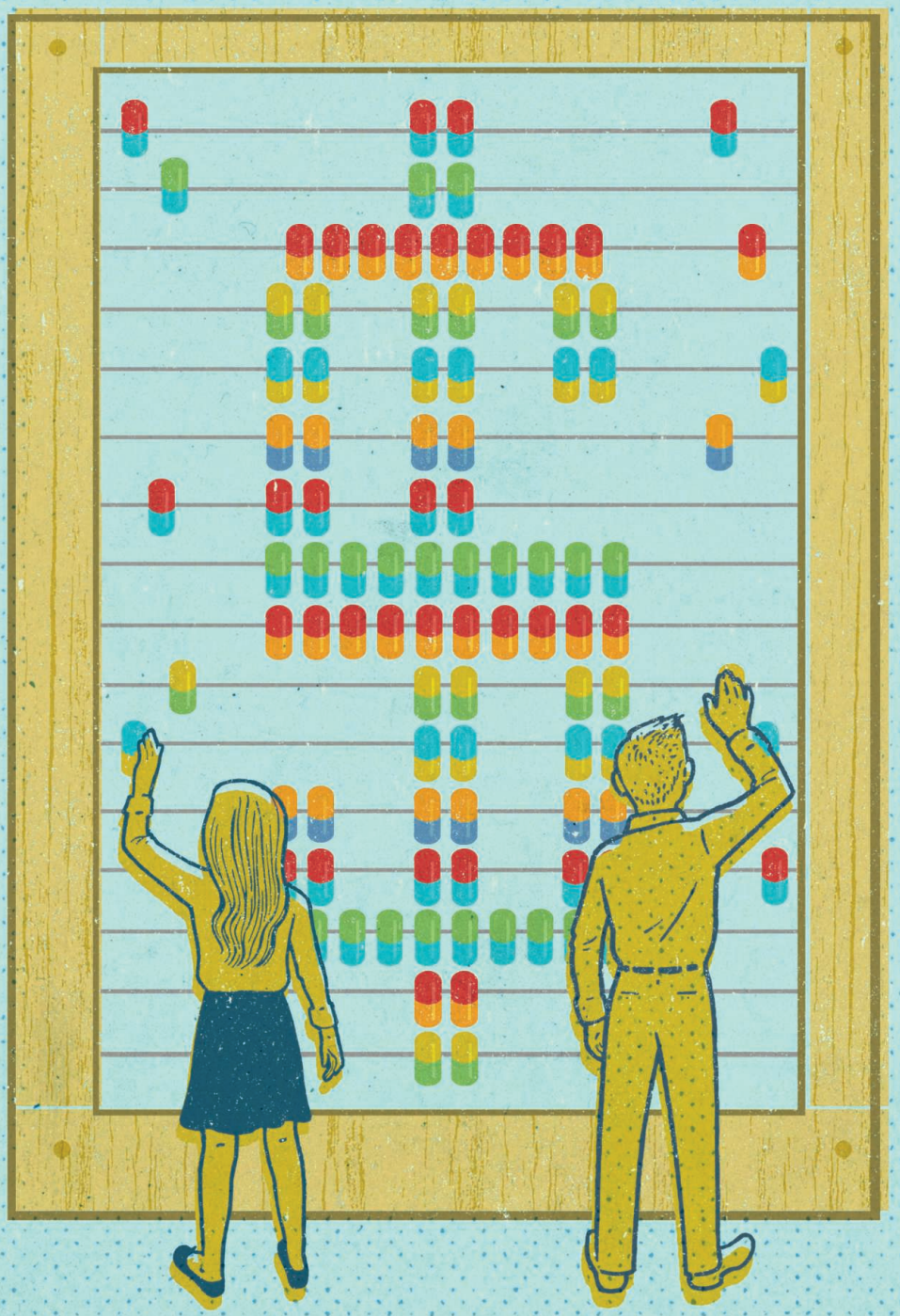

Published by AAAS

Physician Peter Bach is appalled at the sky-high price of cancer treatments in the United States, and he is watching new immune therapies drive them higher. Checkpoint inhibitors for various solid tumors cost about $150,000 a year, and a personalized treatment called chimeric antigen receptor–T cell therapy tops out at $475,000. Dozens more immunotherapies are in clinical trials, as companies race to reap the monetary rewards. In 1995, the cost of cancer drugs for an extra year of life was $54,000. Today, it's about $250,000.

"This is a chase after riches, and it doesn't advance science," says Bach, who works at Memorial Sloan Kettering Cancer Center in New York City. For the past decade, he has immersed himself in health policy and economics to decipher and publicize what's driving these high prices. The details can seem wonkish. Ultimately, though, they come down to an ever-more-popular buzzword in cancer care: value. What's the best way to calculate a drug's benefit to patients, and how much is society willing to pay for an extra month or year of life? There's no agreed-on formula. Does value per person drop, and by how much, if a drug has serious side effects? How much more valuable does it become if it's the only therapy for a particular type of cancer? Bach and his colleagues created an online tool called DrugAbacus to help the public and policymakers consider these questions (https://drugpricinglab.org/tools/drug-abacus/).

On a personal level, Bach understands the value of extra time more than most. His wife Ruth died of breast cancer in 2012 at 46 years old, leaving behind Bach and their young son. Ruth received the best care available, he says, but he recognizes that for many others, the most cutting-edge cancer treatments are increasingly out of reach. *Science* spoke with Bach last month. This interview has been edited for brevity and clarity.

Q: You're a pulmonary and critical care doctor. How did you get into studying drug pricing?
A: I thought that I should devote my energy to trying to address health problems from multiple angles. If you're black, you're less likely to get surgery that can prevent you from dying of cancer; 2.7 million people who have [been] diagnosed [with] hepatitis C haven't received the treatments that cost pennies to make. We had maxed out our science, but we weren't maxing out the health of the people in front of us. I got a public policy degree. I moved to Sloan Kettering and started to study the development of cancer care in the U.S.

Q: And that led you to take a couple years off in 2007 to act as a senior adviser at the Centers for Medicare & Medicaid Services in Washington, D.C. What did you take away from that experience?
A: I realized that the system for drug pricing was rigged. It was geared to ensure that drug companies in the U.S. could charge anything they wanted for cancer drugs. Since I was working in the Medicare program, I knew about all the breaks on price and [sales] volume that existed everywhere else in Medicare. For cancer drugs, [there are] no breaks. I started to think that the only thing we could do about drug prices was to bring attention to these problems. Literally the only thing we could do to get companies to lower drug prices was to embarrass them. We had our chance in 2012.

Q: That was when you helped stop Zaltrap, a new drug for colorectal cancer made by the company Sanofi, from being offered to patients at Sloan Kettering because it cost double the competition with apparently no extra benefit. How did you make that decision?
A: We had a discussion with Leonard Saltz [chief of gastrointestinal oncology at Sloan Kettering]. Zaltrap was about $10,000 a month for Medicare patients, [versus] about $5000 for Avastin. Studies showed 1.4 months [of survival benefit] at the median [for each drug]. If Zaltrap had had 1.5 months and Avastin had had 1.4 months, I don't think we would have done it. We would have been concerned that someone would say, "Sloan Kettering put a value on human life." It's still 3 days—that could be the day you see your daughter get married. It was also serendipitous that the mechanism of action was identical. Sanofi lowered the price by half.

Q: Given today's prices, $10,000 a month sounds almost quaint to me. Is there a tipping point where drugs are simply so expensive no one will use them?
A: No. [But] the understanding that we have to pay these price hikes that Europeans don't pay is starting to hold more sway. I think we are barreling towards a system that makes health care a luxury good for the wealthy. Employers will literally not be able to afford it, state budgets won't be able to afford it. That is a policy decision we are making. One of my jobs is to try and articulate that policy decision, so we can take a hard look at it.

Q: How are you doing that?
A: I'm proud of the DrugAbacus, launched in 2015. The abacus is a thought experiment, where people can go and find out what drugs should cost. We know what the components are—we can measure efficacy, toxicity, novelty, rarity. The question is, how do you combine them? The abacus walks you through. As you change the formula, it changes the price of the drug. A lot of our energy goes into trying to help policymakers and the public [understand] how the system actually works, with respect to the levers at their disposal.

Q: Is there a role for doctors here? Should they be considering the cost of different drugs when they advise their patients?
A: I worry about the difficulty of physicians in a small practice focusing on this, when they have other things to focus on. I think this would be a regressive feature if we felt doctors were rationing. These are policy decisions. And doctors rarely have the ability to know the prices of drugs for their patients.

Q: Why is it important to conduct rigorous studies of cancer drug pricing?
A: Ideology is a poor guide to public policy. The classic pharma argument [is that] we need to pay high prices to drive innovation. X is prices paid, Y is innovation; their argument is you increase X, Y goes up. I think we need to know a little bit about the shape of that curve. Is it linear? Does it flatten? I published an article in *Forbes* suggesting it eventually turns down. You make it so remunerative to do copycat [drugs] that you end up with less risk-taking behavior. Human subjects flow onto trials that aren't asking important questions. The average [survival] benefit of cancer drugs approved over the last 20 years is about 2 months.

Q: A lot of people just think about what a company charges for a drug. But it sounds like what a drug company charges is just the beginning when we're adding up costs.
A: Yes. You hear Pfizer charges $50 for X. The amount of money that goes into you getting X is more than $50. A wholesaler buys it, there's a markup, then the pharmacy buys it, there's a markup. There are inventory costs. Your insurer finances it, there's a markup. It's the money that's really hard to track. But it turns out it's really, really important, because it's half a trillion dollars floating around.

Q: How much power do people like you have to change a system that feels stacked against them?
A: I'm in it for the long haul. I really believe that data can be compelling, as resistant as some of our [society] is to it. My mom always said, "You can't convince the last 20% of people." ■

ILLUSTRATION (OPPOSITE PAGE): 2018 DAN PAGE C/O THEISPOT

REVIEW

Cancer immunotherapy using checkpoint blockade

Antoni Ribas[1]* and Jedd D. Wolchok[2,3]*

The release of negative regulators of immune activation (immune checkpoints) that limit antitumor responses has resulted in unprecedented rates of long-lasting tumor responses in patients with a variety of cancers. This can be achieved by antibodies blocking the cytotoxic T lymphocyte–associated protein 4 (CTLA-4) or the programmed cell death 1 (PD-1) pathway, either alone or in combination. The main premise for inducing an immune response is the preexistence of antitumor T cells that were limited by specific immune checkpoints. Most patients who have tumor responses maintain long-lasting disease control, yet one-third of patients relapse. Mechanisms of acquired resistance are currently poorly understood, but evidence points to alterations that converge on the antigen presentation and interferon-γ signaling pathways. New-generation combinatorial therapies may overcome resistance mechanisms to immune checkpoint therapy.

In 2013, *Science* named cancer immunotherapy its Breakthrough of the Year on the basis of therapeutic gains being made in two fields: chimeric antigen receptor (CAR)–modified T cells and immune modulation using antibodies that block immune regulatory checkpoints. It is critical to note that the apparent rapid clinical progress reported in the past few years was the result of decades of investment in basic science in numerous fields. Without basic mechanistic knowledge in molecular biology, virology, immunology, cell biology, and structural biology, clinical advances in cancer immunotherapy never would have been realized. It is also important to consider the long history of efforts to use the potency of the immune system as a therapeutic modality for cancer. The field traces its earliest efforts to the observations of William Coley, a surgeon who correlated the occurrence of postoperative infection with improved clinical outcomes in cancer patients. After a series of fits and starts throughout the ensuing century, several immunotherapeutics were approved for use in cancer, including bacillus Calmette-Guerin, interferon-α, and interleukin-2 (IL-2). The latter is particularly important in that it demonstrated, for the first time, that advanced metastatic cancer, specifically melanoma and renal cell carcinoma, could be durably controlled in a small subset of patients by using a cytokine capable of expanding T cells. The activity of IL-2 substantiated the importance of adaptive immunity in controlling tumors and provided a solid foundation for the incorporation of basic science knowledge of T cell regulation into the development of new immunotherapy strategies.

[1]Department of Medicine, Division of Hematology-Oncology; Department of Surgery, Division of Surgical Oncology; and Department of Molecular and Medical Pharmacology, Jonsson Comprehensive Cancer Center and Parker Institute for Cancer Immunotherapy, University of California, Los Angeles, Los Angeles, CA 90095, USA. [2]Department of Medicine, Ludwig Center and Parker Institute for Cancer Immunotherapy at Memorial Sloan Kettering Cancer Center, New York, NY 10065, USA. [3]Weill Cornell Medical and Graduate Colleges, New York, NY 10065, USA.
*Corresponding author. Email: aribas@mednet.ucla.edu (A.R.); wolchokj@mskcc.org (J.D.W.)

CTLA-4 as a nonredundant immune checkpoint and clinical activity

A pivotal moment occurred when a protein known as cytotoxic T lymphocyte–associated protein 4 (CTLA-4) was demonstrated to have a potent inhibitory role in regulating T cell responses by two groups, one led by James Allison and the other by Jeffrey Bluestone (*1*–*3*). In resting T cells, CTLA-4 is an intracellular protein; however, after T cell receptor (TCR) engagement and a costimulatory signal through CD28, CTLA-4 translocates to the cell surface, where it outcompetes CD28 for binding to critical costimulatory molecules (CD80, CD86) and mediates inhibitory signaling into the T cell, resulting in arrest of both proliferation and activation (Fig. 1) (*1*). The generation of mouse models lacking CTLA-4 provided additional support of CTLA-4 as a nonredundant coinhibitory pathway, as those animals died of fulminant lymphocytic infiltration of almost all organs (*1*). While Bluestone went on to apply this critical knowledge to control autoimmune diseases, Allison theorized that if this molecular "brake" could be transiently blocked with an antibody, then this might allow for the T cell repertoire to proliferate and become activated to a higher point than normal physiology would allow (*1*). After initial preclinical proof-of-principle studies conclusively showed that checkpoint blockade with a CTLA-4–blocking antibody could lead to durable regression of established tumors in syngeneic animal models (*1*, *2*), the strategy moved toward clinical evaluation.

Initially, two fully human CTLA-4–blocking antibodies (ipilimumab and tremelimumab) entered clinical trials in patients with advanced cancer in 2000 (Fig. 2). It quickly became apparent that durable tumor regressions could occur, although these were relatively infrequent and accompanied by a set of mechanism-related toxicities resulting from tissue-specific inflammation (*4*, *5*). The most common of these toxicities included enterocolitis, inflammatory hepatitis, and dermatitis. Algorithmic use of corticosteroids or other forms of immune suppression readily controlled these symptoms without any apparent loss of antitumor activity (*6*). However, less frequent adverse events also included inflammation of the thyroid, pituitary, and adrenal glands, with the need for lifelong hormone replacement. Clinical activity of CTLA-4 blockade was most apparent in patients with advanced metastatic melanoma, with a 15% rate of objective radiographic response that has been durable in some patients for >10 years since stopping therapy (*7*, *8*). The patterns of clinical response shown by radiographic imaging after ipilimumab were sometimes distinct from those associated with therapies that have more direct antiproliferative mechanisms of action (*9*). Patients treated with ipilimumab on occasion showed delayed response after initial progression or new tumors appearing and then regressing while baseline tumors decreased in size. This led to challenges in securing regulatory approval on the basis of the commonly used surrogate metrics of objective response rate, or progression-free survival. Instead, it necessitated assessment of overall survival, a much longer-term outcome, as the primary endpoint registration trials. Eventually, two large phase 3 trials showed that ipilimumab was the first treatment to significantly extend survival in metastatic melanoma when compared with a peptide vaccine (*10*) or with standard dacarbazine chemotherapy (*11*). Approval from the U.S. Food and Drug Administration (FDA) was granted in 2011. Tremelimumab is still under investigation in clinical trials, and additional CTLA-4–blocking antibodies have recently entered clinical trials (NCT02694822).

Given the relatively low response rate and frequent toxicity associated with CTLA-4 blockade, identification of predictive and pharmacodynamic biomarkers emerged as research priorities. Analysis of tumors from patients with or without a response to anti–CTLA-4 therapy supports that a higher tumor mutational burden is associated with higher likelihood of response (*12*, *13*). On-treatment increases in peripheral blood absolute lymphocyte counts and induction of the inducible costimulator ICOS both correlate with eventual treatment response (*14*). Despite numerous preclinical mouse studies showing that CTLA-4–blocking antibodies with appropriate Fc domains could mechanistically deplete regulatory T cells (T_{regs}) in regressing tumors, data associating this with clinical response in humans remain scarce. A recently initiated clinical trial (NCT03110307) is being used to investigate a version of ipilimumab with enhanced depleting capability by means of a nonfucosylated Fc domain to test this hypothesis further.

PD-1 as a nonredundant immune checkpoint

The programmed cell death 1 (PD-1) receptor has emerged as a dominant negative regulator of antitumor T cell effector function when engaged by

its ligand programmed cell death ligand 1 (PD-L1), expressed on the surface of cells within a tumor. PD-1 bears its name from its initial description as a receptor inducing cell death of an activated T cell hybridoma (*15*). However, further work demonstrated that it is instead an immune checkpoint, with its inhibitory function mediated by the tyrosine phosphatase SHP-2, which dephosphorylates signaling molecules downstream of the TCR (*16*). PD-1 has two ligands, PD-L1 (also known as CD274 or B7-H1), which is broadly expressed by many somatic cells mainly upon exposure to proinflammatory cytokines (*16*), and PD-L2 (also known as CD273 or B7-DC), which has more restricted expression in antigen-presenting cells (*16*). Inflammation-induced PD-L1 expression in the tumor microenvironment results in PD-1–mediated T cell exhaustion, inhibiting the antitumor cytotoxic T cell response (*16*–*18*) (Figs. 1 and 3).

Antitumor T cells repeatedly recognize cognate tumor antigen as the cancer advances from primary to metastatic lesions over time. Triggering of the TCR results in the production of proinflammatory cytokines, including interferon-γ (IFN-γ), which is the strongest stimulator of reactive PD-L1 expression (*16*, *19*). Chronic exposure of T cells to cognate antigen results in reactive PD-L1 expression by target cells, and continuous PD-1 signaling in T cells induces an epigenetic program of T cell exhaustion (*20*, *21*). Several other interactions in the PD-1 pathway have a less clear functional meaning. PD-L1 has been shown to bind the costimulatory molecule CD80 (B71) expressed on T cells, delivering an inhibitory signal (*16*). Repulsive guidance molecule b (RGMb) binds to PD-L2, but not PD-L1, and seems to be relevant for pulmonary tolerance (*16*).

PD-1 is therefore a negative regulator of preexisting immune responses, which becomes relevant to cancer because its blockade results in preferential stimulation of antitumor T cells (Fig. 3). The restricted effect of PD-1 is highlighted by the limited phenotype of PD-1–deficient mice compared to that of CTLA-4–deficient mice, as the former are mostly devoid of autoimmune diseases unless these are induced by other means (*16*). Consequently, PD-1–pathway blockade has a more specific effect on antitumor T cells, perhaps because of their chronically stimulated state, resulting in increased therapeutic activity and more limited toxicity compared to CTLA-4 blockade (*22*, *23*).

Clinical effects of PD-1– and PD-L1–blockade therapies

The underlying biology and durable response rates in patients with multiple types of cancer indicate that therapeutic blockade of the PD-1 pathway is arguably one of the most important advances in the history of cancer treatment. There are currently five anti–PD-1 or anti–PD-L1 antibodies approved by the FDA in 11 cancer indications (Table 1 and Fig. 2). The first evidence of the antitumor activity of PD-1 blockade was with the fully human monoclonal antibody nivolumab (previously known as MDX-1106/BMS936558). Nivolumab was first administered to a patient in October 2006 in a phase 1 single-infusion dose-escalation trial and represents the first instance of PD-1 blockade in humans (Fig. 2). Among the 16 initial patients who received nivolumab every 2 weeks, six (37.5%) had objective tumor responses, including patients with melanoma, renal cell carcinoma, and non–small cell lung cancer (NSCLC) (*24*). The notable early evidence of antitumor activity in this phase 1 trial was accompanied by limited toxicity, although the rare development of pneumonitis was an indicator of occasional serious toxicities (*24*, *25*). The presentation of the phase 1 data with nivolumab triggered rapid acceleration of clinical trial plans with this and other anti–PD-1 and anti–PD-L1 antibodies (Fig. 2). The anti–PD-1 antibody pembrolizumab entered clinical testing in April 2011. With the encouraging clinical data from nivolumab, pembrolizumab's clinical development focused on patients with metastatic melanoma and NSCLC, resulting in the largest phase 1 trial ever conducted in oncology, eventually enrolling 1235 patients (*26*, *27*).

The first FDA approvals of PD-1–blocking antibodies were through accelerated and breakthrough filing pathways, with pembrolizumab and nivolumab approved for the treatment of patients with refractory melanoma in 2014 and, in 2015, for patients with advanced NSCLC (Fig. 2). The first anti–PD-L1 antibody approved was atezolizumab for urothelial cancers in 2016, followed by avelumab for Merkel cell carcinoma in 2017 (Fig. 2). This class of agents was the first to be granted FDA approval on the basis of a genetic characteristic as opposed to the site of origin of the cancer, with the approval of pembrolizumab and nivolumab for the treatment of microsatellite-unstable cancers of any origin in 2017 (*28*). This rapid drug development and broad range of approvals are based on a series of characteristics of the clinical activity of PD-1 pathway–blocking antibodies and are outlined below.

Antitumor activity of PD-1–pathway blockade has been observed in a subset of patients within a broad range of cancers, particularly in carcinogen-induced cancers or cancers driven by viral infections (Table 1). The highest antitumor activities of single-agent PD-1–blockade therapy are in Hodgkin's lymphoma, in which there is constitutive expression of PD-L1 through a common amplification of the PD-L1–encoding locus together with PD-L2 and Janus kinase 2 (JAK2) (termed PDJ amplicon) (*29*); the virally induced Merkel cell carcinoma of the skin (*30*); microsatellite-instability cancers with high mutational load from mismatch-repair deficiency, leading to a high frequency of insertions and/or deletions (indels) (*28*); and desmoplastic melanoma, a rare subtype of melanoma that has a very high mutational load arising from chronic ultraviolet light–induced point mutations (*31*). In these cases, response rates are now 50 to 90%. A second group of cancers with relatively high response rates are carcinogen-induced cancers, such as the more common variants of melanoma arising from intermittently exposed skin, where upfront response rates are presently in the range of 35 to 40%, and a series of cancers associated with the carcinogenic effects of cigarette smoking, such as NSCLC and head and neck, gastroesophageal, and bladder and urothelial cancers, with response rates in the range of 15 to 25% (*26*, *32*–*34*). The other two approvals of single-agent anti–PD-1 therapies are in hepatocellular

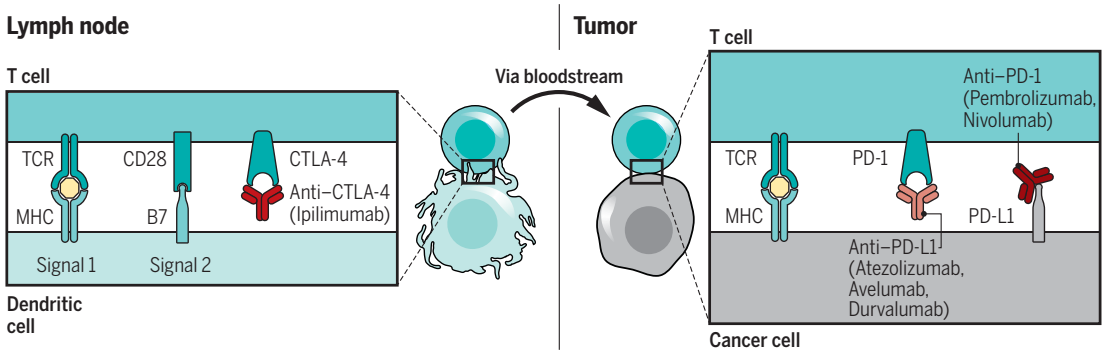

Fig. 1. Blockade of CTLA-4 and of PD-1 and PD-L1 to induce antitumor responses. (**Left**) CTLA-4 is a negative regulator of costimulation that is required for initial activation of an antitumor T cell in a lymph node upon recognition of its specific tumor antigen, which is presented by an antigen-presenting cell. The activation of CTLA-4 can be blocked with anti–CTLA-4 antibodies. (**Right**) Once the T cells are activated, they circulate throughout the body to find their cognate antigen presented by cancer cells. Upon recognition, the triggering of the TCR leads to the expression of the negative regulatory receptor PD-1, and the production of IFN-γ results in the reactive expression of PD-L1, turning off the antitumor T cell responses. This negative interaction can be blocked by anti–PD-1 or anti–PD-L1 antibodies.

carcinoma, with its known relationship to hepatitis virus infection (*35*), and renal cell carcinoma (*36*), which has a low single-nucleotide mutational load but a higher frequency of indels than other common cancers, resulting in increased immunogenicity (*37*).

Once an objective tumor response has been achieved, most remain durable. As opposed to targeted oncogene therapies, in which most tumor responses last until the cancer develops a way to reactivate the pathway or alternate oncogene signaling to bypass the blocked oncogene, in cancer immunotherapies, the rate of relapse is lower. It was hoped that immunotherapy could induce long-lasting responses, because of the ability of T cells to maintain memory to their target, and a polyclonal response that the cancer should have trouble escaping. However, primary refractoriness and acquired resistance after a period of response are major problems with checkpoint blockade therapy [reviewed in (*38*)].

Single-agent PD-1–pathway blockade has a relatively favorable toxicity profile, with toxicities requiring medical intervention (grades 3 to 4) in the range of 10 to 15% in most series (*22*, *26*, *27*, *33*, *39*). Most patients treated with single-agent anti–PD-1 or anti–PD-L1 antibodies have no toxicities above what would be expected from placebo, and treatment-related deaths are very uncommon. Very few patients (~5%) discontinue therapy because of toxicities. The most common treatment-related adverse events of any grade are fatigue, diarrhea, rash, and pruritus in 15 to 20% of patients (*22*, *26*, *27*, *33*, *39*). In a smaller percentage of patients, toxicities are more serious and include several endocrinopathies, in which the immune system infiltrates a hormone-producing gland, leading to permanent dysfunction that requires lifelong substitutive hormonal therapy, such as thyroid disorders (10 to 15%), hypophysitis, adrenal gland disorders (1 to 3%), and type 1 diabetes (1%). Serious visceral organ inflammatory toxicities are uncommon (~1%) but can affect any organ, including the brain (encephalopathy), meninges (meningitis), lung (pneumonitis), heart (myocarditis), gastrointestinal tract (esophagitis, colitis), liver (hepatitis), and kidney (nephritis), in addition to muscles (myositis) and joints (arthritis). These can be life-threatening. The cornerstone of treatment for clinically relevant toxicities with both PD-1– and CTLA-4–blockade therapies is immune suppressive therapy, with high doses of corticosteroids, and sometimes tumor necrosis factor antagonists (which are counter-indicated in patients with hepatitis) and mycophenolate mofetil (*6*).

Mechanisms of response and resistance to single-agent PD-1 therapy

Most of the data support a model in which patients respond to single-agent anti–PD-1 or anti–PD-L1 therapy because of a preexisting antitumor T cell response. Such a response retains therapeutic potential until the infiltrating T cells engage their TCR through recognition of a tumor antigen, triggering expression of PD-1 on T cells and release of IFN-γ, resulting in reactive expression of PD-L1 by cancer-resident cells (*16*–*18*, *31*, *40*, *41*) (Fig. 3). This process, termed adaptive immune resistance, occurs when tumor cells disarm specific T cells through PD-L1 expression (*17*, *18*). It results in a specific state of immune privilege that does not require a systemic immune deficiency and is reversible simply by blocking the PD-1–PD-L1 interaction (*41*) (Fig. 3).

The first step in this mechanism is the differential recognition of cancer cells from normal cells by the immune system, in a situation in which the cancer cells had autovaccinated the patient to induce a specific T cell response. The most common mechanism for this differential recognition is related to the increased mutational load in cancers (*41*, *42*). However, not all mutations seem to have the necessary qualities to give rise to robust targets of an antitumor immune response. Mutations that appear in the founder cancer cell and are carried on by most of the progeny cells (clonal mutations) are favorable, whereas mutations that appear later in the course of the cancer and may vary among different cancer cells (subclonal mutations) are not sensitive to PD-1 blockade (*43*). The processing and presentation by major histocompatibility complex (MHC) molecules of neoepitopes that result from mutations further shapes the landscape of neoantigens recognized by antitumor T cells (*44*, *45*).

The most common reason why a cancer would not have preexisting T cell infiltration is likely a state of low immunogenicity resulting from a lack of mutations that become recognized neoantigens

Table 1. Major indications approved for the use of anti–PD-1 and anti–PD-L1 therapies and the suspected mechanism of action of the antitumor response.

Group	Indication	Objective response rate (%)	Agents approved*	Main driver of response
High response rate	Hodgkin's disease	87	nivolumab pembrolizumab	PDJ amplicon
	Desmoplastic melanoma	70	nivolumab pembrolizumab	Mutations from chronic sun exposure
	Merkel cell	56	avelumab pembrolizumab	Merkel cell virus
	MSI-h cancers	53	nivolumab pembrolizumab	Mutations from mismatch-repair deficiency
Intermediate response rate	Skin melanoma	35 to 40	nivolumab pembrolizumab	Mutations from intermittent sun exposure
	NSCLC	20	atezolizumab nivolumab pembrolizumab	Mutations from cigarette smoking
	Head and neck	15	nivolumab pembrolizumab	Mutations from cigarette smoking
	Gastroesophageal	15	pembrolizumab	Mutations from cigarette smoking
	Bladder and urinary tract	15	atezolizumab avelumab durvalumab nivolumab pembrolizumab	Mutations from cigarette smoking
	Renal cell carcinoma	25	nivolumab pembrolizumab	Insertions and deletions (indels)
	Hepatocellular carcinoma	20	nivolumab	Hepatitis virus

*In alphabetical order

(*42*), or an active means of T cell exclusion (*38*). Certain cancer phenotypes resulting from expression of specific transcriptomic programs may contribute to the lack of T cell recognition, such as expression of genes of the Wnt pathway (*46*) or a series of partially overlapping gene sets that are related to stemness, mesenchymal transition, and wound healing, collectively termed IPRES (for innate anti–PD-1 resistance) because they are enriched in biopsies of patients with melanoma that does not respond to anti–PD-1 therapy (*47*). It is also possible that antitumor T cells are impaired by earlier checkpoints, such as CTLA-4, or immune suppressive cells in the tumor microenvironment, such as myeloid lineage cells or T_{regs} (*38*).

The expression of PD-L1 by cells within a cancer was explored as a biomarker to identify patients who may be more likely to respond to PD-1–blockade therapies (*25*, *26*, *48*). PD-L1 is most frequently expressed reactively upon T cell infiltration and sensing of IFN-γ production, in which case it could be considered a "canary in a coal mine," where its presence is a surrogate for a preexisting T cell response (Fig. 3). In this setting, colocalization of PD-L1, PD-1, and $CD8^+$ T cells in an area of the tumor termed the invasive margin is associated with response to PD-1 blockade (*31*, *49*). PD-L1 can also be expressed constitutively through a series of processes, and it is currently unclear if the mere presence of PD-L1 without detecting a T cell infiltrate is a favorable or detrimental event for PD-1–blockade therapy. Therefore, tumors that may be strongly positive for PD-L1, but do not contain a preexisting cytotoxic $CD8^+$ T cell response, would be unlikely to respond to therapy. The notable exception is Hodgkin's lymphoma, in which the Reed-Stenberg cells have the PDJ amplicon, resulting in constitutive PD-L1 expression (*29*). Of note, this is a cancer that is notorious for both a reactive T cell infiltrate mostly composed of CD4 T helper cells and Reed-Stenberg cells that are frequently deficient in β_2-microglobulin (β_2M), the required subunit for surface expression of MHC class I (*50*). These facts are at odds with the notion that PD-1–blockade therapy mainly reactivates preexisting intratumoral MHC class I–restricted $CD8^+$ T cells.

Once a tumor is immunogenic enough to trigger a specific T cell response, the cancer cells may undergo a series of genetic and nongenetic processes to avoid being eliminated by the immune system, termed cancer immunoediting (*51*). Cancer immunoediting may result in the loss of mutations that are most immunogenic or the mutation or decreased expression of genes involved in the antigen-presentation pathway. Any of these events would be expected to result in primary resistance to PD-1 blockade or lead to acquired resistance, if they developed during therapy. Strong immune selective pressure can lead to a shaping of the mutational landscape of cancer (*44*, *45*, *52*), specific deletion of human leukocyte antigen (HLA) class I alleles that putatively present strong neoantigens (*45*), or loss of β_2M (*53*–*55*). Genetic immunoediting events that can be found at baseline, and, in particular, homozygous loss-of-function mutations in the gene encoding β_2M, have been reported to be associated with both primary and acquired resistance to PD-1 blockade (*53*–*55*).

The process that leads to the reactive expression of PD-L1 upon T cell attack of cancer is mediated by IFN-γ pathway signaling (*16*, *19*, *21*) (Fig. 3). If the cancer cell is unable to sense IFN-γ and signal through the pathway, then PD-L1 will not be reactively expressed. In this setting, it could be futile to give antibodies blocking the PD-1–PD-L1 interaction (*19*, *21*, *56*). Within the IFN-γ receptor pathway, the bottleneck for signaling seems to be JAK1 and JAK2, as absence of either one results in complete lack of signaling (*19*, *21*). Homozygous loss-of-function mutations in the *JAK1/2* genes are rare baseline events but are more frequent than would be expected randomly, suggesting an active immunoediting process to delete them (*21*, *57*). In the setting of fully inactivating *JAK1/2* mutations, patients do not respond to anti–PD-1 therapy (*21*, *57*). Mutating *JAK1/2* provides an advantage to the cancer cells, as it limits favorable effects of IFN-γ, such as increased expression of antigen-presenting machinery molecules, production of chemokines that potently attract other T cells to that area and amplify the immune response, or avoiding the direct antiproliferative effects of interferon (*56*). In some cases of acquired resistance to anti–PD-1 therapy, homozygous loss of *JAK1* or *JAK2* has been documented (*54*, *57*). These are rare genetic events that could explain a minority of cases

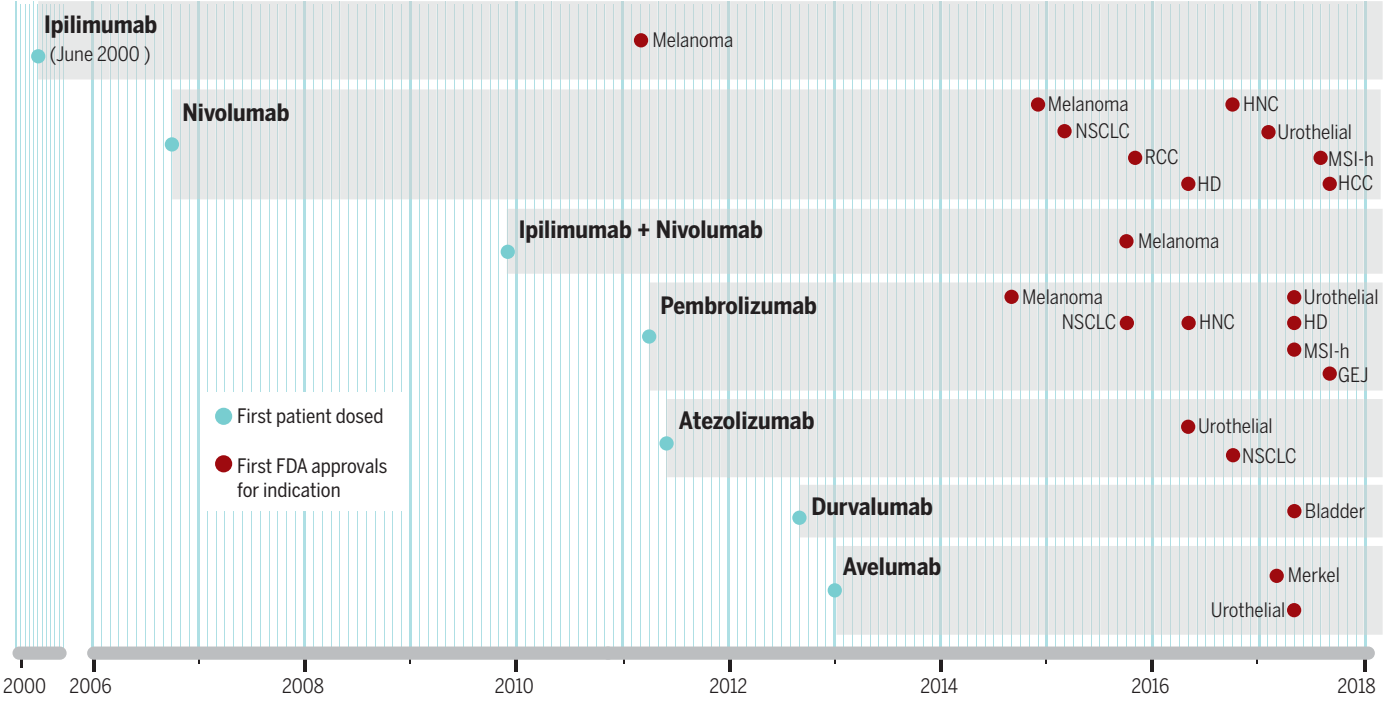

CREDITS (GRAPHIC): V. ALTOUNIAN/*SCIENCE*

Fig. 2. Timing of clinical development of anti–CTLA-4, anti–PD-1, and anti–PD-L1 antibodies, from first administration to humans to FDA approval. Thus far, there has been drug regulatory approval for six antibodies that block immune checkpoints and a combination of two immune checkpoint-blocking antibodies. The gray shading represents the period of clinical development for each of these antibodies, from the dosing of the first patient until regulatory approval (red circles) in different indications. HNC, head and neck cancer; RCC, renal cell carcinoma; MSI-h, high microsatellite instability; HD, Hodgkin's disease; HCC, hepatocellular carcinoma; GEJ, gastroesophageal junction.

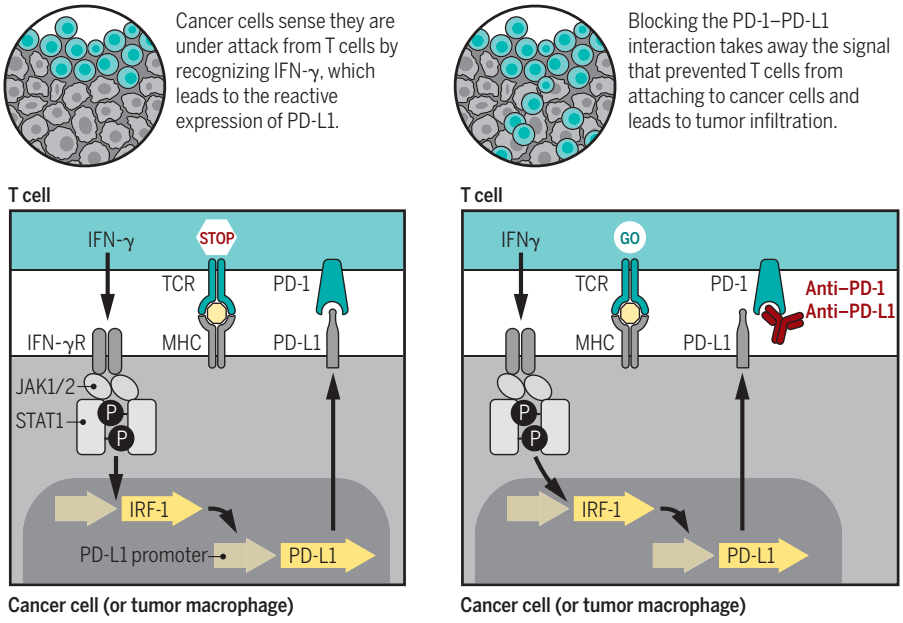

Fig. 3. Mechanism of action of PD-1–blockade therapy. (**Left**) TCR recognition of the cognate antigen presented by MHC molecules on the surface of cancer cells results in T cell activation. T cells then produce IFN-γ and other cytokines. Cancer cells and other cells in the tumor microenvironment have IFN-γ receptors (IFN-γR) that signal through JAK1/2, which phosphorylate (P) and activate signal transducers and activators of transcription (STAT) proteins that dimerize and turn on a series of interferon-response genes, including interferon regulatory factor 1 (IRF-1), which binds to the promoter of PD-L1, leading to its surface expression. The reactive expression of PD-L1 turns off the T cells that are trying to attack the tumor, and these T cells remain in the margin of the cancer. (**Right**) Blockade of the PD-1–PD-L1 interaction with therapeutic antibodies results in T cell proliferation and infiltration into the tumor, inducing a cytotoxic T cell response that leads to an objective tumor response.

with primary or acquired resistance to PD-1 blockade, and they highlight the ability to mechanistically understand these processes. This body of data suggests that molecular mechanisms of resistance to anti–PD-1 therapy converge in alterations in the antigen-presentation machinery and the IFN-γ receptor pathway, an observation recently confirmed in unbiased CRISPR-Cas9 screens in preclinical models (*58*, *59*).

The current understanding of response and resistance to PD-1–blockade therapy suggests that there cannot be a single biomarker to select patients. Therefore, selection of patients who are highly likely to respond to single-agent anti–PD-1 therapy (as opposed to being exposed to the greater toxicity and expense of combined therapy) would require a combination of studies in baseline tumor biopsies with sufficient tissue to include: (i) DNA analyses for tumor mutational load and absence of deleterious mutations in key immune signaling pathways, (ii) RNA analyses to detect the presence or absence of IFN-γ signaling and a favorable tumor phenotype, and (iii) morphological analyses documenting the colocalization of $CD8^+$ T cells expressing PD-1 and interacting with reactively expressed PD-L1 in the tumor microenvironment. However, such extensive testing is currently not done routinely and in a timely enough manner to inform therapeutic decisions in patients with advanced cancer.

Combination CTA-4 and PD-1–blockade therapy

In December 2009, the first patient was treated with combination checkpoint blockade by using ipilimumab to block CTLA-4 and concurrent nivolumab to block PD-1 (Fig. 2). This was designed on the basis of the nonredundant coinhibitory roles of the two pathways, after preclinical studies showed evidence of synergy in syngeneic mouse models (*60*). Further, the distinct immune microenvironments in which CTLA-4 and PD-1–pathway blockade could act provided an additional mechanistic rationale (Fig. 1). CTLA-4 is mainly associated with affecting inhibitory cross-talk in the draining lymph node. Although PD-1 blockade may also have activity in that immunologic space, the presence of PD-L1 on tumor and immune cells in the immediate tumor microenvironment provides an additional anatomic venue for activity (Fig. 1). Most recently, by using mass cytometry (or CyTOF), the Allison lab has shown that CTLA-4 and PD-1 blockade results in distinct phenotypic signatures in T cell subsets (*61*). The initial phase 1 dose-ranging trial of ipilimumab plus nivolumab was conducted in patients with metastatic melanoma and demonstrated a >50% objective response rate in the dose level that was chosen to move to phase 2 and 3 trials (*60*). Importantly, this was associated with a higher frequency of high-grade immune-related toxicities (up to 60%) in comparison to data from monotherapy trials. Phase 2 and 3 studies of the combination of ipilimumab plus nivolumab confirmed a response rate of approximately 60%, and the most recent analysis showed that patients initially randomized to the combination had a slightly higher 3-year survival than patients initially receiving nivolumab alone (58 versus 52%), yet with higher frequency of toxicity (*23*). Initial attempts to identify which patients require the combination have focused on tumor expression of PD-L1 and do suggest that patients with tumors that have little or no PD-L1 expression (<1% of tumor cells with surface staining) have improved survival with combination therapy compared to that with nivolumab alone. Ongoing trials are examining an adaptive dosing regimen with early assessment for response in an attempt to minimize the dosage of the combination and reduce toxicity (NCT03122522).

Other combination therapies and conclusions

Immune checkpoint–blocking antibodies are actively being investigated in combination with an ever-widening spectrum of agents. Although the goal of such investigations—to increase the number of patients who may benefit from this type of therapy—is laudable, the sometimes empiric manner of how agents are brought together is leading to an unrealistic number of trials and expected volunteers, making it unlikely that all hypotheses will be robustly answered. Yet, there are some combination strategies that are in late-stage development and are mechanism based. The description of cellular and molecular mechanisms of primary and acquired resistance to checkpoint blockade therapy allows for designing combination immunotherapy approaches to overcome these resistance mechanisms. In the setting of low preexisting levels of T cells in the tumor, besides the combination of anti–CTLA-4 and anti–PD-1 therapies, other potential approaches include changing the tumor microenvironment by direct injection of interferon-inducing molecules such as toll-like receptor agonists or oncolytic viruses, blocking T cell–excluding proteins like indoleamine 2,3-dioxygenase or arginase, or inhibiting immune suppressive cells like T_{regs} or macrophages [reviewed in (*60*)]. Furthermore, other modes of cancer therapy, such as radiotherapy, chemotherapy, or oncogene-targeted therapies, have been shown to change the immune suppressive tumor microenvironment and potentially synergize with immune checkpoint blockade therapy [reviewed in (*60*)]. Building on recent success in this field is important, but continuing to incorporate the emerging knowledge from mechanistic basic-science studies is critical to achieve greater therapeutic success.

REFERENCES AND NOTES

1. C. A. Chambers, M. S. Kuhns, J. G. Egen, J. P. Allison, *Annu. Rev. Immunol.* **19**, 565–594 (2001).
2. D. R. Leach, M. F. Krummel, J. P. Allison, *Science* **271**, 1734–1736 (1996).
3. T. L. Walunas *et al.*, *Immunity* **1**, 405–413 (1994).

4. F. S. Hodi *et al.*, *Proc. Natl. Acad. Sci. U.S.A.* **100**, 4712–4717 (2003).
5. A. Ribas *et al.*, *J. Clin. Oncol.* **23**, 8968–8977 (2005).
6. M. A. Postow, R. Sidlow, M. D. Hellmann, *N. Engl. J. Med.* **378**, 158–168 (2018).
7. D. Schadendorf *et al.*, *J. Clin. Oncol.* **33**, 1889–1894 (2015).
8. Z. Eroglu *et al.*, *Eur. J. Cancer* **51**, 2689–2697 (2015).
9. J. D. Wolchok *et al.*, *Clin. Cancer Res.* **15**, 7412–7420 (2009).
10. F. S. Hodi *et al.*, *N. Engl. J. Med.* **363**, 711–723 (2010).
11. C. Robert *et al.*, *N. Engl. J. Med.* **364**, 2517–2526 (2011).
12. A. Snyder *et al.*, *N. Engl. J. Med.* **371**, 2189–2199 (2014).
13. E. M. Van Allen *et al.*, *Science* **350**, 207–211 (2015).
14. B. C. Carthon *et al.*, *Clin. Cancer Res.* **16**, 2861–2871 (2010).
15. Y. Ishida, Y. Agata, K. Shibahara, T. Honjo, *EMBO J.* **11**, 3887–3895 (1992).
16. S. H. Baumeister, G. J. Freeman, G. Dranoff, A. H. Sharpe, *Annu. Rev. Immunol.* **34**, 539–573 (2016).
17. D. M. Pardoll, *Nat. Rev. Cancer* **12**, 252–264 (2012).
18. A. Ribas, *Cancer Discov.* **5**, 915–919 (2015).
19. A. Garcia-Diaz *et al.*, *Cell Reports* **19**, 1189–1201 (2017).
20. D. R. Sen *et al.*, *Science* **354**, 1165–1169 (2016).
21. D. S. Shin *et al.*, *Cancer Discov.* **7**, 188–201 (2017).
22. C. Robert *et al.*, *N. Engl. J. Med.* **372**, 2521–2532 (2015).
23. J. D. Wolchok *et al.*, *N. Engl. J. Med.* **377**, 1345–1356 (2017).
24. M. Sznol *et al.*, *J. Clin. Oncol.* **28** (15_suppl), 2506 (2010).
25. S. L. Topalian *et al.*, *N. Engl. J. Med.* **366**, 2443–2454 (2012).
26. E. B. Garon *et al.*, *N. Engl. J. Med.* **372**, 2018–2028 (2015).
27. A. Ribas *et al.*, *JAMA* **315**, 1600–1609 (2016).
28. D. T. Le *et al.*, *Science* **357**, 409–413 (2017).
29. S. M. Ansell *et al.*, *N. Engl. J. Med.* **372**, 311–319 (2015).
30. P. T. Nghiem *et al.*, *N. Engl. J. Med.* **374**, 2542–2552 (2016).
31. Z. Eroglu *et al.*, *Nature* **553**, 347–350 (2018).
32. R. L. Ferris *et al.*, *N. Engl. J. Med.* **375**, 1856–1867 (2016).
33. J. E. Rosenberg *et al.*, *Lancet* **387**, 1909–1920 (2016).
34. J. Bellmunt *et al.*, *N. Engl. J. Med.* **376**, 1015–1026 (2017).
35. A. B. El-Khoueiry *et al.*, *Lancet* **389**, 2492–2502 (2017).
36. R. J. Motzer *et al.*, *N. Engl. J. Med.* **373**, 1803–1813 (2015).
37. S. Turajlic *et al.*, *Lancet Oncol.* **18**, 1009–1021 (2017).
38. P. Sharma, S. Hu-Lieskovan, J. A. Wargo, A. Ribas, *Cell* **168**, 707–723 (2017).
39. C. Robert *et al.*, *N. Engl. J. Med.* **372**, 320–330 (2015).
40. J. M. Taube *et al.*, *Sci. Transl. Med.* **4**, 127ra37 (2012).
41. C. U. Blank, J. B. Haanen, A. Ribas, T. N. Schumacher, *Science* **352**, 658–660 (2016).
42. T. N. Schumacher, R. D. Schreiber, *Science* **348**, 69–74 (2015).
43. N. McGranahan *et al.*, *Science* **351**, 1463–1469 (2016).
44. M. Łuksza *et al.*, *Nature* **551**, 517–520 (2017).
45. N. McGranahan *et al.*, *Cell* **171**, 1259–1271.e11 (2017).
46. S. Spranger, R. Bao, T. F. Gajewski, *Nature* **523**, 231–235 (2015).
47. W. Hugo *et al.*, *Cell* **165**, 35–44 (2016).
48. D. P. Carbone *et al.*, *N. Engl. J. Med.* **376**, 2415–2426 (2017).
49. P. C. Tumeh *et al.*, *Nature* **515**, 568–571 (2014).
50. J. Reichel *et al.*, *Blood* **125**, 1061–1072 (2015).
51. R. D. Schreiber, L. J. Old, M. J. Smyth, *Science* **331**, 1565–1570 (2011).
52. M. S. Rooney, S. A. Shukla, C. J. Wu, G. Getz, N. Hacohen, *Cell* **160**, 48–61 (2015).
53. M. Sade-Feldman *et al.*, *Nat. Commun.* **8**, 1136 (2017).
54. J. M. Zaretsky *et al.*, *N. Engl. J. Med.* **375**, 819–829 (2016).
55. S. Gettinger *et al.*, *Cancer Discov.* **7**, 1420–1435 (2017).
56. E. A. Bach, M. Aguet, R. D. Schreiber, *Annu. Rev. Immunol.* **15**, 563–591 (1997).
57. A. Sucker *et al.*, *Nat. Commun.* **8**, 15440 (2017).
58. R. T. Manguso *et al.*, *Nature* **547**, 413–418 (2017).
59. S. J. Patel *et al.*, *Nature* **548**, 537–542 (2017).
60. M. A. Postow, M. K. Callahan, J. D. Wolchok, *J. Clin. Oncol.* **33**, 1974–1982 (2015).
61. S. C. Wei *et al.*, *Cell* **170**, 1120–1133.e17 (2017).

ACKNOWLEDGMENTS

This work was supported by NIH grants R35 CA197633, P01 CA168585, and P30 CA016042 (A.R.) and R01 CA056821 and P30 CA008748 (J.D.W.), with additional support from the Ressler Family Fund, the Grimaldi Family Fund, and the Garcia-Corsini Family Fund (A.R.) and Swim Across America, Ludwig Cancer Research, the Hazen-Polsky Family Fund, the Hogan Family Fund, Live4Life Foundation, and the Etta Weinheim Fund (J.D.W.). Both authors are members of the Parker Institute for Cancer Immunotherapy.

10.1126/science.aar4060

REVIEW

Personalized vaccines for cancer immunotherapy

Ugur Sahin[1,2,3]* and Özlem Türeci[4]

Cancer is characterized by an accumulation of genetic alterations. Somatic mutations can generate cancer-specific neoepitopes that are recognized by autologous T cells as foreign and constitute ideal cancer vaccine targets. Every tumor has its own unique composition of mutations, with only a small fraction shared between patients. Technological advances in genomics, data science, and cancer immunotherapy now enable the rapid mapping of the mutations within a genome, rational selection of vaccine targets, and on-demand production of a therapy customized to a patient's individual tumor. First-in-human clinical trials of personalized cancer vaccines have shown the feasibility, safety, and immunotherapeutic activity of targeting individual tumor mutation signatures. With vaccination development being promoted by emerging innovations of the digital age, vaccinating a patient with individual tumor mutations may become the first truly personalized treatment for cancer.

Driver mutations promote the oncogenic process, whereas passenger mutations have long been considered as functionally irrelevant (*1*). Both types of mutations, however, can alter the sequence of proteins and create new epitopes, which are processed and presented on major histocompatibility complex (MHC) molecules. The sequence-altered proteins are termed "neoantigens," and their mutated epitopes that are recognized by T cells are called "neoepitopes" (*2*). Neoepitopes are absent from normal tissues and new to a given individual's immune system. In 1916, Ernest Tyzzer, who introduced the term "somatic mutation," recognized their role in the "acquisition of new immunogenic characteristics" by cancer cells (*3*). The idea of taking advantage of their "foreignness" and using mutations as targets against cancer has attracted generations of scientists. How to realize a specific targeting of cancer, however, has remained obscure since its proposal by Paul Ehrlich in 1909 (*4*).

In the 1950s, studies to understand why mice with syngeneic carcinogen-induced tumors are protected from rechallenge with the same cancer cells led to the concept of adaptive tumor immunity (*5*). In the 1970s, tumor-derived T cell clones were shown to recognize human tumor cell lines and were identified as cellular correlates of adaptive immunity. The molecular nature of tumor antigens remained unknown until cloning techniques were introduced in the late 1980s (*6*). Screening of patient tumor–derived expression libraries with autologous tumor-reactive $CD4^+$ or $CD8^+$ T cells revealed two categories of spontaneously recognized T cell antigens: (i) nonmutated proteins with tumor-associated expression and (ii) mutated gene products (*7*). An oncogenic loss-of-function mutation of cyclin-dependent kinase 4 (CDK4) was the first example of the latter category in humans (*8*).

However, the vast majority of discovered mutated antigens were unique to individual patients, and a viable concept for exploiting "personal" targets for therapy could not be envisaged. Therefore, in the 1990s and 2000s, nonmutated tumor antigens shared by patients were favored for cancer vaccine development, yet outcomes were disappointing. Technological and scientific breakthroughs brought somatic mutations back into focus. Next-generation sequencing (NGS) allows rapid sequencing of genomes at low cost. Together with dedicated bioinformatics tools, NGS enables comprehensive mapping of all mutations in a cancer (collectively called the "mutanome") and prediction of MHC molecule–binding neoepitopes. Neoepitope-specific T cells have been shown to be associated with durable clinical responses mediated by immune checkpoint blockade and adoptive transfer of autologous tumor-infiltrating lymphocytes (TILs) (*9*, *10*). Mutational burden, tumor immune cell infiltration, and survival correlate across various cancer types (*11*, *12*). Collectively, these findings strongly indicate that immune recognition of neoepitopes is clinically meaningful. However, profiling of individual cancer patients revealed spontaneous immune responses against only a small fraction of their mutations (<1%) (*13*), casting doubt on the immunogenicity of mutations per se. This led to the presumption that only tumors with a high mutational load, and accordingly a higher diversity of spontaneously occurring cancer-reactive T cell specificities, may qualify for neoantigen-based immunotherapy.

Preclinical studies and clinical translation of personalized mutanome vaccines

Whether the examples of mutated tumor rejection antigens were rare cases of incidental immunogenicity, or were the tip of the iceberg, remained unclear until systematic studies in syngeneic mouse models provided deeper insights. To address which portion of a mutation induced a neoepitope-specific immune response, our laboratory vaccinated mice with long peptides or antigen-encoding RNA, representing 50 mutations identified by NGS in their syngeneic tumor; a considerable fraction of the mutations were immunogenic and mediated tumor rejection (*14*, *15*). Notably, the vast majority of neoepitopes, accounting for 20 to 25% of the randomly selected mutations, were recognized by $CD4^+$ T helper cells. Vaccination with these neoepitopes resulted in growth control of advanced mouse tumors. Most cancers are constitutively MHC class II–negative, and recognition by $CD4^+$ T cells requires uptake and presentation of released tumor antigens by dendritic cells (DCs) in the tumor microenvironment or draining lymph node. As this mechanism should work most efficiently for highly expressed antigens, MHC class II binding prediction and expression thresholds of the mutated allele were combined to enrich for immune-dominant MHC class II neoepitopes. Mice were vaccinated with a computationally designed synthetic mRNA incorporating multiple predicted MHC class II neoepitopes. The mice experienced complete rejection of established tumors associated with strong $CD4^+$ T cell responses and a $CD8^+$ T cell response against an epitope not represented in the vaccine, indicating antigen spread (*15*).

In a concurrent study, the feasibility of using NGS and MHC class I prediction to identify MHC class I–restricted tumor rejection antigens was shown in a highly immunogenic mouse sarcoma model (*16*). The antitumor effect of checkpoint blockade in this model was mediated by neoepitope-specific $CD8^+$ T cells and was fully reproducible by vaccination with long synthetic peptides representing an identified neoepitope (*17*). Another study systematically tested protective antitumor activity of mutated 9-amino acid oligomer (9-mer) peptides in mice. The difference in predicted affinity for a given wild-type/mutant peptide pair, and the predicted conformational stability of MHC class I peptide interaction, were both found to positively correlate with the likelihood of the mutated peptide to be recognized by $CD8^+$ cytotoxic T lymphocytes (CTLs) (*18*). A combination of mass spectrometry and exome sequencing was shown to enrich for immune-dominant MHC class I neoantigens in mouse models (*19*).

Clinical translation from syngeneic mice to humans who have "one-of-a-kind" cancers is more complex because it requires personalization of the process, including identification of mutations, prediction of potential neoepitopes, and design and manufacture of the vaccine (Fig. 1). This was recently accomplished by three first-in-human studies in malignant melanoma patients (*20*–*22*). In one trial, three melanoma patients received autologous DCs loaded ex vivo with seven synthetic 9-mer peptides representing individual mutations of each patient predicted to bind to the frequent class I haplotype HLA-A2 (*20*). Vaccine-induced $CD8^+$ T cell immune responses with confirmed specificity for the respective immunogen were detected against 9 of the 21 peptides. However, recognition of autologous melanoma cells was not assessed, and the relevance of the vaccine responses remained unclear. Two subsequently

[1]Biopharmaceutical New Technologies (BioNTech) Corporation, 55131 Mainz, Germany. [2]TRON–Translational Oncology at the University Medical Center of Johannes Gutenberg University gGmbH, 55131 Mainz, Germany. [3]University Medical Center of the Johannes Gutenberg University, 55131 Mainz, Germany. [4]CI3 Cluster for Individualized Immunointervention e.V., 55131 Mainz, Germany.
*Corresponding author. Email: sahin@uni-mainz.de

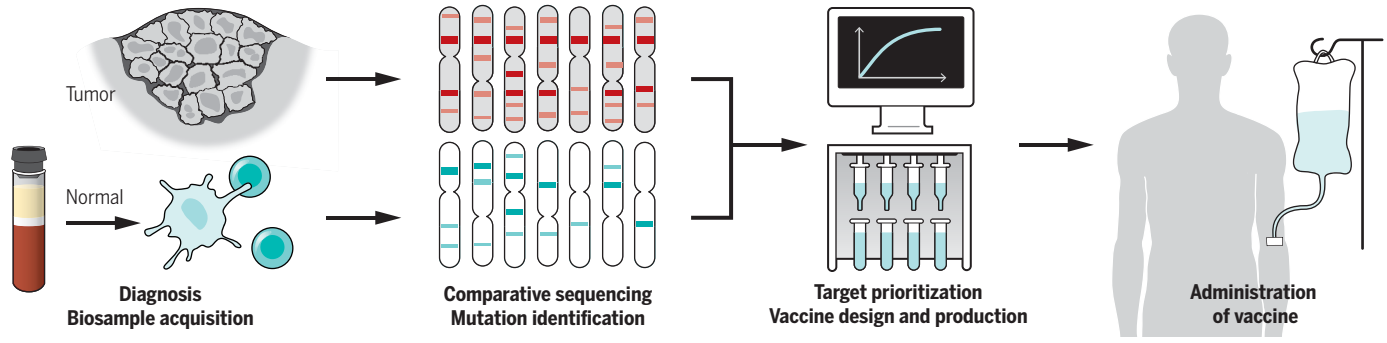

Fig. 1. Customizing a patient-specific cancer vaccine. Patient tumor biopsies and healthy tissue (e.g., peripheral blood white blood cells) are subjected to next-generation sequencing. By comparing the sequences obtained from tumor and normal DNA, tumor-specific nonsynonymous single-nucleotide variations or short indels in protein-coding genes are identified. A computational pipeline is used to examine the mutant peptide regions for binding to the patient's HLA alleles (based on predicted affinity) and other features of the mutated protein deemed relevant for prioritization of potential vaccine targets. These data can facilitate selection of multiple mutations to design unique neoepitope vaccines that are manufactured under GMP conditions.

reported clinical trials in resected stage III-IV melanoma patients exploited the broader potential of the concept irrespective of the HLA haplotype. In one trial, six patients were vaccinated subcutaneously with long peptides representing up to 20 mutations per patient coadministered with adjuvants (*21*). In the second trial, 13 patients were injected with RNA encoding 10 of their individual mutations as 27-mers (*22*). Thus, induction of T cell responses in both studies required processing and presentation of neoepitopes by the patient's antigen-presenting cells. Both studies showed a high overall immunogenicity rate of 60%, as demonstrated by analyzing T cell responses against the individual mutations in interferon-γ (IFN-γ) secretion assays. Each patient developed strong T cell reactivity against several of their tumor mutations. Preexisting T cells were expanded; moreover, the majority of vaccine-induced T cell responses in both studies were newly primed and not detectable before vaccination.

In accordance with the preclinical findings, the majority of neoepitopes induced functional $CD4^+$ T helper 1 (T_H1) cells, both in the RNA trial (which combined MHC class I and class II prediction for neoepitope selection) and in the peptide trial (which relied on MHC class I binding prediction only). Neoepitope-specific $CD8^+$ T cell responses were detected against 25% versus 16% of the mutations in the RNA or the peptide vaccine, respectively. In most cases, the identified minimal epitopes recognized by these $CD8^+$ T cells showed a strong predicted binding affinity, supporting the usefulness of this criterion for neoepitope prioritization. In the RNA trial, multiple $CD8^+$ responses were of high magnitude, allowing detectability without prior expansion. A number of neoepitopes were also concurrently recognized by both $CD4^+$ and $CD8^+$ T cells, the meaning of which is currently unclear. Both trials showed recognition of autologous tumor cell lines for selected vaccine-induced immune responses. In two RNA-vaccinated patients, there was evidence of CTL infiltration and tumor cell killing with neoepitope-specific T cells.

Despite the small cohort sizes, these studies provide intriguing evidence for clinical activity of the vaccine alone and in combination with subsequently administered checkpoint inhibitors. In the RNA trial, vaccination significantly reduced the cumulative number of disease recurrences in the 13 high-risk melanoma patients, translating to a long progression-free survival. Eight of the patients did not have radiographically detectable lesions at study entry and remained recurrence-free for the entire follow-up period. In five patients with progressing disease at entry, there were two objective responses attributable to the vaccine alone (one complete, one partial response), one mixed response, and one stable disease. One patient discontinued vaccination because of fast progression and had a rapid complete remission after subsequent checkpoint blockade therapy. In the peptide trial, four of six vaccinated patients remained recurrence-free for the full follow-up period, while two developed progressive disease and achieved complete tumor regression after subsequent anti–PD-1 treatment.

"...a personalized mutanome vaccine has the potential to become a universally applicable therapy irrespective of cancer type."

Using neoantigens to stimulate tumor immunity

Whereas clinical oncology has relied on targeting oncogenic pathways for decades, lessons learned in recent years by studying immunotherapy-mediated durable clinical responses have indicated that mobilization of the host's immune system represents a powerful therapeutic modality. In cancer patients, the complex interactions between immune system and tumor are considered dysfunctional. A key principle of rational immunotherapy is to restore this process, known as the cancer immunity cycle (*23*, *24*), and to expand and broaden the CTL response against cancer cells (Fig. 2). For many years, tumor rejection has mainly been attributed to cytotoxic $CD8^+$ T cells, and vaccine approaches have relied on potential MHC class I epitopes. There is a growing body of data, however, indicating that neoantigen-specific $CD4^+$ T cells contribute critically to the effectiveness of cancer immunotherapy (*25*). As the cancer mutanome turned out to provide an exceptionally rich source for potent MHC class II neoepitopes, mutanome vaccines have potential for mobilizing the broad repertoire of T_H1 $CD4^+$ T cells (*15*).

Whereas the primary mode of action of $CD8^+$ effectors is cytotoxic killing of cells presenting their cognate antigen (*26*), $CD4^+$ effectors have a wider range of functions, including orchestration of various cell types of the adaptive and innate immune system (*27*). $CD4^+$ T cells are gatekeepers for the induction of effective $CD8^+$ T cells. T_H1 $CD4^+$ T cells in different compartments activate DCs presenting antigens released from tumor cells through cognate CD40 ligand/CD40 receptor interaction. DCs then undergo maturation, produce interleukin-12 and chemoattractants, and up-regulate costimulatory molecules. These events are characteristically linked to the generation of sustained CTL responses to tumor antigens, which are released by tumor cell death and cross-presented. Multi-neoepitope vaccines have been shown to concurrently mobilize neoantigen-specific $CD8^+$ as well as $CD4^+$ T cells, and by furnishing collaborative synergy they may actuate a non-performing cancer immunity cycle at several key points (Fig. 2): In the priming phase of the vaccine

response in the lymphatic compartment, effective licensing of DCs by T_H1 cells can robustly induce potent neoepitope-specific CTLs with improved ability to infiltrate into the tumor and can generate long-lived memory $CD8^+$ T cells (*28*). In the tumor, vaccine-induced T_H1 $CD4^+$ T cells may promote an inflammatory microenvironment by acting on various immune cell types (*15*, *29*). IFN-γ, the key cytokine of T_H1 cells, up-regulates MHC class I on tumor cells to improve killing by $CD8^+$ effectors. Concurrently, by inducing MHC class II expression, IFN-γ sensitizes tumor cells for recognition and direct killing by cytotoxic T_H1 $CD4^+$ effectors. Overall, by promoting tumor cell death and neoantigen release for uptake by DCs in combination with an immunogenic microenvironment, $CD4^+$ T cells may crank up consecutive cycles of T cell priming, expansion, and antigen spread, thus broadening the antitumor T cell repertoire.

Mutation discovery, neoepitope prediction, and selection of target antigens for vaccine design

One of the critical challenges for personalized cancer vaccines is to accurately map the cancer mutanome, so as to select the most suitable mutations for optimal immune responses. Mutations are detected by comparing exome sequencing data generated by NGS from tumor tissue and a matched healthy tissue sample (e.g., the patient's blood cells), thereby preventing the incorrect classification of germline variants as neoepitopes. NGS analysis is being continuously improved, and clinical application requires standard operating procedures that ensure data reproducibility, quality control, and privacy. Current protocols allow efficient nucleic acid extraction in NGS-grade quality from fresh, frozen, and formalin-fixed paraffin-embedded tissues. Typically, these analyses rely on a small biopsy from a single tumor lesion collected for routine diagnostics, and thus sequence data may not be representative of the tumor's full clonal spectrum. Another concern to be addressed is erroneous mutation determination. Standardized algorithms to sensitively determine true mutations in individual NGS data sets work well for single-nucleotide variations (SNVs). SNVs are the most abundant type of tumor mutations, and if they occur in an expressed protein and are nonsynonymous, they can give rise to T cell–recognized neoepitopes. Other mutation types of potential relevance are gene fusions or small insertions and deletions (indels) that can lead to highly immunogenic frameshifts (*30*). Besides these well-defined mutation classes, less characterized cancer-associated epigenetic, transcriptional, translational, or posttranslational aberrations may generate neoepitopes and expand the discovery space for vaccine targets considerably (*31*). Their cancer specificity and usability as neoantigens are difficult to assess with existing technologies and are currently under investigation.

The processing and presentation of antigens is a complex, multistep process following stochastic principles in which protease cleavage products of thousands of proteins compete for binding into

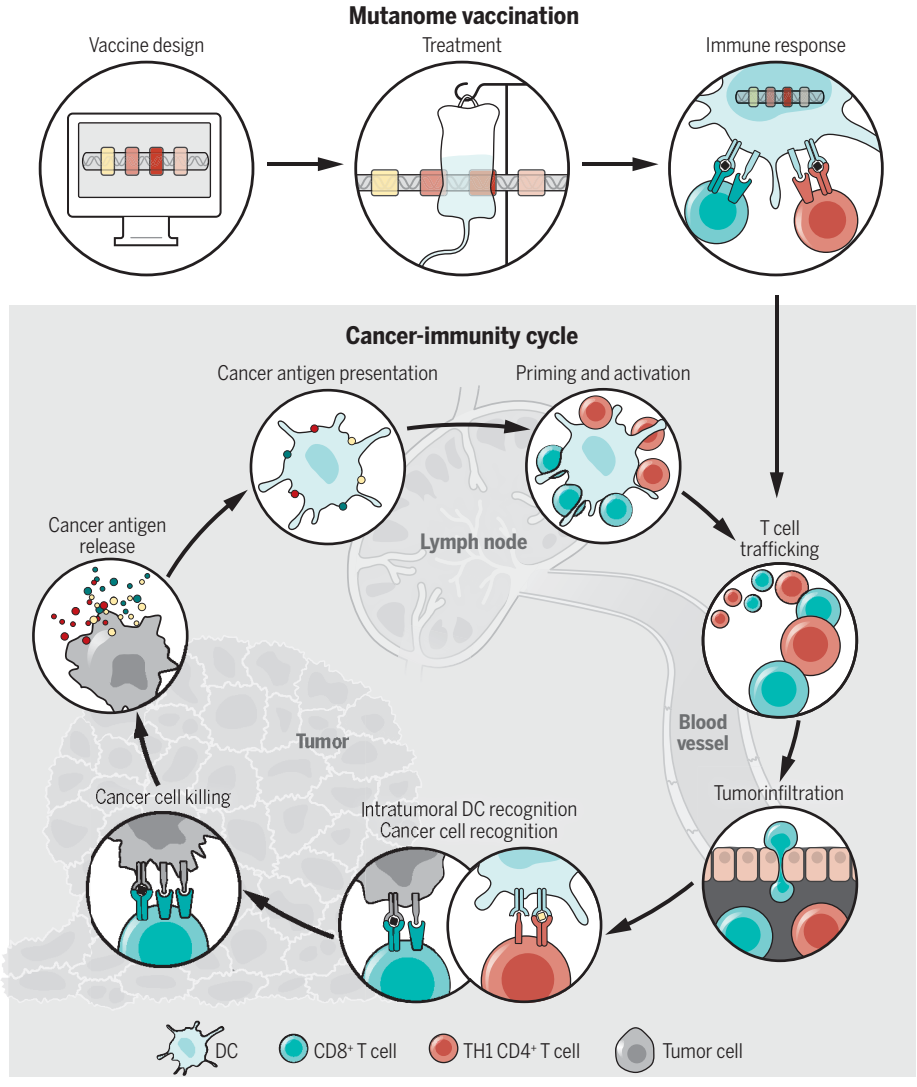

Fig. 2. Neoepitope vaccines promote a functional cancer immunity cycle. The goal of cancer immunotherapy is to ensure self-propagating revolution of the dysregulated cancer immunity cycle through its various steps (*24*). Vaccine-induced neoepitope-specific $CD4^+$ T_H1 cells may intersect at discrete rate-limiting steps considered as potentially difficult to overcome. These include the promotion of T cell priming and expansion, proinflammatory reshaping of the tumor microenvironment, and recruitment of $CD4^+$ T cells for direct killing of tumor cells. By concomitantly inducing $CD8^+$ and $CD4^+$ T cell responses, multi-neoepitope vaccines may contribute to tipping the balance from tolerance toward productive immunity against tumor cells, rendering the cancer immunity cycle functional.

pockets of MHC molecules. Only a portion of mutated sequences are presented on MHC at levels sufficient to trigger an effective T cell response. Technical feasibility and costs limit the number of mutations that can be incorporated into a drug product. Selecting the mutations with the highest likelihood of immunogenicity and therapeutic relevance is critical for designing personalized vaccines. So far, there is no consensus on how to prioritize mutations in this regard. The minimum requirements are (i) expression of the mutated gene in the tumor, and (ii) its capability of producing a sequence-altered epitope presented on one of the patient's MHCs. NetMHC and IEDB consensus methods are most frequently used to estimate MHC binding and enrich for neoepitopes recognized by $CD8^+$ T cells [reviewed in (*32*)]. The stability of the MHC-peptide complex is considered a better predictor for immunogenicity than MHC binding affinity alone. However, the currently available prediction algorithms for MHC-peptide stability cover only a few MHC alleles and rely on small data sets. Only a fraction of mutant peptides predicted as high-affinity binders to human MHC class I alleles are naturally presented MHC class I ligands. Presentation on MHC class I is affected by the transcription level of the mutated gene. Generally, in mammalian cells, the gene expression level, the amount of translated protein, the cell surface density of MHC ligands derived from it, immune recognition, and lysis of the respective cell are all positively

correlated (*33*). Consequently, high expression can to some extent compensate for weak MHC class I binding and vice versa (*34*), which suggests that neoantigen prioritization can be achieved by combining predicted MHC class I binding and the expression level of the mutation. Expression levels can be mined from NGS data via the number of mRNA sequencing reads containing the mutation. However, not every mutant MHC class I ligand (that is presented) is immunogenic. Even so, the current class I prediction algorithms seem to enrich sufficiently for processed, strongly immunogenic CTL neoepitopes (*2*, *22*).

Accurate prediction of ligands binding to MHC class II is challenging. MHC II binds denatured proteins or large peptides that are subsequently trimmed, whereas MHC I relies on pre-generated, sized peptides. Because the binding groove of MHC II molecules is open at both ends, the length and binding register of peptides are less defined and thus less predictable. On the other hand, this may be one of the reasons for higher abundance of MHC class II binding epitopes relative to MHC class I binding epitopes, and may explain why MHC class II binding prediction efficiently enriches for immunogenic neoantigens. Depending on the affinity prediction cutoff, 70%, 45%, or 34% of mutations selected for a HLA class II binding score of <1, 1 to 10, or >10, respectively, induced neoepitope-specific $CD4^+$ T cell responses (*22*).

One concept currently being explored to enrich for tumor rejection–mediating neoantigens is to target mutations that are expressed across all clones within a heterogeneous tumor. This is expected to reduce the likelihood of outgrowth of antigen-negative clones and is supported by the observation that advanced non–small cell lung cancer and melanoma patients with tumors enriched for clonal neoantigens respond better to checkpoint blockade (*35*). An alternative explanation may be that subclonal antigens have occurred later in a tumor's life cycle, or under conditions of potent immunosuppression, which are less likely to generate immunity. This again would be better addressed by a vaccine combining mutations of various subclones and capable of de novo priming of immune responses. Inclusion of mutated driver genes critical for proliferation, survival, or metastasis of tumor cells into a multi-neoantigen vaccine may further mitigate immune editing of tumors. A caveat is that functional validation and authentication as a driver gene is not trivial.

In patients treated with immune checkpoint inhibitors, the composition of the gut microbiome affects the efficacy of cancer immunotherapy (*36*–*38*). A detailed discussion of the gut microbiome and immunotherapy is provided in a recent review (*39*). One explanation may be a direct effect of the microbiome on antitumor immunity—for example, T cell modulation by tertiary bile acids produced by specific microbial communities, or induction of inflammation by pattern recognition receptor signaling. Another explanation is molecular mimicry between microbial and cancer neoantigens. An interesting idea in this regard is that neoantigens sharing structural features with microbial antigens are more likely immune-dominant and recognized by the T cell receptor (TCR) repertoire evolutionarily optimized for the detection of pathogen-derived epitopes. Shared epitope-string patterns in neoantigens of patients responding to anti–CTLA-4 checkpoint blockade were hypothesized (*11*) but not confirmed in two meta-analyses in larger patient cohorts (*40*). Recent studies introduced a composite neoantigen quality model, which confers a clinically relevant stronger immunogenicity to neoantigens with (i) sequence homology with pathogen-derived peptides and (ii) stronger predicted HLA binding affinity of the neoepitope relative to its wild type (differential neoepitope presentation). When this "neoantigen quality" model was applied to cancer mutanome data from pancreatic cancer, lung cancer, and melanoma patient cohorts, it was capable of discriminating long- and short-term survivors (*41*, *42*).

Manufacturing and clinical application of personalized mutanome vaccines

A critical challenge for clinical application of personalized vaccines is the fast manufacturing

Table 1. Current vaccine formats explored for delivery of neoepitopes.

Vaccine format	Advantages	Challenges
Synthetic peptides (*45*)	Cell-free manufacturing Automated synthesis established Proven clinical activity of long peptides Compatible with a wide range of formulations to improve delivery Transient activity and complete degradation	Lack of clinical-grade manufacturability of a substantial portion of sequences High variability in the physicochemical properties of individual peptides, complicating manufacturing Irrelevant immune responses against artificial epitopes created by peptide degradation in the extracellular space
Messenger RNA (*46*)	Cell-free manufacturing Inherent adjuvant function via TLR7, TLR8, and TLR3 signaling Proven clinical activity Highly efficient systemic delivery into DCs established Transient activity and complete degradation All types of epitopes can be encoded	Fast extracellular degradation of mRNA if not protected by appropriate formulation Interpatient variability of TLR7-driven adjuvant activity
DNA plasmids (*47*)	Cell-free manufacturing Inherent adjuvant activity driven by TLR9 Cost-effective and straightforward manufacturing All types of epitopes can be encoded	Potential safety risks by insertional mutagenesis Successful transfection requires entry into nucleus, thereby limiting effective delivery of vaccines into DCs
Viral vectors (*48*) (adenoviral and vaccinia)	Strong immunostimulatory activity Extensive clinical experience with vector formats in the infectious disease field All types of epitopes can be encoded	Complex manufacturing Immune responses against components of the viral vector backbone, limiting successful in vivo vaccine delivery and efficacy
Engineered attenuated bacterial vectors (*49*) (*Salmonella*, *Listeria*)	Strong immunostimulatory activity Could be combined with plasmid DNA All types of epitopes can be encoded	Complex manufacturing and "sterility" testing Immune responses against bacterial components, limiting vaccine delivery and vaccine immunogenicity Potential safety risks due to delivery of live, replication-competent bacteria
Ex vivo antigen-loaded DCs (*50*)	Strong immunostimulatory activity Proven clinical efficacy of DC vaccines Can be loaded with various antigen formats	Higher costs and resources required for adoptive cell therapy approaches

and timely delivery of the individually tailored vaccine. The turnaround time for vaccine production depends on the vaccine format, which is also critical for the magnitude and quality of the induced immune response. Formats under consideration for personalized vaccines are long peptides, RNA, DNA plasmids, viral vectors, engineered bacteria, and antigen-loaded DCs (Table 1). The recently reported fully personalized clinical trials used either a mixture of peptides (15 to 30 amino acids in length) corresponding to the mutated sequences with poly-ICLC (carboxymethylcellulose, polyinosinic-polycytidylic acid, and poly-L-lysine double-stranded RNA) as adjuvant, or mRNA with intrinsic adjuvant activity and encoding a strand of multiple predicted neoepitopes. The overall timeline for good manufacturing practice (GMP)–compliant on-demand production, from the start of processing of the patient's sample for mutation discovery to vaccine release for administration, was about 3 to 4 months. Patients were treated with other standard or experimental compounds until their personal vaccine had been produced. For both peptide and mRNA vaccine platforms, reduction of lead times to less than 4 weeks is expected.

Another challenge is to define the most suitable clinical setting for mutanome vaccination. A therapeutic vaccine most likely works particularly well in the adjuvant or minimal residual disease settings, where tumor load is low and immune-suppressive mechanisms are not firmly established. Efficient control of a larger tumor load may require combination immunotherapies. Neoepitope vaccination can turn "cold" tumors into "hot" ones and mediate up-regulation of PD-L1 in the tumor microenvironment. Thus, it may extend application of anti–PD-1/PD-L1 therapies to patients without preexisting T cell response. This is particularly attractive for patients with a lower tumor mutational burden, who are less likely to have endogenous immunity to be unleashed by anti–PD-1/PD-L1 treatment. In addition, neoepitope vaccine–primed T_H1^+ and $CD8^+$ memory T cells may enhance durability of anti–PD-1/PD-L1–mediated effects by promoting robust memory responses. Clinical trials NCT02897765 and NCT03289962, evaluating PD-1/PD-L1 blockade in combination with neoepitope vaccination, are currently recruiting patients. Similarly, inhibition of factors such as CTLA4, LAG-3, TIM-3, IDO, or TGF-β, as well as stimulation of costimulatory molecules (e.g., OX40, GITR, CD137) and addition of T cell–agonistic cytokines, were preclinically shown to synergize with cancer vaccines. With regard to escape mechanisms, the risk of outgrowth of neoantigen loss variants can be mitigated by the multi-neoepitope–targeting nature of personalized mutanome vaccines. In contrast, selection of clones with defects in the antigen processing and presentation machinery (e.g., HLA or β_2-microglobulin loss) is likely to occur (*22*, *43*, *44*). This risk again can be addressed by combining mutanome vaccines with compounds that do not depend on intact MHC class I presentation. These could be, for example, bispecific T cell engagers or antibodies against cancer cell surface targets, which are capable of Fc-mediated activation of natural killer cells or of complement.

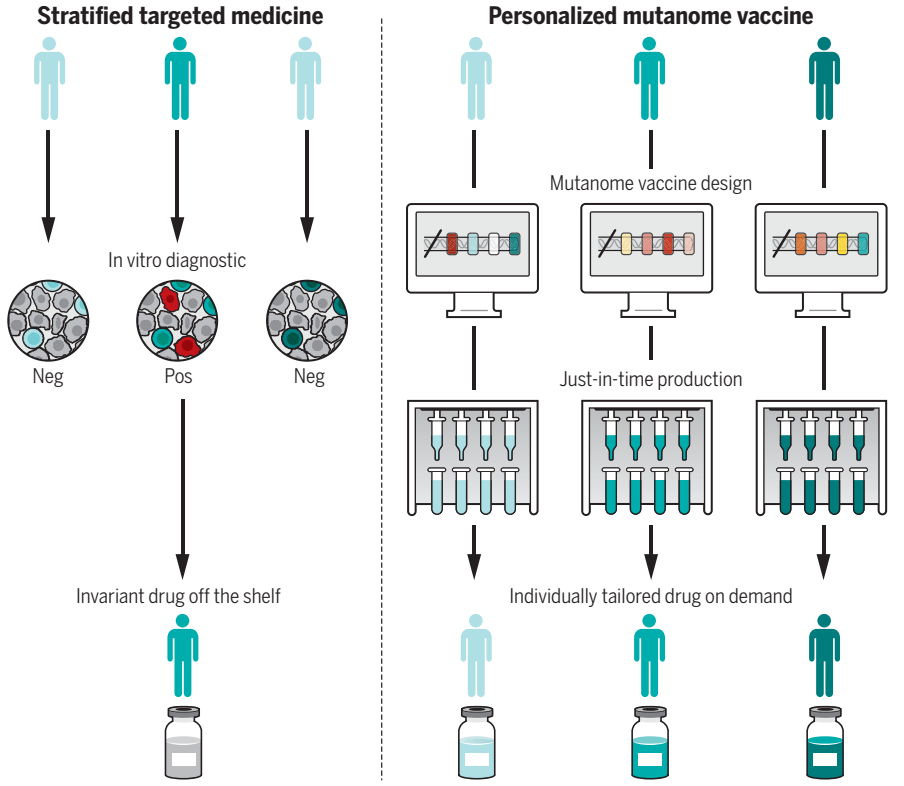

Fig. 3. Personalized cancer medicine. Left: Conventional stratified medicine matches a patient to an existing off-the-shelf drug using biomarker assays. Right: As opposed to a preformed drug, mutanome vaccination is a patient-specific therapy that targets cancer mutations per se, irrespective of their primary sequence. Thus, mutanome vaccines may qualify as universal and tailorable therapy from which each cancer patient may benefit.

The broader impact of realizing personalized mutanome vaccines

Mutanome vaccines may become the first therapeutic modality to truly realize personalized treatment of cancer. In the era dominated by the "one-size-fits-all" paradigm, stratified treatment has been considered a synonym for personalized medicine. However, this is not strictly the case. Stratified therapies identify patients carrying a defined biomarker (generally a shared cancer-driving genetic aberration) and subject them to a treatment targeting this biomarker. Unfortunately, such therapeutically targetable biomarkers are not available for most cancer types and are restricted to patient subsets. Thus, each stratified drug excludes the majority of patients who do not harbor the respective aberration (Fig. 3). In contrast, true patient-specific therapy should be achievable by neoantigen vaccination. The large repertoire of individual driver and passenger mutations (irrespective of their functional relevance) can be leveraged, and all patients with a sufficient frequency of cancer mutations could be offered their tailored and targeted treatment.

The number of somatic mutations in tumors ranges from less than 10 to several thousand, and they are largely unique for every patient. This is not the only dimension of heterogeneity (Fig. 4). A delicate interplay between the tumor and a set of host and environmental factors (e.g., HLA haplotype and other genetic polymorphisms, the microbiome, age, comorbidity, the immune cell repertoire, the composition of the tumor microenvironment), which define the immunological status ("cancer-immune set point"), shapes each individual cancer (*23*) (Fig. 4). Personalized mutanome vaccines hold promise to address tumor heterogeneity, which accounts for the failure of conventional anticancer treatments. A patient's vaccine composition can be directed against various clones because of its ability to target multiple epitopes within a tumor and can be adjusted upon tumor changes.

Concluding thoughts

Personalized cancer vaccines have moved beyond the first critical hurdle of clinical translation. Challenges remaining on the path forward include identifying the most suitable clinical settings, reducing production turnaround time, upscaling manufacturing, and ensuring affordability. New trends and technologies of the digital age, such as big data science, cloud and high-performance computing, and digitalized manufacturing solutions, are expected to add momentum. Predictive neoepitope algorithms will continue to improve by applying machine learning tools to big data sets.

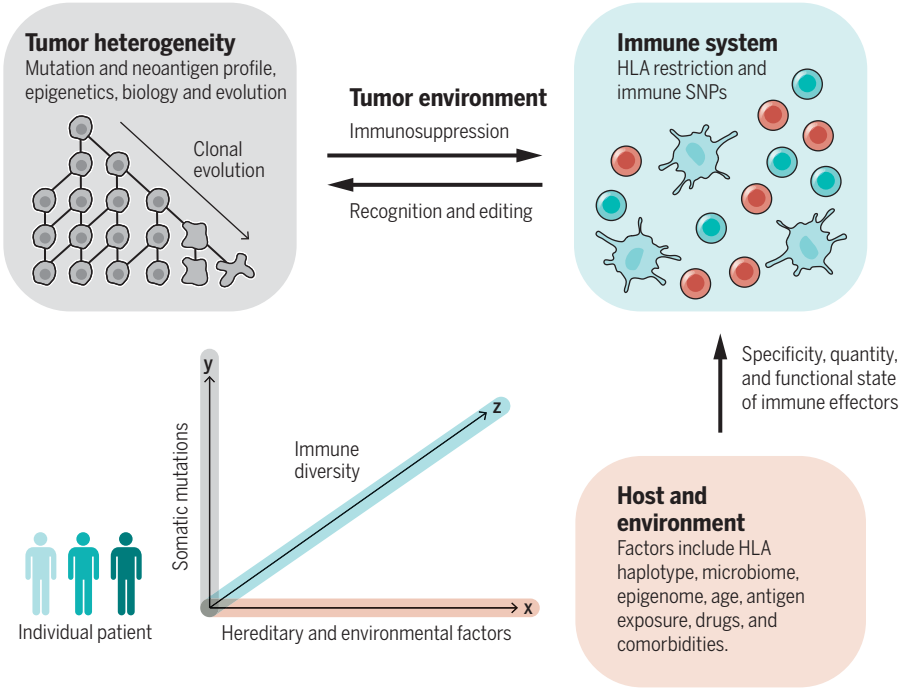

Fig. 4. The interconnected dimensions of cancer heterogeneity. The interaction between cancer and immune system is shaped by various host, tumor and environmental factors. The complex interplay of these sources of interpatient heterogeneity affects both the course of disease and the efficacy of immunotherapy, and calls for personalized approaches.

Higher-resolution analysis of tumors, the microenvironment, and immunity is becoming feasible by TCR repertoire analysis, high-throughput single-cell sequencing, and circulating tumor DNA detection. Computational inference of the phenotype and functional status of infiltrating cells from transcriptome data may support the selection of combination treatments. Lastly, insights into immunotherapy success or failure are expected to increase the spectrum of biomarkers for vaccine design and combination treatment. It is well worth the effort, as mutations constitute critical promoters of the oncogenic process and treatment failure and are the common denominator across all cancers. Therefore, a personalized mutanome vaccine has the potential to become a universally applicable therapy irrespective of cancer type.

REFERENCES

1. D. Hanahan, R. A. Weinberg, *Cell* **144**, 646–674 (2011).
2. T. N. Schumacher, R. D. Schreiber, *Science* **348**, 69–74 (2015).
3. E. E. Tyzzer, *J. Cancer Res.* **1**, 125–156 (1916).
4. P. Ehrlich, *Ned. Tijdschr. Geneeskd.* **5**, 273–290 (1909).
5. E. J. Foley, *Cancer Res.* **13**, 835–837 (1953).
6. P. van der Bruggen *et al.*, *Science* **254**, 1643–1647 (1991).
7. P. G. Coulie, B. J. Van den Eynde, P. van der Bruggen, T. Boon, *Nat. Rev. Cancer* **14**, 135–146 (2014).
8. T. Wölfel *et al.*, *Science* **269**, 1281–1284 (1995).
9. N. van Rooij *et al.*, *J. Clin. Oncol.* **31**, e439–e442 (2013).
10. P. F. Robbins *et al.*, *Nat. Med.* **19**, 747–752 (2013).
11. A. Snyder *et al.*, *N. Engl. J. Med.* **371**, 2189–2199 (2014).
12. N. A. Rizvi *et al.*, *Science* **348**, 124–128 (2015).
13. E. Tran *et al.*, *Science* **350**, 1387–1390 (2015).
14. J. C. Castle *et al.*, *Cancer Res.* **72**, 1081–1091 (2012).
15. S. Kreiter *et al.*, *Nature* **520**, 692–696 (2015).
16. H. Matsushita *et al.*, *Nature* **482**, 400–404 (2012).
17. M. M. Gubin *et al.*, *Nature* **515**, 577–581 (2014).
18. F. Duan *et al.*, *J. Exp. Med.* **211**, 2231–2248 (2014).
19. M. Yadav *et al.*, *Nature* **515**, 572–576 (2014).
20. B. M. Carreno *et al.*, *Science* **348**, 803–808 (2015).
21. P. A. Ott *et al.*, *Nature* **547**, 217–221 (2017).
22. U. Sahin *et al.*, *Nature* **547**, 222–226 (2017).
23. D. S. Chen, I. Mellman, *Nature* **541**, 321–330 (2017).
24. D. S. S. Chen, I. Mellman, *Immunity* **39**, 1–10 (2013).
25. E. Tran *et al.*, *Science* **344**, 641–645 (2014).
26. N. Zhang, M. J. Bevan, *Immunity* **35**, 161–168 (2011).
27. B. J. Laidlaw, J. E. Craft, S. M. Kaech, *Nat. Rev. Immunol.* **16**, 102–111 (2016).
28. E. M. Janssen *et al.*, *Nature* **421**, 852–856 (2003).
29. T. Schumacher *et al.*, *Nature* **512**, 324–327 (2014).
30. Ö. Türeci *et al.*, *Clin. Cancer Res.* **22**, 1885–1896 (2016).
31. C. M. Laumont, C. Perreault, *Cell. Mol. Life Sci.* **75**, 607–621 (2018).
32. X. S. Liu, E. R. Mardis, *Cell* **168**, 600–612 (2017).
33. M. Bassani-Sternberg, S. Pletscher-Frankild, L. J. Jensen, M. Mann, *Mol. Cell. Proteomics* **14**, 658–673 (2015).
34. J. G. Abelin *et al.*, *Immunity* **46**, 315–326 (2017).
35. N. McGranahan *et al.*, *Science* **351**, 1463–1469 (2016).
36. V. Gopalakrishnan *et al.*, *Science* **359**, 97–103 (2018).
37. B. Routy *et al.*, *Science* **359**, 91–97 (2018).
38. V. Matson *et al.*, *Science* **359**, 104–108 (2018).
39. L. Zitvogel, Y. Ma, D. Raoult, G. Kroemer, T. F. Gajewski, *Science* **359**, 1366–1370 (2018).
40. E. M. Van Allen *et al.*, *Science* **350**, 207–211 (2015).
41. V. P. Balachandran *et al.*, *Nature* **551**, 512–516 (2017).
42. M. Łuksza *et al.*, *Nature* **551**, 517–520 (2017).
43. C. M. D'Urso *et al.*, *J. Clin. Invest.* **87**, 284–292 (1991).
44. J. M. Zaretsky *et al.*, *N. Engl. J. Med.* **375**, 819–829 (2016).
45. C. J. M. Melief, in *Oncoimmunology*, L. Zitvogel, G. Kroemer, Eds. (Springer Cham, 2018), pp. 249–261.
46. N. Pardi, M. J. Hogan, F. W. Porter, D. Weissman, *Nat. Rev. Drug Discov.* 10.1038/nrd.2017.243 (2018).
47. J. Rice, C. H. Ottensmeier, F. K. Stevenson, *Nat. Rev. Cancer* **8**, 108–120 (2008).
48. K. J. Ewer *et al.*, *Curr. Opin. Immunol.* **41**, 47–54 (2016).
49. I. Lin, T. Van, P. Smooker, *Vaccines* **3**, 940–972 (2015).
50. J. Banchereau, B. Schuler-Thurner, A. K. Palucka, G. Schuler, *Cell* **106**, 271–274 (2001).

10.1126/science.aar7112

REVIEW

CAR T cell immunotherapy for human cancer

Carl H. June,[1,2,3]* Roddy S. O'Connor,[1,2] Omkar U. Kawalekar,[1] Saba Ghassemi,[1,2] Michael C. Milone[1,3]

Adoptive T cell transfer (ACT) is a new area of transfusion medicine involving the infusion of lymphocytes to mediate antitumor, antiviral, or anti-inflammatory effects. The field has rapidly advanced from a promising form of immuno-oncology in preclinical models to the recent commercial approvals of chimeric antigen receptor (CAR) T cells to treat leukemia and lymphoma. This Review describes opportunities and challenges for entering mainstream oncology that presently face the CAR T field, with a focus on the challenges that have emerged over the past several years.

By applying sophisticated ex vivo culture and cellular engineering approaches to adoptive T cell transfer (ACT), durable clinical responses of otherwise treatment-refractory cancers have recently been achieved, revealing the power and potential of ACT. On the basis of dramatic results, autologous T cells engineered to express a chimeric antigen receptor (CAR) specific for the CD19 B lymphocyte molecule have recently been approved by the U.S. Food and Drug Administration (FDA) for treatment of refractory pre-B cell acute lymphoblastic leukemia and diffuse large B cell lymphoma. In this Review, we focus on (i) the prospects for universal CAR T cells, (ii) the use of CAR T cell therapy for solid tumors, and (iii) emerging disparities in the use and commercialization of CAR T cell therapy.

Three forms of ACT are being developed for cancer therapy; these include tumor-infiltrating lymphocytes (TILs), T cell receptor (TCR) T cells, and CAR T cells. TILs have been shown to induce durable complete responses in patients with metastatic melanoma in a variety of clinical trials. The rationale for TIL therapy has been strengthened by recent data demonstrating that TILs can target neoantigens in melanoma (*1*); the status of TIL therapy is further discussed in (*2*). Similarly, gene transfer technology has been applied to peripheral blood T lymphocytes to generate cells with transgenic TCRs or CARs. A number of pharmaceutical and biotechnology companies are now commercializing these various forms of ACT (*3*).

Genetically engineered T cells: TCR versus CAR T cell immunotherapy

TCRs consist of an α- and a β-chain noncovalently associated with the CD3 complex on the T cell surface (Fig. 1). Activation of T cells occurs when the TCR recognizes peptides noncovalently bound to major histocompatibility complex (MHC) on the surface of antigen-presenting cells or tumor cells. The first TCR T cell cancer immunotherapy used in the clinic was tested against metastatic melanoma and utilized a TCR that bound a human lymphocyte antigen A2 (HLA-A2)–restricted peptide from a melanocytic differentiation antigen (*4*). Subsequently, a higher-avidity TCR targeting the MART-1 (melanoma antigen recognized by T cells 1) epitope was developed, with the aim of achieving enhanced recognition of malignant cells with lower MART-1 expression. Although an improved response rate was demonstrated, it came with a cost of also targeting normal melanocytes in the skin, eye, and cochlea (*5*). Such on-target, off-tumor toxicity occurred in more than half of the treated patients, providing the first clues that the line between efficacy and toxicity when targeting shared antigens may be thin. The onset of fatal neurotoxicity and cardiotoxicity associated with two separate TCR-based therapies directed to the cancer-testis antigen MAGE-A3 further highlighted the challenge (*6*, *7*). However, targeting the cancer-testis antigen NY-ESO-1 with T cells expressing an affinity-enhanced TCR specific for an HLA-A2–restricted peptide produced evidence of clinical efficacy without appreciable toxicity. These observations raised hope that the therapeutic window may not be so narrow for all shared antigenic targets (*8*); engineered NY-ESO-1 T cells are now under evaluation in a late-stage clinical trial (NCT01343043, clinicaltrials.gov). Efforts to develop TCR T cell therapies with TCRs specific to particular tumor neoantigens would likely be safer than targeting shared antigens (*3*); however, this has not been tested clinically.

A CAR combines antigen-binding domains—most commonly, a single-chain variable fragment (scFv) derived from the variable domains of antibodies with the signaling domains of the TCRς chain and additional costimulatory domains from receptors such as CD28, OX40, and CD137 (Fig. 1). CARs overcome some limitations of engineered TCRs, such as the need for MHC expression, MHC identity, and costimulation. Groups led by Kuwana and Eshhar first showed that these types of synthetic receptor molecules enabled MHC-independent target recognition by T cells (*9*, *10*). The independence of CAR recognition from MHC restriction endows the CAR T cell with a fundamental antitumor advantage, because a major mechanism of immunoevasion by cancer is loss of MHC-associated antigen presentation by tumor cells (*11*). One limitation of current CAR T cell strategies is that they require extracellular surface targets on the tumor cells. The characteristics of CAR and TCR T cells are compared in Table 1.

B cell malignancies: Unexpected success with CAR T cells

The results from the initial clinical trials using first-generation CAR designs in patients with various cancers were disappointing. However, in 2011, second-generation CAR T cells targeting CD19 and encoding costimulatory domains emerged as the lead paradigm for engineered T cell therapies in cancer (*12*–*15*). Several features make CD19 a nearly ideal target. It displays frequent and high-level expression in B cell malignancies, it is required for normal B cell development in humans (*16*), and it is not expressed outside of the B cell lineage. Patients successfully treated with CD19 CARs often have profound B cell aplasia (*13*) with some preservation of plasma cells and prior humoral immunity (*17*). The loss of B cells after CAR T cell therapy is largely managed by replacement therapy with intravenous immunoglobulin, not unlike the treatment for individuals

Table 1. Characteristics of CAR- and TCR-engineered T cells.

CAR T cells	TCR T cells
Signal amplification from synthetic biology: 200 targets can trigger CAR T cells (*57*)	Sensitive signal amplification derived by evolution of the TCR
Avidity-controllable	Low-avidity, unless engineered (*58*)
CAR targets surface structures: proteins, glycans	TCR targets intracellular proteome
MHC-independent recognition of tumor targets	Requires MHC class I expression and HLA matching on tumor
At least decade-long persistence (*59*)	Lifelong persistence
Serial killers of tumor cells (*60*)	Serial killers of tumor cells (*60*)
Cytokine release syndrome more severe than with TCR-based therapy	Off-tumor toxicity difficult to predict (*7*)

[1]Center for Cellular Immunotherapies, Perlman School of Medicine, Philadelphia, PA, USA. [2]Parker Institute for Cancer Immunotherapy, University of Pennsylvania, Philadelphia, PA, USA. [3]Department of Pathology and Laboratory Medicine, Perlman School of Medicine, Philadelphia, PA, USA.
*Corresponding author. Email: cjune@exchange.upenn.edu

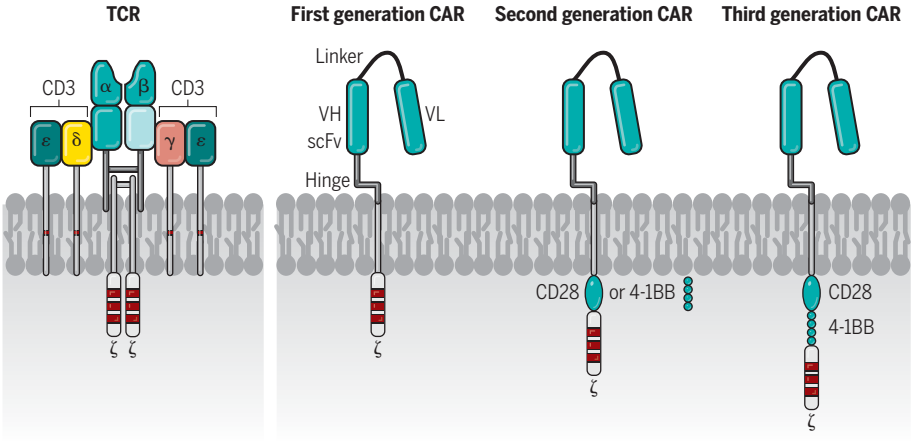

Fig. 1. Engineered T cells: design of TCR versus CAR T cells. T cells can be redirected to have specificity for tumors by the introduction of (**left**) transgenic TCRs (T cell receptors) or (**right**) CAR (chimeric antigen receptor) proteins. CARs are fusion proteins composed of an extracellular portion that is usually derived from an antibody and intracellular signaling modules derived from T cell signaling proteins. First-generation CARs contain CD3ζ, whereas second-generation CARs possess a costimulatory endodomain (e.g., CD28 or 4-1BB) fused to CD3ζ. Third-generation CARs consist of two costimulatory domains linked to CD3ζ. scFv, single-chain variable fragment; VH, variable heavy chain; VL, variable light chain.

with genetic deficiencies in B cells owing to CD19 mutations (*16*).

Early results from CAR T cell trials evaluating other targets indicated that the CD19 off-tumor cross-reactions are not a singular example, but may be generally observed with other lineage-dependent targets. Multiple myeloma, which expresses low levels of CD19, has responded to CD19 CAR T cell therapy (*18*). In ongoing trials (NCT02546167, clinicaltrials.gov) with CARs targeting B cell maturation antigen (BCMA or CD269) in advanced myeloma, the nonmalignant plasma cells that also express BCMA are eradicated in addition to the malignant myeloma cells (*19*). The tolerability of off-tumor reactions will depend greatly on the types of noncancerous cells that are targeted.

Most patients with relapsed leukemia achieve complete remission after CD19-specific CAR T cell treatment. However, two forms of resistance to this therapy have emerged. In patients with acute leukemia, the loss of the antigenic epitope on CD19 that is targeted by CAR T cells appears to be a dominant mechanism of tumor escape. This is analogous to mechanisms of antigenic escape due to acquired defects in antigen presentation or antigen loss observed with TCR T cell–based therapies (*15*, *20*). The frequency of relapse with CD19-negative loss variants was 28% in the international trial for young adult and pediatric patients with acute leukemia (*21*). CD19 loss has not been reported as a form of resistance in patients with chronic lymphocytic leukemia (CLL); resistance in CLL is likely due to a failure of the CAR T cells to proliferate after infusion (*22*). Table 2 lists several important translational challenges that need to be overcome in advancing CAR T cell therapy to clinical fruition.

Table 2. Strategies to overcome current clinical challenges associated with CAR T cell therapies.

Issue	Strategy	Expected outcome
Cytokine release syndrome (*13*, *61*)	Tocilizumab, siltuximab, JAK kinase inhibitors, corticosteroids	Blocking IL-6 effects rapidly reverses fevers, hypotension, and hypoxia
Development of anti-CAR idiotypic antibodies to murine scFvs	Use humanized scFv (*62*)	Longer persistence of CAR T cells
Lack of persistence of CAR T cells	Understand mechanisms of signaling domains that impart increased longevity (*63*); use sorted memory or stem cells (*64*)	Long-term persistence of CAR T cells when desired by clinical situation
Relapse owing to loss of CD19 epitope	Target CD22 and CD19	Combinatorial surface targeting prevents escape (*23*)

CAR T moving beyond B cells

CAR T technology has now been shown to have broader applications beyond CD19, and early-phase clinical trials of CAR T cells targeting BCMA and CD22 have reported similarly potent antitumor activity in multiple myeloma and acute lymphoblastic leukemia, respectively (*19*, *23*). However, BCMA and CD22, like CD19, are highly restricted to the B cell lineage, which resides in tissue that can be targeted with manageable toxicity. Attempts to target tumor-associated antigens in solid tumors have achieved limited success so far.

The ERBB2/HER2 protein is a receptor tyrosine kinase that is frequently overexpressed in cancer and is a validated target for antibody or antibody-drug conjugates. CAR T cell therapy targeting ERBB2/HER2 led to a fatal toxicity in the first patient treated. By using a third-generation CAR with a high-affinity scFV based on Herceptin and CD28 and 4-1BB intracellular signaling domains, it was revealed that the toxicity was apparently caused by recognition and killing of ERBB2-positive cells expressed at low density on the lung epithelium, triggering pulmonary failure and massive cytokine release (*24*). Lower doses of CAR T cells that have a scFv with lower affinity than the Herceptin-based CAR have proven safe in sarcoma patients but only have modest clinical activity (*25*).

A phase 1 trial of T cells expressing a first-generation CAR targeting the carbonic anhydrase IX (CAIX) antigen on renal cell carcinoma also encountered unexpected hepatotoxicity, owing to low-density expression of the CAIX antigen on normal biliary epithelium that was not discovered in preclinical studies (*26*). Delayed respiratory toxicity coinciding with peak T cell expansion in a trial of CAR T cell therapy targeting CEACAM5 also suggested the potential for on-target, off-tumor toxicity with this cancer-associated antigen (*27*). Clinical trials of CARs targeting other shared antigens associated with solid tumors including mesothelin, carcinoembryonic antigen, and the GD2 ganglioside have not reported notable toxicity; however, the antitumor activity observed in these trials has also been minimal. GD2-specific CAR T cells with enhanced antitumor activity are capable of inducing fatal neurotoxicity in preclinical models, highlighting the challenge (*28*). Local-regional injection of CAR T cell therapy targeting the interleukin (IL)–13 receptor α2 on glioblastoma multiforme demonstrated on-target activity without the appreciable toxicity that would be expected if intravenous administration were performed, suggesting that the therapeutic index may be enhanced by direct intratumoral injection for some antigens (*29*). CAR T cell therapy targeting a tumor-specific antigen, the alternately spliced variant of epidermal growth factor receptor (EGFRvIII), has demonstrated that this antigen can be safely targeted, but EGFRvIII antigen loss

within the tumor was also observed in some treated subjects, further illustrating the need to target multiple antigens to prevent antigen escape (*30*).

The tumor microenvironment presents additional barriers to the successful application of ACT, especially in solid tumors. Well-described pathways that inhibit T cell immunity within tumors include immune checkpoints (e.g., expression of PD-L1, a ligand for the programmed death 1 receptor), alterations in the tumor metabolic environment (e.g., hypoxia or expression of indolamine-1-oxidase and arginase), regulatory T cells, and suppressive myeloid cells (*31*). Many of these immunologic and metabolic checkpoints increase in tumors after ACT, suggesting adaptive resistance (*30*). Clinical trials that combine PD-1/PD-L1–blocking antibodies with CD19-specific CAR T cell therapies are under way (e.g., NCT02926833, NCT02650999, and NCT02706405; clinicaltrials.gov). In addition to combinations with other checkpoint inhibitors, alternative approaches to disrupting these suppressive pathways, such as switch receptors or gene editing, are also under study (*32*).

Toxicities with CAR T cell therapy

Although some degree of immune stimulation and inflammation was expected with T cell activation after ACT, severe cytokine release syndrome (CRS) has been observed with CD19-specific, BCMA-specific, and CD22-specific CAR T cells (Fig. 2). This syndrome can be more severe than the influenza-like syndrome commonly observed with TIL- and TCR-based therapies (*33*). The severity of the CAR T cell–associated CRS correlates with tumor burden (*14*, *34*). In the most severe form, CRS shares many features with hemophagocytic lymphohistiocytosis and macrophage activation syndrome (*35*).

Although CRS was an expected toxicity with T cell immunotherapy, unexpected neurologic complications ranging in severity from mild to life-threatening have also been reported across different clinical studies with CD19- and BCMA-specific CAR T cells. The neurologic toxicities described with CD19-specific CAR T cells have been largely reversible (Box 1). It is not known whether the cerebral edema resulting from CAR T cell therapy is an extreme manifestation of CRS or whether there is a separate mechanism of action. In support of the latter, there is evidence for endothelial injury, perhaps related to inflammatory cytokines, contributing to the onset of neurotoxicity (*36*). The mechanisms underlying T cell immunotherapy–mediated CRS and cerebral edema are poorly understood, in part because the field lacks informative animal models to study these important toxicities.

Improving engineered T cells through cellular engineering

The strength of binding between a ligand and its receptor (affinity) is a fundamental biophysical parameter affecting the outcome of most receptor signaling. Characterizing the affinity of a single TCR for its cognate peptide presented within MHC (pMHC) is complex. In the most simplistic form, the binding reaction between TCR and pMHC can be represented by the equation

$$\mathrm{TCR} + \mathrm{pMHC} \underset{k_{off}}{\overset{k_{on}}{\rightleftharpoons}} \mathrm{TCR{:}pMHC}$$

However, there is considerable debate regarding whether the equilibrium binding constant ($K_D = k_{on}/k_{off}$, where k_{on} and k_{off} are the association and dissociation rates, respectively) or the dissociation half-life ($t_{1/2} = 0.693/k_{off}$) is the most important parameter affecting the outcome of TCR signaling. Using surface plasmon resonance measurements of TCR affinity, the apparent K_D values of most functional TCRs for pMHC range from 1 to 100 μM (*37*). The role of TCR affinity may be especially relevant to tumor-associated cancer-testis antigens, which are nonmutated self-antigens to which some degree of tolerance likely exists, unlike for foreign antigens (*38*).

Similar to TCRs, affinity engineering may also be applicable in CAR design to increase the antitumor potency of CAR T cells and modulate on-target, off-tumor toxicity. *ERBB2/HER2* encodes a cell surface receptor implicated in the pathogenesis of numerous epithelial malignancies (*39*). Varying the affinity of a CAR against ERBB2/HER2 increases the discrimination between low antigen density, such as that found on healthy epithelial cells, and higher antigen load on tumor cells (*40*). However, identifying the optimal affinity is not straightforward, as evidenced by improved antitumor activity (but with the emergence of severe neurotoxicity) associated with enhanced binding of a GD2-specific CAR in a preclinical model (*28*). Beyond affinity, substantial effort has been expended to evaluate the impacts of CAR ectodomain structure, transmembrane domain, and signaling (*41*), which all can affect CAR function. Unfortunately, few standards have been defined, and CAR design remains largely empiric. In many cases, the functional consequences are also not fully apparent in preclinical experiments, further complicating the CAR design process.

Universal CAR T cells

Although ACT evolved from allogeneic bone marrow transplantation, ACT strategies have focused on autologous T cells owing to the inherent barriers imposed by the MHC. A return to allogeneic donor or "universal" T cells could provide considerable advantages over autologous T cells if the MHC barriers could be eliminated. Universal CAR T cells derived from healthy donors have the potential to overcome the many immune defects associated with cancer treatment. In addition, the use of universal CAR T cell therapies might provide

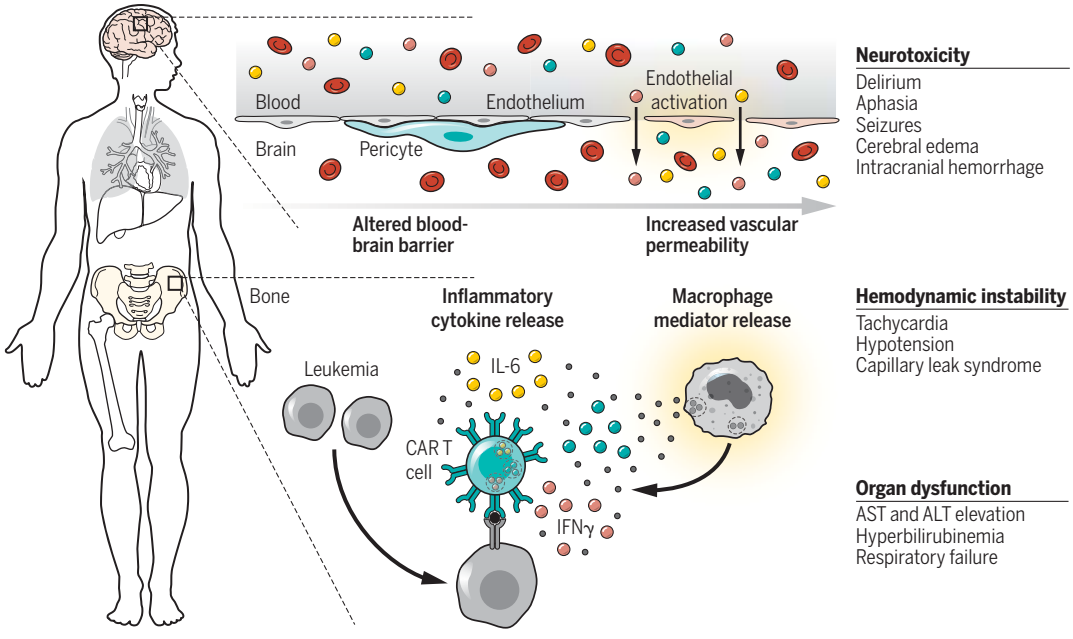

Fig. 2. CAR T cell therapy is associated with cytokine release syndrome and neurotoxicity. Cytokine release syndrome has occurred with CAR T cells targeting CD19 or BCMA. When the CAR T cell engages surrogate antigens, it releases a variety of cytokines and chemokines. Macrophages and other cells of the innate immune system also become activated and contribute to the release of soluble mediators. CAR T cells are routinely observed in cerebral spinal fluid, and the cytokines may increase permeability to soluble mediators and permit increased trafficking of CAR T cells and other lymphocytes to central nervous system parenchyma. IFN, interferon; AST, aspartate aminotransferase; ALT, alanine aminotransferase.

CREDITS (GRAPHIC): A. KITTERMAN/*SCIENCE*

opportunities to simplify the manufacturing of engineered cells, perhaps even allowing for the creation of "off-the-shelf" ACT products (*42*), facilitating more rapid and less expensive treatment compared with autologous patient-specific T cells.

The first study to report the use of gene editing to generate universal CAR T cells without a functional endogenous TCR was by Torikai *et al.* (*43*). A pilot trial using TALEN (transcription activator–like effector nuclease)–based engineering in two patients recently demonstrated the feasibility of applying off-the-shelf universal CD19-specific CAR T cell therapy (*44*). Engraftment of the genetically universal CAR T cells was limited in both subjects, constraining the therapeutic efficacy of the approach in the pilot study. Importantly, subject 1, who was mismatched at all MHC class I alleles, experienced graft-versus-host disease that was associated with the expansion of contaminating, nonedited T cells that retained the endogenous TCR, indicating that more complete editing will be required for the success of this approach. Recognition of MHC class I–deficient cells by natural killer (NK) cells also might have limited engraftment, despite profound immunosuppression induced by alemtuzumab. One appealing strategy to prevent NK lysis of universal CAR T cells is to insert HLA-E and delete HLA-A, -B, and -C, which prevents host T cells from killing the universal CAR T cells (*45*). Given the rapid progress in the field, it is likely that universal CAR T cells will become widely used. However, the major question remaining is whether the approach will be sufficiently potent to serve as a stand-alone therapy, or whether it will rather act as a bridge for a definitive therapy, such as a stem cell transplant or autologous CAR T cell therapy.

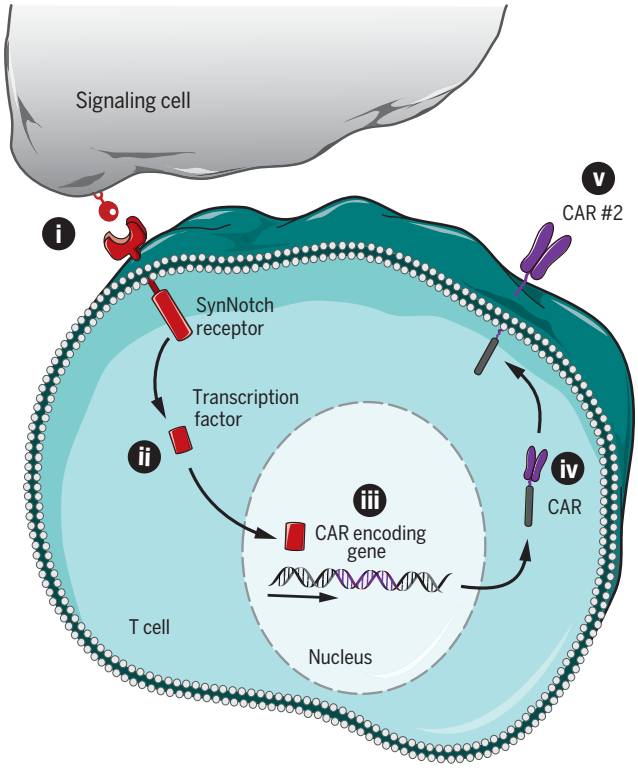

Fig. 3. Conditionally expressed CAR using Notch as a signal induction and response pathway system. The extracellular ligand-binding domain of CAR 1, upon engagement with its cognate ligand (i), induces proteolysis of the intracellular domain of a synthetic Notch (synNotch) receptor, which contains a transcriptional regulator. Upon release, the notch intracellular domain is translocated to the nucleus (ii) to regulate transcription (iii) of the gene encoding CAR 2 downstream of the transcription factor binding site. Translation of the protein (iv) is followed by the surface expression of the CAR (v). In this manner, a conditional CAR expression specific to a second antigen in the presence of the first antigen–specific ligand safely arms the T cell for highly specific recognition.

Genome editing and multipurpose CARs

Many technologies can introduce targeted double-stranded breaks in DNA, permitting efficient creation of insertion or deletion mutations, which generally inactivates the targeted gene. Homology-directed repair can be used to insert genes of interest at the targeted site. There are many genome-editing tools, including zinc finger nucleases, meganucleases, TALENs, homing endonucleases, and CRISPR-Cas9 nucleases. These technologies have all been successfully applied to engineer T cells. The major issue in the field now is whether bacterially derived Cas9 will be sufficiently immunogenic to interfere with the delivery of CRISPR-Cas9–edited T cells (*46*).

Human genome editing offers the opportunity to eliminate immunosuppressive signals such as CTLA-4 and PD-1, enhancing the function of T cells, possibly without the toxicity associated with global blockade of immune checkpoint molecules (*47*). Gene editing has also been used to eliminate genes for CAR targets that are also expressed by the T cell, which may allow targeting of tumor-associated antigens that would otherwise not be amenable to T cell immunotherapy (*48*). Recently, Eyquem *et al.* introduced a CAR into the TCR locus so that receptor expression could be controlled under physiologic conditions of the endogenous TCR promoter, thereby markedly enhancing CAR T cell function (*49*).

Single antigen–based approaches are limited in their ability to discriminate tumor cells from healthy tissue. To provide enhanced specificity toward tumors, combined sensing approaches are increasingly being developed that target two or more antigens. One of the earliest strategies involved splitting of the primary CD3ζ and costimulatory signals from second-generation CARs into two separate chimeric receptors that are co-expressed within the same T cell (*50*). A synthetic Notch receptor system has also been described that integrates the dual antigenic signals through transcription rather than signaling (*51*) (Fig. 3). Understanding the pharmacokinetic features of CAR expression in combinatorial antigen-sensing systems will be important because trafficking between physiologic compartments can occur within hours after CAR infusion, when cells retaining CAR expression might still be capable of mediating toxicity.

To mitigate the potential risk of self-reactive immunity associated with ACT, synthetic molecular systems for achieving inducible death of the genetically engineered T cells, often called "suicide switches," have been developed. The most notable approach uses the pro-apoptotic protein caspase-9 fused to a domain of FKBP12 (inducible caspase-9, or iCasp9). Upon introduction of a dimeric small molecule such as rimiducid, the FKBP12 domains of iCasp9 dimerize, and the T cells undergo rapid apoptotic cell death. The iCasp9 approach has been evaluated in allogeneic donor lymphocyte infusions after hematopoietic stem cell transplantation and has demonstrated

Box 1. Cerebral edema associated with CAR T cell therapy.

An unanticipated toxicity from CAR T cell therapy has been cerebral edema. Five deaths attributed to cerebral edema were reported in patients treated with JCAR015, the CD19 CAR originally developed by Brentjens and colleagues (*14*). The company Juno announced that it terminated clinical development of JCAR015 in March 2017. The cause of the cerebral edema occurring in patients treated with JCAR015 was a capillary leak owing to endothelial damage that was restricted to the central nervous system (*36*). Edema has classically been accepted as a consequence of some forms of physiologic immune activation. Swelling of tumor masses followed by tumor regression occurs after checkpoint therapy (*65*). However, swelling of tumors in patients treated with CAR T cells has not been reported. The underlying cause of cerebral edema after CAR T cell treatment remains unknown, and the lack of a suitable animal model to study the toxicity hinders research in this area.

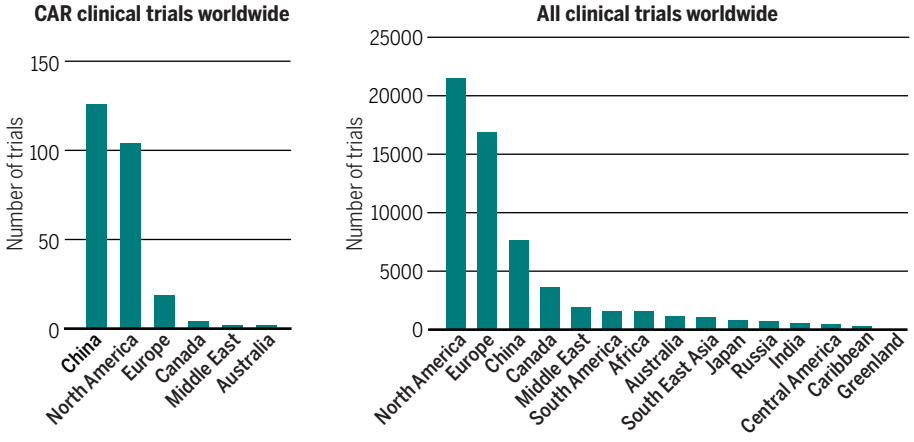

Fig. 4. Regional disparities in studies of CAR T cell therapies. (**Left**) Geographic localization of clinical trials presently testing CAR T cell therapies, identified using the search term "chimeric antigen receptor." Worldwide, 253 trials are testing CAR T cells (clinicaltrials.gov, accessed 16 January 2018). China is now the most active area of clinical research for CAR T cells. (**Right**) Comparison with the geographic localization of all clinical trials worldwide.

robust T cell elimination with the ability to abrogate graft-versus-host disease (*52*).

Commercialization of CAR T cells

The field of immuno-oncology has emerged as one of the great success stories of the past decade. However, the advent of numerous but often noncurative targeted therapies will increase life span and the prevalence of patients living with cancer (*53*). There are now more than 250 clinical trials testing CAR T cells. It is notable that there are disparities in the geographic locations of the trials, with hotspots for translational research occurring in China and the United States and far fewer trials taking place in Europe, Japan, and the Southern Hemisphere (Fig. 4). The reasons for the geographic disparity are likely complex and related to the willingness to adopt and invest in new therapies, divergent regulatory policies by health authorities, and societal differences.

The financial burdens imposed by effective but noncurative therapies that are encountered by patients with hematologic malignancies, particularly CLL and multiple myeloma, also present challenges. CLL is the most common form of leukemia in the United States; about 100,000 patients were living with the disease in 2000, and, because of improved but noncurative targeted therapies such as ibrutinib and idelalisib, an increase to ~200,000 cases in the United States is projected (*54*). However, targeted therapies for CLL present a substantial economic burden for both patients and the economy, now estimated at a lifetime cost of $604,000 per patient, and the total cost of CLL management in the United States alone is estimated to exceed $5 billion per year by 2025 (*54*). It is likely that CAR T cell therapies are more cost-effective than current standard-of-care therapies for leukemia and lymphoma. The bespoke manufacturing processes now used for highly personalized engineered T cell therapies incur high costs. The cost of manufacturing CAR T cells is expected to decrease (*55*). A detailed analysis of the public health considerations of the pricing of gene-modified cells is beyond the scope of this Review, but some aspects have recently been summarized (*56*).

Future opportunities and applications

The advent of CAR T cells for leukemia and lymphoma is noteworthy from several perspectives. Perhaps most important is that CAR T cells are the first form of gene transfer therapy to gain commercial approval by the U.S. FDA. Because of the risk of CRS and neurologic toxicities, CAR T cells were approved contingently with a risk evaluation and mitigation strategy, whereby the FDA requires that physicians complete training for management of adverse effects. One of the greatest challenges in developing cell-based therapeutic approaches is the paucity of preclinical models to evaluate the safety and efficacy of these complex therapies before human studies or in response to safety issues that are uncovered in early-phase clinical studies. Although CAR T cells are transforming the management of hematologic malignancies, there are still many hurdles to successfully applying these therapeutic approaches more broadly to solid tumors. Ongoing advances in T cell engineering, gene editing, and cell manufacturing have the potential to broaden T cell–based therapies to other cell types such as induced pluripotent stem cells, hematopoietic stem cells, and NK cells and to foster new applications beyond oncology in infectious diseases, organ transplantation, and autoimmunity.

REFERENCES AND NOTES

1. E. M. Verdegaal *et al.*, *Nature* **536**, 91–95 (2016).
2. S. A. Rosenberg, N. P. Restifo, *Science* **348**, 62–68 (2015).
3. C. H. June, S. R. Riddell, T. N. Schumacher, *Sci. Transl. Med.* **7**, 280ps7 (2015).
4. R. A. Morgan *et al.*, *Science* **314**, 126–129 (2006).
5. L. A. Johnson *et al.*, *Blood* **114**, 535–546 (2009).
6. R. A. Morgan *et al.*, *J. Immunother.* **36**, 133–151 (2013).
7. B. J. Cameron *et al.*, *Sci. Transl. Med.* **5**, 197ra103 (2013).
8. A. P. Rapoport *et al.*, *Nat. Med.* **21**, 914–921 (2015).
9. Y. Kuwana *et al.*, *Biochem. Biophys. Res. Commun.* **149**, 960–968 (1987).
10. G. Gross, T. Waks, Z. Eshhar, *Proc. Natl. Acad. Sci. U.S.A.* **86**, 10024–10028 (1989).
11. F. Garrido, N. Aptsiauri, E. M. Doorduijn, A. M. Garcia Lora, T. van Hall, *Curr. Opin. Immunol.* **39**, 44–51 (2016).
12. J. N. Kochenderfer *et al.*, *Blood* **116**, 4099–4102 (2010).
13. D. L. Porter, B. L. Levine, M. Kalos, A. Bagg, C. H. June, *N. Engl. J. Med.* **365**, 725–733 (2011).
14. R. J. Brentjens *et al.*, *Sci. Transl. Med.* **5**, 177ra38 (2013).
15. S. A. Grupp *et al.*, *N. Engl. J. Med.* **368**, 1509–1518 (2013).
16. M. C. van Zelm *et al.*, *N. Engl. J. Med.* **354**, 1901–1912 (2006).
17. V. G. Bhoj *et al.*, *Blood* **128**, 360–370 (2016).
18. A. L. Garfall *et al.*, *N. Engl. J. Med.* **373**, 1040–1047 (2015).
19. S. A. Ali *et al.*, *Blood* **128**, 1688–1700 (2016).
20. E. Sotillo *et al.*, *Cancer Discov.* **5**, 1282–1295 (2015).
21. S. L. Maude *et al.*, *N. Engl. J. Med.* **378**, 439–448 (2018).
22. D. L. Porter *et al.*, *Sci. Transl. Med.* **7**, 303ra139 (2015).
23. T. J. Fry *et al.*, *Nat. Med.* **24**, 20–28 (2018).
24. R. A. Morgan *et al.*, *Mol. Ther.* **18**, 843–851 (2010).
25. N. Ahmed *et al.*, *J. Clin. Oncol.* **33**, 1688–1696 (2015).
26. C. H. Lamers *et al.*, *Mol. Ther.* **21**, 904–912 (2013).
27. F. C. Thistlethwaite *et al.*, *Cancer Immunol. Immunother.* **66**, 1425–1436 (2017).
28. S. A. Richman *et al.*, *Cancer Immunol. Res.* **6**, 36–46 (2018).
29. C. E. Brown *et al.*, *N. Engl. J. Med.* **375**, 2561–2569 (2016).
30. D. M. O'Rourke *et al.*, *Sci. Transl. Med.* **9**, eaaa0984 (2017).
31. J. A. Joyce, D. T. Fearon, *Science* **348**, 74–80 (2015).
32. W. A. Lim, C. H. June, *Cell* **168**, 724–740 (2017).
33. M. Kalos *et al.*, *Sci. Transl. Med.* **3**, 95ra73 (2011).
34. S. L. Maude *et al.*, *N. Engl. J. Med.* **371**, 1507–1517 (2014).
35. D. M. Barrett, D. T. Teachey, S. A. Grupp, *Curr. Opin. Pediatr.* **26**, 43–49 (2014).
36. J. Gust *et al.*, *Cancer Discov.* **7**, 1404–1419 (2017).
37. M. M. Davis *et al.*, *Annu. Rev. Immunol.* **16**, 523–544 (1998).
38. M. Aleksic *et al.*, *Eur. J. Immunol.* **42**, 3174–3179 (2012).
39. M. Marotta *et al.*, *Sci. Rep.* **7**, 41921 (2017).
40. H. G. Caruso *et al.*, *Cancer Res.* **75**, 3505–3518 (2015).
41. S. Srivastava, S. R. Riddell, *Trends Immunol.* **36**, 494–502 (2015).
42. J. L. Zakrzewski *et al.*, *Nat. Biotechnol.* **26**, 453–461 (2008).
43. H. Torikai *et al.*, *Blood* **119**, 5697–5705 (2012).
44. W. Qasim *et al.*, *Sci. Transl. Med.* **9**, eaaj2013 (2017).
45. G. G. Gornalusse *et al.*, *Nat. Biotechnol.* **35**, 765–772 (2017).
46. C. T. Charlesworth, P. S. Deshpande, D. P. Dever, B. Dejene, N. Gomez-Ospina, S. Mantri, M. Pavel-Dinu, J. Camarena, K. I. Weinberg, M. H. Porteus, Identification of pre-existing adaptive immunity to Cas9 proteins in humans. bioRxiv 243345 [Preprint]. 5 January 2018.
47. C. H. June, J. T. Warshauer, J. A. Bluestone, *Nat. Med.* **23**, 540–547 (2017).
48. R. Galetto, I. Chion-Sotinel, A. Gouble, J. Smith, *Blood* **126**, 116 (2015).
49. J. Eyquem *et al.*, *Nature* **543**, 113–117 (2017).
50. C. C. Kloss, M. Condomines, M. Cartellieri, M. Bachmann, M. Sadelain, *Nat. Biotechnol.* **31**, 71–75 (2013).
51. K. T. Roybal *et al.*, *Cell* **164**, 770–779 (2016).
52. A. Di Stasi *et al.*, *N. Engl. J. Med.* **365**, 1673–1683 (2011).
53. P. J. Neumann, J. T. Cohen, *N. Engl. J. Med.* **373**, 2595–2597 (2015).
54. Q. Chen *et al.*, *J. Clin. Oncol.* **35**, 166–174 (2017).
55. B. L. Levine, C. H. June, *Nature* **498**, S17 (2013).
56. R. Hettle *et al.*, *Health Technol. Assess.* **21**, 1–204 (2017).
57. J. D. Stone, D. H. Aggen, A. Schietinger, H. Schreiber, D. M. Kranz, *OncoImmunology* **1**, 863–873 (2012).
58. M. P. Tan *et al.*, *Clin. Exp. Immunol.* **180**, 255–270 (2015).
59. J. Scholler *et al.*, *Sci. Transl. Med.* **4**, 132ra53 (2012).
60. A. J. Davenport *et al.*, *Cancer Immunol. Res.* **3**, 483–494 (2015).
61. J. N. Kochenderfer *et al.*, *Blood* **119**, 2709–2720 (2012).
62. D. Sommermeyer *et al.*, *Leukemia* **31**, 2191–2199 (2017).
63. M. C. Milone *et al.*, *Mol. Ther.* **17**, 1453–1464 (2009).
64. X. Wang *et al.*, *Blood* **127**, 2980–2990 (2016).
65. M. A. Postow, R. Sidlow, M. D. Hellmann, *N. Engl. J. Med.* **378**, 158–168 (2018).

ACKNOWLEDGMENTS

This work was supported by NIH grants RO1CA226983 (C.H.J.), 5R01CA165206 (C.H.J.), and 1P01CA214278 (M.C.M.). We apologize that because of space constraints, we were unable to cite many studies.

10.1126/science.aar6711

REVIEW

The microbiome in cancer immunotherapy: Diagnostic tools and therapeutic strategies

Laurence Zitvogel,[1,2,3,4]* Yuting Ma,[5,6] Didier Raoult,[7] Guido Kroemer,[8,9,10] Thomas F. Gajewski[11]*

The fine line between human health and disease can be driven by the interplay between host and microbial factors. This "metagenome" regulates cancer initiation, progression, and response to therapies. Besides the capacity of distinct microbial species to modulate the pharmacodynamics of chemotherapeutic drugs, symbiosis between epithelial barriers and their microbial ecosystems has a major impact on the local and distant immune system, markedly influencing clinical outcome in cancer patients. Efficacy of cancer immunotherapy with immune checkpoint antibodies can be diminished with administration of antibiotics, and superior efficacy is observed with the presence of specific gut microbes. Future strategies of precision medicine will likely rely on novel diagnostic and therapeutic tools with which to identify and correct defects in the microbiome that compromise therapeutic efficacy.

Cancer cells frequently express tumor-associated antigens that are targetable by T lymphocytes; however, concomitant immune regulatory molecules often suppress these functional immune responses. Therapeutic agents uncoupling these immune checkpoints have recently been shown to have a major impact on patient treatment outcomes. In particular, monoclonal antibodies (mAbs) that block the engagement of the inhibitory receptor PD-1 by its main ligand PD-L1 have to date been approved by the U.S. Food and Drug Administration (FDA) for use in the treatment of patients with 10 distinct tumor types (*1*). However, the majority of tumors appear to lack infiltration with T cells, and expression of immune genes indicative of an active immune response. Major efforts are being made to overcome the mechanisms of primary resistance to immunotherapy (*1*). Besides tumor cell–intrinsic oncogenic pathways, additional host and environmental factors can have a major impact on the degree of endogenous immune responses and hence the efficacy of cancer immunotherapeutics (*1*). The composition of the gut microbiome has emerged as one major factor that exerts a profound impact on the peripheral immune system, including in the cancer context (*2*). The mammalian microbiome represents all host-associated microorganisms, a complex and diverse ecosystem residing at portals of entry on all epithelial barriers. It encompasses the bacterial microbiome, the archaeal microbiome, the virome (bacteriophages and eukaryotic viruses), the mycobiome (fungi), and the meiofauna (unicellular protozoa and helminthic worms) (*3*) and is acquired after birth through vertical transmission and then shaped by environmental exposure throughout life. Disrupting the repertoire of the gut microbiome, which is sometimes referred to as "intestinal dysbiosis," has been epidemiologically (and sometimes causally) associated with a variety of chronic inflammatory disorders (*4*). Here, we discuss the impact of the bacterial microbiome on the relationship between cancer and the immune system, and the potential therapeutic utility of directly manipulating commensal microbiota as an approach to enhance the efficacy of cancer immunotherapy.

[1]Gustave Roussy Cancer Campus (GRCC), Equipe Labellisée–Ligue Nationale contre le Cancer, Villejuif, France. [2]Institut National de la Santé et de la Recherche Medicale (INSERM) U1015, Villejuif, France. [3]Université Paris-Sud, Université Paris-Saclay, Gustave Roussy, Villejuif, France. [4]Center of Clinical Investigations in Biotherapies of Cancer (CICBT) 1428, Villejuif, France. [5]Center for Systems Medicine, Institute of Basic Medical Sciences, Chinese Academy of Medical Sciences and Peking Union Medical College, 100005 Beijing, China. [6]Suzhou Institute of Systems Medicine, Suzhou, Jiangsu 215123, China. [7]Unité de Recherche sur les Maladies Infectieuses et Tropicales Emergentes, Aix Marseille Université, UM63, CNRS 7278, IRD 198, INSERM 1095, Institut Hospitalo-Universitaire (IHU)–Méditerranée Infection, 19-21 Boulevard Jean Moulin, 13005 Marseille. [8]Centre de Recherche des Cordeliers, Université Paris Descartes, Sorbonne Paris Cité, Université Pierre et Marie Curie, Paris, France. [9]Metabolomics and Cell Biology Platforms, GRCC, Villejuif, France. [10]Equipe 11 Labellisée–Ligue Nationale Contre le Cancer, UMRS 1138, Paris, France. [11]Department of Pathology, Department of Medicine, and the Ben May Department of Cancer, University of Chicago, Chicago, IL 60615, USA.
*Corresponding author. Email: laurence.zitvogel@gustaveroussy.fr (L.Z.); tgajewsk@medicine.bsd.uchicago.edu (T.F.G.)

Early steps: A role for the microbiome in cancer

The cardinal role of the intestinal microbiota in regulating health and diseases has only recently been fully appreciated (Fig. 1) (*4*). The human gut microbiome contains ~3×10^{13} bacteria, most of which are commensals (*5*). From birth, the intestinal microbiota plays a crucial role in the life-long programming of innate and acquired immune responses; it fine-tunes the delicate balance between inflammation, infection, and tolerance of food and commensal antigens (*4*, *6*). Beyond effects on intestinal and local immune physiology, the gut microbiome has systemic effects throughout the meta-organism (*6*). Exemplifying this notion, critical host fitness-promoting traits are missing in laboratory mice maintained under specific pathogen–free (SPF) conditions, compared with wild free-living animals. Transfer of the wild gut microbiome to laboratory mice induces long-lasting immune modulatory effects (over several generations), which improves disease outcome against viral infection and mutagen- and inflammation-induced carcinogenesis (*7*).

The microbiome has been discovered to be involved in the initiation and progression of various types of cancer, both at epithelial barriers and within sterile tissues (*8*). Commensal ecosystems inhabiting the intestine or other mucosae play a role in both local and distant carcinogenesis. Microbes can directly act as cancer-transforming agents, by providing a toxic metabolite or an oncogenic product, or indirectly by inducing inflammation or immunosuppression. Moreover, fecal microbial transplantation can transfer the neoplasia-prone phenotype from knockout mice lacking some immune-relevant genes (such as *Tbx21*, *Nod2*, *Nlrp6*, or *Tlr5*) of wild-type mice (*8*). By contrast, accumulating evidence supports a positive role for bacteria in combating cancer located at sites that are distant from the gut, through potentiation of host antitumor immune responses (table S1) (*9*). Epidemiological studies supported by experiments in rodents suggest a dose-dependent association between antibiotic use and risk of cancer (*9*). Taken together, these studies laid the theoretical framework to identify microbes that may bestow anticancer activities.

The gut microbiome and immuno-oncology

An early hint suggesting an immunotherapeutic effect of the microbiome came from studies of total-body irradiation, which enhanced the efficacy of tumor-specific T cell transfer through translocation of a bacterial product, the toll-like receptor 4L (TLR4L) lipopolysaccharide, from the intestinal lumen to secondary lymphoid organs (*10*). Soon after, it was observed that several anticancer treatment modalities showed reduced therapeutic effects in germ-free mice as well as in mice treated with broad-spectrum antibiotics (*11–14*), or in mice lacking specific immune-potentiating bacterial species originating from different vendors (*15*). Such results were obtained with metronomic cyclophosphamide (*12*), chemotherapy with platinum salts (*11*), immunotherapy through a combination of TLR9 antagonist and antibody to interleukin-10R (IL-10R) (*11*), or administration of mAbs to CTLA-4 and/or PD-1/PD-L1 (*13*, *14*). In each case, therapeutic efficacy was curtailed when the gut microbiota was absent or manipulated. The fine mechanisms explaining the contribution of the microbiome to therapy-induced anticancer immune responses may differ for each treatment modality. For instance, cyclophosphamide increases the permeability of the upper gastrointestinal (GI) tract, leading to translocation of the small intestine–residing *Enterococcus*

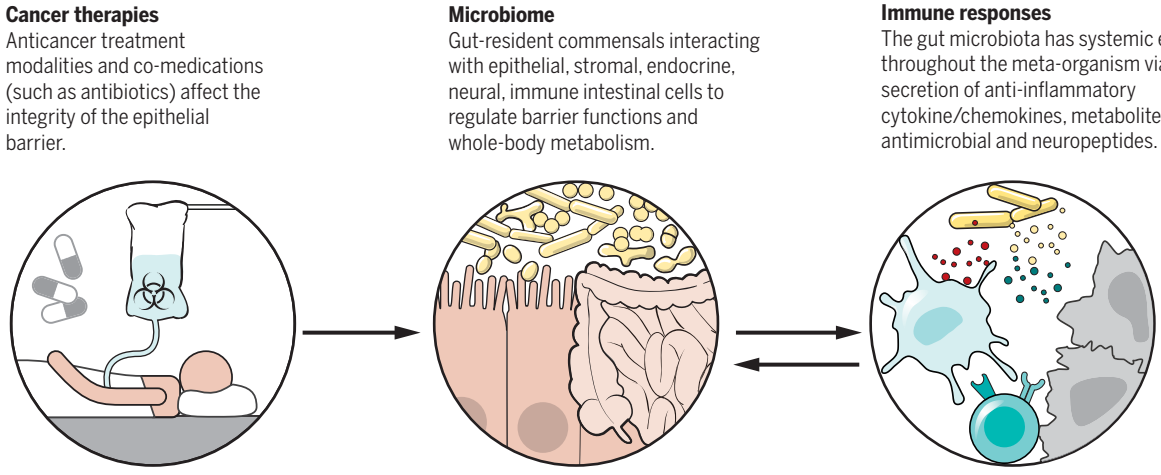

Fig. 1. The microbiome at the crossroads between physiology and pathology in cancer. The intestinal microbiota plays a crucial role in the life-long programming of innate and acquired immune responses because it fine-tunes the delicate balance between inflammation, infection, and tolerance of food and commensal antigens. Several therapeutic modalities could be harnessed to restore the homeostasis of the gut and the metaorganism during cancer progression and treatment.

hirae to the spleen, but also the accumulation of *Barnesiella intestinihominis* in the colon, which together exert a coordinated immunostimulatory effect on antitumor immune responses (*16*). Upon CTLA-4 blockade, intraepithelial lymphocytes damage ileal epithelial cells, stimulating the accumulation of *Bacteroides fragilis* and *Burkholderiales* spp., activating IL-12–producing dendritic cells (DCs) and T helper 1 (T_H1) immune responses (*13*). Therapeutic efficacy of PD-1/PD-L1 blockade was associated with the presence of *Bifidobacterium* spp., which activate antigen-presenting cells (*15*). The immunizing effects of antibody to IL-10R + the TLR9 agonist CpG were linked to the activation of myeloid cells and tumor necrosis factor–α (TNFα) secretion within the tumor microenvironment (*11*). The causal relationship between the dominance of distinct commensals and the efficacy of anticancer therapies in these examples has been proven with mouse cohousing experiments or oral gavage with defined species (table S1).

Corroborating these experimental findings, several independent retrospective analyses in human cohorts of metastatic lung, kidney, and bladder cancer patients indicated the deleterious role of different classes of antibiotics taken around the initiation of mAbs to PD1/PDL-1 (*14*). These retrospective analyses of patients treated with second-line therapies for FDA-approved indications needs to be confirmed in future prospective clinical trials and validated in other treatment contexts (for example, first-line versus second-line immunotherapies, and additional cancer types). In hematological malignancies, intestinal bacteria also modulate the risk of infection and graft-versus-host disease (GVHD) after allogeneic hematopoietic stem cell transplantation (ASCT). Early administration of systemic broad-spectrum antibiotics in ASCT was associated with increased GVHD, and worse transplant-related mortality, presumably by depleting protective *Clostridiales* and *Blautia* in the intestinal microbiota (*17*).

Perhaps the most provocative data suggesting the importance of commensal microbiota in clinical efficacy of cancer immunotherapy have been derived from the sequencing of baseline stool samples from patients being treated with antibody to PD-1–based therapies. Recent advances in sequencing technologies have improved our capacity to stratify patients on the basis of their microbial metagenomic fingerprint (*13*–*15*, *18*–*20*). 16*S* ribosomal RNA (rRNA)–based sequencing of gene amplicons and shotgun DNA sequencing of patient stool samples have identified subsets of bacteria more abundant in responding versus nonresponding patients. In some cases, decreased α diversity or richness of fecal bacterial composition was correlated with worse patient survival. It should be highlighted that variations exist between the different research studies, which included patients with distinct genetic and nutritional patterns, clinical trials that were conducted in different geographic locations within the United States or Europe, and different types of tumors, including lung cancer, renal cell cancer, and melanoma. Given these considerations, it is perhaps even more striking that bacteria generally associated with health (such as *Clostridiales*, *Ruminococcaceae*, *Faecalibacterium* spp., *Akkermansia muciniphila*, *B. fragilis*, and *Bifidobacteria*) (*13*, *14*, *18*–*20*) or immunogenicity (*Enterococci*, *Collinsella*, and *Alistipes*) (*11*, *13*, *14*, *20*) were found to be abundant in responding patients. Further corroborating these findings of solid malignancies, a study performed in 541 patients with hematologic malignancies reported that the gut microbiome at diagnosis influenced the probability of relapse within 2 years after ASCT. In this context, a high abundance of a bacterial group composed mostly of *Eubacterium limosum* had a positive prognostic impact (*21*).

"The microbiome has been discovered to be involved in the initiation and progression of various types of cancer, both at epithelial barriers and within sterile tissues."

Data supporting a causal role for improved immunotherapy efficacy have been derived by using transfer of patient fecal samples into germ-free (GF) or antibiotics-treated SPF mice, that subsequently were inoculated with mouse syngeneic tumors and then treated with mAbs to CTLA-4 and/or PD-1/PD-L1 (table S1) (*13*, *14*, *19*, *20*). Notably, fecal microbial transplantation (FMT) of feces from patients (who showed clinical response to immune checkpoint blockade) transferred a "responder" phenotype to recipient mice, whereas "nonresponder" patient feces tended to confer nonresponsiveness to recipients (*13*, *14*, *19*, *20*). These results highlight that the responder/nonresponder status of recipient mice was derived from the composition of the donor microbiome via FMT. Several defined bacteria species were identified that conferred improved immune-mediated tumor control in reconstituted mouse systems in vivo. This effect depended on distinct *Bacteroides* species in melanoma treated with ipilimumab (*13*) and at least partly on *Faecalibacterium* (*19*) in melanoma and on *Verrucomicrobiacae* [more specifically, *A. muciniphila* (*14*)] in lung cancer patients treated with the PD-1 inhibitors pembrolizumab or nivolumab.

Uncoupling efficacy from toxicity has always been a holy grail in clinical oncology. Evidence suggests that a microbiome rich in *Blautia* and *E. limosum* (which results from avoiding antibiotics that kill anaerobic bacteria) favors longer

survival after ASCT because such a microbiome simultaneously reduces GVHD and boosts graft-versus-leukemia effects (*17*, *21*). In patients with metastatic melanoma treated with the checkpoint inhibitor ipilimumab (antibody to CTLA-4), the abundance of *Bacteroidetes* inversely correlated with the severity of colitis (*22*). Accordingly, *B. fragilis* and *Burkholderia cepacia* administered via gavage to mice reduced the severity of colitis induced by mAb to CTLA-4 (*13*, *22*).

In parallel lines of investigation beyond immunotherapy, there is growing awareness that microbial metabolism of anticancer drugs may promote tumor chemoresistance (table S1). For example, the majority of pancreatic adenocarcinomas were reported to be invaded by high densities of *Gammaproteobacteria* expressing the long isoform of cytidine deaminase, an enzyme that deactivates gemcitabine. Colorectal cancers enriched in *Fusobacterium nucleatum* also demonstrated worse prognosis, in part because the bacteria conveyed resistance to oxaliplatin and 5-fluorouracil by inducing autophagy as a cellular defense mechanism in malignant cells (table S1). Altogether, these observations support the impact of intestinal microbiome composition—and that of individual phyla and species with contrasting activities—on the evolution of cancers and their response to treatment with immunotherapy or chemotherapy.

Immunostimulation by the microbiome: Mechanisms of action

Defining the mode of action of microbes will likely become crucial for monitoring their beneficial effects in the context of cancer treatments. On theoretical grounds, the gut flora may activate anticancer immune responses in numerous ways. The main hypothetical mechanisms are (i) through the stimulation of T cell responses against microbial antigens, which either provide help for tumor-specific immune responses, or may cross-react against tumor-specific antigens; (ii) through engagement of pattern recognition receptors that mediate pro-immune or anti-inflammatory effects; or (iii) via small metabolites that mediate systemic effects on the host.

Peptide or lipid structures from bacteria can activate a range of distinct T cell receptors, thus selecting a surge of T lymphocytes that might be expanded and enter the circulation. Recent data have suggested that bacterial epitope-specific T cells can be found within the tumor microenvironment in mouse models, perhaps because of the high level of chemokines that can be produced by tumor cells, which in turn recruits the normal gut-homing $CCR9^+$ T cells (*14*). In principle, such T cells could produce cytokines or express CD40L and thereby provide help to tumor antigen–specific $CD8^+$ T cells. Alternatively, it is conceivable that they could recognize cross-reactive antigens expressed by normal or cancer cells. Such a molecular mimicry across the meta-organism has been insinuated to support the development of autoimmune diseases (*23*). However, thus far there are very scarce reports indicating that such cross-reactivities may provide an etiological link between the microbiome and responses to tumor-associated antigens expressed by malignant cells (*24*).

"One of the striking findings that distinguishes cancer patient responders from nonresponders after PD-1 blockade immunotherapy is the ratio of putatively favorable to unfavorable bacteria."

In terms of effects on pattern recognition receptors, DCs exposed to microbes (such as *B. fragilis* or *A. muciniphila*) associated with anticancer properties induce systemic IL-12–dependent T_H1/Tc1 immune responses beneficial against tumors treated with antibody to CTLA-4 (*13*) or PD-1/PD-L1 (*14*). In the presence of *Bifidobacteria*, type I interferon (IFN)–related immune genes are up-regulated in antigen-presenting cells of secondary lymphoid organs (*15*). Ligands of TLRs or Nod-like receptors (NLRs) may mediate the effects of such bacteria, as documented for *E. hirae* (*16*, *25*), *B. fragilis* (*13*), and *A. muciniphila* (table S1). Indeed, *Alistipes shahii* stimulates TNFα production by tumor-associated myeloid cells during immunotherapy combining TLR9 agonists with IL-10R blockade in a TLR4-dependent fashion (*11*). However, the microbial stimulation of anticancer memory T_H1/Tc1 cell responses only partially rely on TLR2/TLR4 in the context of treatments with cyclophosphamide (*16*) or CTLA-4 blockade (*13*). What is not yet clear is whether DC precursors attain exposure to bacterial-derived products in the vicinity of the intestinal mucosa and then traffic to the tumor and tumor-draining lymph node, or whether systemically circulating mediators dependent on specific gut bacteria can have distant effects on DCs elsewhere in the host. On a different note, nociceptive neuropeptides produced by bacteria may also affect the host, not only through the activation of sensory neurons but also by eliciting immunoregulatory T cell subsets in the gut (*26*). These findings suggest that the enteric nervous system may constitute yet another target for local (and perhaps systemic) immunomodulation.

The gut microbiome has a major impact on host metabolism, including immunometabolism. Polyamines generated in the gut—such as spermidine, as well as vitamin B6—can stimulate autophagy at distant sites of the body, eliciting anticancer immune responses in the context of chemotherapy (*27*). The capacity of the microbiome to generate polyamines has also been associated with reduced toxicity of antibody to CTLA-4 in melanoma patients (*22*). Short-chain fatty acids produced by gut bacteria are sensed by a variety of cell types, including DCs and regulatory T cells expressing the G protein–coupled receptors GPR41 or GPR43 (*28*). A microbe-associated metabolite, desaminotyrosine (DAT), derived from *Clostridium orbiscindens* has been reported to protect from influenza virus–mediated lung immunopathology through type I IFN signaling (table S1). Bacterium-derived dipeptide aldehydes mediate cathepsin L inhibition, which may enable gut mutualists to stably occupy a niche in the phagolysosome and interfere with antigen presentation of epithelial or immune cells (*28*). It can be anticipated that these and other, yet-to-be-discovered bacterial metabolites may profoundly

Box 1. Culturomics approaches to discover new biotherapeutics.

The description of cancer-associated intestinal dysbiosis constitutes an unmet medical need. So far, techniques aimed at identifying microbes were based almost exclusively on metagenomic studies. Metagenomics has several limitations, mostly related to DNA extraction methods, amplification steps, and big-data computerized analyses. Only 15% of bacteria grown from feces are detectable with metagenomics. The absence of clear definitions of uncultivatable species led to a considerable number of operational taxonomic units with a marginal taxonomic value. A large part of the bacterial cells in stools analyzed with metagenomics are nonviable at the time of defecation. The sensitivity of polymerase chain reaction is often incompatible with the detection of bacterial species located in the upper GI tract, where the vast majority of metabolic and immune functions are regulated. Automatic sampling of small intestinal content and mucosal specimens by means of ingested capsules containing miniaturized devices may constitute a technique to circumvent this limitation. Culturomics, the cultivation of all microbes living in mucosae, was developed in 2008 by using a combination of diversified culture media and rapid identification of bacterial colonies by means of matrix-assisted laser desorption/ionization–time-of-flight (MALDI-TOF) mass spectrometry alone or combined with 16S rRNA sequencing (*40*). Thus, the development of new culture media for anaerobic bacteria or metanogenic oxygen-sensitive archae or slowly growing populations forming microcolonies has been carried out (*40*), enabling the description of more than 400 new species. To render the microbiome "druggable," one needs to develop good manufacturing processes to grow commensals by using chemically defined media, without natural products originating from animals. Last, the ability to lyophilize the microorganisms while maintaining their viability after freeze-drying remains crucial for future implementations.

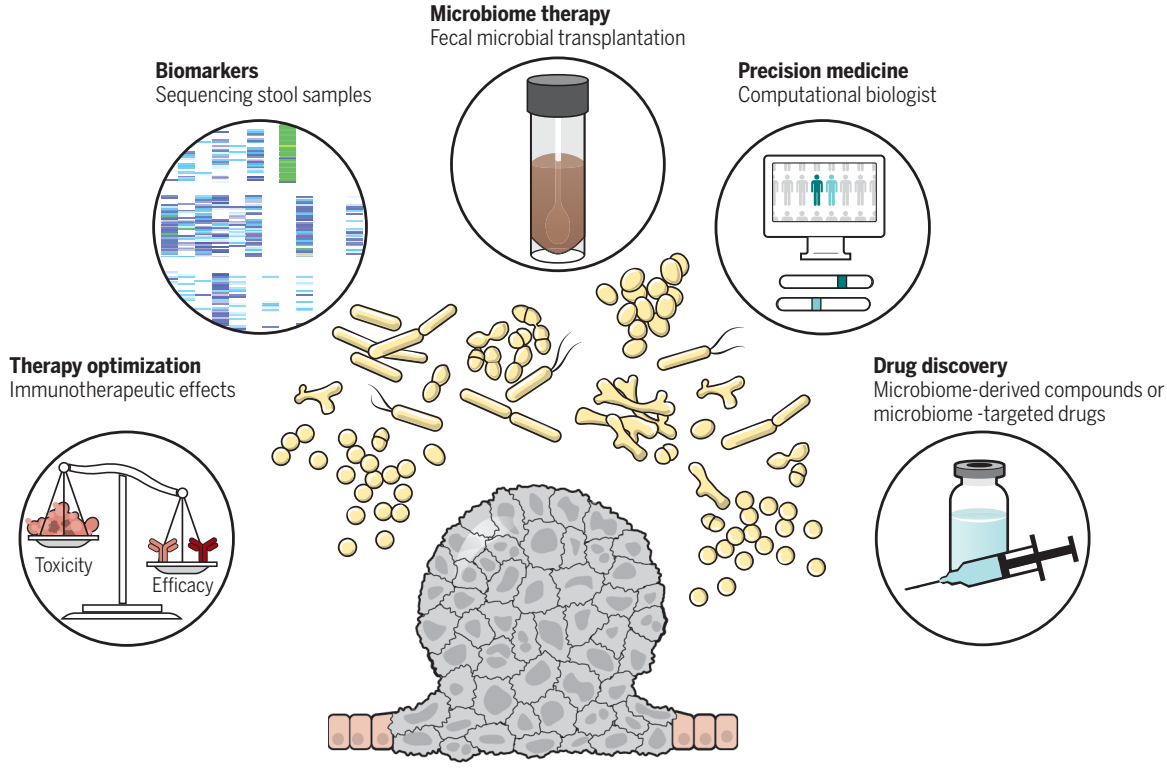

Fig. 2. Harnessing the microbiome for the discovery of diagnosis and therapeutic tools in cancer. The complex interplay between cancer, immunity, and microbiota may be partially elucidated by novel "omics" technologies: metagenomics, metatranscriptomics, culturomics, metabolomics, co-occurrence analyses, and three-dimensional crypt stem cell–derived enteroid in contact with distinct species of the microbiome and immune subsets, all integrated through computational biology. Such an apothecary of omics technologies will generate diagnosis tools for dysbiosis, for drug screening and novel therapeutics, such as artificial ecosystems or new microbial species, as well as small bioactives that either act on the microbiota to induce favorable shifts in its composition or mimic desirable microbial effects on the host. Microbial intervention as a cancer therapeutic includes prebiotics, probiotics or live bacteria (and associated phages), and natural products (autologous or allogeneic fecal microbial transplantation). These interventions will have to be adapted according to the patient's life style, comorbidities, comedications, and genetic inheritance for an optimized personalization of his or her therapy. Building on pioneering studies (*14*, *19*, *20*), new biomarkers based on microbial composition of the stool will likely emerge. Monitoring the microbiome will also be essential as a pharmacokinetic and dynamic parameter, longitudinally on new interventional studies aimed at targeting the intestinal ecosystem.

influence the host immune system. The generation of diagnostic tools and novel therapeutics will provide a challenge that will require molecular analysis of the microbiome, metabolism, and immunity cycle via novel "omics" technologies and subsequent integration through systems biology methods (Fig. 2).

Microbial interventions as a cancer therapeutic

If patients lack colonization with a community of commensal microbes that support endogenous T cell priming against tumor antigens, it is somewhat intuitive to consider FMT from a donor patient who has a favorable microbiome. Impressive results of FMT (up to 81% response rate) are well known to be effective for the treatment of refractory *Clostridium difficile* diarrhea (*29*). However, there are multiple critical parameters to consider for this approach, most notably the selection of the ideal donor. In principle, it should be an individual with a diverse microbial composition that includes bacteria associated with favorable treatment outcomes. One consideration could be to use material from cancer patients that had a major clinical response to mAbs to PD-1. However, there are reasons to approach this strategy with caution. In addition to modulating immune responses, the composition of commensal microbiota has been linked to chronic diseases, with a theoretical risk of transferring obesity from donor to recipient (*30*). Transfer of pathogens is also a potential concern—either bacterial, viral, or parasitic—necessitating careful screening. In addition, some bacteria appear to contribute to inflammation-induced carcinogenesis. FMT from colorectal patients into germ-free mice can elicit dysplasia and polyp formation, which did not occur with transplantation from normal donors (*31*). Additional variables are whether to use fresh or frozen donor fecal material, identification of optimal storage conditions, and whether a single FMT is sufficient, or multiple will be required (*32*).

A desirable alternative to transfer of a mixed population of commensal bacteria from a given donor is to use defined bacteria, either singly or in combination. This strategy will depend on identification of the precise bacterial isolates capable of supporting improved antitumor immunity in the human host, combined with culture conditions that can support their expansion in vitro and encapsulation protocols that preserve biologic activity upon oral administration. The current 16*S* rRNA and shotgun sequencing strategies are likely preferentially detecting the most abundant bacteria correlated with favorable clinical outcome. However, it is conceivable that less abundant bacterial entities that coexist with the more abundant species are functionally important. Therefore, careful culture, isolation, and mechanistic testing of rare species (some of which may reside in the small intestine and be less abundant in stool samples) will need to be considered. Communities of bacteria also may be involved in the immune-potentiating effects of gut microbes, rather than a single major species. For protection against vancomycin-resistant *Enterococci feacium*, a consortium of five bacteria was identified that functioned together in vivo (*33*). Because only a minority of bacterial entities identified through sequencing appear to be culturable with standard methods, improvement of protocols for optimal

in vitro growth will become a critical component for moving this strategy forward (Box 1). It is essential that great care be taken to use actual bacterial isolates that have the desired biological properties, which will necessitate focusing beyond the species and down to the strain level. A panel of cultured *Bifidobacterium* and *E. hirae* species and strains showed major distinctions based on genome sequencing, and clearly not all strains will be efficacious in vivo (*16*, *34*). Once specific bacteria candidates are identified, then a final challenge would be to use preclinical systems for functional screening. For in vivo testing, several mouse models have been used, including SPF mice having defined commensal bacterial compositions or preconditioned with antibiotics, or germ-free mice that lack commensals at baseline. To date, *Bifidobacteria* spp. (*15*, *20*), *Akkermansia muciniphilia* (*14*), *E. hirae* (*16*), and *Bacteroides* spp. (*13*) have been shown to improve antitumor T cell responses and support better tumor control in vivo. Although it is likely that mice cannot support colonization with all commensals that have been adapted to the human GI tract—and thus represent an imperfect system—it may be sufficient to focus on bacteria that do successfully thrive in both hosts during these early days of therapeutic development.

One of the striking findings that distinguishes cancer patient responders from nonresponders after PD-1 blockade immunotherapy is the ratio of putatively favorable to unfavorable bacteria (*20*). Thus, it is conceivable that a subset of commensal organisms have a negative impact on immunotherapy efficacy. Strategies aimed at specifically eliminating unfavorable bacteria while providing immune-potentiating effects should be pursued. While standard antibacterial antibiotics may lack specificity and pose a risk, more precise strategies are warranted. It is noteworthy that bacteriophages can be highly selective for a given bacterial species and are already being used in the food industry to eliminate unfavorable bacteria (*35*). Dietary or chemical entities that support the colonization and expansion of selected bacteria are collectively referred to as prebiotics. In principle, prebiotics should favor the relative expansion of specific bacterial entities that could have a favorable impact on antitumor immunity. Much investigation has been done with dietary fiber, components of which are metabolized to short-chain fatty acids that can have immunomodulatory properties (*36*). However, prebiotics rely on expansion of the types of bacteria that are already present in the host or ingested naturally over time. Hence, controlling for interpatient heterogeneity and experimental variables may make pharmacologic development of prebiotics as a stand-alone therapy challenging. Combinatorial administration of a prebiotic with specific bacteria (called "synbiotics") may be attractive as an integrated approach. Dietary interventions are already being evaluated for GVHD, with the goal of modulating host microbiota (ClinicalTrials.gov, NCT02763033). Besides diet interventions, other factors such as exercise, concomitant medications, and likely sleep cycles can modulate gut microbial composition (*37*). Therefore, at minimum these parameters should be tracked in clinical trial databases and evaluated for correlation with efficacy of checkpoint inhibitors and other immunotherapies.

Future challenges and regulatory considerations

The regulation of microbial consumption as a category of drug provide a therapeutic challenge. In the United States, current commercial probiotics can be purchased over the counter; however, they are only regulated as food products/dietary supplements, not as drugs (*38*). Yet if the intent of the probiotic is to have therapeutic impact such as for cancer immunotherapy, then the FDA has indicated that development and regulation as a drug is indicated, including filing of an Investigational New Drug application and the usual reporting requirements. General guidelines include the clear identification of the genus and species of the probiotic strain, including genomic sequencing, potency and mechanistic laboratory studies, human clinical trials with efficacy endpoints, human safety and adverse event evaluation, and potential for infectivity. The latter point has been made relevant by studies of the yeast-based probiotic *Saccharomyces boulardii*, which has been marketed as a probiotic and also investigated for the treatment of *C. difficile* infection. Multiple cases of disseminated infection have been identified in apparent association with this probiotic, particularly in immune-suppressed individuals (*39*). Future challenges that merge the microbiome and oncology fields will include the development of rapid and cost-effective methods for the diagnosis of intestinal dysbiosis and the precise mapping of the biological effects and modes of action of pre-, pro-, and synbiotics for each cancer type. Addressing these challenges should forge a path toward a reproducible way of manipulating the intestinal ecosystem for optimizing precision medicine and improved patient survival.

REFERENCES AND NOTES

1. P. Sharma, S. Hu-Lieskovan, J. A. Wargo, A. Ribas, *Cell* **168**, 707–723 (2017).
2. D. S. Chen, I. Mellman, *Nature* **541**, 321–330 (2017).
3. T. S. Stappenbeck, H. W. Virgin, *Nature* **534**, 191–199 (2016).
4. W. M. de Vos, E. A. de Vos, *Nutr. Rev.* **70** (suppl. 1), S45–S56 (2012).
5. R. Sender, S. Fuchs, R. Milo, *PLOS Biol.* **14**, e1002533 (2016).
6. Y. Belkaid, S. Naik, *Nat. Immunol.* **14**, 646–653 (2013).
7. S. P. Rosshart *et al.*, *Cell* **171**, 1015–1028.e13 (2017).
8. A. Dzutsev *et al.*, *Annu. Rev. Immunol.* **35**, 199–228 (2017).
9. L. Zitvogel, R. Daillère, M. P. Roberti, B. Routy, G. Kroemer, *Nat. Rev. Microbiol.* **15**, 465–478 (2017).
10. C. M. Paulos *et al.*, *J. Clin. Invest.* **117**, 2197–2204 (2007).
11. N. Iida *et al.*, *Science* **342**, 967–970 (2013).
12. S. Viaud *et al.*, *Science* **342**, 971–976 (2013).
13. M. Vétizou *et al.*, *Science* **350**, 1079–1084 (2015).
14. B. Routy *et al.*, *Science* **359**, 91–97 (2018).
15. A. Sivan *et al.*, *Science* **350**, 1084–1089 (2015).
16. R. Daillère *et al.*, *Immunity* **45**, 931–943 (2016).
17. R. R. Jenq *et al.*, *Biol. Blood Marrow Transplant.* **21**, 1373–1383 (2015).
18. N. Chaput *et al.*, *Ann. Oncol.* **28**, 1368–1379 (2017).
19. V. Gopalakrishnan *et al*, *Science* **358**, eaan4236 (2017).
20. V. Matson *et al.*, *Science* **359**, 104–108 (2018).
21. J. U. Peled *et al.*, *J. Clin. Oncol.* **35**, 1650–1659 (2017).
22. K. Dubin *et al.*, *Nat. Commun.* **7**, 10391 (2016).
23. R. Hebbandi Nanjundappa *et al.*, *Cell* **171**, 655–667.e17 (2017).
24. V. P. Balachandran *et al.*, *Nature* **551**, 512–516 (2017).
25. H. Takada *et al.*, *Infect. Immun.* **63**, 57–65 (1995).
26. N. Yissachar *et al.*, *Cell* **168**, 1135–1148.e12 (2017).
27. F. Pietrocola *et al.*, *Cancer Cell* **30**, 147–160 (2016).
28. P. Joglekar, J. A. Segre, *Cell* **169**, 378–380 (2017).
29. E. van Nood *et al.*, *N. Engl. J. Med.* **368**, 407–415 (2013).
30. N. Alang, C. R. Kelly, *Open Forum Infect. Dis.* **2**, ofv004 (2015).
31. S. H. Wong *et al.*, *Gastroenterology* **153**, 1621–1633.e6 (2017).
32. P. Moayyedi, Y. Yuan, H. Baharith, A. C. Ford, *Med. J. Aust.* **207**, 166–172 (2017).
33. S. Caballero *et al.*, *Cell Host Microbe* **21**, 592–602.e4 (2017).
34. T. Odamaki *et al.*, *Int. J. Genomics* **2015**, 567809 (2015).
35. J. Zhang, Y. Hong, N. J. Harman, A. Das, P. D. Ebner, *Genome Announc.* **2**, e00521-14 (2014).
36. S. J. Bultman, *Semin. Oncol.* **43**, 97–106 (2016).
37. C. A. Thaiss *et al.*, *Cell* **167**, 1495–1510.e12 (2016).
38. V. Venugopalan, K. A. Shriner, A. Wong-Beringer, *Emerg. Infect. Dis.* **16**, 1661–1665 (2010).
39. A. Enache-Angoulvant, C. Hennequin, *Clin. Infect. Dis.* **41**, 1559–1568 (2005).
40. J. C. Lagier *et al.*, *Nat. Microbiol.* **1**, 16203 (2016).

ACKNOWLEDGMENTS

L.Z. and G.K. were supported by the Ligue Contre le Cancer (Équipe Labelisée); Agence Nationale de la Recherche (ANR)–Projets blancs; ANR under the frame of E-Rare-2, the ERA-Net for Research on Rare Diseases; Association pour la Recherche sur le Cancer (ARC); Cancéropôle Ile-de-France; Institut National du Cancer (INCa); Institut Universitaire de France; Fondation pour la Recherche Médicale (FRM); the European Commission (ArtForce); the European Research Council (ERC); the LeDucq Foundation; the LabEx Immuno-Oncology; the Site de Recherche Intégrée sur le Cancer (SIRIC) Stratified Oncology Cell DNA Repair and Tumor Immune Elimination (SOCRATE); the SIRIC Cancer Research and Personalized Medicine (CARPEM); Recherche Hospitalo-Universitaire–LUMIERE; the Seerave Foundation; Institut Suisse de Recherche Expérimentale sur le Cancer (ISREC) Foundation; Swiss Foundation; the Paris Alliance of Cancer Research Institutes (PACRI); and philanthropy (from E. Badinter and N. Meyer). L.Z. is inventor on patent EP17305206 and European license 16306779.6 held by Institut Gustave Roussy that covers use of microbial modulators for anti-PD1/PD-L1/PD-L2 antibody-based treatments. Y.M. is supported by the Natural Science Foundation of China (NSFC, grants 81722037 and 81671630), China Ministry of Science and Technology (National key research and development program, grant 2017YFA0506200), Natural Science Foundation of Jiangsu Province (grants BK20170006 and BK20160379), Chinese National Thousand Talents Program, Chinese Academy of Medical Sciences (CAMS) Initiative for Innovative Medicine (grants CAMS-I2M and 2016-I2M-1-005), and the Non-profit Central Research Institute Fund of CAMS (grants 2016ZX310194, 2017NL31004, and 2017RC31008). D.R. is supported by the French Ministery/IHU Méditerranée Infections. T.G. was supported by Team Science Award R35 CA210098 from the Melanoma Research Alliance, the American Cancer Society–Jules L. Plangere Jr. Family Foundation Professorship in Cancer Immunotherapy, and funds from the University of Chicago Medicine Comprehensive Cancer Center; by Institutional Training Grant T32 CA009594, and from The Center for Research Informatics of The University of Chicago Biological Science Division. T.F.G. is an advisory board member for Roche-Genentech, Merck, Abbvie, Bayer, Aduro, and Fog Pharma. T.F.G. receives research support from Roche-Genentech, BMS, Merck, Incyte, Seattle Genetics, and Ono. T.F.G. is a shareholder/cofounder of Jounce Therapeutics. L.Z., D.R., and G.K. are shareholders/founders of everImmune. The University of Chicago holds a licensing arrangement with Evelo. T.F.G. is an inventor on patent 15/170,284 submitted by the University of Chicago that covers the use of microbiota to improve cancer immunotherapy.

SUPPLEMENTARY MATERIALS

www.sciencemag.org/content/359/6382/1366/suppl/DC1
Table S1
References (*41*–*74*)

10.1126/science.aar6918

RESEARCH

A phosphide salt is a versatile precursor

Geeson and Cummins, p. 1383

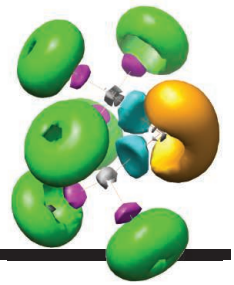

IN *SCIENCE* JOURNALS

Edited by **Stella Hurtley**

Collapsed houses and damaged cars, 1 month after a series of earthquakes struck Kumamoto, Japan, in April 2016.

GEOPHYSICS

Building better early warning systems

Earthquake early warning systems are designed to alert the public in time to seek shelter before a devastating seismic event. Typically, they are triggered when a minimum threshold of earthquake-related ground motion is sensed. However, the time required for this motion to reach the sensors depends on their distance from the earthquake source. Minson *et al.* found that triggering such systems at low levels of ground motion provided substantially faster warning than waiting until strong ground motion was sensed. These results offer a foundation for better responses to earthquake hazards in high-risk regions. —KVH

Sci. Adv. 10.1126/sciadv.aaq0504 (2018).

PLANT SCIENCE

Keeping the channels open

When the rice blast fungus enters a rice cell, the plasma membrane stays intact, so the rice cell remains viable. The fungus then moves to adjacent cells via plasmodesmata, the plant's intercellular channels. Sakulkoo *et al.* used a chemical genetic approach to selectively inhibit a single MAP (mitogen-activated protein) kinase, Pmk1, in the blast fungus. Inhibition of Pmk1 trapped the fungus within a rice cell. Pmk1 regulated the expression of a suite of effector genes involved in suppression of host immunity, allowing the fungus to manipulate plasmodesmal conductance. At the same time, Pmk1 regulated the fungus's hyphal constriction, which allows movement into new host cells. —PJH

Science, this issue p. 1399

INFECTION

Metabolic syndrome, leaky guts, and infection

Metabolic syndrome often accompanies obesity and hyperglycemia and is associated with a breakdown in the integrity of the intestinal barrier and increased risk of systemic infection. Thaiss *et al*. found that mice with systemic infection of a *Salmonella* analog, *Citrobacter rodentium*, also exhibited hyperglycemia. Deletion of the glucose transporter GLUT2 altered sensitivity to chemically induced epithelial permeability and protected mice from pathogen invasion. The authors also found a correlation in humans between glycated hemoglobin (an indicator of hyperglycemia) and serum levels of pathogen recognition receptor ligands. —CA

Science, this issue p. 1376

NEURODEVELOPMENT

Genomic plasticity during brain development

Mice genomes contain many mobile retrotransposons. Bedrosian *et al*. analyzed DNA from the mouse hippocampus during development (see the Perspective by Song and Gleeson). They found that the amount of maternal care in the first few weeks of a mouse pup's life affected the number of copies of the L1 retrotransposon. The experience of maternal care was thus "recorded" in the DNA of these mice pups during a time when the brain was still actively developing. —PJH

Science, this issue p. 1395; see also p. 1330

CONDUCTING POLYMERS

Moving charges with radicals

Conducting polymers usually contain backbones with multiple bonds. After chemical doping to remove some of the electrons, charge carriers can move freely. These conjugated backbones can also make the polymers rigid and hard to process. Joo *et al*. synthesized a redox-active, non-conjugated radical polymer that exhibited high conductivity (see the Perspective by Lutkenhaus). The polymer has a low glass transition temperature, allowing it to

CREDITS: (TOP TO BOTTOM) M. B. GEESON AND C. C. CUMMINS; KAREL PICHA/CTK/AP IMAGES

form intermolecular percolation networks for electrons. —PDS

Science, this issue p. 1391; see also p. 1334

CELL BIOLOGY

Local control of localized protein synthesis

Localized protein synthesis provides spatiotemporal precision for injury responses and growth decisions at remote positions in nerve axons. Terenzio *et al*. show that this process is controlled by local translation of preexisting axonal mRNA encoding the master regulator mTOR (see the Perspective by Riccio). mTOR controls both its own synthesis and that of most newly synthesized proteins at axonal injury sites, thereby determining the subsequent survival and growth of the injured neuron. —SMH

Science, this issue p. 1416; see also p. 1331

MATERIALS SCIENCE

More than just simple folding

Origami involves folding two-dimensional sheets into complex three-dimensional objects. However, some shapes cannot be created using standard folds. Faber *et al*. studied the wing of an earwig, which can fold in ways not possible using origami and can alter its shape for flight. The authors replicated this ability by using a membrane that allows for deformations and variable stiffness. Prestretching generated energetically bistable origami patterns that exhibited passive self-folding behavior. —MSL

Science, this issue p. 1386

The foldaway wings of an earwig inspire materials design.

CANCER

For cancer, think globally, act locally

Systemic immunotherapy in cancer treatment can have major side effects because it stimulates the entire immune system and is not necessarily tumor-specific. Surgery, a classic mainstay of cancer treatment, has the drawback of temporarily suppressing the immune response at the site of tumor resection. To address both concerns, Park *et al*. designed hydrogel scaffolds to gradually release agonists of innate immunity. They implanted these scaffolds into mice at the sites of tumor resection. This approach was safe and more effective than systemic or even locally injected immunotherapy. —YN

Sci. Transl. Med. **10**, eaar1916 (2018).

CANCER

An alternate route for metastatic cells

Metastatic tumor cells are thought to reach distant organs by traveling through the blood circulation or the lymphatic system. Two studies of mouse models now suggest a hybrid route for tumor cell dissemination. Pereira *et al*. and Brown *et al*. used distinct methodologies to monitor the fate of tumor cells in lymph nodes. They found that tumor cells could invade local blood vessels within a node, exit the node by entering the blood circulation, then go on to colonize the lung. Whether this dissemination route occurs in cancer patients is unknown; the answer could potentially change the way that affected lymph nodes are treated in cancer. —PAK

Science, this issue p. 1403, p. 1408

IN OTHER JOURNALS

Edited by **Sacha Vignieri** *and* **Jesse Smith**

Ancient forest fragmentation is a result of direct human impacts, not climate.

PLANT SCIENCE

Natural variation in salt tolerance

Salt stress in agriculture is not just a matter of being near the ocean; as much as half of irrigated farmland is overly salty. Plants have strategies to adjust to saline conditions, such as reducing sodium uptake or altering the architecture of their root systems. Julkowska *et al*. analyzed a range of *Arabidopsis thaliana* genotypes to identify genetic loci that could drive changes in root architecture in response to salt. Natural variation across 347 *A. thaliana* accessions affected the angle of roots and the distribution of bulk between main and lateral roots, leading to identification of the genes responsible. For example, variation in gene expression in response to salt showed that the *CYP79B2* (cytochrome P450 family 79 subfamily B2) gene serves to reduce lateral root growth in salt-stressed conditions. —PJH

Plant Cell **29**, 3198 (2017).

PHYSICS

A circular solution for quantum simulation

Quantum simulation can map challenging problems in complex materials onto better defined ones in simpler, easier-to-manipulate systems. Physical implementations range from trapped ions to superconducting qubits, each having distinct strengths and weaknesses. Nguyen *et al*. propose a quantum simulator that seems to combine many of the best features of the existing simulators in one system, while being within current experimental reach. The simulator is based on circular Rydberg atoms—with a highly excited electron orbiting the nucleus along a roughly circular path—where the atoms can be trapped by laser light, can be read out one by one, and have very long lifetimes. The interactions between such atoms would make it possible to simulate some of the most challenging problems in many-body physics. —JS

Phys. Rev. X **8**, 011032 (2018).

PHOTOS: (LEFT TO RIGHT) JAKOB FABER/ETH ZÜRICH; MOKHAMAD EDLIADI/CIFOR

PALEOECOLOGY

Human impact on African forests

About 2600 years ago, continuous forest in western central Africa was replaced by a mosaic of forest and savanna. It has been unclear, however, whether this was caused by climate change or expansion of the contemporary human population. Using a sedimentary record of vegetation and hydrological history from Cameroon, Garcin *et al.* confirm the key role of humans in this transition. Although the pollen record indicates an abrupt fragmentation of the forest, there is no signature of an accompanying hydrological change. Nor did the hydrology alter 500 years later when the landscape reverted once more to forest, indicating a negligible role for climate. —AMS

Proc. Natl. Acad. Sci. U.S.A. 10.1073/pnas.1715336115 (2018).

OPTICAL COMMUNICATION

Faster, faster, faster

With consumer broadband speeds on the rise and the prospect of "fiber to the home" effectively providing access to unlimited bandwidth, actual end-user data rates will nevertheless be limited by the radio-frequency wireless routers. One solution (avoiding hardwiring) is optical wireless communication, whereby an optical system replaces the wireless link. The obvious issue is that gadgets in a room tend to move, and a direct line-of-sight connection between sender and receiver stations is required. Zhang *et al.* propose an optical beam-steering scheme that provides a sufficiently wide field of view and demonstrate a data rate of 40 gigabits per second. The ability to stream content in high definition on multiple devices without the "wheel of patience" would be a thing of the past. —ISO

Opt. Lett. **43**, 723 (2018).

CLIMATE EXTREMES

The chill of a warming world

Why have some winters been so cold in some of the northern midlatitudes, even though global climate is getting hotter? Paradoxically, the answer may be that the Arctic itself is warming so quickly. Cohen *et al.* show that there is a clear relationship between Arctic temperatures and severe winter weather for the United States over the past two decades and that severe winter weather in the eastern United States has become more frequent as Arctic temperatures have risen. Although they were not included in the analysis, this relationship is likely valid for northern Europe and East Asia as well. —HJS

Nat. Commun. 10.1038/s41467-018-02992-9 (2018).

The blizzard Jonas of 2016, in the Bronx, New York, USA

PHOTO: EDDTORO/SHUTTERSTOCK

NEUROGENESIS

Neurogenesis and the sleeping fly

As we have all experienced, the body's alertness, cognitive abilities, and stress threshold depend on obtaining sufficient sleep. But why? Studies suggest that sleep is needed to set up the right brain connections. Szuperak *et al.* looked at the earliest stages of sleep by monitoring fruitfly larvae. To test for periods of rest, or sleep, they tried to arouse larvae by exposing them to a bright light. Fly larvae were indeed aroused from periods of rest, and as a result of this sleep disruption, they slept more at a later time, like other animals. Sleep-deprived larvae also showed decreased neurogenesis. This work suggests that flies may be a model for sleep, with possible implications for brain development. —BAP

eLife 10.7554/eLife.33220.001 (2018).

BIOPHYSICS

Cell geometry regulates differentiation

The size and shape (geometry) of cells regulate tension on the cytoskeleton and the contractility of the cell membrane. von Erlach *et al.* show that mesenchymal stem cells grown in different shapes have varying amounts of cell membrane microdomains known as lipid rafts. These are thought to be focal points for membrane-associated signaling, and the authors demonstrate that their occurrence was dependent on cytoskeletal contraction and cell geometry. Activation of signaling by the AKT kinase occurred at lipid rafts, and this was dependent on cell geometry and membrane contractility. Interestingly, AKT activation at lipid rafts was an important determinant of mesenchymal stem cell lineage, once differentiated. —GKA

Nat. Mater. **17**, 237 (2018).

ALSO IN *SCIENCE* JOURNALS

Edited by **Stella Hurtley**

INORGANIC CHEMISTRY

Silicon clears a wet path to phosphines

Phosphoric acid is produced on a massive scale for fertilizer by treating phosphate rock with sulfuric acid. In contrast, preparation of more elaborate phosphorus compounds used in chemical catalysis, pharmaceutical, and battery applications requires laborious generation and chlorination of elemental phosphorus. Geeson and Cummins now show that phosphoric acid may also be a practical source of such compounds (see the Perspective by Protasiewicz). They isolated and characterized a phosphide salt derived from treatment of dehydrated phosphoric acid with trichlorosilane, a compound already used at the commercial scale to produce high-purity silicon. The salt proved to be a versatile precursor for a range of alkylated and fluorinated phosphorus compounds. —JSY

Science, this issue p. 1383; see also p. 1333

BIOCHEMISTRY

Using iron to generate a copper ligand

Many microbial enzymes are metal-dependent, and the microbe must acquire scarce metals from the environment. Microbes that use methane as a carbon source have a copper-dependent enzyme that oxidizes the methane. Peptides known as methanobactins (Mbns) acquire copper by using a pair of ligands comprising a nitrogen-containing ring and an adjacent thioamide. Kenney *et al*. describe the biosynthetic machinery that adds the copper-binding groups to a precursor peptide. This involves a complex of two homologs: MbnB, a member of a functionally uncharacterized protein family that includes a diiron cluster, and MbnC, which is even less well characterized. The iron cofactor is required for ligand synthesis. MbnB and MbnC homologs are encoded in many genomes, suggesting that they may have roles beyond Mbn biosynthesis. —VV

Science, this issue p. 1411

NEURODEGENERATION

Pinpointing amyloid's toxicity

Alzheimer's disease patients have decreased activity of the peptidyl-prolyl cis-trans isomerase Pin1, an enzyme that structurally alters phosphorylated proteins and reduces amyloid-β (Aβ) production. Using mouse models of Alzheimer's disease, Stallings *et al*. found that Pin1 was dephosphorylated and inactivated by the phosphatase calcineurin, which is stimulated by Aβ-induced changes in Ca^{2+} signaling. Aβ-induced dendritic spine loss, which underlies the synaptic dysfunction in Alzheimer's disease, was prevented by treating mice with the calcineurin inhibitor FK506, an immunosuppressant that reduces organ transplant rejection. —LKF

Sci. Signal. **11**, eaap8734 (2018).

CLIMATE

How green is burning wood?

To fulfill its renewable energy pledges, the European Union is increasingly using wood rather than coal to fuel power stations. In a Perspective, Schlesinger cautions that this policy is having unintended consequences. This is particularly so in the southeastern United States, from which millions of tons of wood pellets are shipped to Europe each year. Wood is only a carbon-neutral fuel if the areas from which it is harvested can fully regrow. Offsetting the carbon used in production and transport requires additional biomass to accumulate on the land after harvest. Furthermore, carbon emissions from wood burning enter the atmosphere now, whereas forest growth removes carbon from the atmosphere over the course of several decades. —JFU

Science, this issue p. 1328

METABOLISM

An emerging target for vascular diseases

Various pathologies, including cancer and ocular diseases, are associated with hypervascularization—a localized increase in blood vessels. Recent studies have revealed the importance of metabolism in driving endothelial cell activity to form new blood vessels (angiogenesis). In a Perspective, Li and Carmeliet discuss the therapeutic opportunities to target metabolic pathways in endothelial cells to disrupt or promote vascularization in a range of different pathological conditions. —GKA

Science, this issue p. 1335

RESEARCH ARTICLE

INFECTION

Hyperglycemia drives intestinal barrier dysfunction and risk for enteric infection

Christoph A. Thaiss,[1] Maayan Levy,[1] Inna Grosheva,[2] Danping Zheng,[1] Eliran Soffer,[1] Eran Blacher,[1] Sofia Braverman,[1] Anouk C. Tengeler,[1] Oren Barak,[1,3] Maya Elazar,[1] Rotem Ben-Zeev,[1] Dana Lehavi-Regev,[1] Meirav N. Katz,[1] Meirav Pevsner-Fischer,[1] Arieh Gertler,[4] Zamir Halpern,[5,6,7] Alon Harmelin,[8] Suhail Aamar,[9] Patricia Serradas,[10] Alexandra Grosfeld,[10] Hagit Shapiro,[1] Benjamin Geiger,[2] Eran Elinav[1]*

Obesity, diabetes, and related manifestations are associated with an enhanced, but poorly understood, risk for mucosal infection and systemic inflammation. Here, we show in mouse models of obesity and diabetes that hyperglycemia drives intestinal barrier permeability, through GLUT2-dependent transcriptional reprogramming of intestinal epithelial cells and alteration of tight and adherence junction integrity. Consequently, hyperglycemia-mediated barrier disruption leads to systemic influx of microbial products and enhanced dissemination of enteric infection. Treatment of hyperglycemia, intestinal epithelial–specific GLUT2 deletion, or inhibition of glucose metabolism restores barrier function and bacterial containment. In humans, systemic influx of intestinal microbiome products correlates with individualized glycemic control, indicated by glycated hemoglobin levels. Together, our results mechanistically link hyperglycemia and intestinal barrier function with systemic infectious and inflammatory consequences of obesity and diabetes.

The obesity pandemic has reached alarming magnitudes, affecting more than 2 billion people worldwide and accounting for more than 3 million deaths per year (*1*). A poorly understood feature of the "metabolic syndrome" is its association with dysfunctions of the intestinal barrier, leading to enhanced permeability and translocation of microbial molecules to the intestinal lamina propria and systemic circulation (*2*). This influx of immune-stimulatory microbial ligands into the vasculature, in turn, has been suggested to underlie the chronic inflammatory processes that are frequently observed in obesity and its complications (*3*), while entry of pathogens and pathobionts through an impaired barrier leads to an enhanced risk of infection in obese and diabetic individuals (*4*, *5*), particularly at mucosal sites (*6*). However, the mechanistic basis for barrier dysfunction accompanying the metabolic syndrome remains poorly understood. Beyond metabolic disease, enhanced intestinal permeability has also been linked with systemic inflammation in a variety of conditions, including cancer (*7*), neurodegeneration (*8*), and aging (*9*). Thus, there is an urgent scientific need to better define the molecular and cellular orchestrators and disruptors of intestinal barrier function, to devise strategies to counteract the detrimental systemic consequences of gut barrier alterations.

Obesity is associated with, but not required for, intestinal barrier dysfunction

We began our investigation of the drivers of gastrointestinal barrier dysfunction in obesity by hypothesizing that the adipokine leptin, a major orchestrator of mammalian satiety, may act as an obesity-associated regulator of barrier integrity. Leptin deficiency and resistance to leptin signaling are strongly associated with morbid obesity in mice and humans, and both leptin deficiency and resistance were previously suggested to contribute to intestinal barrier dysfunction and susceptibility to enteric infection (*10*–*13*). We used a mouse model featuring genetic dysfunction of the leptin receptor (LepR), leading to hyperphagia and morbid obesity (*db/db*, fig. S1A). Indeed, we detected elevated amounts of microbial pattern recognition receptor (PRR) ligands at multiple systemic sites in leptin-unresponsive *db/db* mice (Fig. 1, A to C), indicative of enhanced influx of gut commensal-derived products. A similar phenomenon was observed in leptin-deficient mice (*ob/ob*, fig. S1, B and C). To gain insight into the molecular signatures accompanying barrier dysfunction under aberrant leptin signaling, we performed RNA sequencing of colonic tissue, obtained from *db/db* mice and their wild-type (WT) littermates under steady-state conditions. Leptin unresponsiveness was associated with global alterations of transcription (fig. S1D), with several hundred genes featuring differential expression between both groups (fig. S1E). Among the genes whose expression was most strongly abrogated in obese mice were members of the tight and adherence junction structures (fig. S1F), protein complexes that inhibit paracellular flux of intestinal molecules into the lamina propria (*14*). Consequently, tight junction integrity was compromised in *db/db* mice (Fig. 1, D and E), leading to enhanced influx of luminal molecules and electrical current measured across the epithelial layer (Fig. 1, F and G).

To determine the consequences of barrier dysfunction in leptin-resistant mice, we used the murine *Citrobacter rodentium* model simulating human enteropathogenic *Escherichia coli* infection (*15*). A bioluminescent variant of *C. rodentium* allowed us to noninvasively track infection in vivo (*16*). In WT mice, *C. rodentium* caused a self-limiting, mainly gut-contained infection (Fig. 1, H to L). In contrast, *db/db* mice did not clear the pathogen from their intestine (Fig. 1, H and I), in line with previous reports (*12*). Notably, *db/db* mice also showed a significantly enhanced bacterial attachment to the intestinal wall (fig. S1, G and H) and featured *C. rodentium* colonization at systemic sites (Fig. 1, J to L, and fig. S1I). Similar susceptibility to *C. rodentium* was noted for leptin-deficient *ob/ob* mice (fig. S1, J to N).

To understand which cell type was responsible for LepR-mediated protection from enteric infection, we generated bone marrow chimeras, in which WT and *db/db* mice were used as either recipients or donors of bone marrow transplanted into lethally irradiated mice. Exacerbated infection and systemic spread of *C. rodentium* was observed whenever the bone marrow recipient was LepR-deficient, regardless of the source of bone marrow (Fig. 1, M and N, and fig. S1O), indicating that the nonhematopoietic compartment mediated resistance against infection. LepR expression on nonhematopoietic cells has been reported in multiple tissues, including the gut, liver, and most prominently the nervous system (*17*). Mice lacking LepR in intestinal epithelial cells (Villin-Cre:LepR$^{fl/fl}$) or hepatocytes (Albumin-Cre:LepR$^{fl/fl}$) did not show any signs of enhanced susceptibility to *C. rodentium* infection (fig. S2, A to F), whereas mice with LepR deficiency specifically in the nervous system (Nestin-Cre:LepR$^{fl/fl}$) featured an exacerbated (fig. S2, G to I), yet highly variable (fig. S2, J to O), bacterial growth. To further explore the possibility of neuronal leptin signaling driving barrier dysfunction and risk of infection, we generated mice with a specific

[1]Department of Immunology, Weizmann Institute of Science, Rehovot, Israel. [2]Department of Molecular Cell Biology, Weizmann Institute of Science, Rehovot, Israel. [3]Department of Obstetrics and Gynecology, Kaplan Medical Center, Rehovot, affiliated with the Hebrew University and Hadassah School of Medicine, Jerusalem, Israel. [4]The Robert H. Smith Faculty of Agriculture, Food and Environment, The Hebrew University, Rehovot, Israel. [5]Sackler Faculty of Medicine, Tel Aviv Sourasky Medical Center, Tel Aviv, Israel. [6]Research Center for Digestive Tract and Liver Diseases, Tel Aviv Sourasky Medical Center, Tel Aviv, Israel. [7]Digestive Center, Tel Aviv Sourasky Medical Center, Tel Aviv, Israel. [8]Department of Veterinary Resources, Weizmann Institute of Science, Rehovot, Israel. [9]Department of Medicine, Hadassah–Hebrew University Hospital, Jerusalem, Israel. [10]INSERM Centre de Recherche des Cordeliers, Sorbonne Université, Sorbonne Cités, UPD Univ. Paris 05, CNRS, IHU ICAN, Paris, France.
***Corresponding author. Email: eran.elinav@weizmann.ac.il**

deletion of LepR in the paraventricular hypothalamus (Sim1-Cre:LepR$^{fl/fl}$), in the ventromedial hypothalamus (SF1-Cre:LepR$^{fl/fl}$), in cholinergic neurons (ChAT-Cre:LepR$^{fl/fl}$), and in the arcuate nucleus of the hypothalamus (POMC-Cre:LepR$^{fl/fl}$ and AgRP-Cre:LepR$^{fl/fl}$) and infected them with *C. rodentium*. However, none of these mice showed enhanced susceptibility to pathogenic invasion when compared to littermate controls (fig. S3, A to O). Collectively, these results suggested that leptin deficiency per se might not provide a sufficient explanation to barrier dysfunction and enhanced risk of enteric infection.

A feature common to all leptin- and LepR-deficient mice exhibiting an impaired barrier function and enhanced *C. rodentium* dissemination in our studies (*db/db, ob/ob* and Nestin-Cre:LepR$^{fl/fl}$) was their tendency to develop obesity. We therefore hypothesized that an obesity-related factor distinct from leptin signaling may predispose these mice to impaired barrier function and exacerbated intestinal infection. Thus, to complement the above genetic models of obesity, we fed WT mice a high-fat diet (HFD) to induce weight gain (fig. S4A). Similarly to obese leptin- and LepR-deficient mice, HFD-fed obese mice showed elevated steady-state systemic PRR ligand influx (Fig. 2A), as well as exacerbated *C. rodentium* infection and systemic dissemination (Fig. 2, B to E, and fig. S4B). To further test whether obesity is the major driver for barrier dysfunction and impaired *C. rodentium* containment in LepR-deficient mice, we performed paired-feeding experiments, in which the food access for *db/db* mice was restricted to the amount consumed by their WT littermates, thereby equalizing body weight between both groups (Fig. 2F). Surprisingly, even after weight reduction to control levels, lean *db/db* mice were still unable to cope with *C. rodentium* infection (Fig. 2, G and H), ruling out that obesity per se was directly driving barrier dysfunction and risk for enteric infection in these mice. The lack of a direct causal relationship between obesity and barrier dysfunction was further supported by experiments using a chemical inhibitor of leptin signaling (*18*), which rendered WT mice susceptible to exacerbated infection and systemic bacterial spread even before the onset of marked obesity (Fig. 2, I to L, and fig. S4, C to F). Together, these data indicated that neither leptin signaling nor obesity per se sufficiently explain the severity of barrier dysfunction and systemic enteric infection in mice with the metabolic syndrome.

In search of a unifying explanation for the above results in multiple mouse models of genetic and acquired obesity and leptin deficiency, we investigated other common features of the metabolic syndrome that could potentially contribute to barrier dysfunction. One such manifestation

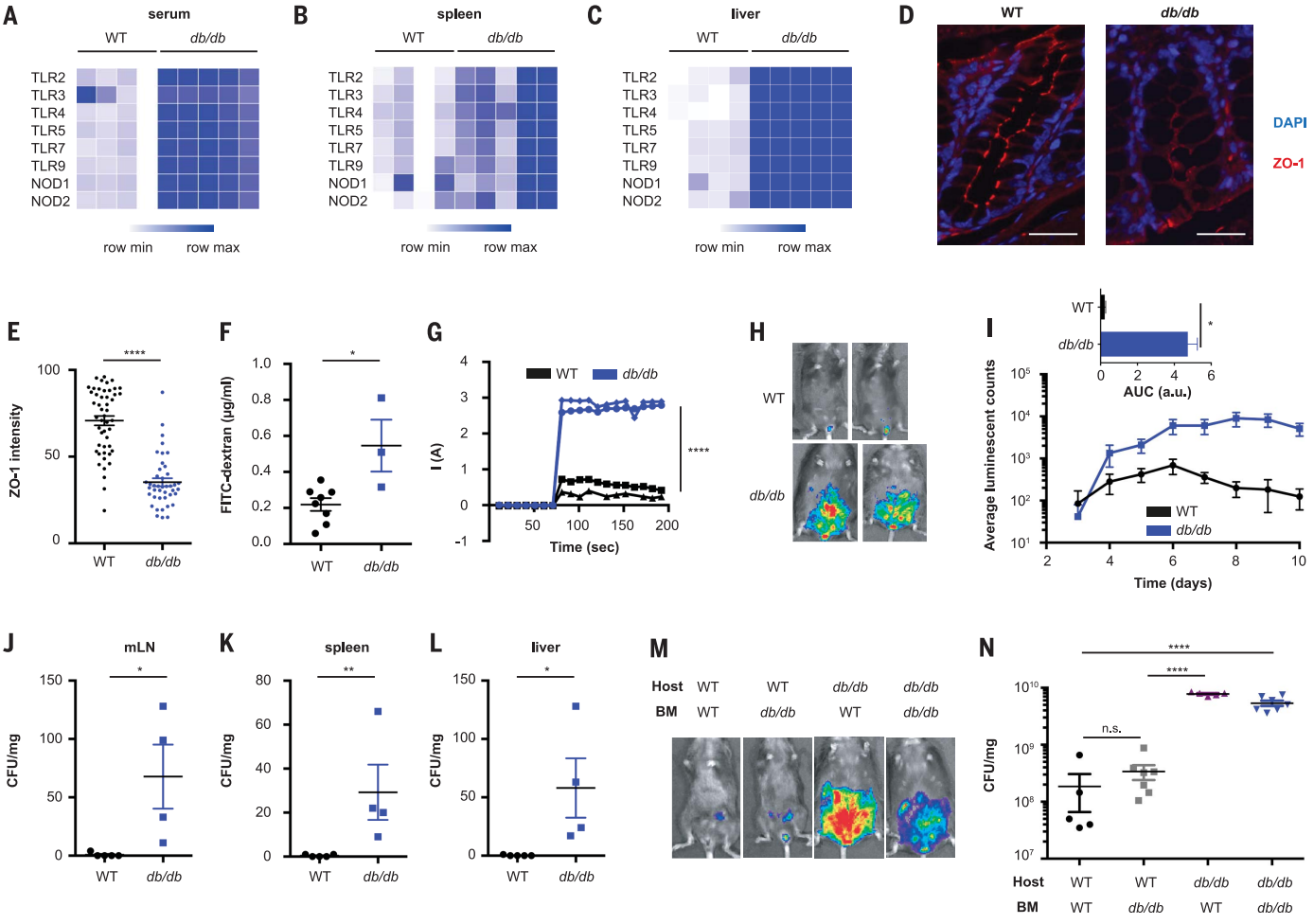

Fig. 1. Obesity is associated with intestinal barrier dysfunction and enteric infection. (**A** to **C**) PRR stimulation by sera (A) and splenic (B) and hepatic extracts (C) from *db/db* mice and WT littermates. (**D** and **E**) ZO-1 staining (D) and quantification (E) of colonic sections from *db/db* mice and WT littermates. Scale bars, 100 µm. (**F**) FITC (fluorescein isothiocyanate)–dextran recovered from the serum of *db/db* mice and WT littermates after oral gavage. (**G**) Ussing chamber recording of colons from *db/db* mice and controls. (**H** to **L**) Abdominal luminescence (H and I) and colony-forming units (CFUs) recovered from mesenteric lymph nodes (J), spleens (K), and livers (L) from *db/db* mice infected with *C. rodentium*. (**M** and **N**) Total abdominal luminescence (M) and epithelial-adherent colonies (N) of *C. rodentium* in bone marrow chimeras of *db/db* and WT mice. All data represent at least two independent experiments. Means ± SEM are plotted. *P < 0.05, **P < 0.01, ****P < 0.0001 by analysis of variance (ANOVA) (N) or Mann-Whitney U test (all other panels). ns, not significant.

of the metabolic syndrome, typically accompanying obesity and potentially contributing to barrier dysfunction, is glucose intolerance and resultant hyperglycemia. Notably, all mice featuring marked susceptibility *C. rodentium* infection, including obese *db/db*, pair-fed lean *db/db* mice, Nestin-Cre:LepR$^{fl/fl}$ mice, mice fed a HFD, and mice treated with leptin antagonist, showed elevated blood glucose concentrations (Fig. 2, M to O, and fig. S4, G and H). In contrast, all mouse groups and models that did not develop enhanced *C. rodentium* susceptibility (Villin-Cre:LepR$^{fl/fl}$, Albumin-Cre:LepR$^{fl/fl}$, Sim1-Cre:LepR$^{fl/fl}$, SF1-Cre:LepR$^{fl/fl}$, ChAT-Cre:LepR$^{fl/fl}$, POMC-Cre:LepR$^{fl/fl}$, and AgRP-Cre:LepR$^{fl/fl}$, as well as those Nestin-Cre:LepR$^{fl/fl}$ mice that did not feature a tendency for severe infection) collectively showed normoglycemic levels (fig. S4, I and J). Together, these results suggested that hyperglycemia, rather than obesity or alterations in leptin signaling, may predispose to barrier dysfunction leading to enhanced enteric infection in the setup of the metabolic syndrome in mice.

Hyperglycemia drives intestinal barrier disruption

To test whether elevated glucose concentrations were causally involved in host defense against intestinal infection, we induced hyperglycemia in the absence of obesity in a mouse model of type 1 diabetes mellitus through administration of streptozotocin [STZ (*19*), fig. S5A]. Indeed, STZ-treated mice developed severe *C. rodentium* infection and systemic translocation, accompanied by enhanced bacterial growth, epithelial adherence, and systemic spread (Fig. 3, A to E). STZ treatment also resulted in dysfunction of intestinal epithelial adherence junctions under steady-state conditions (Fig. 3, F and G), coupled with systemic dissemination of microbial products (fig. S5, B and C), and enhanced transepithelial flux (Fig. 3, H and I).

Oral antibiotic treatment prevented the detection of bacterial products at systemic sites in STZ-treated mice (Fig. 3, J to L), demonstrating that the intestinal microbiota was the probable source of disseminated microbial molecules. In contrast to the load of bacterial products at distal organs (fig. S5D), the microbial load in the intestinal lumen was unaffected by hyperglycemia (fig. S5E). We next sought to test the possibility that barrier dysfunction in STZ-treated mice was mediated by compositional microbiota alterations. Indeed, 16*S* ribosomal DNA (rDNA) sequencing revealed a taxonomic change in the configuration of the intestinal microbiota of hyperglycemic mice, which was corrected by insulin treatment and resultant normalization of serum glucose concentrations (fig. S6, A to D). However, these compositional microbial changes did not seem to play a critical role in glucose-mediated barrier dysfunction, as microbiota transfer from STZ-treated

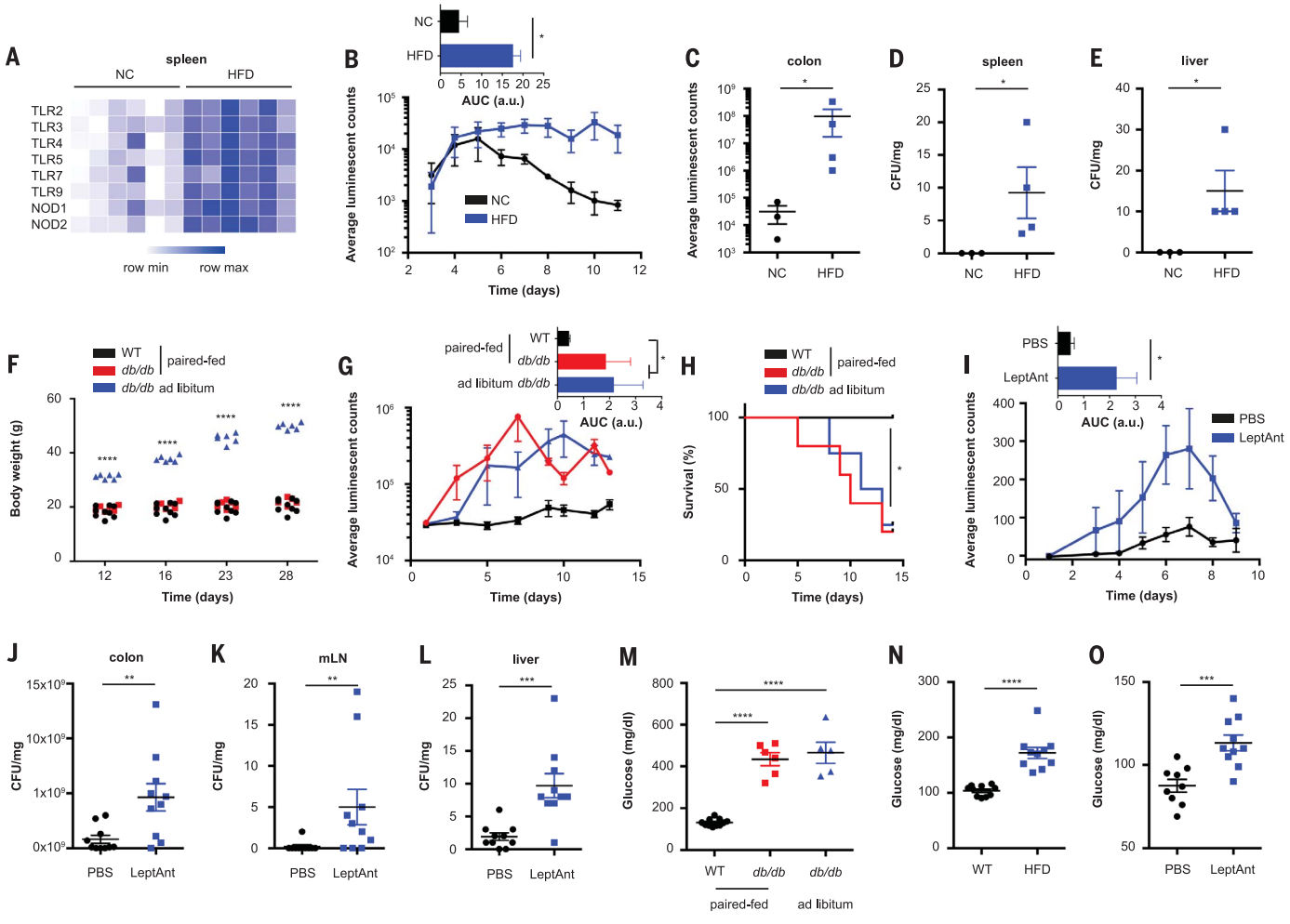

Fig. 2. Obesity does not suffice to explain susceptibility to enteric infection. (**A**) PRR stimulation by splenic extracts from mice fed a high-fat diet (HFD). (**B** to **E**) Abdominal luminescence (B) and CFUs recovered from colonic tissue (C), spleens (D), and livers (E) of HFD-fed mice infected with luminescent *C. rodentium*. (**F** to **H**) Body weight (F), *C. rodentium* luminescence (G), and *C. rodentium*-induced mortality (H) in paired-fed *db/db* mice and controls. (**I** to **L**) Total abdominal luminescence signals (I) and live CFUs recovered from colonic tissue (J), mesenteric lymph nodes, (K) and livers (L) from leptin antagonist (LeptAnt)-treated mice infected with bioluminescent *C. rodentium*. (**M** to **O**) Blood glucose concentrations in paired-fed *db/db* mice (M), HFD-fed mice (N), and LeptAnt-treated mice (O). All data represent at least two independent experiments. Means ± SEM are plotted. *P < 0.05, **P < 0.01, ***P < 0.001, ****P < 0.0001 by ANOVA (F and M) or Mann-Whitney U test (all other panels).

donors and controls to normoglycemic germ-free mice neither induced dissemination of bacterial products to systemic sites (fig. S6E) nor increased susceptibility to *C. rodentium* infection (fig. S6, F to J). These data indicate that although the commensal microbiota serves as the reservoir of microbial molecules that translocate to the systemic circulation upon disruption of the intestinal barrier, compositional microbiota alterations arising under hyperglycemic conditions do not directly affect barrier integrity.

To corroborate the specificity of hyperglycemia as a driver of susceptibility to intestinal infection, we used hyperglycemic *Akita* mice (fig. S7A), an STZ-independent model of type I diabetes mellitus that harbors a spontaneous mutation in the gene encoding insulin 2 (*20*). As in STZ-treated mice, we observed in this model elevated *C. rodentium* growth and pathogenic translocation to systemic tissues (Fig. 3, M and N, and fig. S7, B and C). To further validate the specific impact of hyperglycemia as a driver of the barrier dysfunction phenotype, we administered 0.25 U per day of insulin to STZ-treated mice via hyperosmotic pumps for 4 weeks, which restored normoglycemic levels (fig. S7D). Treatment with insulin also prevented the loss of adherence junction integrity (Fig. 4A and fig. S7E), systemic dissemination of microbial products (Fig. 4B), and enhanced *C. rodentium* growth and pathogenic translocation (Fig. 4, C and D). Together, these experiments establish hyperglycemia as a direct and specific cause for intestinal barrier dysfunction and susceptibility to enteric infection.

Hyperglycemia reprograms intestinal epithelial cells

To determine whether glucose acted directly on intestinal epithelial cells to affect barrier function, we used an in vitro system of cultured intestinal epithelial (Caco-2) cells exposed to different concentrations of glucose in the culture medium. We assessed tight junction integrity through automated high-throughput analysis of ZO-1 staining patterns. Indeed, glucose induced barrier alterations in a dose- and time-dependent manner, manifesting visually as increased tortuosity and altered appearance of cell-cell junctions (Fig. 4, E to H). To investigate the mechanisms by which elevated blood glucose concentrations compromise intestinal epithelial cell function in vivo, we performed RNA sequencing of purified intestinal epithelial cells from STZ-treated mice and controls. Global reprogramming of the epithelial transcriptome was detected in hyperglycemic mice (Fig. 4I), in which more than 1000 genes were differentially expressed compared to vehicle-treated controls (Fig. 4J). These genes were predominantly involved in metabolic pathways, and specifically in N-glycan biosynthesis and pentose-glucuronate interconversion (Fig. 4K), two intracellular functions critically involved in the maintenance of epithelial barrier function (*21*–*29*). For example, hyperglycemia affected the entire pathway of protein N-glycosylation by provoking marked downregulation of central genes (Fig. 4L and fig. S8). In contrast, epithelial proliferation or cell death were not affected by STZ treatment (fig. S9, A to D).

In addition to the above epithelial changes, hyperglycemia modestly affected the intestinal

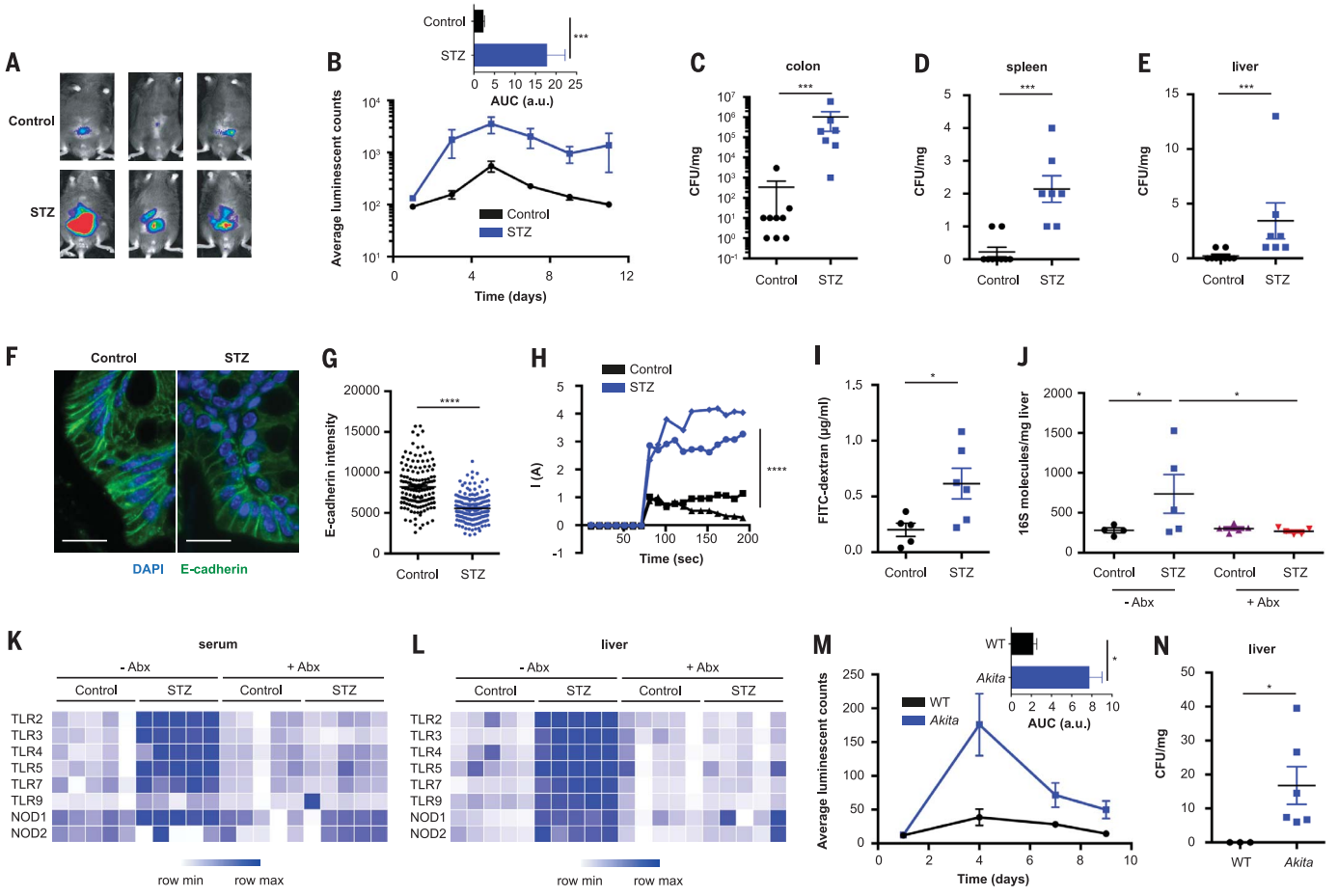

Fig. 3. Hyperglycemia causes susceptibility to enteric infection. (**A** to **E**) Abdominal luminescence (A and B) and CFUs recovered from colonic tissue (C), spleens (D), and livers (E) from STZ-treated mice infected with bioluminescent *C. rodentium*. (**F** and **G**) E-cadherin staining (F) and quantification (G) of colons from STZ-treated mice and controls. Scale bars, 25 µm. (**H**) Ussing chamber recordings from colons of STZ-treated mice and controls. (**I**) FITC-dextran recovered from the serum of STZ-treated mice after oral gavage. (**J**) Detection of 16*S* rDNA in livers of STZ- and Abx-treated mice. (**K** and **L**) PRR stimulation by sera (K) and hepatic extracts (L) from STZ-treated mice and controls, with or without antibiotic (Abx) treatment. (**M** and **N**) Abdominal luminescence (M) and hepatic CFUs (N) from *C. rodentium*–infected *Akita* mice. All data represent at least two independent experiments. Means ± SEM are plotted. *$P < 0.05$, ***$P < 0.001$, ****$P < 0.0001$ by ANOVA (J) or Mann-Whitney *U* test (all other panels).

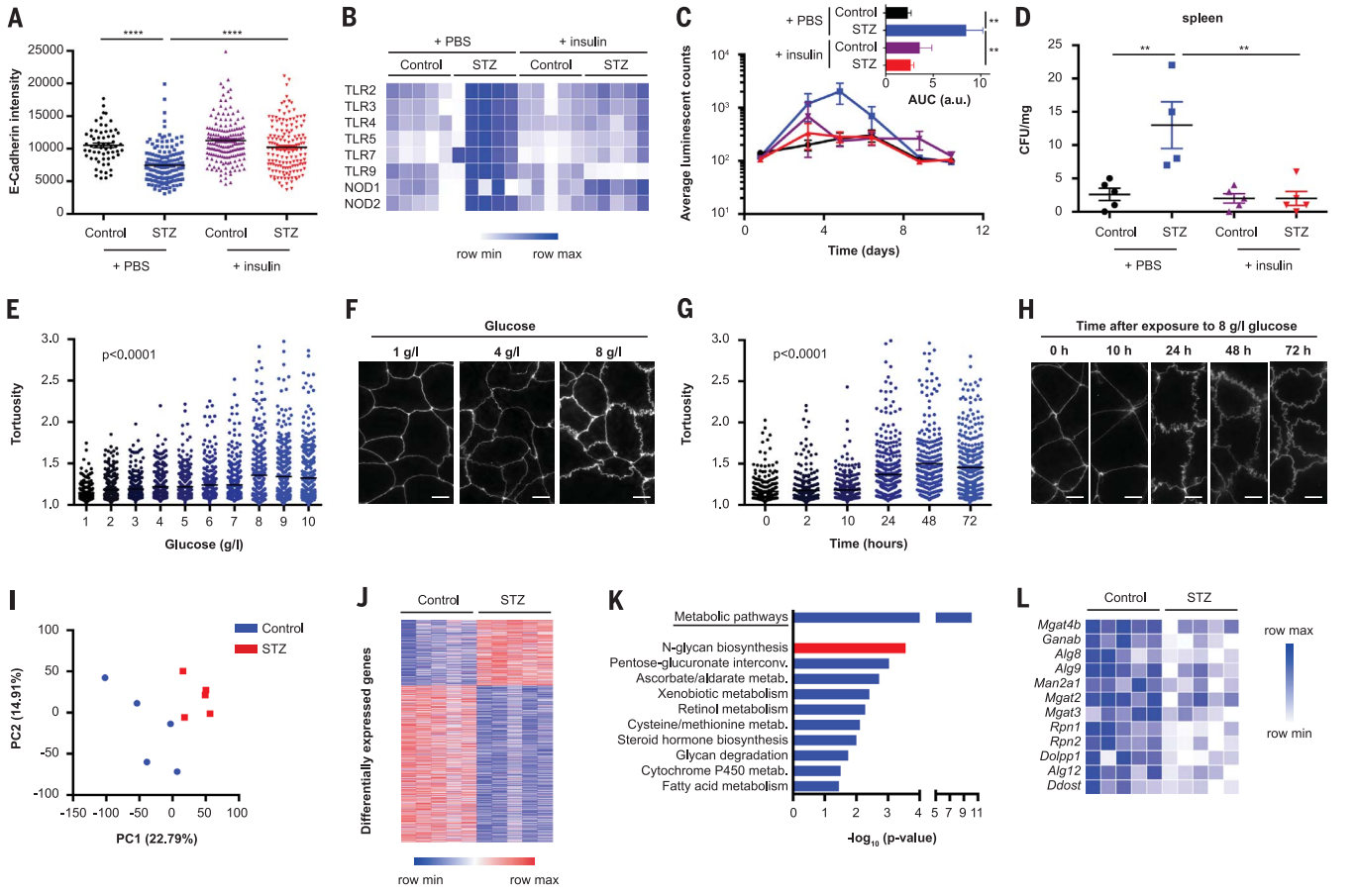

Fig. 4. Hyperglycemia alters intestinal epithelial cell function. (**A** and **B**) Colonic E-cadherin intensity (A) and PRR ligand stimulation by sera (B) from STZ-treated mice and controls, with or without insulin administration. (**C** and **D**) Abdominal luminescence (C) and CFUs recovered from the spleen (D) of STZ- and insulin-treated mice after *C. rodentium* infection. (**E** to **H**) Quantification of barrier tortuosity (E and G) and representative ZO-1 staining (F and H) of Caco-2 cells treated with different concentrations and exposure times of glucose. Scale bars, 10 μm. (**I** to **K**) Principal component analysis (I), heatmap (J), and pathway annotation (K) of differentially expressed genes in the epithelium of STZ-treated mice and controls. (**L**) Differentially expressed genes contributing to N-glycan biosynthesis. All data represent at least two independent experiments. Means ± SEM are plotted. $^{**}P < 0.01$, $^{****}P < 0.001$ by ANOVA.

and splenic immune system, specifically by causing an increased representation of myeloid cells (fig. S10, A to J), in line with previous reports (*30*). However, STZ treatment did not provoke an overt inflammatory state in the intestine (fig. S11, A to E). In particular, cytokines involved in interleukin-22 (IL-22)–mediated barrier function and host defense, which has been implicated in the susceptibility of obese mice to infection (*12*), were unaltered, as was the epithelial transcriptional response to IL-22 (fig. S11F). Indeed, hyperglycemia and IL-22 appeared to have additive effects in mediating host defense against *C. rodentium*, because STZ-treated IL-22–deficient mice featured accelerated bacterial growth and mortality when compared to IL-22–deficient controls (fig. S11, G and H). We further compared the involvement of epithelial and immune cells in host defense against another gastrointestinal pathogen, *Salmonella* Typhimurium. STZ-treated mice orally infected with *Salmonella* showed enhanced systemic colonization, whereas intestinal luminal growth was comparable to that of vehicle-treated controls (fig. S12, A to E). In contrast to this marked susceptibility of STZ-treated mice to oral *Salmonella* Typhimurium infection, susceptibility of these mice to systemic infection was only apparent in the liver (fig. S12, F to H). Notably, systemic infection with *Salmonella* caused enhanced intestinal colonization in STZ-treated mice, potentially indicative of retrograde spread of bacteria across a compromised barrier (fig. S12, I and J).

Epithelial reprogramming by hyperglycemia involves glucose metabolism and GLUT2

We next assessed whether epithelial glucose metabolism was involved in the transcriptional reprogramming of STZ-treated mice. Isolated intestinal epithelial cells from hyperglycemic mice featured elevated amounts of metabolites along the glycolytic cascade (fig. S13A). Inhibition of glucose metabolism via 2-deoxyglucose (2-DG) rescued glucose-induced barrier aberrations in vitro in a dose-dependent manner (Fig. 5, A to C). In addition, 2-DG administration blocked transcriptional reprogramming in STZ-treated mice (Fig. 5D and fig. S13B), including the N-glycan pathway (fig. S13C); prevented the systemic dissemination of microbial products (Fig. 5, E and F); and restored host defense against *C. rodentium* (Fig. 5G and fig. S13, D to F). Bacterial growth in the intestinal lumen was unaffected by 2-DG treatment (fig. S13G). To test whether 2-DG could be used to counteract hyperglycemia-mediated loss of barrier integrity beyond the STZ model, we administered 2-DG to *C. rodentium*-infected *db/db* mice and assessed its impact on systemic dissemination of the pathogen. Notably, the detectable pathogen load in the mesenteric lymph nodes, spleens, and livers of 2-DG–treated *db/db* mice was strongly reduced under 2-DG treatment (Fig. 5H and fig. S13, H and I). Together, these data suggest that glucose-mediated reprogramming of epithelial cell metabolic function leads to transcriptional alterations, abrogation of the intestinal barrier, and impaired host defense against enteric infection.

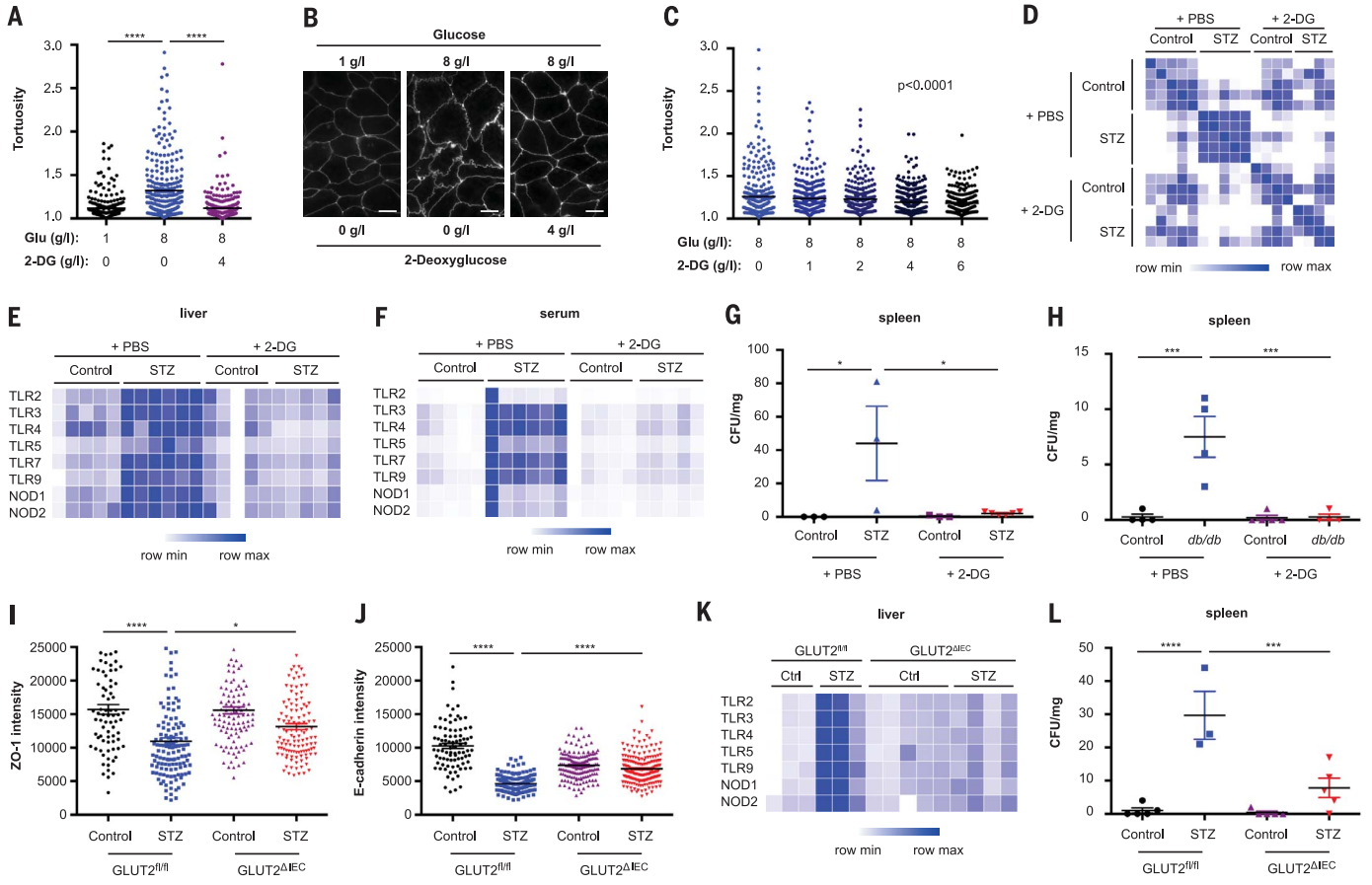

Fig. 5. Epithelial reprogramming by hyperglycemia involves glucose metabolism and GLUT2. (**A** to **C**) Quantification of barrier tortuosity (A and C) and representative ZO-1 staining (B) of Caco-2 cells treated with the indicated concentrations of glucose and 2-deoxyglucose (2-DG). Scale bars, 10 μm. (**D**) Similarity matrix of the epithelial transcriptomes of STZ-treated mice, with or without 2-DG administration. (**E** and **F**) PRR stimulation by hepatic extracts (E) and sera (F) from STZ-treated mice, with or without 2-DG administration. (**G** and **H**) Splenic CFUs from *C. rodentium*–infected and 2-DG–treated STZ (G) and *db/db* mice (H). (**I** to **K**) Colonic ZO-1 (I) and E-cadherin intensity (J) and PRR stimulation by hepatic extracts (K) from STZ-treated GLUT2$^{\Delta IEC}$ mice and controls. (**L**) CFUs recovered from spleens of STZ-treated GLUT2$^{\Delta IEC}$ mice and controls infected with *C. rodentium*. All data represent at least two independent experiments. Means ± SEM are plotted. $^{*}P < 0.05$, $^{**}P < 0.01$, $^{***}P < 0.001$, $^{****}P < 0.0001$ by ANOVA.

Glucose transport between the intestinal epithelium and circulation is mediated by the bidirectional glucose transporter GLUT2 (*31*). To determine the role of this transporter in hyperglycemia-mediated epithelial reprogramming, we next used mice selectively lacking GLUT2 in intestinal epithelial cells (GLUT2$^{\Delta IEC}$) (*32*) and induced hyperglycemia in these mice by STZ administration. Indeed, GLUT2$^{\Delta IEC}$ mice were resistant to STZ-induced transcriptional reprogramming and retained epithelial transcriptomes similar to those of controls (fig. S14, A and B). GLUT2$^{\Delta IEC}$ mice also retained intact tight and adherence junction complexes (Fig. 5, I and J, and fig. S14, C and D), reduced transepithelial flux (fig. S14E), and intestinal containment of microbial PRR ligands (Fig. 5K), despite sustained STZ-induced hyperglycemia (fig. S14F). Ablation of GLUT2 also ameliorated the STZ-induced susceptibility to *C. rodentium* growth and systemic dissemination (Fig. 5 L, and fig. S14, G to I). Collectively, these results indicate that GLUT2 is involved in the hyperglycemia-induced metabolic and transcriptional alterations in intestinal epithelial cells, resulting in barrier dysfunction and microbial translocation to the systemic circulation.

Blood glucose concentrations are associated with microbial product influx in humans

Finally, we sought to determine whether glycemic levels similarly correlate with intestinal barrier function in humans. To this end, we recruited 27 healthy individuals (fig. S15, A and B) and performed measurements of multiple serum parameters and microbial products in the circulation. Of all variables measured, hemoglobin A1c (HbA1c), indicative of an individual's 3-month average plasma glucose concentration, showed the strongest correlation with serum levels of PRR ligands (Fig. 6, A to C, and fig. S15, C to E). In contrast, high body mass index and other hallmarks of metabolic disease did not significantly associate with the influx of microbial products (Fig. 6, A and B, and fig. S15F). Total stool bacterial content did not correlate with HbA1c levels (fig. S15G). Together, these data suggest that similar to their effects in mice, serum glucose concentrations, rather than obesity, may associate with or potentially even drive intestinal barrier dysfunction in humans.

Discussion

Serum glucose is among the most strictly controlled physiological variables of organismal homeostasis. Chronically elevated glucose concentrations, as observed in diabetes mellitus, obesity, and associated metabolic disorders, such as nonalcoholic fatty liver disease, result from altered homeostatic set points of the tightly regulated normoglycemic levels (*33*). Long-standing hyperglycemia, in turn, leads to a myriad of potentially devastating biochemical and physiological consequences, such as the generation of advanced glycation end products, pancreatic glucose toxicity (*34*, *35*), macrovascular and microvascular complications affecting virtually every organ (*36*), risk of infection (*37*), and enhanced mortality (*38*).

In this study, we have identified glucose as an orchestrator of intestinal barrier function. Hyperglycemia markedly interfered with homeostatic epithelial integrity, leading to abnormal influx of

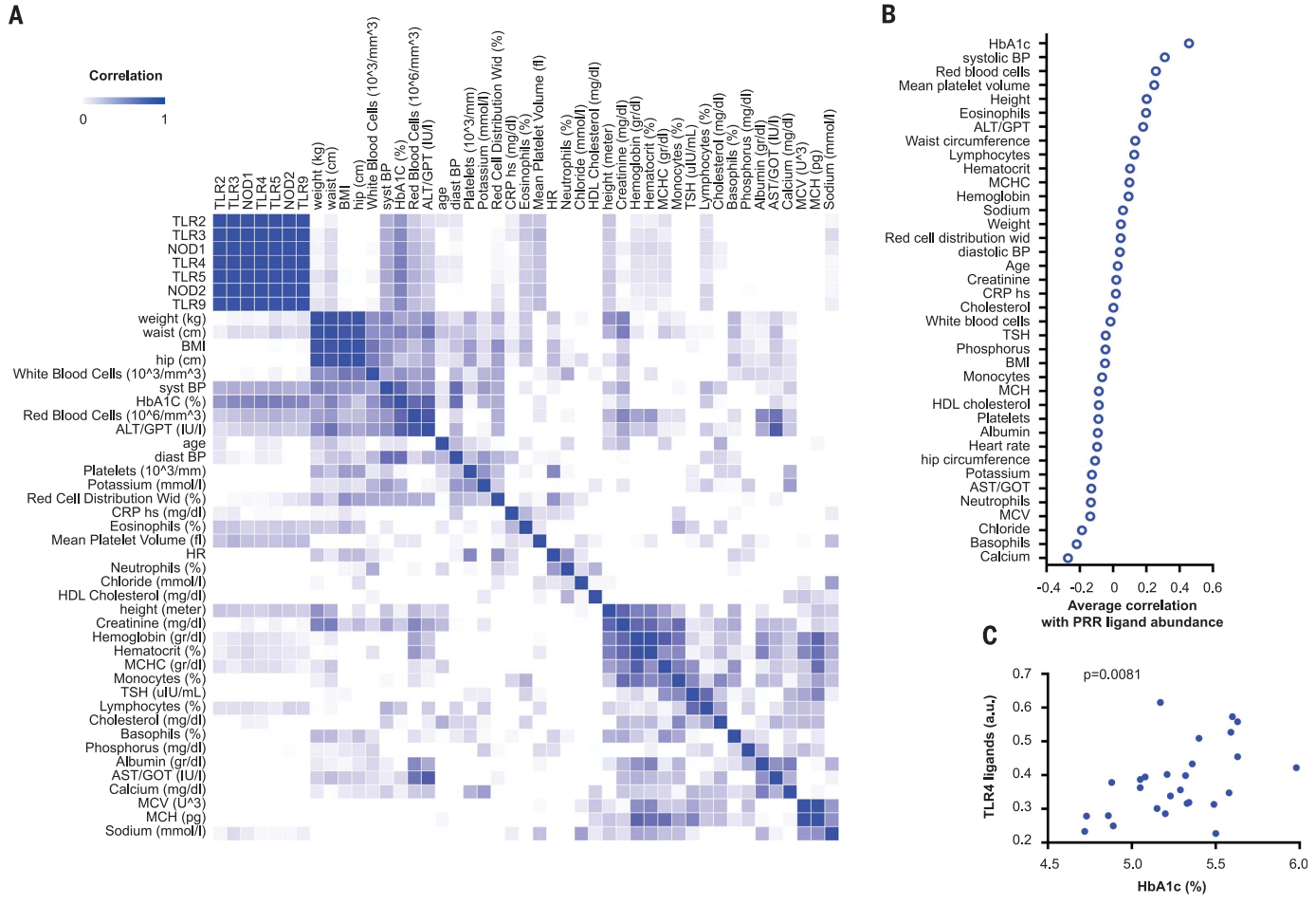

Fig. 6. Hyperglycemia is associated with influx of microbial products in humans. (**A** and **B**) Correlation matrix (A) and average correlations with systemic PRR ligands (B) of the indicated parameters in the serum of 27 healthy volunteers. (**C**) Correlation of HbA1c with serum levels of TLR4 ligands.

immune-stimulatory microbial products and a propensity for systemic spread of enteric pathogens. Our results indicate that hyperglycemia causes retrograde transport of glucose into intestinal epithelial cells via GLUT2, followed by alterations in intracellular glucose metabolism and transcriptional reprogramming (fig. S16). One of the most strongly affected pathways by hyperglycemia in our study involves the N-glycosylation of proteins in the endoplasmic reticulum and Golgi apparatus, which has been implicated as a key regulator of a multitude of epithelial functions (*25*). Although our study focused on the impact of systemic glucose concentrations on the intestinal barrier, similar effects might be caused by a high-glucose diet, which may affect intestinal epithelial cells in a similar manner, potentially resulting in diet-induced alterations of barrier function. Such potential physiologically important dietary effects on barrier function merit further studies. Furthermore, the impact of hyperglycemia on epithelial barrier function might be relevant beyond the gastrointestinal tract and affect other mucosal surfaces, such as the respiratory tract, as was indicated by a recent study of close to 70,000 diabetes patients highlighting a positive correlation between HbA1c values and a variety of mucosal community- and hospital-acquired infections (*39*).

Collectively, our findings provide a potential molecular explanation for altered barrier function in the context of the metabolic syndrome and the resultant enhanced mucosal infection noted in patients suffering from obesity (*5*) and diabetes mellitus (*40*). Furthermore, the link that we highlight between hyperglycemia and gut barrier alterations may provide a mechanistic basis for a variety of seemingly unrelated inflammatory manifestations, complications, and associations of the metabolic syndrome—collectively termed "metaflammation" or "para-inflammation" (*41*, *42*). Examples of these include adipose tissue inflammation driving exacerbated obesity and glucose intolerance (*43*), nonalcoholic fatty liver disease progressing to detrimental nonalcoholic steatohepatitis (*44*), inflammation contributing to atherosclerosis and associated cardiovascular disease (*45*), and even recently suggested associations between the metabolic syndrome and neurodegeneration (*46*). Ultimately, our results may present the starting point for harnessing glucose metabolism or other regulators of intestinal barrier integrity as potential therapeutic targets in the prevention and amelioration of enteric infection and gut-related systemic inflammation.

REFERENCES AND NOTES

1. N. Stefan, F. Schick, H. U. Häring, *Cell Metab.* **26**, 292–300 (2017).
2. D. A. Winer, H. Luck, S. Tsai, S. Winer, *Cell Metab.* **23**, 413–426 (2016).
3. P. D. Cani *et al.*, *Diabetes* **57**, 1470–1481 (2008).
4. M. E. Falagas, M. Kompoti, *Lancet Infect. Dis.* **6**, 438–446 (2006).
5. K. A. Kaspersen *et al.*, *Epidemiology* **26**, 580–589 (2015).
6. J. Casqueiro, J. Casqueiro, C. Alves, *Indian J. Endocrinol. Metab.* **16** (suppl. S1), 27–36 (2012).
7. S. I. Grivennikov *et al.*, *Nature* **491**, 254–258 (2012).
8. T. R. Sampson *et al.*, *Cell* **167**, 1469–1480.e12 (2016).
9. N. Thevaranjan *et al.*, *Cell Host Microbe* **21**, 455–466.e4 (2017).
10. R. Ahmad, B. Rah, D. Bastola, P. Dhawan, A. B. Singh, *Sci. Rep.* **7**, 5125 (2017).
11. N. M. Mackey-Lawrence, W. A. Petri Jr., *Mucosal Immunol.* **5**, 472–479 (2012).
12. X. Wang *et al.*, *Nature* **514**, 237–241 (2014).
13. R. Madan *et al.*, *Infect. Immun.* **82**, 341–349 (2014).
14. C. Guillot, T. Lecuit, *Science* **340**, 1185–1189 (2013).
15. J. W. Collins *et al.*, *Nat. Rev. Microbiol.* **12**, 612–623 (2014).
16. M. Wlodarska *et al.*, *Cell* **156**, 1045–1059 (2014).
17. M. G. Myers Jr., H. Münzberg, G. M. Leinninger, R. L. Leshan, *Cell Metab.* **9**, 117–123 (2009).
18. E. Elinav *et al.*, *Endocrinology* **150**, 3083–3091 (2009).
19. M. S. Islam, D. T. Loots, *Methods Find. Exp. Clin. Pharmacol.* **31**, 249–261 (2009).
20. J. Wang *et al.*, *J. Clin. Invest.* **103**, 27–37 (1999).
21. D. W. Scott *et al.*, *Mol. Biol. Cell* **26**, 3205–3214 (2015).
22. M. Nita-Lazar, I. Rebustini, J. Walker, M. A. Kukuruzinska, *Exp. Cell Res.* **316**, 1871–1884 (2010).

23. B. T. Jamal *et al*., *Cell Health Cytoskelet.* **2009**, 67–80 (2009).
24. Y. Goto *et al*., *Science* **345**, 1254009 (2014).
25. Y. Goto, S. Uematsu, H. Kiyono, *Nat. Immunol.* **17**, 1244–1251 (2016).
26. T. A. Pham *et al*., *Cell Host Microbe* **16**, 504–516 (2014).
27. J. M. Pickard *et al*., *Nature* **514**, 638–641 (2014).
28. K. S. Bergstrom *et al*., *PLOS Pathog.* **6**, e1000902 (2010).
29. M. Van der Sluis *et al*., *Gastroenterology* **131**, 117–129 (2006).
30. S. Niu *et al*., *J. Immunol.* **197**, 3293–3301 (2016).
31. B. Thorens, *Diabetologia* **58**, 221–232 (2015).
32. C. C. Schmitt *et al*., *Mol. Metab.* **6**, 61–72 (2016).
33. M. E. Kotas, R. Medzhitov, *Cell* **160**, 816–827 (2015).
34. A. Bangert *et al*., *Proc. Natl. Acad. Sci. U.S.A.* **113**, E155–E164 (2016).
35. Y. Tanaka, P. O. Tran, J. Harmon, R. P. Robertson, *Proc. Natl. Acad. Sci. U.S.A.* **99**, 12363–12368 (2002).
36. R. Madonna, R. De Caterina, *Vascul. Pharmacol.* **54**, 68–74 (2011).
37. S. O. Butler, I. F. Btaiche, C. Alaniz, *Pharmacotherapy* **25**, 963–976 (2005).
38. S. A. Leite *et al*., *Diabetol. Metab. Syndr.* **2**, 49 (2010).
39. A. Mor *et al*., *Am. J. Epidemiol.* **186**, 227–236 (2017).
40. L. M. Muller *et al*., *Clin. Infect Dis.* **41**, 281–288 (2005).
41. R. Medzhitov, *Nature* **454**, 428–435 (2008).
42. G. S. Hotamisligil, *Nature* **542**, 177–185 (2017).
43. D. Okin, R. Medzhitov, *Cell* **165**, 343–356 (2016).
44. A. Nakamura *et al*., *J. Diabetes Investig.* **2**, 483–489 (2011).
45. F. Pistrosch, A. Natali, M. Hanefeld, *Diabetes Care* **34** (suppl. 2), S128–S131 (2011).
46. M. Barbagallo, L. J. Dominguez, *World J. Diabetes* **5**, 889–893 (2014).

ACKNOWLEDGMENTS

We thank the members of the Elinav lab for discussions, J. Friedman for providing mice, and A. Erez and S. Limanovich for helpful advice. **Funding:** C.A.T. received a Boehringer Ingelheim Fonds PhD Fellowship. B.G. holds the Erwin Neter professorial Chair in cell and tumor biology. B.G. and E.E. are supported by the Leona M. and Harry B. Helmsley Charitable Trust; E.E. is supported by Y. and R. Ungar; the Adelis Foundation; the Gurwin Family Fund for Scientific Research; the Crown Endowment Fund for Immunological Research; the estate of J. Gitlitz; the estate of L. Hershkovich; the Benoziyo Endowment Fund for the Advancement of Science; J. L. and V. Schwartz; A. and G. Markovitz; A. and C. Adelson; the French National Center for Scientific Research (CNRS); D. L. Schwarz; the V. R. Schwartz Research Fellow Chair; L. Steinberg; J. N. Halpern; A. Edelheit; and by grants funded by the European Research Council; a Marie Curie Integration grant; the German-Israeli Foundation for Scientific Research and Development; the Israel Science Foundation; the Helmholtz Foundation; and the European Foundation for the Study of Diabetes. P.S. and A.G. acknowledge ANR-ALIA 007-01 Nutra2-sense for the generation of the intestinal epithelial-specific GLUT2 knockout mice. E.E. holds the Sir Marc & Lady Tania Feldmann professorial Chair in immunology, is a senior fellow of the Canadian Institute for Advanced Research (CIFAR), and an international researcher of the Bill & Melinda Gates Foundation and Howard Hughes Medical Institute (HHMI). **Author contributions:** C.A.T. conceived the study; designed, performed, analyzed, and interpreted experiments; and wrote the manuscript. M.L., I.G., D.Z., E.S., E.B., S.B., A.C.T., M.N.K. and M.P.-F. performed and analyzed experiments. O.B., M.E., R.B.-Z., D.L-R., Z.H., and S.A. carried out the human study. A.G., A.H., P.S., A.G., H.G., and B.G. provided critical tools, insights, and advice. E.E. conceived the study, supervised and mentored its participants, interpreted results, and wrote the manuscript. **Competing interests:** The authors declare that they have no competing interests. **Data and materials availability:** All data and code to understand and assess the conclusions of this research are available in the main text, supplementary materials, and via the following repositories: European Nucleotide Archive (ENA) accession no. PRJEB24760.

SUPPLEMENTARY MATERIALS

www.sciencemag.org/content/359/6382/1376/suppl/DC1
Materials and Methods
Figs. S1 to S16
References (*47*–*56*)

26 October 2017; accepted 6 February 2018
Published online 8 March 2018
10.1126/science.aar3318

REPORT

INORGANIC CHEMISTRY

Phosphoric acid as a precursor to chemicals traditionally synthesized from white phosphorus

Michael B. Geeson and Christopher C. Cummins*

White phosphorus, generated in the legacy thermal process for phosphate rock upgrading, has long been the key industrial intermediate for the synthesis of phosphorus-containing chemicals, including herbicides, flame-retardants, catalyst ligands, battery electrolytes, pharmaceuticals, and detergents. In contrast, phosphate fertilizers are made on a much larger scale from phosphoric acid, obtained by treating phosphate rock with sulfuric acid. Dehydration of phosphoric acid using sodium chloride gives trimetaphosphate, and here we report that trichlorosilane, primarily used for the production of high-purity silicon, reduces trimetaphosphate to the previously unknown bis(trichlorosilyl)phosphide anion. This anion offers an entry point to value-added organophosphorus chemicals such as primary and secondary alkyl phosphines, and thus to organophosphinates, and can also be used to prepare phosphine gas and the hexafluorophosphate anion, all previously available only downstream from white phosphorus.

Present industrial practice for production of most phosphorus-containing chemicals relies on energy-intensive reduction of phosphate to white phosphorus (termed the "thermal process"), followed by oxidation with hazardous chlorine to generate phosphorus trichloride (*1*). This route is followed even for mass-produced compounds, such as the herbicide glyphosate and the battery electrolyte lithium hexafluorophosphate, that in the end contain no chlorine (*2*, *3*). Chemists have sought alternative, more direct reactions to transform elemental phosphorus into valuable compounds featuring phosphorus-carbon bonds, thereby omitting chlorine from the sequence (*4*, *5*). A paradigm shift would be to obtain value-added phosphorus chemicals in a manner that bypasses both elemental phosphorus and chlorine with substantial reduction of energy inputs, waste, and potential for harm to the environment. Here, we describe a process that bypasses elemental phosphorus and borrows from the semiconductor industry for its energy inputs in the form of trichlorosilane, a high production-volume chemical made using HCl (*6*), that is the precursor to high-purity elemental silicon for the manufacture of solar panels (*7*).

Global production of white phosphorus (P_4) is near 1 Mt per year, with most production taking place in China and to a much lesser degree in Vietnam and Kazakhstan; production in the United States is limited to one plant, and the European Union has no capacity for production, relying entirely on imports (*8*, *9*). In 2017, the EU added P_4 to its list of critical materials (*10*). Worldwide, a shift has taken place to manufacture of high-purity phosphoric acid via phosphate treatment with sulfuric acid (termed the "wet process") due to lower production costs and the appealing elimination of hazardous waste disposal issues connected with P_4 production (*11*). Like elemental chlorine, P_4 has been used for chemical warfare, and it is also toxic and pyrophoric (*12*). Because the wet process accounts for ~95% of all phosphate rock processed (*1*), a shift to wet-process phosphate as the starting point for production of nonfertilizer phosphorus chemicals would benefit from the economics of scale (Fig. 1). The foregoing considerations give substantial impetus for finding synthetic routes that use wet-process phosphate, instead of P_4, as the starting point for making value-added phosphorus chemicals.

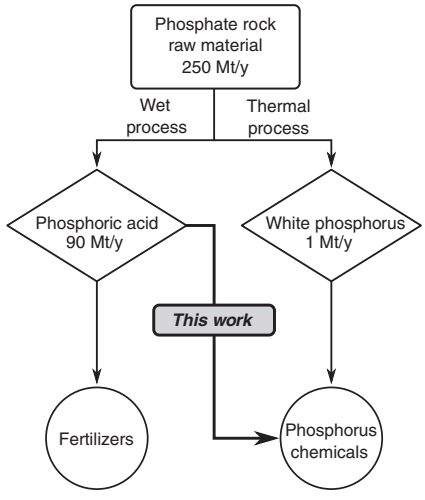

Fig. 1. Production routes to commercial phosphorus compounds from mineral sources.

Phosphate rock used for fertilizer production, underpinning global agriculture, is initially converted into phosphoric acid by the wet process (*11*). It was shown recently that phosphoric acid can be dehydrated conveniently by reaction with sodium chloride at elevated temperatures to provide sodium trimetaphosphate (*13*). We targeted trimetaphosphate, $[P_3O_9]^{3-}$, for direct conversion to value-added chemicals, positing an analogy between the monomeric unit, metaphosphate ion (PO_3^-), and carbon dioxide. Both are Lewis acids that may act as oxide ion acceptors to provide phosphate and carbonate, respectively (*14*). We hypothesized that the Lewis acidic character of metaphosphate vis-à-vis phosphate would make this form of the raw material more prone to favorable kinetics for a reductive process.

We began our investigations by converting the sodium salt of trimetaphosphate to the tetrabutylammonium (TBA) salt, $[TBA]_3[P_3O_9]\cdot 2H_2O$, (*15*) a variant more compatible with homogeneous reaction conditions in organic solvent and analysis of products by common laboratory characterization techniques such as nuclear magnetic resonance (NMR) spectroscopy. Upon heating $[TBA]_3[P_3O_9]\cdot 2H_2O$ in neat trichlorosilane (selected because of its known ability to reduce phosphine oxides (*16*) and used here in an unoptimized 33:1 Si/P molar ratio, the excess being potentially recyclable), ^{31}P NMR spectroscopy indicated clean conversion to one new phosphorus-containing product that was identified as the bis(trichlorosilyl)phosphide anion (**1**) (Fig. 2). Anion **1** gives rise to a diagnostic ^{31}P NMR singlet at −171.7 parts per million, displaying ^{29}Si satellites ($^1J_{P-Si}$ = 150 Hz) (Fig. 3A). Optimization of the reaction conditions by using a steel pressure reactor heated to 110°C for 72 hours provided [TBA][**1**] in 65% yield on a gram scale. The identity of [TBA][**1**] was confirmed by multinuclear NMR spectroscopy, x-ray crystallography (Fig. 3B), and elemental analysis. Anion **1** is also unambiguously observable by negative-mode electrospray ionization mass spectrometry and has a characteristic isotope pattern with an average mass/charge ratio of 299.86 (fig. S45).

Recently, the carbon (*17*) and silicon (*18*) analogs of anion **1** were also successfully synthesized, suggesting a general stability of trichlorosilyl stabilized p-block anions. As the only phosphorus-containing species observable by ^{31}P NMR spectroscopy in the crude reaction mixture, **1** appears to be a stable thermodynamic sink for phosphorus under these reaction conditions. The stability of **1** is presumably a result of the electron-withdrawing trichlorosilyl groups. The phosphorus-silicon bonds are notably short at 2.128(5) Å (the sum of the single bond covalent radii is 2.27 Å) (*19*), a distance contraction indicative of delocalization of phosphorus electron density into the six σ*(Si–Cl) bonds. This bonding paradigm is supported by natural bond orbital (NBO) and natural resonance theory (NRT) calculations (*20*) revealing that multiple resonance structures are needed to describe the total electron density of

Department of Chemistry, Massachusetts Institute of Technology, 77 Massachusetts Avenue, Cambridge, MA 02139, USA.
*Corresponding author. Email: ccummins@mit.edu

1 (table S5). The chemical bonding in anion **1** is visually summarized by an electron localization function (ELF) (*21*) isosurface plot (Fig. 3C), where elongations of ELF P–Si bonding basins above and below the Si–P–Si plane are indicative of phosphorus-silicon multiple bonding. The packing of [TBA][**1**] in the solid state, as determined by an x-ray diffraction study, shows that the shortest contacts between the bis(trichlorosilyl)phosphide anion and the TBA cation are between the chlorine and hydrogen centers, respectively (2.78 to 2.94 Å). The phosphorus center, although it carries the formal negative charge, has longer contact distances to the TBA cation (≥3.07 Å).

With [TBA][**1**] in hand, we were eager to see if this salt could be used to make phosphorus-carbon bonds. An alkyl halide, (4-chlorobutyl)benzene $[Ph(CH_2)_4Cl]$, was selected as the reaction partner to target organophosphorus products of low volatility and of relevance to the pharmaceutical industry (*22*). Treatment of [TBA][**1**] with $Ph(CH_2)_4Cl$ (5 equivalents) in toluene gave the corresponding dialkylsilylphosphine $[Ph(CH_2)_4]_2PSiCl_3$ which was not isolated but rather converted during workup to the borane-protected secondary phosphine $[Ph(CH_2)_4]_2P(BH_3)H$ using a solution of $THF{\cdot}BH_3$ followed by treatment with a solution of aqueous sodium hydroxide. Before the workup procedure, silicon tetrachloride was detected as a by-product in the crude reaction mixture using ^{29}Si NMR spectroscopy. Air-stable phosphine-borane adduct $[Ph(CH_2)_4]_2P(BH_3)H$ could be purified by column chromatography and isolated in 19% yield (unoptimized).

Conditions selective for monoalkylation of anion **1** were discovered when a preparation of the same secondary phosphine was attempted in a one-pot procedure. Accordingly, heating a mixture of $[TBA]_3[P_3O_9]{\cdot}2H_2O$, $Ph(CH_2)_4Cl$ and trichlorosilane was found to yield clean alkylsilylphosphine $Ph(CH_2)_4P(SiCl_3)H$, which was identified by ^{31}P NMR spectroscopy. Cleavage of the phosphorus-silicon bond using either water or basic alumina gave the corresponding primary phosphine, $Ph(CH_2)_4PH_2$, which was purified by distillation and isolated in 64% yield. Anion **1** was implicated as a likely intermediate in this one-pot procedure because the same primary phosphine was also obtained when pure [TBA][**1**] was used as the phosphorus-containing starting material under otherwise identical conditions. The presence or absence of trichlorosilane in alkylation reactions of **1** therefore provides tunably selective conditions for the preparation of primary and secondary phosphines, respectively. Existing routes from primary and secondary phosphines to several important classes of phosphorus-containing compounds such as phosphonates (*23*) and trialkylphosphines (*24*) are already well established. Secondary phosphines in particular are valuable starting materials for hydrophosphination reactions (*25*, *26*).

With (4-phenylbutyl)phosphine in hand as the product of a one-pot procedure from trimetaphosphate, we pursued a formal synthesis of fosinopril—an angiotensin-converting enzyme inhibitor used against hypertension and chronic heart failure—by oxidizing the primary phosphine to (4-phenylbutyl)phosphinic acid. This was accomplished with excellent selectivity upon treatment with hydrogen peroxide along the lines of a literature procedure (Fig. 4) (*27*). The resulting (4-phenylbutyl)phosphinic acid may be converted to the target prodrug fosinopril, as reported by a group at Bristol-Myers Squibb (*22*). Using their synthetic scheme, the key phosphorus-carbon bond-forming step involving radical addition of hypophosphorous acid was not entirely selective for addition to the terminal, olefinic carbon of 3-buten-1-yl-benzene. Chromatographic purification was necessary to assess the impact of regioisomeric impurities on the quality of intermediates downstream. In the case of the new phosphorus-carbon bond-forming methodology reported here (Fig. 2), in which an alkyl chloride was used as the source of the 4-phenylbutyl group in the (4-phenylbutyl)phosphinic acid synthesized, no such regioisomeric impurities are produced as side products. This example illustrates how the P–C bond-forming methodology, proceeding by way of in situ–generated bis(trichlorosilyl)phosphide,

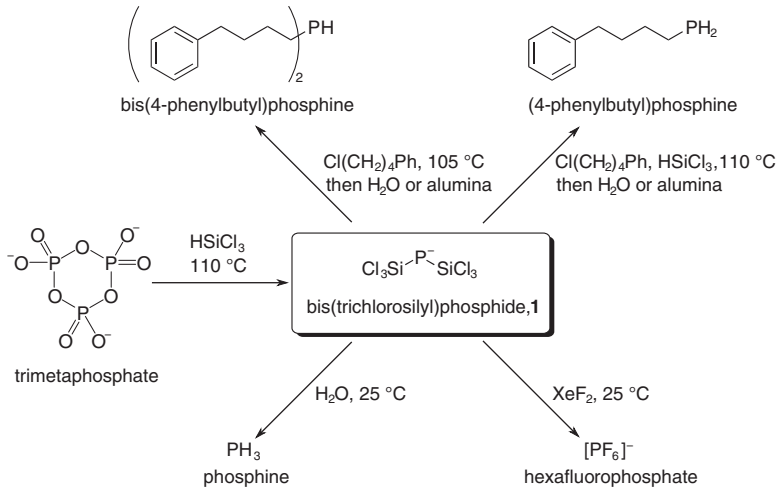

Fig. 2. Formation of bis(trichlorosilyl)phosphide (1) from trimetaphosphate and its subsequent reactivity. Compounds with phosphorus bonds to carbon, hydrogen, and fluorine are accessible.

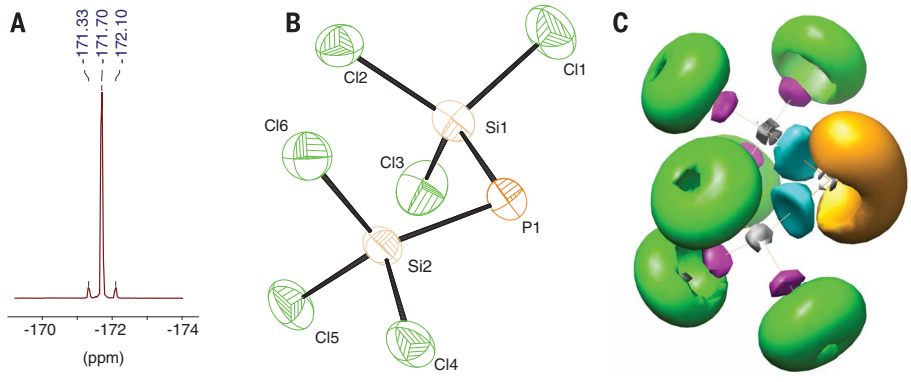

Fig. 3. Characterization of phosphide 1. (**A**) ^{31}P NMR spectrum of [TBA][**1**] displaying ^{29}Si satellites. (**B**) Crystallographic structure of **1** with thermal ellipsoids shown at the 50% probability level and the TBA cation omitted for clarity. Selected bond and angle metrics: P1–Si1: 2.141(2) Å, P1–Si2: 2.1439(19) Å, Si1–P1–Si2: 97.86(8)°. (**C**) Plot of the 0.83 ELF isosurface. Color key: orange, P lone pair basin; cyan, P–Si bond basins; magenta, Si–Cl bond basins; and green, Cl lone pair basins.

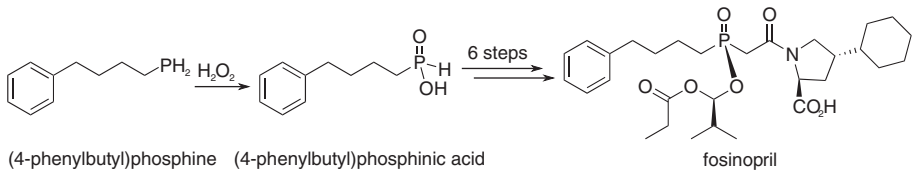

Fig. 4. Further synthetic application. Conversion of (4-phenylbutyl)phosphine to (4-phenylbutyl) phosphinic acid, an intermediate in the reported synthesis of fosinopril (*22*).

can be plugged into existing synthetic pathways to value-added phosphorus chemicals.

After observing hydrolytic cleavage of phosphorus-silicon bonds, we wondered whether anion **1** might react in a similar manner to produce phosphine (PH_3) (Fig. 2), which is primarily used in the fumigation industry and is typically produced by hydrolysis of metal phosphides (*28*). Treatment of a dichloromethane solution of [TBA][**1**] with water (15 equivalents) gave clean formation of PH_3 in at least 65% yield, as determined by quantitative ^{31}P NMR spectroscopy. This reactivity is reminiscent of that reported for trisilylphosphines, such as $P(SiMe_3)_3$, which also react with water to give phosphine, indicative of a highly reduced phosphorus center (*29*). Such compounds, traditionally synthesized from white phosphorus, are used as versatile reagents for the synthesis of metal phosphides (*30*) and quantum dots (*31*).

Having established the reduced nature of the phosphorus atom in **1**, we sought to determine whether oxidation of the phosphorus-silicon bonds with a source of fluorine might give the hexafluorophosphate anion, which is extensively employed as an electrolyte component in lithium ion batteries (*2*). Treatment of [TBA][**1**] with xenon difluoride, a convenient laboratory source of elemental fluorine (*32*), gave clean conversion to the hexafluorophosphate anion as assayed by its characteristic ^{19}F and ^{31}P NMR multiplets; the hexafluorophosphate could be isolated as its lithium salt after precipitation with lithium tetrakis(pentafluorophenyl)borate ethyl etherate (Fig. 2) in 70% yield.

In the past, when high-purity phosphoric acid for the detergent industry was manufactured from white phosphorus, the latter was a linchpin synthetic intermediate for phosphorus fine chemicals (*33*), and it is still essential for those derived today from phosphorus trichloride. With the present work, we illustrate an alternative pathway to phosphorus chemicals originating with wet-process phosphate. It is clear that several classes of phosphorus chemicals will be accessible using the chemistry described here, passing through the key molecular intermediate bis(trichlorosilyl)phosphide anion, a simple inorganic anion produced in a reaction using trichlorosilane, a high-production-volume chemical. In a possible future in which white phosphorus production were to cease, this methodology could be adopted as a replacement, keeping supply chains open for critical chemicals that currently rely on the manufacture of P_4.

REFERENCES AND NOTES

1. H. Diskowski, T. Hofmann, "Phosphorus," *Ullmann's Encyclopedia of Industrial Chemistry* (Wiley, 2000).
2. R. Younesi, G. M. Veith, P. Johansson, K. Edström, T. Vegge, *Energy Environ. Sci.* **8**, 1905–1922 (2015).
3. J. E. Franz, J. A. Sikorski, M. K. Mao, *Glyphosate: A Unique Global Herbicide* (American Chemical Society, Washington DC, 1997).
4. M. Peruzzini, L. Gonsalvi, A. Romerosa, *Chem. Soc. Rev.* **34**, 1038–1047 (2005).
5. J. E. Borger, A. W. Ehlers, J. C. Slootweg, K. Lammertsma, *Chemistry* **23**, 11738–11746 (2017).
6. R. A. Benkeser, *Acc. Chem. Res.* **4**, 94–100 (1971).
7. W. Simmler, "Silicon Compounds, Inorganic," *Ullmann's Encyclopedia of Industrial Chemistry* (Wiley, Weinheim, Germany, 2000).
8. Deloitte Sustainability, British Geological Survey, Bureau de Recherches Géologiques et Minières, Netherlands Organisation for Applied Scientific Research, Study on the review of the list of critical raw materials, *Tech. Rep.* https://doi.org/10.2873/398823 (2017).
9. W. Schipper, *Eur. J. Inorg. Chem.* **2014**, 1567–1571 (2014).
10. European Commission, 2017 List of Critical Raw Materials for the EU (2017); http://ec.europa.eu/growth/sectors/raw-materials/specific-interest/critical_en.
11. K. Schrödter *et al.*, "Phosphoric Acid and Phosphates," *Ullmann's Encyclopedia of Industrial Chemistry* (Wiley, Weinheim, Germany, 2008).
12. J. Emsley, *The 13th Element: The Sordid Tale of Murder, Fire and Phosphorus* (Wiley, New York, 2000).
13. D. Pham Minh, J. Ramaroson, A. Nzihou, P. Sharrock, *Ind. Eng. Chem. Res.* **51**, 3851–3854 (2012).
14. J. Rebek Jr., *Tetrahedron* **35**, 723–731 (1979).
15. C. J. Besecker, V. W. Day, W. G. Klemperer, *Organometallics* **4**, 564–570 (1985).
16. D. Hérault, D. H. Nguyen, D. Nuel, G. Buono, *Chem. Soc. Rev.* **44**, 2508–2528 (2015).
17. U. Böhme, M. Gerwig, F. Gründler, E. Brendler, E. Kroke, *Eur. J. Inorg. Chem.* **2016**, 5028–5035 (2016).
18. M. Olaru *et al.*, *Angew. Chem. Int. Ed.* **56**, 16490–16494 (2017).
19. P. Pyykkö, M. Atsumi, *Chemistry* **15**, 12770–12779 (2009).
20. F. Weinhold, C. R. Landis, *Valency and Bonding: A Natural Bond Orbital Donor-Acceptor Perspective* (Cambridge Univ. Press, Cambridge, UK; New York, 2005).
21. A. D. Becke, K. E. Edgecombe, *J. Chem. Phys.* **92**, 5397–5403 (1990).
22. N. G. Anderson *et al.*, *Org. Process Res. Dev.* **1**, 315–319 (1997).
23. L. D. Quin, "The Common 3-Coordinate Functions (σ^3, λ^3)," in *A Guide to Organophosphorus Chemistry* (Wiley, 2000), pp. 82–83.
24. H. Werner, G. Canepa, K. Ilg, J. Wolf, *Organometallics* **19**, 4756–4766 (2000).
25. V. S. Chan, I. C. Stewart, R. G. Bergman, F. D. Toste, *J. Am. Chem. Soc.* **128**, 2786–2787 (2006).
26. D. K. Wicht, D. S. Glueck, "Hydrophosphination and Related Reactions," in *Catalytic Heterofunctionalization*, A. Togni, H. Grützmacher, Eds. (Wiley, 2001), pp. 143–170.
27. S. Buckler, M. Epstein, *Tetrahedron* **18**, 1221–1230 (1962).
28. G. Bettermann, W. Krause, G. Riess, T. Hofmann, "Phosphorus Compounds, Inorganic," *Ullmann's Encyclopedia of Industrial Chemistry* (Wiley, Weinheim, Germany, 2000).
29. D. C. Gary, B. M. Cossairt, *Chem. Mater.* **25**, 2463–2469 (2013).
30. M. D. Healy, P. E. Laibinis, P. D. Stupik, A. R. Barron, *J. Chem. Soc. Chem. Commun.* **1989**, 359 (1989).
31. S. Tamang, C. Lincheneau, Y. Hermans, S. Jeong, P. Reiss, *Chem. Mater.* **28**, 2491–2506 (2016).
32. N. Bartlett, F. O. Sladky, *Chem. Commun.* **1968**, 1046–1047 (1968).
33. R. Gilmour, *Phosphoric Acid: Purification, Uses, Technology, and Economics* (CRC Press/Taylor & Francis, Boca Raton, FL, 2014).

ACKNOWLEDGMENTS

We thank W. J. Transue for his insightful discussion throughout the course of this work and for collecting Raman spectra; M. L. Riu for independently reproducing the procedure for the synthesis of [TBA][**1**]; Y. Surendranath, A. Radosevich, D. Nocera, and D. Dhiba (OCP Group) for stimulating discussions; and D. Darensbourg for the gift of a steel pressure reactor. **Funding:** The authors gratefully acknowledge financial and logistical support received through the Université Mohammed VI Polytechnique-MIT Research Program, a partnership between UM6P and OCP Group in Morocco and the Massachusetts Institute of Technology dedicated to promoting sustainable development in Africa. The authors acknowledge the Commonwealth Computational Cloud for Data Driven Biology for computing resources. **Author contributions:** M.B.G. contributed to conception and design of experiments, data collection, analysis and interpretation, and drafting and critical revision of the manuscript; C.C.C. contributed to conception and design of experiments, analysis and interpretation, and drafting and critical revision of the manuscript. **Competing interests:** M.B.G. and C.C.C. are inventors on patent application 62/583,472, submitted by the Massachusetts Institute of Technology, which covers a method for producing phosphorus chemicals from wet-process phosphate. **Data and materials availability:** Crystallographic data are available from the Cambridge Structural Database under refcode 1815508. Full synthetic details, including preparative procedures and spectroscopic data for characterization of compounds, are in the supplementary materials.

SUPPLEMENTARY MATERIALS

www.sciencemag.org/content/359/6382/1383/suppl/DC1
Materials and Methods
Figs. S1 to S48
Tables S1 to S7
References (*34*–*50*)

4 December 2017; accepted 23 January 2018
Published online 8 February 2018
10.1126/science.aar6620

MATERIALS SCIENCE

Bioinspired spring origami

Jakob A. Faber,[1] Andres F. Arrieta,[2]* André R. Studart[1]*

Origami enables folding of objects into a variety of shapes in arts, engineering, and biological systems. In contrast to well-known paper-folded objects, the wing of the earwig has an exquisite natural folding system that cannot be sufficiently described by current origami models. Such an unusual biological system displays incompatible folding patterns, remains open by a bistable locking mechanism during flight, and self-folds rapidly without muscular actuation. We show that these notable functionalities arise from the protein-rich joints of the earwig wing, which work as extensional and rotational springs between facets. Inspired by this biological wing, we establish a spring origami model that broadens the folding design space of traditional origami and allows for the fabrication of precisely tunable, four-dimensional–printed objects with programmable bioinspired morphing functionalities.

Programmable matter that can self-shape, morph, and actuate through "instructions" embedded into its own material architecture is widespread in nature and has opened exciting possibilities in robotics, biomedical technologies, arts, and design (*1*–*3*). Origami is particularly attractive because it allows folding simple, two-dimensional (2D) sheets into complex, 3D geometries. This simplicity and effectiveness of folding has inspired mathematicians, engineers, and materials scientists to exploit origami (*4*, *5*) as programmable metamaterials (*6*, *7*), reconfigurable structures (*8*–*10*), adaptive architectures (*11*, *12*), and soft robotic parts (*13*, *14*).

Despite its exciting prospects, major drawbacks remain when using classic origami principles. Classic origami, or rigid origami, uses two building blocks: rigid, planar facets of zero thickness and distinct, straight-line creases. These rigidity assumptions lead, in theory, to a limited design space of possible folding patterns (*15*). Besides these pattern constraints, a second aspect that limits functionality is that rigid origami mechanisms have only one degree of freedom, which is not associated with any stiffness during folding or unfolding. This lack of stiffness renders the resulting mechanisms purely kinematic (only describing motions) and thus hinders many engineering applications, particularly those involving load-bearing functions.

Attempts to extend the purely kinematic rigid origami principles have mainly been pursued by introducing bending energy in the creases (*5*, *16*). The addition of bending energy in the form of stiffness to the crease allows for forces and moments to be linked to the folding process; however, the design space for folding patterns remains unchanged. To account for additional folding patterns and programmability observed in practice on thin sheets, facet bending or twisting has been identified as an extra degree of freedom (*17*, *18*).

Despite these efforts, synthetic origami structures developed so far are still far from reaching the range of functionalities and design freedom observed in nature. An impressive natural example of folding pattern and functionality is the wings of Dermaptera, an order of insects commonly known as earwigs (Fig. 1A). The folding ratio (closed/open area) of these highly specialized wings is among the highest in the animal kingdom, with reported values of 1:10 (*19*) to 1:18 (*20*). This exceptionally high ratio concurrently allows for a large wing area during flight and a short, folded package to navigate the earwig's tight underground habitat (*21*). There are three very distinct features separating the wing-folding mechanism of Dermaptera from the assumptions of rigid origami. First, the earwig wing employs a pattern (Fig. 1B) that is incompatible with rigid origami theory because of angle mismatches and curved creases (*22*). Second, the wing has evolved to fully and rapidly self-fold from the open toward the closed state. The self-folding is achieved without the use of muscles. Instead, it

[1]Complex Materials, Department of Materials, ETH Zürich, 8093 Zürich, Switzerland. [2]Programmable Structures Lab, School of Mechanical Engineering, Purdue University, West Lafayette, IN 47907, USA.
*Corresponding author. Email: andre.studart@mat.ethz.ch (A.R.S.); aarrieta@purdue.edu (A.F.A.)

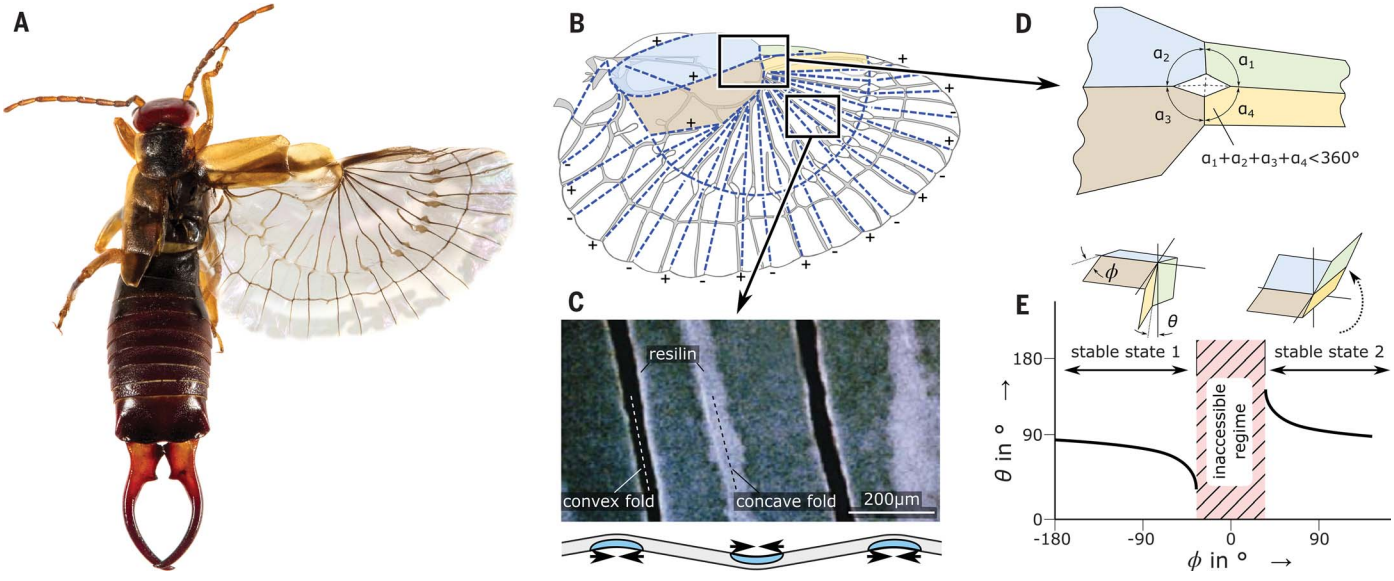

Fig. 1. Earwig wing as a natural example of multifunctional programmable folding. (**A**) The earwig *Forficula auricularia* with unfolded wing. [Image reprinted with permission from G. Wizen] (**B**) The folding pattern is incompatible with rigid origami assumptions. [Image adapted from Haas *et al*. (*19*)] (**C**) Alternating, asymmetric resilin distribution throughout the wing drives the self-folding process. The schematic under the microscopic image indicates the resilin-rich regions (in blue) along the cross-section of the wing. [Microscope image reprinted from (*19*) with permission by Elsevier] (**D**) Bistable central mechanism and angle mismatch. [Image adapted from Haas *et al*. (*19*)] (**E**) The inaccessible regime is responsible for the bistable function, but not accessible by origami kinematics. [Graph adapted from Haas (*23*) for a missing angle of 60°]

is preprogrammed in asymmetrically arranged, prestrained resilin in the joints (*19*) (Fig. 1C). Finally, a bistable snap-through mechanism (Fig. 1D) is incorporated in the structure to keep the unfolded wing in its open state. The open, locked state is stable enough to resist the aerodynamic loads during flight. The rigid origami model of this mechanism describes angular motions near the stable states (Fig. 1E), but exhibits a "forbidden range" (*23*) or inaccessible regime. Notably, this regime near the snap-through angle determines all functionality of the earwig wing. Thus, although the morphing of the earwig wing arises solely from the folding pattern and crease design, current origami models are not sufficient to describe its exceptional functionality even if bending facets are considered.

Our aim in this study is to identify design principles of the earwig wing and implement them in synthetic structures with pronounced stiffness and fast-morphing programmability. Therefore, we first investigate the earwig wing's self-folding behavior by finite element analysis (FEA) and derive the underlying principles embedded in the design of its natural joints. We then simplify the identified joint design using analogous mechanical springs. Using the newly introduced spring elements, we build a model of the wing's core mechanism to quantify its bistability and self-folding functions. Finally, these functions are transferred into 4D-printed, synthetic folding systems with unmatched and tunable functionality inspired by the natural example.

The self-folding and locking capability of the earwig wing relies on the presence of resilin-based joints. Resilin is an elastic biopolymer commonly linked to energy storage in natural systems, which has been found in symmetrical as well as asymmetrical arrangements in the earwig wing's joints (*19*). This through-thickness distribution of resilin in the joints determines the spring type: A symmetric distribution corresponds to an extensional spring, whereas an asymmetric distribution corresponds to a rotational spring. Combinations of both forms are possible. Whereas rotational springs have been discussed elsewhere (*5*, *16*), we now describe the role and resulting design capabilities of extensional springs for extending the pattern design space and generating locking, multistable folding systems.

To exploit the effect of the proposed extensional springs on the wing's self-folding behavior, we conducted folding simulations assuming either strict origami or spring-modified origami conditions (Fig. 2). Our results show that the geometrically incompatible folding pattern of the wing prevents complete folding if the strict conditions of traditional origami are considered (Fig. 2C). By contrast, full closure of the wing following the same pattern as the natural example is observed if the joints are treated as extensional and rotational springs. More details of these FEA simulations are provided in the supplementary materials. To assess the feasibility of this simulation, we produced a replica of the wing pattern by multimaterial 4D printing of stiff polymer facets (acrylonitrile butadiene styrene, ABS) and rubber-like hinges (thermoplastic polyurethane, TPU). The manually folded package confirms the stacking order and shape of the simulation results (Fig. 2D).

Despite the complexity of the simulated biological example and therefore the rather qualitative nature of these results, such proof-of-concept computational analysis clearly hints at the crucial role of membrane extensibility in making previously incompatible fold designs accessible.

The extensibility of joints not only facilitates the folding of complex patterns, but also paves the way to understand and synthetically design bioinspired features that were previously out of reach. The most notable feature of the earwig wing is its central mid-wing mechanism. It is bistable with two possible states: During folding, it is a classic Miura-Ori pattern with three convex and one concave fold. After fully opening and passing through an unstable flat state, it becomes a concave pyramid (Fig. 3A). In this shape, the mid-wing mechanism maintains the wing in its open flying configuration. Although it consists of only four facets, this crucial part of the wing simultaneously exhibits the mentioned features of interest; namely, self-folding, self-locking (bistability), and imperfect-pattern tolerance. Thus, a fundamental investigation of the interplay between membrane (extensional) and bending (rotational) elastic energy stored in folds of the mid-wing region provides valuable insights into the design principles of this morphing structure. To analytically model this four-facet unit cell, we use simple rotational and extensional springs (Fig. 3). The four rigid facets are interconnected by rotational and extensional springs at each joint (Fig. 3A). The spring constants of possible materials and geometries can easily be retrieved from the formulas given in the supplementary

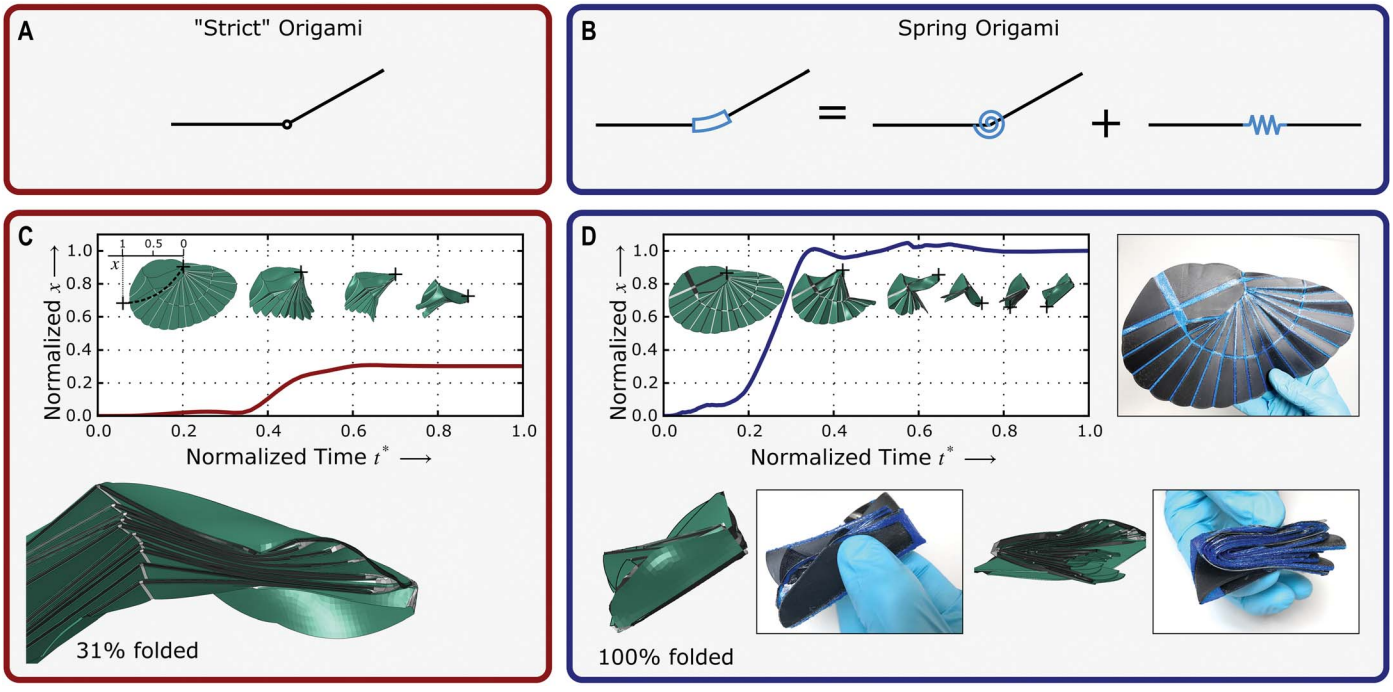

Fig. 2. Assumptions and FEA simulations describing the self-folding behavior of the earwig wing. (**A**) Strict (rigid) origami model. (**B**) Proposed interpretation of resilin occurrence as extensional and rotational spring elements. (**C**) Origami-inspired simulation approach leads to incomplete self-folding, whereas (**D**) the incorporation of spring elements in the origami structure results in complete self-folding of the simulated wing (movie S1). A multimaterial printed wing model confirms the shape and fold order of the simulated folded package.

materials. The energy stored in one rotational spring equals $\frac{1}{2}c_B(\Delta\phi)^2$, where c_B is the rotational spring stiffness and $\Delta\phi$ is the difference between the interfacet angle ϕ and the angle under which no bending stress occurs, $\phi_{0,B}$ (Fig. 3B). Similarly, the extensional spring energy is $\frac{1}{2}c_M(\Delta x)^2$, where c_M is the extensional spring stiffness and Δx is the spring extension x compared to its stress-free state $x_{0,M}$. Simple trigonometry links the spring extension x and the folding parameter ϕ (see Eq. S3), allowing for a convenient description of all energies in terms of ϕ (Fig. 3C). The extension-free angle obtained, $\phi_{0,M}$, is determined by the missing angle between the facets (see Eq. S10).

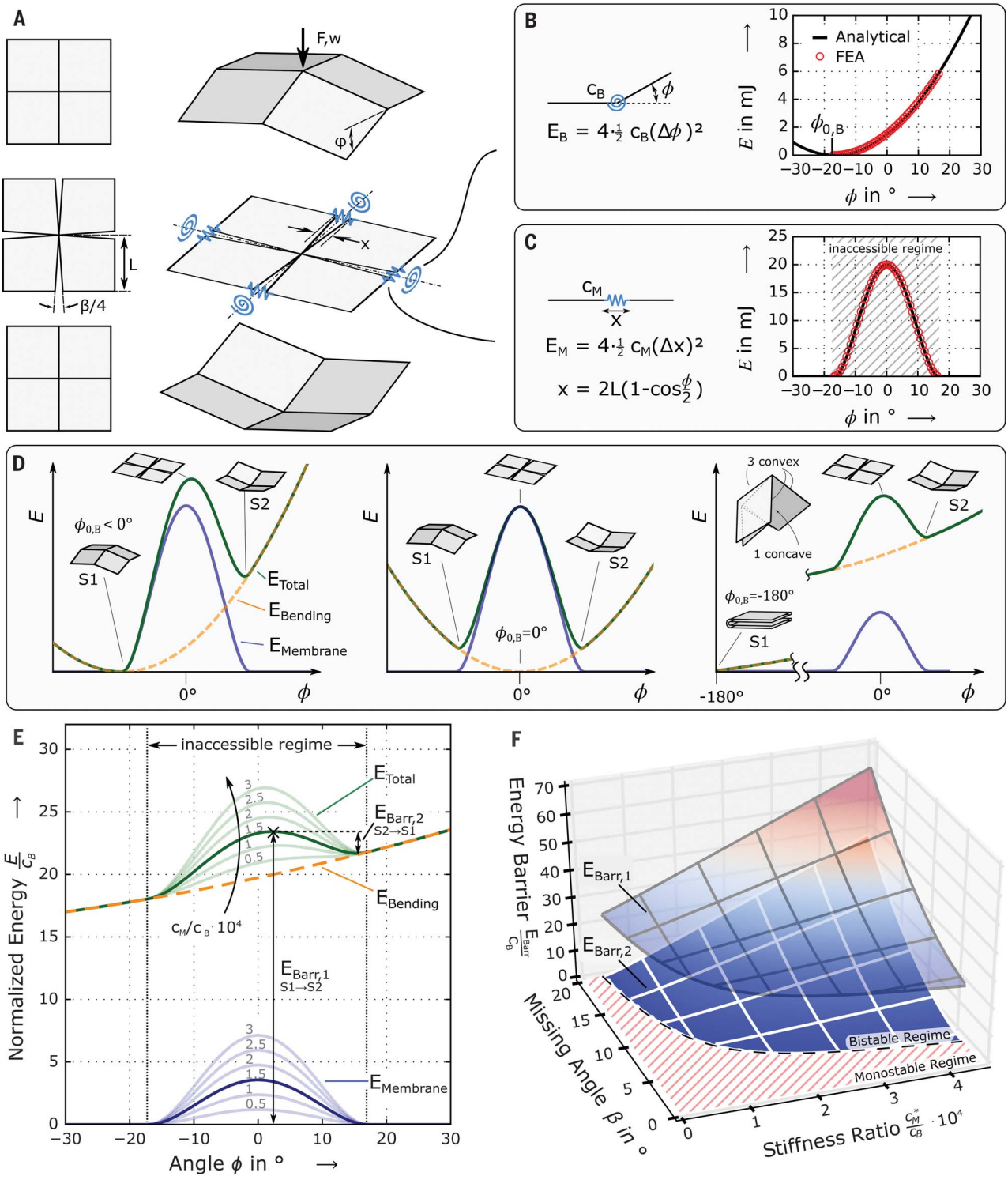

Fig. 3. Generalized model of bistable four-fold spring origami structures. (**A**) Geometry and spring arrangement. Analytical (**B**) rotational and (**C**) extensional spring energies and corresponding FEA evaluations. (**D**) Possible configurations and associated energy landscapes of selected four-faced spring origami structures. (**E**) Influence of the extensional spring stiffness on the energy landscape for β = 5° and definition of energy barriers. (**F**) Design map illustrating the effect of the missing angle and stiffness ratio on the magnitude of the energy barriers $E_{Barr,1}$ and $E_{Barr,2}$.

By computing the rotational and extensional contributions of the total energy stored in the joints of the mid-wing region, it is now possible to establish the energy landscape of the four-facet structure in different configurations (see assumptions in supplementary materials). In the inaccessible regime, the missing angle β must be compensated for by membrane extension, giving rise to an energy peak (Fig. 3, C and D). The rotational and extensional energy contributions can then be combined in endless configurations, depending on the folding patterns, each joint's stiffness values, and the programming parameters $\phi_{0,B}$ and $\phi_{0,M}$. Three exemplary configurations are shown in Fig. 3D. The initially

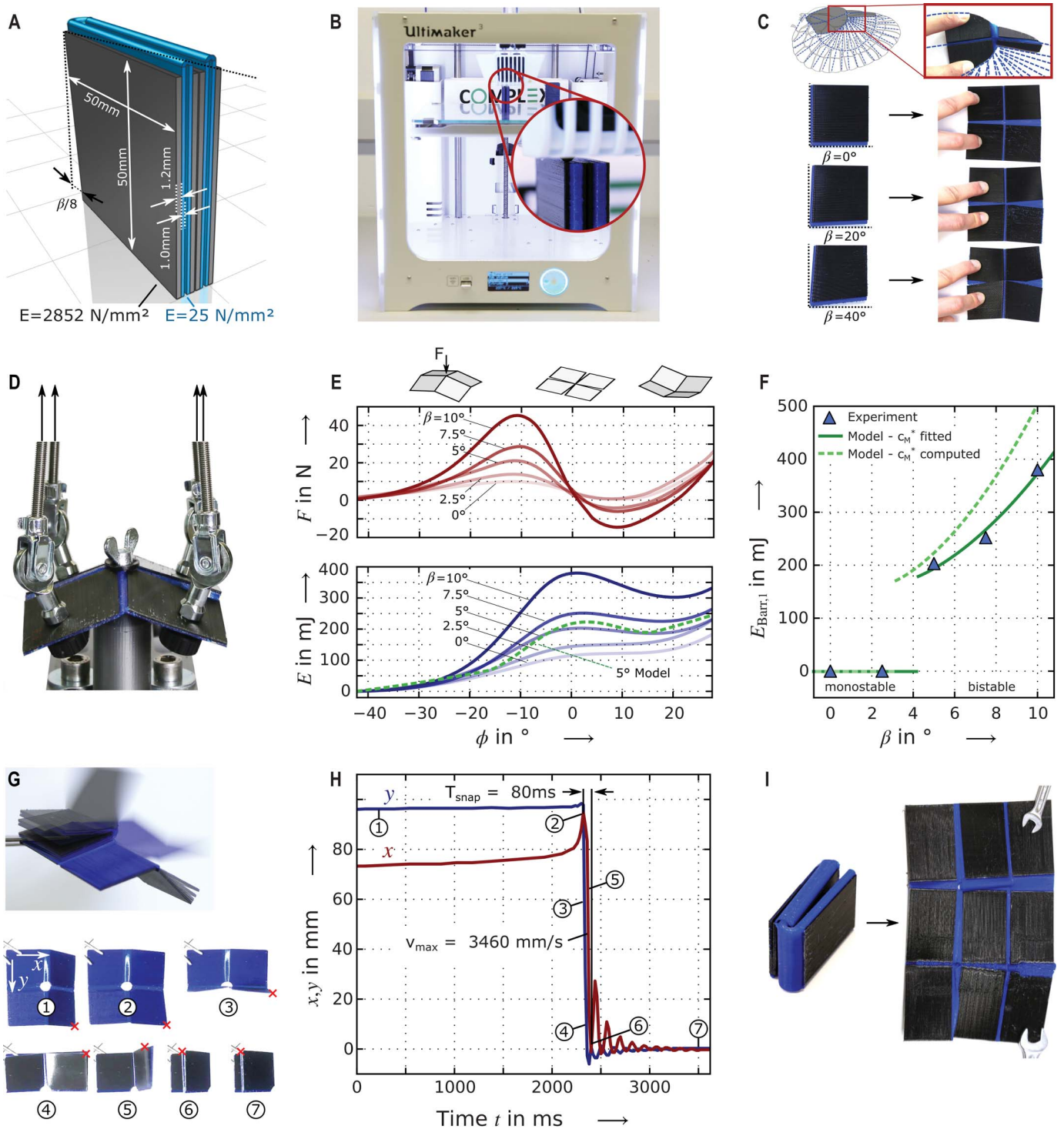

Fig. 4. Four-dimensional printing and experimental investigation of spring origami mechanisms. (**A**) Geometry and material properties. (**B**) FDM printing in the folded, upright state. (**C**) Nondevelopable, 4D-printed designs using the earwig wing's central mechanism contours (top) and simplified rectangular facet contours with different missing angles. (**D**) Cardan test rig. (**E**) Measured forces and related energy plots for mechanisms with increasing missing angle β. Model prediction for β = 5° is shown by the dashed green curve. (**F**) Effect of the missing angle on the energy barrier magnitudes and model predictions. (**G** and **H**) Fast self-folding after slow internal stimulus (movie S1). (**I**) A 4D-printed, nondevelopable 3 × 3–panel array.

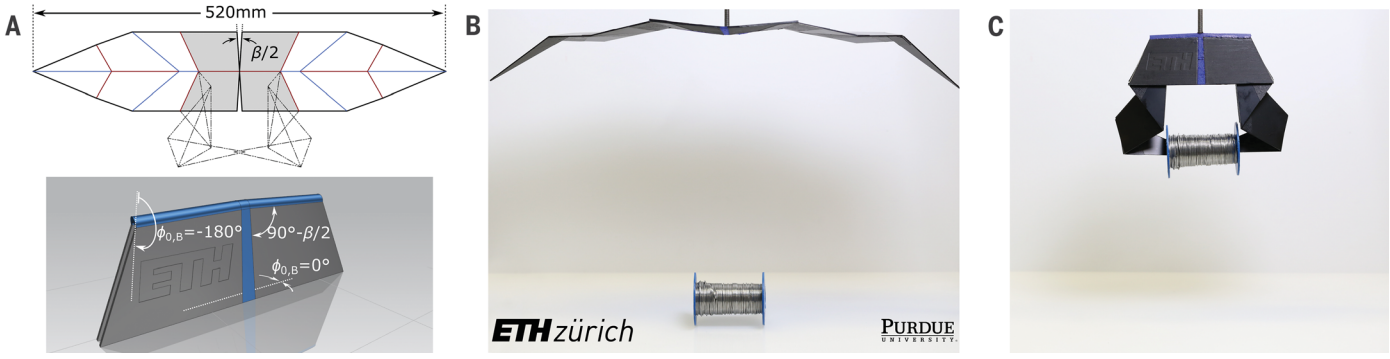

Fig. 5. Spring origami gripper (movie S2). (**A**) Fold pattern. Gray facets and computer-assisted design model: preprogrammed control cell. White facets: passive part of mechanism. (**B**) Stable state 1: open. (**C**) Stable state 2: closed. The closed state exerts force on the gripped object without constant actuation.

mentioned case of a stress-free "pyramid" as the base state leads to an asymmetrical energy landscape (Fig. 3D, left). A symmetrical case can be reached by planar assembly of facets, including a missing angle and using prestretched joint regions (Fig. 3D, center). Assembling three convex ($\phi_{0,B} = -\pi$) and one concave fold ($\phi_{0,B} = +\pi$), as in the case of the earwig wing, yields the exemplary Miura-Ori configuration, which serves as our base system. These preprogrammed angles lead to a fully folded pattern as the stress-free state (Fig. 3D, right).

For a technical application of the described unit cell, it is necessary to understand and model the relation between design parameters and resulting morphing and mechanical properties. Applying the basic building blocks from Fig. 3, A to D, we computed design maps of two kinds: First, Fig. 3E shows the bending, membrane, and total stored energies over ϕ for the self-folding Miura-Ori configuration, displaying a constant missing angle β. A low membrane stiffness ratio (c_M/c_B) leads to monostable systems resulting from the lack of an energy barrier that could give rise to two distinct mechanical states. These systems are bending-dominated and will return to their preprogrammed shape immediately. For stiffness ratios of $\frac{c_M}{c_B} > 0.5 \times 10^4$, a barrier develops in the energy landscape, leading to the two minima that characterize a bistable system. This threshold from mono- to bistability changes with the missing angle, which increases the energy barrier and therefore shifts the overall behavior toward more pronounced bistability. The combined effect of both stiffness values c_M and c_B, as well as the missing angle β, on the magnitude of the energy barriers $E_{Barr,1}$ and $E_{Barr,2}$ is shown in the design map depicted in Fig. 3F. E_{Barr} scales proportionally with c_M and c_B as long as their ratio is constant (see Eqs. S1 and S2). For each $\frac{c_M}{c_B}$ ratio, there is a critical missing angle β_c that makes the folding pattern bistable, and vice versa (Fig. 3F). The parameter space revealed by these maps allows us to determine appropriate variables to design folding behavior, stable states, and tuned energy barriers in spring origami systems. Such features control the direction and order of folding, the obtainable geometries, and the self-locking strength. Furthermore, the derivatives of the energy plots allow one to directly obtain folding moments and forces, which are relevant for the design of load-bearing functions in both stable states (see Eqs. S1 and S5). As is the case in the earwig wing, this unit cell can serve as an embedded control unit for much larger folding patterns and complex geometries. In the following section, we discuss how this Miura-Ori configuration can be exploited in exemplary synthetic systems to achieve fast folding and locking mechanisms with minimal actuation inspired by the earwig wing.

We transferred the biological design principles extracted from the earwig wing into a functional synthetic folding system that can be directly manufactured by 4D printing using a conventional additive manufacturing process (Fig. 4). The base configuration was a fourfold structure of 100 mm by 100 mm unfolded edge length with 1.2-mm-thick facets made of a stiff component [polylactic acid (PLA) or ABS] and joints made from an elastomeric component (TPU) with a thickness of 1.0 mm (Fig. 4A). Using multimaterial fused deposition modeling (FDM, Fig. 4B), we can overcome several limitations of conventional origami-type folding approaches. First, printing allows us to preprogram the folding pattern in an elegant way: Instead of using selective shrinking or swelling of a bilayer architecture to induce bending (*14*, *24*, *25*), we printed the samples in the fully folded configuration. This allows us to set $\phi_{0,B} = \pm\pi$ in the desired combination. If bistability is simultaneously required, simple folding techniques also fail. Any missing angle $\beta \neq 0$ renders the fold pattern nondevelopable, which means not foldable from a flat sheet. Our folded-printing approach allows us to program $\phi_{0,M}$ by directly implementing the missing angle β in the geometry. Figure 4C demonstrates the relationship between the printed and the unfolded geometry with the missing angle β ranging from 0° to 40°.

To illustrate the distinctive folding and mechanical functionalities of the printed spring origami, we measured the force required to keep the structure at a constant interfacet angle near and within the inaccessible region (Fig. 1E). The energy curves obtained through integration of the measured forces feature the two-well landscapes characteristic of bistable systems (Fig. 4E, blue curves). The experimental curves and the earlier model predictions match quantitatively very well the dependence of the stored energy on the folding angle (Fig. 4E, dashed line). The magnitude of the energy barrier observed in these curves rises in a progressive manner with increasing missing angles β and shows the predicted bistability threshold behavior (Fig. 4F). Small missing angles lead to the monostable systems predicted by our model (compare Fig. 3E), whereas bistability arises above the expected threshold.

Our ability to tune the energy barrier between bistable states using simple geometrical and material properties (Fig. 3F) enables the design and fabrication of spring origami structures that can undergo fast morphing, triggered by an environmental stimulus. As opposed to other common biological and synthetic morphing systems that react to external stimuli (*26*–*28*), the elastic energy stored in spring origami results in very fast intrinsic folding of the structure. Tracking the motion of a Miura-Ori structure during self-folding allowed us to quantify the dynamics of this fast morphing process (Fig. 4, G and H). The snap-through between the two stable states occurs in 80 ms, much faster than conventional diffusion-driven mechanisms. This is equivalent to the fast actuation mechanism used by the Venus flytrap or the underwater suction trap Utricularia, which also convert a slow stimulus to a rapid movement by bistability concepts (*29*, *30*).

We also demonstrate the scalability of our 4D-printing approach beyond four-facet systems by printing larger arrays (Fig. 4I), or by using a single spring origami element to control more complex structures that fold via conventional mechanisms. To illustrate this possibility, we fabricated a spring origami gripper that actuates with a low-energy input (Fig. 5 and movie S2). The gripper consists of a passive fold pattern (white) responsible for the kinematic gripping movement and a central, 4D-printed spring origami element (gray) that defines the energy landscape of the folding system. By designing the

materials and geometrical parameters (Fig. 5A) of this cell—namely, missing angle, stiffness values, and strain-free fold angles—the inherent energy landscape of the entire gripper mechanism can be programmed. Our spring origami gripper eventually displays the bistable and fast self-folding functionalities of the earwig wing. The programmed stable states (Fig. 5, B and C) and energy landscape allows the spring origami structure to exert a force on the gripped object without the need for constant external actuation. This contrasts with purely passive rigid origami mechanisms, which would yield to any applied load owing to the absence of an energy landscape or stable states. The spring origami gripper can thus remain in both the open (Fig. 5B) or closed positions (Fig. 5C) and lift objects of its own body weight.

Origami structures featuring extensional and rotational joints inspired by the earwig wing show unusual self-locking, fast-morphing, and geometry-tolerant folding patterns that are not allowed in conventional origami theory. The possibility of 4D printing 3D objects whose morphing and mechanical behavior are programmed with the material architecture brings us closer to the design strategies underlying the exquisite dynamics of biological self-shaping structures. The ample design space provided by the proposed spring origami systems can potentially be used to fabricate biomedical devices with patient-specific morphing features, collapsible portable displays, soft robots, or deployable spacecraft modules.

REFERENCES AND NOTES

1. I. Burgert, P. Fratzl, *Philos. Trans. A Math. Phys. Eng. Sci.* **367**, 1541–1557 (2009).
2. L. D. Zarzar, J. Aizenberg, *Acc. Chem. Res.* **47**, 530–539 (2014).
3. A. Ghadban *et al.*, *Chem. Commun. (Camb.)* **52**, 697–700 (2016).
4. A. Lebée, *Int. J. Space Structures* **30**, 55–74 (2015).
5. N. Turner, B. Goodwine, M. Sen, *J. Mec.* **230**, 2345–2362 (2016).
6. J. L. Silverberg *et al.*, *Science* **345**, 647–650 (2014).
7. S. Shan *et al.*, *Adv. Funct. Mater.* **24**, 4935–4942 (2014).
8. E. A. Peraza-Hernandez, D. J. Hartl, R. J. Malak Jr., D. C. Lagoudas, *Smart Mater. Struct.* **23**, 094001 (2014).
9. S. Waitukaitis, R. Menaut, B. G. Chen, M. van Hecke, *Phys. Rev. Lett.* **114**, 055503 (2015).
10. S. Daynes, R. S. Trask, P. M. Weaver, *Smart Mater. Struct.* **23**, 125011 (2014).
11. S. Tibbits, K. Cheung, *Assem. Autom.* **32**, 216–225 (2012).
12. P. M. Reis, F. López Jiménez, J. Marthelot, *Proc. Natl. Acad. Sci. U.S.A.* **112**, 12234–12235 (2015).
13. J. Mu *et al.*, *Sci. Adv.* **1**, e1500533 (2015).
14. S. Felton, M. Tolley, E. Demaine, D. Rus, R. Wood, *Science* **345**, 644–646 (2014).
15. T. Tachi, *Origami* **4**, 175–187 (2009).
16. V. Brunck, F. Lechenault, A. Reid, M. Adda-Bedia, *Phys. Rev. E* **93**, 033005 (2016).
17. F. Lechenault, M. Adda-Bedia, *Phys. Rev. Lett.* **115**, 235501 (2015).
18. J. L. Silverberg *et al.*, *Nat. Mater.* **14**, 389–393 (2015).
19. F. Haas, S. Gorb, R. J. Wootton, *Arthropod Struct. Dev.* **29**, 137–146 (2000).
20. J. Deiters, W. Kowalczyk, T. Seidl, *Biol. Open* **5**, 638–644 (2016).
21. J. F. V. Vincent, in *Deployable Structures*, S. Pellegrino, Ed. (Springer Vienna, Vienna, 2001), pp. 37–50.
22. E. D. Demaine, J. O'Rourke, *Geometric Folding Algorithms: Linkages, Origami, Polyhedra* (Cambridge Univ. Press, Cambridge, 2007), pp. 292–296.
23. F. Haas, Geometry and mechanics of hind-wing folding in Dermaptera and Coleoptera, thesis, University of Exeter (1994).
24. Q. Ge, C. K. Dunn, H. J. Qi, M. L. Dunn, *Smart Mater. Struct.* **23**, 094007 (2014).
25. R. M. Erb, J. S. Sander, R. Grisch, A. R. Studart, *Nat. Commun.* **4**, 1712 (2013).
26. Y. Liu, J. K. Boyles, J. Genzer, M. D. Dickey, *Soft Matter* **8**, 1764–1769 (2012).
27. A. Lendlein, S. Kelch, *Angew. Chem. Int. Ed.* **41**, 2034–2057 (2002).
28. A. Papadopoulou *et al.*, *Addit. Manuf.* **2**, 106–116 (2015).
29. Y. Forterre, J. M. Skotheim, J. Dumais, L. Mahadevan, *Nature* **433**, 421–425 (2005).
30. O. Vincent *et al.*, *Proc. R. Soc. London Ser. B* **278**, 2909–2914 (2011).

ACKNOWLEDGMENTS

We especially thank K. Masania and S. Gantenbein for help with the 3D-printing experiments, M. Binelli for the gripper suggestion, E. Jeoffroy for help with photos and movies, and all colleagues for fruitful discussions. **Funding:** We are grateful for financial support from ETH Zürich, Purdue University, European Office of Aerospace Research and Development (grant FA9550-16-1-0007), and the Air Force Office of Scientific Research (grant FA9550-17-1-0074). **Authors contributions:** All authors designed the research. The analytical, numerical, and experimental work was designed, performed, and evaluated by J.A.F. The manuscript was prepared by J.A.F., A.R.S., and A.F.A. All authors discussed and critically assessed the results and their implications, and revised the manuscript at all stages. **Competing interests:** The authors declare no competing financial interests. **Data and materials availability:** All data are available in the manuscript or supplementary materials.

SUPPLEMENTARY MATERIALS

www.sciencemag.org/content/359/6382/1386/suppl/DC1
Materials and Methods
Figs. S1 and S2
Table S1
Movies S1 to S3
Python Code of Spring Origami Model
Raw Data of Mechanical Testing
Raw Data of Image Analysis
3D-Printing Files

25 August 2017; accepted 30 January 2018
10.1126/science.aap7753

CONDUCTING POLYMERS

A nonconjugated radical polymer glass with high electrical conductivity

Yongho Joo,[1]* Varad Agarkar,[2]* Seung Hyun Sung,[1]
Brett M. Savoie,[1]† Bryan W. Boudouris[1,2]†

Solid-state conducting polymers usually have highly conjugated macromolecular backbones and require intentional doping in order to achieve high electrical conductivities. Conversely, single-component, charge-neutral macromolecules could be synthetically simpler and have improved processibility and ambient stability. We show that poly(4-glycidyloxy-2,2,6,6-tetramethylpiperidine-1-oxyl), a nonconjugated radical polymer with a subambient glass transition temperature, underwent rapid solid-state charge transfer reactions and had an electrical conductivity of up to 28 siemens per meter over channel lengths up to 0.6 micrometers. The charge transport through the radical polymer film was enabled with thermal annealing at 80°C, which allowed for the formation of a percolating network of open-shell sites in electronic communication with one another. The electrical conductivity was not enhanced by intentional doping, and thin films of this material showed high optical transparency.

Conducting polymers have relied on conjugated macromolecular backbones that are subsequently chemically doped so as to achieve high electrical conductivity values [for example, poly(3,4-ethylene dioxythiophene) doped with poly(styrene sulfonate) (PEDOT:PSS)] (*1*, *2*). Despite their impressive electrical conductivity values (*3*, *4*), certain aspects of these macromolecules are not ideal. First, for some applications, optical transparency at visible wavelengths can be difficult to achieve with extended conjugated backbones. Second, the syntheses of advanced conducting polymers can be quite complicated with low yields. Third, chemical doping can depend on processing and lead to performance variability, and the dopants can decrease the materials and device stability.

Charge-neutral macromolecules that achieve relatively high electrical conductivity values without doping could address some of these issues (*5*). Radical polymers (*6*) with nonconjugated backbones and stable open-shell pendant groups (*7*, *8*) can pass charge through a series of oxidation-reduction (redox) reactions between the pendant open-shell sites (*9*). Because of the high density of redox-active sites associated with these materials, they have had an effect on myriad energy storage and energy conversion applications (*10*–*14*). However, the highest solid-state electrical conductivity value reported for radical polymers was ~10^{-2} S m^{-1} (*15*).

Despite the low reported conductivity values, the redox reactions that allow for charge exchange between the pendant groups are rapid (*16*–*18*), so high conductivities should be possible with appropriate molecular engineering of charge-transporting sites (*19*). We synthesized poly(4-glycidyloxy-2,2,6,6-tetramethylpiperidine-1-oxyl) (PTEO) using a ring-opening polymerization methodology, which allowed all of the radical sites in the monomer to be conserved in the polymer. Given its flexible macromolecular backbone and a near–room temperature glass transition temperature (T_g), its flow temperature is well below the degradation temperature of the macromolecule. Thermal annealing of the radical polymer thin film resulted in the formation of percolating networks of radical sites in the solid state that were in electronic communication with one another. This network formation occurred despite the amorphous nature of the polymer thin film. We achieved a >1000-fold increase in the electrical conductivity of PTEO relative to other report values for radical polymers, and the ultimate conductivity of ~20 S m^{-1} is comparable with commercially available, chemically doped conducting polymers.

We polymerized a monomer that contained an open-shell site directly because postpolymerization conversion of closed-shell pendant groups to open-shell forms rarely achieves complete conversion and can lead to undesired by-products (*20*, *21*). We introduced a nitroxide functionality by reacting epichlorohydrin with 4-hydroxy-2,2,6,6-tetramethylpiperidine-1-oxyl (TEMPO-OH) in the presence of a base (Fig. 1A). This small molecule, 4-glycidyloxy-2,2,6,6-tetramethylpiperidine-1-oxyl (GTEMPO), was purified (fig. S1) in order to yield a well-defined monomeric species (*22*) that was stable across a range of different temperatures

[1]Charles D. Davidson School of Chemical Engineering, 480 Stadium Mall Drive, Purdue University, West Lafayette, IN 47906, USA. [2]Department of Chemistry, 560 Oval Drive, Purdue University, West Lafayette, IN 47906, USA.
*These authors contributed equally to this work.
†Corresponding author. Email: bsavoie@purdue.edu (B.M.S.); boudouris@purdue.edu (B.W.B.)

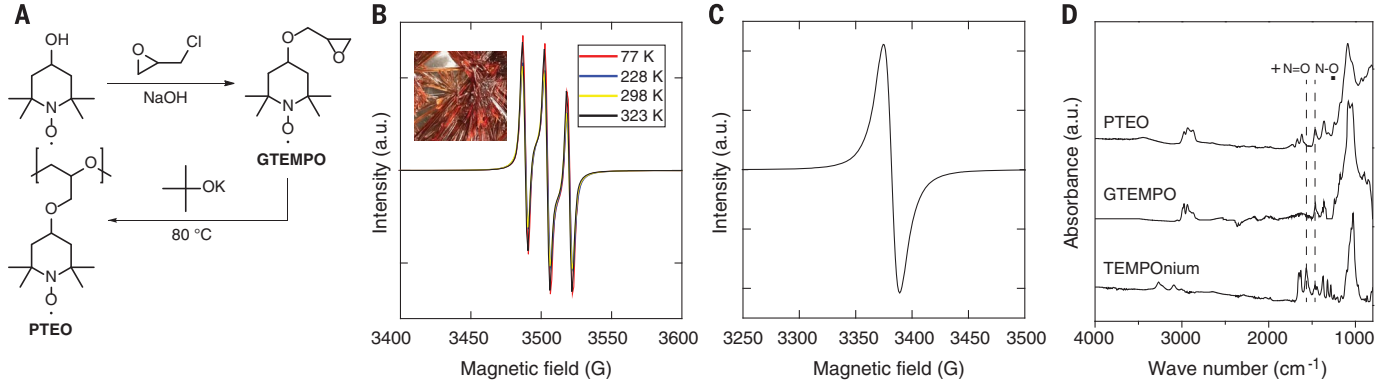

Fig. 1. Controlling and monitoring the amount of open-shell sites in radical polymers is a key objective in the design of high-conductivity open-shell macromolecular species. (**A**) The monomer synthesis and ring-opening polymerization-based synthetic scheme used to generate the PTEO radical polymer. (**B**) The constant radical density (there is an overlapping nature of the spectra acquired at different temperatures) of the PTEO macromolecule in chloroform solutions as a function of temperature, as determined with EPR spectroscopy. (Inset) A photograph of the recrystallized monomer. (**C**) The EPR spectroscopy signal of a radical polymer thin film showing a classic Lorentzian shape, which is indicative of substantial radical-radical interactions in the solid state. (**D**) The ATR-FTIR spectra of the oxoammonium-based TEMPOnium salt, the GTEMPO monomer, and the PTEO polymer, indicating the absence of the oxoammonium cation signal in either the monomer or radical polymer used in this work.

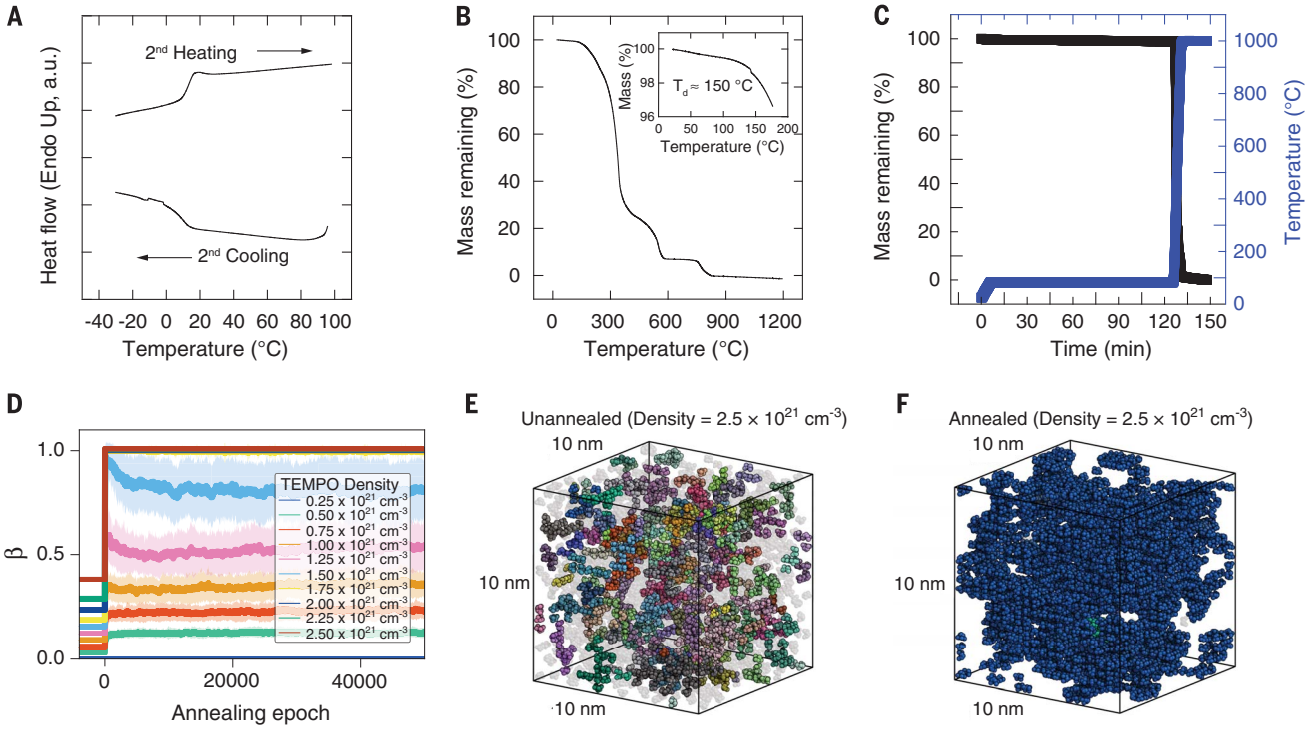

Fig. 2. PTEO flow, thermal, and percolation properties. (**A**) The glass transition temperature at ~20°C for the PTEO macromolecule is clear, and there is no melting or crystallization transition. (**B**) The onset degradation temperature of PTEO is ~150°C. (**C**) No degradation of PTEO was observed when the material was held at 80°C for 2 hours. (**D**) Percolation behavior as a function of radical density and annealing summarized from the Monte Carlo simulations. The average values are shown as solid lines, and standard deviations are shown as the shaded regions. (**E** and **F**) Typical configurations for the (E) unannealed and (F) annealed films at a radical density of 2.5×10^{21} cm^{-3}. Independent networks are drawn with different colors, and any networks composed of less than five molecules are rendered gray and transparent. For example, in (F) almost all of the nitroxide groups are colored navy blue, indicating that there is one large continuous percolation network for charge transport after annealing has occurred.

(Fig. 1B). In the ring-opening polymerization protocol, a potassium *tert*-butoxide initiator generated the PTEO macromolecule with a number-average molecular weight of 2.4 kg mol^{-1} (*23*). The high densities of radical sites present in the monomers were also present in the polymers (Fig. 1C), within experimental error, as determined with electron paramagnetic resonance (EPR) spectroscopy (*24*, *25*). Moreover, no oxoammonium cation sites within either the monomer or polymer products, which increase the electrical conductivity of other nitroxide-bearing radical polymers (*26*), were detected with attenuated total reflectance Fourier transform infrared (ATR-FTIR) spectroscopy (Fig. 1D) at the characteristic frequency (ν) of 1550 cm^{-1}. Identifying these dopants at the levels that can affect charge transport can be difficult with standard chemical characterization methodologies. Thus, although these data suggest that no dopants are present in the ~0.1% (by weight) level, we cannot definitely state that there are no oxoammonium cation (or other dopant) sites present at lower levels. For this relatively low molecular weight of PTEO, the main nitroxide interactions would be between neighboring chains in a thin film. A density functional theory (DFT) characterization of the orientational dependence of TEMPO interactions revealed multiple favorable pairing configurations (fig. S2), with interaction energies on the order of −4 kcal mol^{-1} (−0.17 eV). These interaction energies, an order of magnitude greater than the thermal energy, would result in nitroxide separations between 4 and 6 Å (fig. S3).

High electrical conductivity requires a relatively low T_g, so that the material can be annealed in the molten state and away from the degradation temperature of the radical pendant groups. The bulky nitroxide-containing substituent of the PTEO prevented crystallization of the polymer chains (fig. S4) and resulted in a T_g of ~20°C (Fig. 2A), which is well below the ~150°C onset of degradation for PTEO (Fig. 2B). Thermal processing below 100°C (Fig. 2C) allowed us to create percolating nitroxide networks for charge transport between electrodes, which has not been seen for other systems because of the high T_g of most radical polymers, and this inability to process radical polymer thin films appropriately has contributed to reports of extremely low electrical conductivity values for nitroxide-based radical polymers (*27*).

We modeled radical network formation in PTEO with Monte Carlo (MC) simulations of the annealing process using a Hamiltonian parameterized with DFT calculations and with an implicit treatment of the polymer (supplementary materials). The configurations were then processed to characterize the radical networks and their degree of percolation (β) according to

$$\beta = \frac{1}{3}(s_x + s_y + s_z) \quad (1)$$

Here, s_i is the span of the largest network in each lattice dimension, with β ranging from 0 (no percolation) to 1 (complete percolation across the lattice). The simulations revealed a dramatic effect of annealing on the percolation behavior at all radical densities. Random distributions of the radical groups (an amorphous as-cast film) did not form percolating networks (Fig. 2D). Only after annealing did discontinuous subnetworks (Fig. 2E) combine through aggregation to form percolating networks (Fig. 2F). Moreover, only above a critical radical density could percolating networks form at all.

We monitored this transition for PTEO from the low-charge-transport regime (~10^{-9} S m^{-1}) to the high-charge-transport regime (~10 S m^{-1}) in real time as the material crossed from the as-spin-coated glassy state (the thin film was cast at ~20°C) into a liquid-like molten state (Fig. 3A). In order to evaluate charge transport in this quenched state, the films were transferred to an inert atmosphere vacuum probe station and held at a temperature of 100 K. Heating of the sample occurred inside of the inert atmosphere

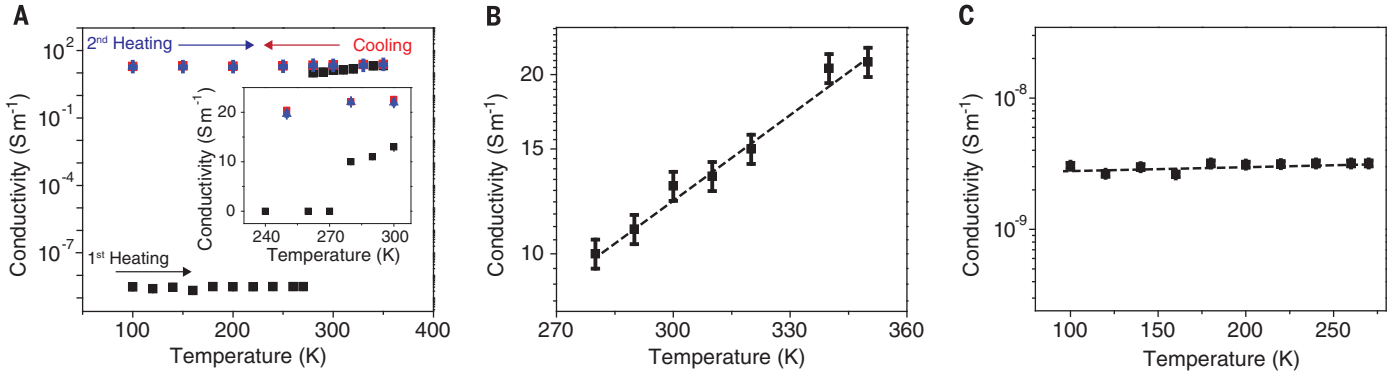

Fig. 3. PTEO conducts charge after annealing has occurred. (**A**) Electrical conductivity as a function of temperature for PTEO in a 0.5-μm channel. Real-time annealing of the thin film allowed for local order to appear within the film so that the electrical conductivity was altered by 10 decades. (**B**) Above the glass transition temperature, there is thermally activated transport, whereas (**C**) below the glass transition temperature, the electrical conductivity is temperature-independent. The data points represent the average value measured for four different PTEO films, and the error bars represent the standard deviation from this average. If no error bars are present, the error is within the size of the point.

vacuum probe station in order to capture the charge transport ability at low temperatures before bringing the PTEO thin films near T_g, so the changes in conductivity appear to be caused by changes in the nanoscale structure as opposed to changes in chemical oxidation. In these experiments, the sample was allowed to reach the desired temperature and held at that temperature for 30 min before collecting the electrical data. Then, the temperature of the sample was moved to the next temperature. Moreover, in a separate experiment, replicate devices were annealed at 80°C for 2 hours in inert atmosphere conditions but without evaluating their low-temperature electrical properties (without the "1st heating" scan in Fig. 3A), and the conductivity of thin films processed in this manner began and remained at ~10 S m^{-1} (in the same manner seen for the "2nd heating" scan of Fig. 3A), indicating that ordering was occurring though thermal annealing (fig. S5).

Once local order was created within the melt, it was retained as the thin film was cooled back into the glassy state, and this enabled rapid charge transport at room temperature both for cooling (Fig. 3A, red squares) and heating (Fig. 3A, blue triangles) of the thin film. Above T_g, thin films displayed thermally activated transport with an activation energy of ~90 meV (Fig. 3B), which is consistent with the increased molecular motion. Moreover, as has been observed with other radical polymers (*22*, *26*, *28*), the transport was independent of temperature below T_g (Fig. 3C).

To study the role of defects, such as impurities or traps, we performed a fragility analysis on the annealed MC networks by removing a random distribution of the TEMPO sites from the annealed MC networks (those shown in Fig. 2, D to F) and recalculating the percolation behavior (Fig. 4A). Defect introduction has adverse effects at all TEMPO densities but was most sensitive near a TEMPO density of ~1.7 × 10^{21} cm^{-3}. We estimate that the TEMPO number density in PTEO is at least 1.75 × 10^{21} cm^{-3}, on the basis of previous characterizations of chemically similar

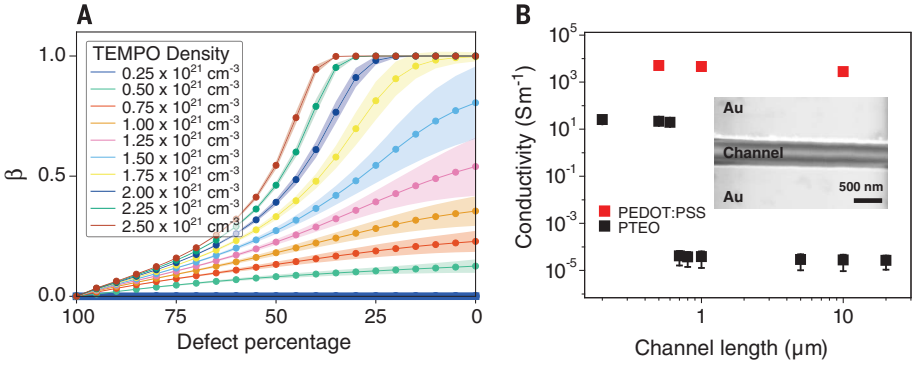

Fig. 4. The charge transport behavior of radical polymers is dictated by percolating domains of paired nitroxide groups. (**A**) Fragility analysis performed on the annealed networks as a function of radical density and defect density. (**B**) The electrical conductivity at T = 350 K for PTEO as a function of channel length (black squares) shows that these localized domains were less than or equal to 600 nm in size in experimental practice. The data points represent the average of the measurements conducted on four different devices of that channel length, and the error bars represent 1 standard deviation from this average. If no error bar is shown, the error is within the size of the point. Equivalent experiments were performed with PEDOT:PSS (red squares) serving as the channel material, and there is almost no dependence on the conductivity as a function of channel length. (Inset) A scanning electron microscopy image of a typical channel used in these studies, showing the spacing between the gold electrode contacts before film deposition.

polymers (*29*), so our PTEO films should be strongly sensitive to the levels of defect incorporation and film processing. Over long enough length scales, defects will render the networks nonpercolative. Given the length scale limitations of our simulations, we can place a lower limit for the percolation length scale of ~20 nm for radical densities greater than 1.75 × 10^{21} cm^{-3}.

The lack of crystallinity in these amorphous conductors made it difficult to experimentally determine the length scale at which the percolation of nitroxide groups ended. We estimated the size of high-charge-transport domains by changing the lengths between the two electrodes (Fig. 4B). At channel lengths >0.7 μm, the conductivity was low, ~10^{-4} S m^{-1} (*21*, *26*). However, for channel lengths of 0.6 μm or less, the conductivity reached ~20 S m^{-1}. These data suggest that the nitroxide percolation network had a characteristic length scale of ~600 nm. Thus, if the high-charge-transport domains do not bridge across the electrodes, the conductivity is limited by the low-charge-transport domains. Bare channels and those containing polystyrene (PS) were fabricated and had conductivities below the detection limit (<10^{-12} S cm^{-1}) of our system (fig. S6). Similar experiments performed with PEDOT:PSS showed some contact resistance but otherwise exhibited high conductivity across this length-scale range, as expected, and the variation of its higher electrical conductivity for the same channel lengths was only twofold (Fig. 4B).

We evaluated how the chemical nature of the thin films affected the observed transport behavior. When the radical group within the PTEO repeat unit was intentionally quenched to form

the N-OH functionality (PTEO-OH), the electrical conductivity for the 0.5-μm channel decreased to ~10^{-7} S m^{-1} (fig. S7A). In order to form an electron donor-acceptor system within the radical polymer thin film, we intentionally doped the PTEO film with 4-acetamido2,2,6,6-tetramethyl-1-oxopiperidinium tetrafluoroborate (TEMPOnium) at a high loading (10%, by weight) (*26*). This intentional doping had little impact on the ultimate electrical conductivity of the film, and the conductivity showed the same marked increase after thermal annealing as was observed for the undoped system (fig. S7B). Moreover, making composite blends of PTEO and PTEO-OH at channel lengths of 0.5 μm allowed for experimental verification of the computational fragility analyses shown in Fig. 4A. That is, for thin films that conained >90% (by weight) PTEO, the electrical conductivity was ~10 S m^{-1}, as expected; however, when >20% (by weight) of the polymer composite was composed of inactive PTEO-OH, the conductivity of the thin film fell to ~10^{-7} S m^{-1} (fig. S7C). Thus, charge exchange from the injecting electrode to the collecting electrode depends on the ability of the nitroxide groups to form a percolating structure and not on any inherent limitations of the radical self-exchange reactions.

Last, the nonconjugated nature of the radical polymers led to weak absorption profiles of the material both in solution and as thin films. That is, the solution absorption spectrum showed the oft-observed signal for nitroxide-based radical polymers (fig. S8). However, the ~1-μm-thick PTEO film showed only minimal absorption in the visible spectrum, with ≥98% transmission at wavelengths of $\lambda \leq 500$ nm and 100% transmission at longer wavelengths. These thin films maintained their high electrical conductivity over multiple weeks (fig. S9) when they were exposed to ambient conditions. Thus, these radical polymer films present as relatively high-electrical-conductivity materials with high optical transparency and ambient stability.

REFERENCES AND NOTES

1. O. Ostroverkhova, *Chem. Rev.* **116**, 13279–13412 (2016).
2. I. Salzmann, G. Heimel, M. Oehzelt, S. Winkler, N. Koch, *Acc. Chem. Res.* **49**, 370–378 (2016).
3. Y. P. Wen, J. K. Xu, *J. Polym. Sci. A Polym. Chem.* **55**, 1121–1150 (2017).
4. Z. Y. Zhu, C. C. Liu, F. X. Jiang, J. K. Xu, E. D. Liu, *Synth. Met.* **225**, 31–40 (2017).
5. T. M. Swager, *Macromolecules* **50**, 4867–4886 (2017).
6. S. Mukherjee, B. W. Boudouris, *Organic Radical Polymers: New Avenues in Organic Electronics* (Springer Science, 2017).
7. A. J. Wingate, B. W. Boudouris, *J. Polym. Sci. A Polym. Chem.* **54**, 1875–1894 (2016).
8. E. P. Tomlinson, M. E. Hay, B. W. Boudouris, *Macromolecules* **47**, 6145–6158 (2014).
9. K. Oyaizu, H. Nishide, *Adv. Mater.* **21**, 2339–2344 (2009).
10. C. Friebe, U. S. Schubert, *Top. Curr. Chem. (Cham.)* **375**, 19 (2017).
11. S. Muench *et al*., *Chem. Rev.* **116**, 9438–9484 (2016).
12. L. Rostro, L. Galicia, B. W. Boudouris, *J. Polym. Sci., B, Polym. Phys.* **53**, 311–316 (2015).
13. E. P. Tomlinson, M. J. Willmore, X. Zhu, S. W. A. Hilsmier, B. W. Boudouris, *ACS Appl. Mater. Interfaces* **7**, 18195–18200 (2015).
14. B. W. Boudouris, *Curr. Opin. Chem. Eng.* **2**, 294–301 (2013).
15. M. E. Hay, S. Hui Wong, S. Mukherjee, B. W. Boudouris, *J. Polym. Sci., B, Polym. Phys.* **55**, 1516–1525 (2017).
16. K. Oyaizu, T. Kawamoto, T. Suga, H. Nishide, *Macromolecules* **43**, 10382–10389 (2010).
17. Y. Sasada, R. Ichinoi, K. Oyaizu, H. Nishide, *Chem. Mater.* **29**, 5942–5947 (2017).
18. H. Tokue, K. Kakitani, H. Nishide, K. Oyaizu, *Chem. Lett.* **46**, 647–650 (2017).
19. K. Sato *et al*., *J. Am. Chem. Soc.* **140**, 1049–1056 (2018).
20. L. Rostro, S. H. Wong, B. W. Boudouris, *Macromolecules* **47**, 3713–3719 (2014).
21. L. Rostro, A. G. Baradwaj, B. W. Boudouris, *ACS Appl. Mater. Interfaces* **5**, 9896–9901 (2013).
22. A. G. Baradwaj, L. Rostro, B. W. Boudouris, *Macromol. Chem. Phys.* **217**, 477–484 (2016).
23. C. Chang *et al*., *Polymer (Guildf.)* **51**, 1947–1953 (2010).
24. H. V. T. Nguyen *et al*., *ACS Cent. Sci.* **3**, 800–811 (2017).
25. M. A. Sowers *et al*., *Nat. Commun.* **5**, 5460 (2014).
26. A. G. Baradwaj *et al*., *Macromolecules* **49**, 4784–4791 (2016).
27. Y. Zhang *et al*., *J. Mater. Chem. C Mater. Opt. Electron. Devices* **6**, 111–118 (2018).
28. A. G. Baradwaj, L. Rostro, M. A. Alam, B. W. Boudouris, *Appl. Phys. Lett.* **104**, 213306 (2014).
29. L. Rostro, A. G. Baradwaj, A. R. Muller, J. S. Laster, B. W. Boudouris, *MRS Commun.* **5**, 257–263 (2015).

ACKNOWLEDGMENTS

We thank D. A. Wilcox for assistance in acquiring the thermogravimetric analysis data. **Funding:** The molecular design and characterization work was supported by the NSF through the CAREER Award in the Polymers Program (award 1554957; program manager, A. Lovinger), and the advanced microelectronic device fabrication was supported by the Air Force Office of Scientific Research through the Organic Materials Chemistry Program (grant FA9550-15-1-0449; program manager, K. Caster). **Authors contributions:** V.A. designed and conducted all experiments associated with molecular synthesis. Y.J. conducted experiments regarding the experimental optoelectronic properties. S.H.S. designed the initial electronic characterization experiments and fabricated the nanoscale electronic devices. B.M.S. designed and conducted all efforts related to the computational work. B.W.B. conceived the project, designed experiments, and directed the research. All authors contributed to the writing and editing of the manuscript. **Competing interests:** None declared. **Data and materials availability:** All data needed to evaluate the conclusions in the paper are present in the paper or the supplementary materials.

SUPPLEMENTARY MATERIALS

www.sciencemag.org/content/359/6382/1391/suppl/DC1
Materials and Methods
Figs. S1 to S9
References (*30*–*34*)

1 September 2017; resubmitted 29 December 2017
Accepted 21 February 2018
10.1126/science.aao7287

NEURODEVELOPMENT

Early life experience drives structural variation of neural genomes in mice

Tracy A. Bedrosian,* Carolina Quayle, Nicole Novaresi, Fred. H. Gage*

The brain is a genomic mosaic owing to somatic mutations that arise throughout development. Mobile genetic elements, including retrotransposons, are one source of somatic mosaicism in the brain. Retrotransposition may represent a form of plasticity in response to experience. Here, we use droplet digital polymerase chain reaction to show that natural variations in maternal care mediate the mobilization of long interspersed nuclear element–1 (LINE-1 or L1) retrotransposons in the hippocampus of the mouse brain. Increasing the amount of maternal care blocks the accumulation of L1. Maternal care also alters DNA methylation at YY1 binding sites implicated in L1 activation and affects expression of the de novo methyltransferase DNMT3a. Our observations indicate that early life experience drives somatic variation in the genome via L1 retrotransposons.

The brain exhibits plasticity in response to environmental experience, particularly during the first weeks of life. A portion of this plasticity can be attributed to modification of DNA through epigenetic changes such as methylation or chromatin remodeling. However, dynamic neuronal DNA sequences suggest a role for mobilization of retrotransposons or induction of other structural variants in experience-driven brain plasticity (*1*, *2*). We developed Taqman assays for droplet digital polymerase chain reaction (ddPCR) to probe the number of long interspersed nuclear element–1 (L1) retrotransposon copies present in mouse genomic DNA (fig. S1). Although L1 is the most abundant class of retrotransposons, comprising about 17% of human and mouse genomes, most copies are truncated or otherwise mutated such that mobilization is no longer possible. The average human genome retains 80 to 100 active L1 copies; the mouse genome retains more than 3000. We designed our assays to enrich for the currently active families of L1 in the mouse genome [L1MdT, L1MdGf, and L1MdA (*3*)] (fig. S1A). Full-length L1 retrotransposons are composed of a 5′ untranslated region (5′UTR) with an internal Pol II promoter, two open reading frames (ORFs), and a 3′UTR followed by a Poly(A) tail. L1 elements mobilize through a "copy and paste" mechanism, in which full-length L1 mRNA is reverse transcribed beginning at the 3′ end and inserted into a new genomic location. In many cases, either reverse transcription stops early or the intermediate single-stranded DNA (ssDNA) is degraded before the insertion is resolved, resulting in 5′ truncated insertions. To account for these multiple forms, we designed four assays spanning different regions of the element to gain insight into the length of L1 copies detected by ddPCR. As expected, assays for the 5′ end of L1 had fewer sequence matches in the mouse reference genome and were more likely to belong to a full-length element than assays for the 3′ end of L1 (fig. S1, B and C). In addition, we developed assays for mouse 5*s* ribosomal DNA and mouse minor satellite DNA for use as stable, multicopy endogenous reference genes (fig. S1, D and E).

Rodents exhibit natural variations in maternal care that influence the neurodevelopment and adult behavior of their offspring (*4*). Some of the lasting effects of maternal care have been linked to epigenetic changes precipitated by the amount of licking/grooming and arched-back nursing that a pup receives from its mother (*5*). Different gene expression patterns, stress responses, and DNA methylation profiles are activated depending on the quality and quantity of maternal care. We leveraged this range of maternal care to examine the effects of neonatal care on L1 copy number in mice. We monitored the behavior of dams with their pups during the first 2 weeks after parturition. Individual variations were observed in maternal style, as previously reported (Fig. 1A) (*6*). We divided mice into two groups based on median total maternal behavior, which revealed two distinctive maternal styles, high maternal care and low maternal care, across the 2-week observation period (Fig. 1B and fig. S2A). Variations in maternal care did not affect body mass gain in the pups (fig. S2B). At weaning on postnatal day (PND) 21, the total percent time dams spent on maternal care was significantly correlated with L1 copy number measured in the hippocampus of their offspring (Fig. 1C and fig. S3) but not in the frontal cortex or heart (fig. S4, A and B). Because this effect was not identified in all tissues, it is unlikely to be a result of inherited differences in L1 copy number. Furthermore, we studied genetically homogeneous inbred mice, in which the L1 copy number was similar among the dams and sires (fig. S4C). To investigate cell-type specificity and to rule out differences in cytoplasmic L1 DNA, we sorted hippocampal nuclei by NeuN expression using fluorescence-activated cell sorting (FACS). By single-nuclei quantitative PCR, we detected a higher hippocampal L1 copy number in $NeuN^+$ nuclei from PND 21 pups reared with low maternal care (Fig. 1, D and E).

Other genomic events besides retrotransposition could account for an increase in L1 copy number. For one, mobile elements could be reverse transcribed and exist as extrachromosomal ssDNA or circular DNA without integrating into the genome. To investigate this possibility, we treated samples with single-stranded deoxyribonuclease or size-selected high-molecular-weight DNA, but neither treatment significantly changed the pattern of L1 3′UTR detected (fig. S5, A and B). Alternatively, L1 copy number could be increased as a result of large-scale genomic duplications. However, we observed similar copy numbers of L1MdV, a nonmobile family of L1, between mice reared with high or low maternal care (fig. S5C). Further, early life experience seemed to specifically affect L1 retrotransposons, because copy numbers of other mobile elements—short interspersed nuclear element (SINE) B1, SINE B2, and intracisternal A particle (IAP) elements—did not correlate with maternal care (fig. S5D).

The generation of genomic diversity by L1 elements is likely a dynamic, lifelong process that begins during embryonic development. Retrotransposition activity is increased as neural progenitors differentiate into neurons (*2*); thus, early life (when the brain is undergoing extensive growth and differentiation) represents a prime stage in which to uncover the sensitivity of L1 to experience. L1 retrotransposition rates are higher in the mouse brain compared with other tissues and, among brain subregions, highest in the hippocampus, a region sensitive to environmental stimuli (*7*, *8*). During the first week of life, the hippocampus is one of the few structures in the rodent brain that is still undergoing extensive cell division and differentiation, making it more likely to foster retrotransposition than other brain regions at that time (*9*).

To confirm that low maternal care was eliciting an increase in hippocampal L1 copy number, we examined the timeline of L1 accumulation and the effects of manipulating maternal behavior (Fig. 2A). We used a paradigm of separation-induced maternal care by exposing dams to 3 hours of maternal separation daily. Maternal separation was initially developed as a rat model of neglect, but mice and some strains of rats actually compensate for the separation by increasing their care upon reunion with the litter (*10*–*13*). Maternal separation in our study did not reduce maternal care, in agreement with previous reports in mice (*12*–*14*), but it did reduce the natural variations between individual mothers, such that dams undergoing maternal separation showed a consistently high level of arched-back nursing, licking-grooming, and contact time when reunited with their litters (Fig. 2, B and C). At PND 0, before the pups received any appreciable maternal care, we measured similar hippocampal L1 copy numbers among mice born to high- or low-maternal-care dams; however, by PND 7, we observed more L1 copies in mice reared with low maternal care (Fig. 2D). The accumulation of L1 copies was blocked in mice reared by highly maternal dams

Laboratory of Genetics, The Salk Institute for Biological Studies, La Jolla, CA 92037, USA.
*Corresponding author. Email: tbedrosian@salk.edu (T.A.B.); gage@salk.edu (F.H.G.)

that compensated for separation (Fig. 2D). In addition, we performed a cross-fostering experiment in which two to four pups from each litter were reared by a foster dam beginning at PND 0. L1 3′UTR copy number was better correlated with the maternal care of the dam that reared the pups and not with the care of the biological dam (Fig. 2E).

To examine the mechanism whereby maternal care affects L1 copy number, we analyzed the rate of neurogenesis. Stimuli that enhance neurogenesis may promote retrotransposition because dividing cells are permissive to the L1 ribonucleoprotein complex entering the nucleus. We injected mice daily, for the first 7 days of life, with EdU, a marker of cell proliferation. Then we collected the hippocampi at PND 21 and used flow cytometry to quantify cells expressing EdU and Prox1, a marker of dentate granule neurons. Mice reared with high or low maternal care had similar numbers of $EdU^+/Prox1^+$ neurons and $EdU^+/Prox1^-$ cells, suggesting no difference in neurogenesis rate (fig. S6, A and B).

Next, we analyzed methylation of L1 because gene- and brain region–dependent effects of maternal care on DNA methylation have been reported (*5*, *15*). We narrowed our analysis to the Tf family of L1 elements, because this is the most active and evolutionarily recent family of mouse L1 elements (*3*). The L1MdTf promoter consists of a variable number of repeat monomers, with each representing a CpG island and including a YY1 transcription factor binding site required for L1 gene expression (Fig. 3A) (*16*). Using bisulfite sequencing, we assessed a region of 13 individual CpGs containing the YY1 binding site to determine the average methylation level in the hippocampus (Fig. 3B). Mice that experienced low maternal care had less methylation across the L1 promoter (Fig. 3C), particularly at the YY1 binding site (Fig. 3D). This difference corresponded to more L1 mRNA expression in the hippocampus at PND 4 (Fig. 3E) but not in the frontal cortex (fig. S7). To investigate how maternal care,

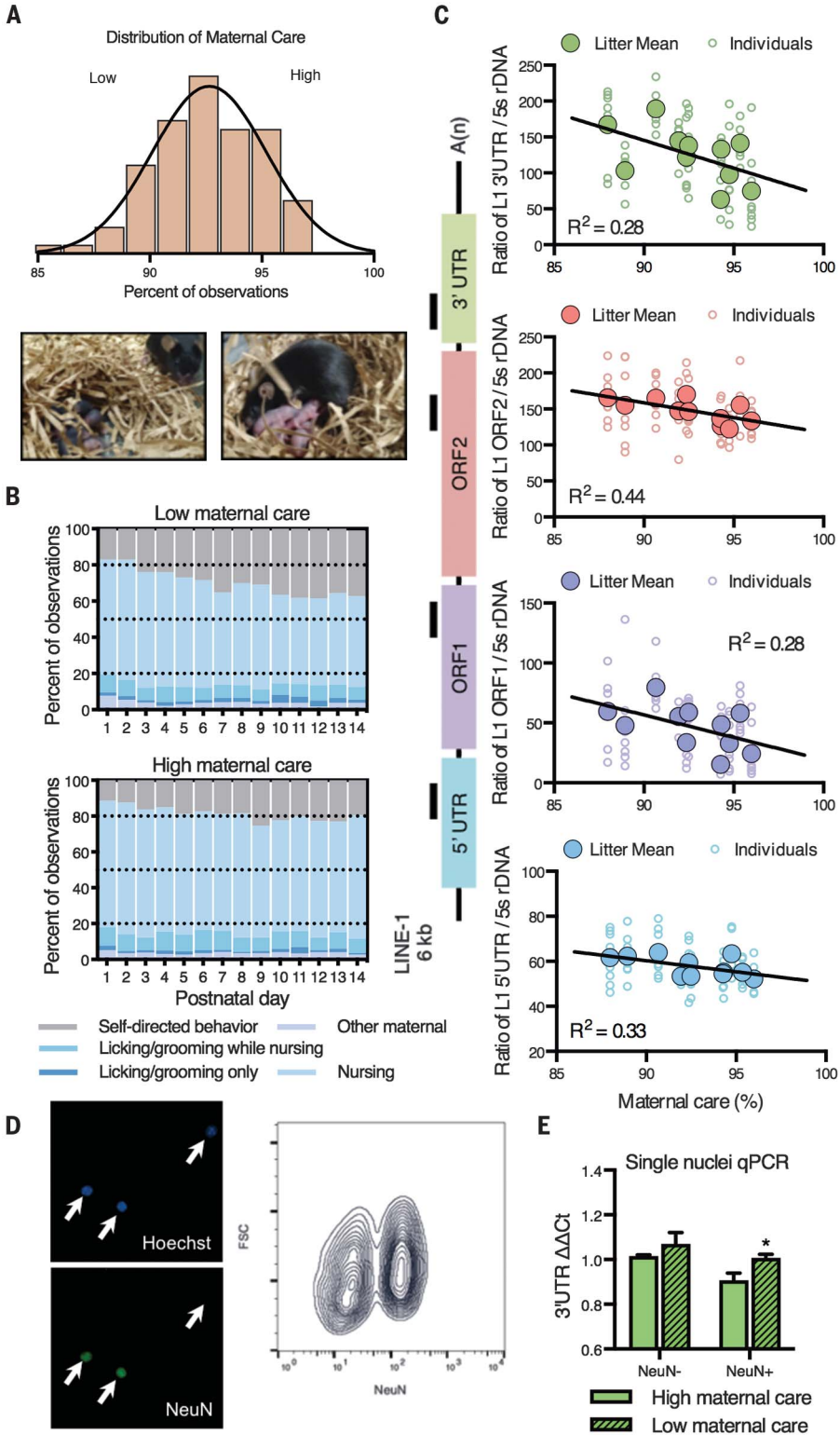

Fig. 1. Natural variations in maternal care predict hippocampal L1 copy number.
(**A**) Distribution of time spent on maternal care. Dams above the median were called "high maternal," and dams below the median were called "low maternal." $N = 84$. Photos show representative low maternal (left) and high maternal (right) dams. (**B**) Breakdown of mean time spent performing maternal versus self-directed behaviors. Low: $N = 41$; High: $N = 43$. (**C**) Hippocampal L1 copy number in PND 21 offspring is inversely correlated with maternal care received during the first two postnatal weeks. Linear mixed model (LMM), with maternal care and sex as fixed factors and a random intercept for litter; $N = 75$ pups from 11 litters. Fixed-effect coefficients for care: 3′UTR, −7.66, $P = 0.049$; ORF2, −4.15, $P = 0.01$; ORF1, −3.60, $P = 0.06$; 5′UTR, −1.05, $P = 0.03$. (**D**) Hippocampal tissue collected at PND 21 was sorted based on NeuN staining. Micropictographs show sorted $NeuN^+$ and $NeuN^-$ single nuclei (arrows). (**E**) L1 copy number was higher in single neuronal nuclei from pups with low maternal care. ddCt (ΔΔCt) values for nuclei were averaged to get one value per mouse used for statistical analysis. Two-tailed *t* test, High $NeuN^-$: $N = 3$ mice (83 nuclei), Low $NeuN^-$: 4 mice (83 nuclei), $t = 0.41$, $P = 0.40$; High $NeuN^+$: 4 mice (125 nuclei); Low $NeuN^+$: 4 mice (131 nuclei), $t = 2.85$, $P = 0.03$. Data represented as mean ± SEM. $^*P < 0.05$.

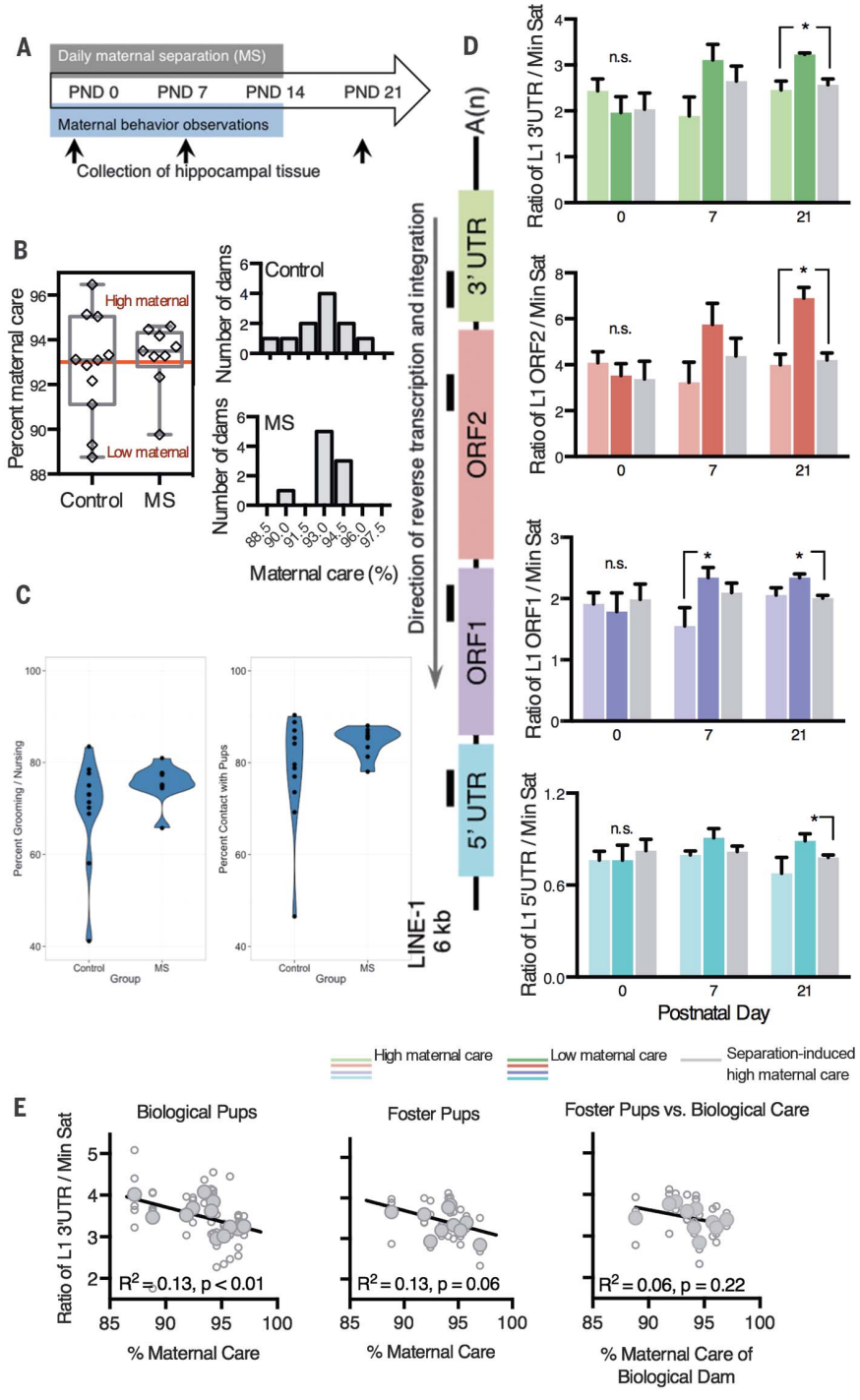

Fig. 2. Manipulating maternal care affects accumulation of L1 copy number.
(**A**) Timeline of experimental design. Dams were either undisturbed or subjected to daily 3-hour separation from their pups during the first 2 weeks postpartum. Pups were collected at PND 0, PND 7, and PND 21. (**B**) Dams exposed to separation were more likely to be highly maternal than control dams. Control: $N = 11$; MS (maternal separation): $N = 9$. (**C**) Separated dams showed less variability in time grooming and nursing their pups and time contacting pups. F test for equality of variances (Grooming/Nursing: $F = 7.58$, $P = 0.0085$; Contact: $F = 15.12$, $P = 0.0008$). Control: $N = 11$; MS: $N = 9$. (**D**) Low maternal care was associated with increased hippocampal L1 copy number beginning at PND 7, but separation (which caused compensatory increases in care) blocked the increase in copy number. Two-tailed t test, P0: High $N = 6$, Low $N = 7$, MS $N = 4$; P7: High $N = 4$, Low $N = 5$, MS $N = 5$; P21: High $N = 5$, Low $N = 4$, MS $N = 9$. 3′UTR high versus low, $t = 2.91$, $P = 0.03$; MS versus low, $t = 2.82$, $P = 0.02$. ORF2 high versus low, $t = 4.14$, $P = 0.01$; MS versus low, $t = 4.64$, $P < 0.01$. ORF1 P7 high versus low, $t = 1.94$, $P = 0.04$, P21 MS versus low, $t = 4.04$, $P < 0.01$. 5′UTR MS versus low, $t = 2.70$, $P = 0.02$. (**E**) In another cohort of mice, two to four pups from each litter were fostered to another dam on PND 0. L1 3′UTR copy number in the hippocampus at PND 21 correlated better with the care the pups received than with the care of the biological mother. Pearson correlation, Biological pups: $N = 64$ pups, Foster pups: $N = 28$ pups. L1 3′UTR copy number in foster pups did not correlate with the care of the biological dam. Data in bar graphs represented as mean ± SEM. *$P < 0.05$.

in general, influences methylation of the L1MdTf promoter, we examined gene expression of DNA methyltransferases in hippocampal tissue from our time point cohort. DNMT1 and DNMT3B expression decreased from PND 0 to PND 21 but did not differ between maternal care groups. In contrast, DNMT3A expression peaked at PND 7, at which point expression was reduced in mice that received low maternal care (Fig. 3F). Methylation of IAP elements, which showed no change in copy number with maternal care, was similar for all mice (fig. S8). These observations suggest that methylation of L1 occurs during normal postnatal development but to varying extents depending on the environment to which the developing pup is exposed. Differential methylation and expression are likely only some of the mechanisms that contribute to changes in L1 copy number; another possibility is differential susceptibility of the DNA to accept new L1 insertions.

Our results suggest that there is plasticity at the level of the DNA sequence in response to environmental perturbations. It will be necessary to confirm these findings in the future using additional methods like single-cell genome sequencing. PCR-based copy number assays have the advantage of detecting relative changes across a large number of L1 elements but lack specificity for targeting somatic insertions or for distinguishing insertions that arise through bona fide retrotransposition versus another mechanism. Because of this lack of specificity, it is difficult to estimate the number of insertions per cell. Nonetheless, de novo insertions may have a variety of consequences depending on the site of insertion, such as altering expression of nearby genes, affecting splicing of transcripts, or shuffling DNA through L1-mediated transduction (*17*, *18*). Somatic retrotransposition could affect neuronal diversity and function, particularly in light of the highly networked state of the brain. As previously reported (*4*), we observed more anxiety-like behavior in adult mice that were reared with low maternal care (fig. S9), although it remains unknown whether somatic mosaicism contributes to these behaviors. Single-cell sequencing has estimated the rate of L1 retrotransposition in the human

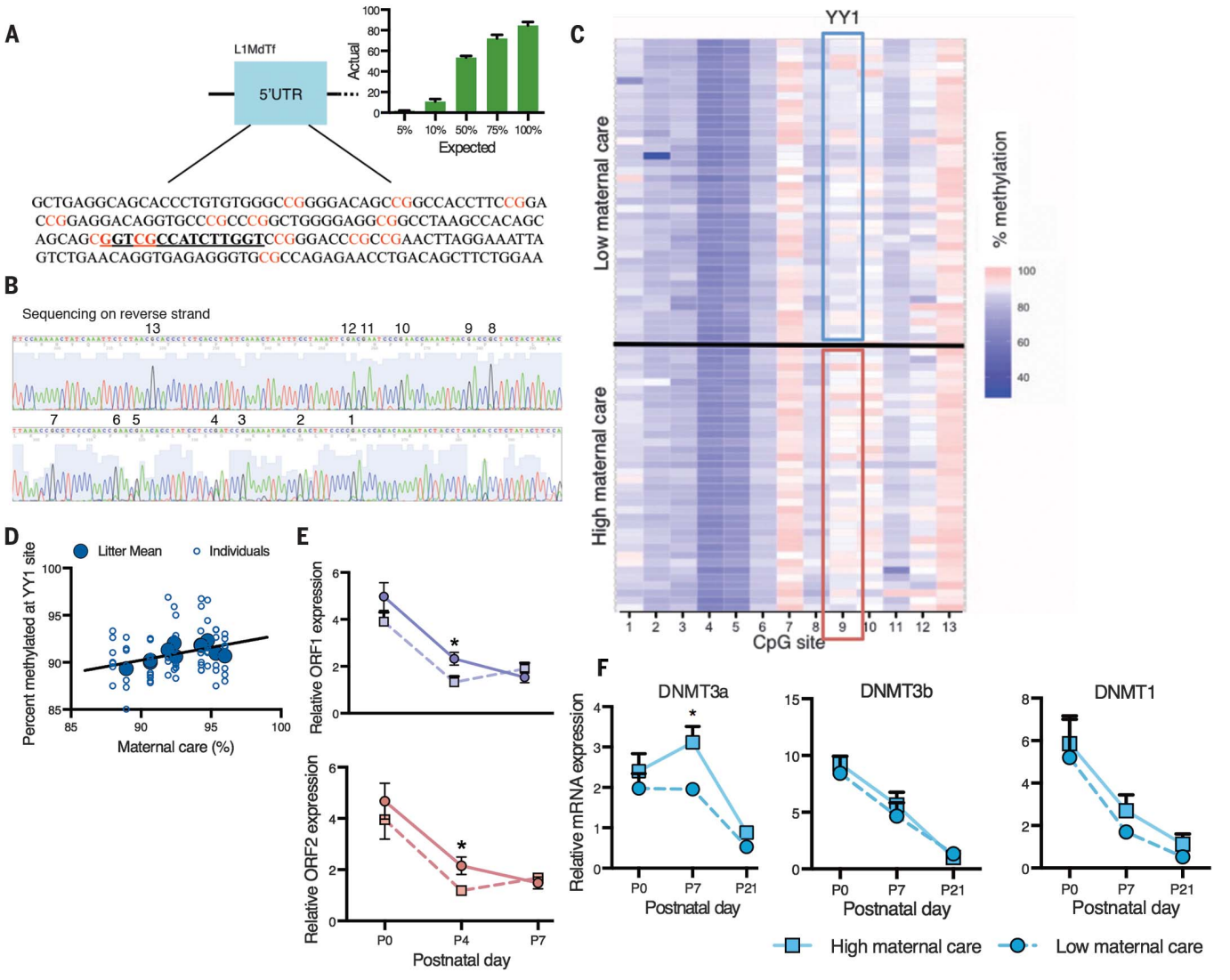

Fig. 3. Maternal care alters methylation of YY1 binding site in the L1 promoter. (**A**) The L1MdTf promoter contains a CpG island and YY1 binding site (underlined and bold) that is important for transcription of the element. Sequencing the bisulfite-converted L1 promoter using methylated DNA standards produced accurate results (inset). (**B**) Methylation was analyzed at 13 individual CpG sites in the L1MdTf promoter of hippocampal DNA from PND 21 mice. (**C**) Low maternal care was associated with less methylation, particularly at the YY1 binding site at position 9. Each row represents an individual mouse. LMM, with maternal care and CpG site as fixed factors and a random intercept for litter. Fixed factor coefficient for care: 0.18, $P = 0.01$. High: $N = 32$; Low: $N = 44$. (**D**) Mice reared with less maternal care had reduced methylation of the YY1 site. LMM, with maternal care as fixed factor and a random intercept for litter. Fixed factor coefficient: 0.21, $P = 0.04$. High: $N = 32$; Low: $N = 44$. (**E**) L1 mRNA expression was elevated in pups raised with low maternal care. Each time point, two-tailed t test, P0: $N = 6$ per group; P4: High: $N = 5$; Low: $N = 3$; P7: High: $N = 4$; Low: $N = 5$. ORF1 P4, $t = 2.5$, $P = 0.04$; ORF2 P4, $t = 3.4$, $P = 0.01$. (**F**) The reduced methylation coincided with reduced expression of DNMT3a, a de novo methyltransferase enzyme, at PND 7. Expression of DNMT3b and DNMT1 did not differ between mice with different maternal care. Each time point, two-tailed t test, P0: $N = 6$ per group; P7: High: $N = 4$; Low: $N = 5$; P21: High: $N = 5$; Low: $N = 4$. DNMT3a P7, $t = 2.97$, $P = 0.02$. Data represented as mean ± SEM. *$P < 0.05$.

brain to be <0.6 to 13 insertions per neuron, depending on the brain region and detection method (*19*, *20*). Mice have thousands more active copies of L1 per cell than humans, but whether species differences in L1 copy number result in a proportionally greater L1 insertion rate is unknown. Even a few insertions could have substantial functional effects in the brain. Moreover, it was recently reported that childhood stress and adversity result in hypomethylation of retrotransposons in humans (*21*, *22*). Our results demonstrate that early life experience can drive structural variation of the genome via L1 retrotransposons.

REFERENCES AND NOTES

1. T. A. Bedrosian, S. Linker, F. H. Gage, *Genome Med.* **8**, 58 (2016).
2. A. R. Muotri *et al.*, *Nature* **435**, 903–910 (2005).
3. A. Sookdeo, C. M. Hepp, M. A. McClure, S. Boissinot, *Mob. DNA* **4**, 3 (2013).
4. I. C. Weaver, M. J. Meaney, M. Szyf, *Proc. Natl. Acad. Sci. U.S.A.* **103**, 3480–3485 (2006).
5. I. C. Weaver *et al.*, *Nat. Neurosci.* **7**, 847–854 (2004).
6. F. A. Champagne, D. D. Francis, A. Mar, M. J. Meaney, *Physiol. Behav.* **79**, 359–371 (2003).
7. N. G. Coufal *et al.*, *Nature* **460**, 1127–1131 (2009).
8. J. K. Baillie *et al.*, *Nature* **479**, 534–537 (2011).
9. S. A. Bayer, *J. Comp. Neurol.* **190**, 87–114 (1980).
10. S. Macrí, G. J. Mason, H. Würbel, *Eur. J. Neurosci.* **20**, 1017–1024 (2004).
11. S. Macrì, H. Würbel, *Horm. Behav.* **50**, 667–680 (2006).
12. R. A. Millstein, A. Holmes, *Neurosci. Biobehav. Rev.* **31**, 3–17 (2007).
13. L. S. Own, P. D. Patel, *Horm. Behav.* **63**, 411–417 (2013).
14. R. D. Romeo *et al.*, *Horm. Behav.* **43**, 561–567 (2003).
15. S. E. Brown, I. C. Weaver, M. J. Meaney, M. Szyf, *Neurosci. Lett.* **440**, 49–53 (2008).

16. S. H. Lee, S. Y. Cho, M. F. Shannon, J. Fan, D. Rangasamy, *PLOS ONE* **5**, e11353 (2010).
17. J. A. Erwin, M. C. Marchetto, F. H. Gage, *Nat. Rev. Neurosci.* **15**, 497–506 (2014).
18. J. V. Moran, R. J. DeBerardinis, H. H. Kazazian Jr., *Science* **283**, 1530–1534 (1999).
19. G. D. Evrony *et al.*, *Cell* **151**, 483–496 (2012).
20. K. R. Upton *et al.*, *Cell* **161**, 228–239 (2015).
21. D. Nätt, I. Johansson, T. Faresjö, J. Ludvigsson, A. Thorsell, *Clin. Epigenetics* **7**, 91 (2015).
22. B. Misiak *et al.*, *Epigenomics* **7**, 1275–1285 (2015).

ACKNOWLEDGMENTS

The authors thank M. L. Gage for critical reading of the manuscript; Q. Zhu for the minor satellite assay; J. Erwin, A. Paquola, I. Gallina, D. Reid, and S. Linker for technical assistance and discussions; and the Salk Institute Functional Genomics Core, Next Generation Sequencing Core, and Flow Cytometry Core facilities for equipment and technical assistance. **Funding**: This work was supported by NIH R01 MH095741, NIH U01 MH106882, The G. Harold and Leila Y. Mathers Charitable Foundation, The Leona M. and Harry B. Helmsley Charitable Trust grant 2012-PG-MED00, The Engman Foundation, Annette C. Merle-Smith, Takeda Pharmaceutical International, The JPB Foundation, NIH F32 MH102983 (T.A.B), and a National Alliance for Research on Schizophrenia and Depression Young Investigator Award (T.A.B.). **Author contributions**: T.A.B. and F.H.G. designed the experiments and wrote the manuscript. T.A.B., N.N., and C.Q. performed the experiments and analyzed the data. **Competing interests**: None declared. **Data and materials availability**: All data needed to evaluate the conclusions in the paper are present in the paper or the supplementary materials.

SUPPLEMENTARY MATERIALS

www.sciencemag.org/content/359/6382/1395/suppl/DC1
Materials and Methods
Figs. S1 to S9
Table S1
References (*23*–*30*)

12 June 2016; resubmitted 4 November 2017
Accepted 25 January 2018
10.1126/science.aah3378

PLANT SCIENCE

A single fungal MAP kinase controls plant cell-to-cell invasion by the rice blast fungus

Wasin Sakulkoo,[1] Miriam Osés-Ruiz,[1] Ely Oliveira Garcia,[2] Darren M. Soanes,[1] George R. Littlejohn,[1]* Christian Hacker,[1] Ana Correia,[1] Barbara Valent,[2] Nicholas J. Talbot[1]†

Blast disease destroys up to 30% of the rice crop annually and threatens global food security. The blast fungus *Magnaporthe oryzae* invades plant tissue with hyphae that proliferate and grow from cell to cell, often through pit fields, where plasmodesmata cluster. We showed that chemical genetic inhibition of a single fungal mitogen-activated protein (MAP) kinase, Pmk1, prevents *M. oryzae* from infecting adjacent plant cells, leaving the fungus trapped within a single plant cell. Pmk1 regulates expression of secreted fungal effector proteins implicated in suppression of host immune defenses, preventing reactive oxygen species generation and excessive callose deposition at plasmodesmata. Furthermore, Pmk1 controls the hyphal constriction required for fungal growth from one rice cell to the neighboring cell, enabling host tissue colonization and blast disease.

Blast diseases of cereals are caused by the filamentous fungus *Magnaporthe oryzae* (synonym of *Pyricularia oryzae*), destroying sufficient rice each year to feed 60 million people (*1*), and wheat blast disease now threatens wheat production in South America and, most recently, Asia (*2*). Plant infection requires an infection cell, called an appressorium, which uses a pressure-driven mechanism to breach the tough cuticle of the leaf (*3*, *4*). Once inside plant tissue, the fungus elaborates pseudohyphal-like invasive hyphae that rapidly colonize living host cells, secreting effector molecules to suppress host immunity and facilitate infection (*5*). *M. oryzae* effectors are delivered into host cytoplasm by means of a biotrophic interfacial complex (BIC), a plant-derived membrane-rich structure in which effectors accumulate during transit to the host (*5*–*8*). Hyphae then appear to locate pit fields, composed of plasmodesmata, which are traversed by constricted, narrow hyphae, enabling the spread of the fungus to adjacent host cells (*9*). The fungus rapidly colonizes host tissue, and disease lesions appear within 4 to 5 days of initial infection by spores.

In this study, we investigated how *M. oryzae* colonizes host tissue and, in particular, how it spreads from one plant cell to the next. We first performed ultrastructural analysis of rice sheath cells infected with the pathogenic strain Guy11. This analysis confirmed constriction of hyphae from an average diameter of 5.0 μm to 0.6 μm during traversal of rice cells (Fig. 1, A and B, and fig. S1). The rice plasma membrane in the second invaded cell remained intact as an electron-dense lining near the rice cell wall, continuous with the plant plasma membrane around hyphae (Fig. 1B) (*5*, *8*, *9*). By contrast, the rice plasma membrane in the first invaded cell lost integrity upon exit of the fungus to the next rice cell (Fig. 1, B and E) (*7*, *9*, *10*).

One of the plant's defenses against infection is to close intercellular plasmodesma channels by deposition of callose (*11*, *12*). We visualized callose using aniline blue staining of rice cells (Fig. 1C and fig. S3). Callose papillae often form at appressorium penetration sites, but no callose occlusions were initially observed at plasmodesmata during infection of the first rice cell at 27 hours post-inoculation (hpi) (fig. S3). Later callose deposition was observed at plasmodesmata by 30 hpi, consistent with the onset of cell death among initially invaded rice cells (figs. S1 and S2). Callose collars then formed around the base of invasive hyphae after they invaded adjacent cells, at 34 hpi (Fig. 1C and fig. S3). These observations suggest that *M. oryzae* is able to clear plasmodesmal occlusion materials before penetrating pit fields (Fig. 1D). We also observed a switch from polarized to isotropic fungal growth by invasive hyphae at rice cell junctions. The polarisome marker Spa2–green fluorescent protein (Spa2-GFP) localized to hyphal tips and then disappeared as hyphal tips swelled upon contact with the host cell wall (fig. S2) (*5*). Spa2-GFP then appeared again at hyphal tips in newly colonized cells (fig. S2). Cell wall crossing was accompanied by reorganization of fungal septins and F-actin into an hourglass shape at the point of maximum hyphal constriction (Fig. 1F, figs. S2 and S10, and movie S1) (*3*, *5*, *13*).

Plasmodesmata are dynamic structures through which proteins diffuse between plant cells (*11*). To test whether the blast fungus can manipulate plasmodesmata by increasing their size exclusion limit to facilitate effector diffusion to adjacent plant cells, we bombarded rice tissue infected with *M. oryzae* at 24 hpi with single- and double-sized mCherry expression vectors. In uninfected rice tissue, a 28.8-kDa single mCherry protein moved into neighboring rice cells but a 57.6-kDa double mCherry fusion protein generally did not, owing to its larger size (Fig. 1, G and H). By contrast, in blast-infected tissue, double mCherry protein diffused to adjacent rice cells. The gating limit of rice plasmodesmata is therefore relaxed during early *M. oryzae* infection. We then carried out time-lapse imaging of the fungal apoplastic effector Bas4 (biotrophy-associated secreted protein 4)–GFP (*8*), expressed under its native promoter, during plant infection (fig. S2 and movie S2). We observed that upon exit of the fungus to an adjacent cell, Bas4-GFP leaked into the host cytoplasm of initially colonized rice cells. However, fluorescence did not diffuse into the newly colonized cells. Plasmodesmata therefore remain open at early stages of infection (24 to 27 hpi) but are closed at later stages, consistent with the increase in plasmodesmal callose deposition at 30 to 34 hpi (fig. S3) (*7*, *14*), suggesting that the blast fungus is able to overcome callose deposition at pit fields to invade neighboring cells. Plasmodesmata may lose their structural integrity after this time, as initially infected rice cells lose their viability.

To study regulatory mechanisms controlling invasive growth, we characterized Pmk1, a fungal mitogen-activated protein kinase (MAPK) essential for appressorium development and pathogenicity that is conserved in many plant-pathogenic fungi (*15*). Pmk1 null mutants of *M. oryzae* cannot infect rice plants even when mutants are inoculated onto wounded leaves (*15*). We decided to conditionally inactivate the Pmk1 MAPK using a chemical genetic approach. We generated an analog-sensitive (AS) allele of *PMK1* (*pmk1*^{AS}) by mutating the gatekeeper residue of the kinase adenosine triphosphate (ATP)–binding site into a small amino acid residue, glycine. The equivalent (Shokat) mutation previously reported in yeast *fus3-as1* confers susceptibility to the ATP analog 1-naphthyl-PP1 (1NA-PP1) (*16*). Expression of the *pmk1*^{AS} allele, under control of its native promoter, restored pathogenicity to a Δ*pmk1* mutant (fig. S4). Addition of 1NA-PP1 selectively inhibited the function of Pmk1^{AS} mutants, preventing appressorium development (fig. S4), a result that was identical to the effects of *PMK1* deletion or expression of a kinase-inactive allele (*17*). We also observed that inhibiting Pmk1 after appressorium formation blocked cuticle penetration by preventing assembly of the septin ring at the appressorium pore (fig. S5).

To test the role of Pmk1 in tissue invasion, we allowed a *pmk1*^{AS} mutant to invade the first rice epidermal cell before adding 1NA-PP1 at 26 hpi. This treatment blocked invasion of adjacent epidermal cells, resulting in the first infected cells becoming filled with fungal hyphae (Fig. 2, A and B). Pmk1 inactivation did not affect the structure

[1]School of Biosciences, University of Exeter, Exeter EX4 4QD, UK. [2]Department of Plant Pathology, Kansas State University, 4024 Throckmorton Plant Sciences Center, Manhattan, KS 66506-5502, USA.
*Present address: School of Biological and Marine Sciences, Plymouth University, Portland Square Building, Drake Circus, Plymouth PL4 8AA, UK.
†Corresponding author. Email: n.j.talbot@exeter.ac.uk

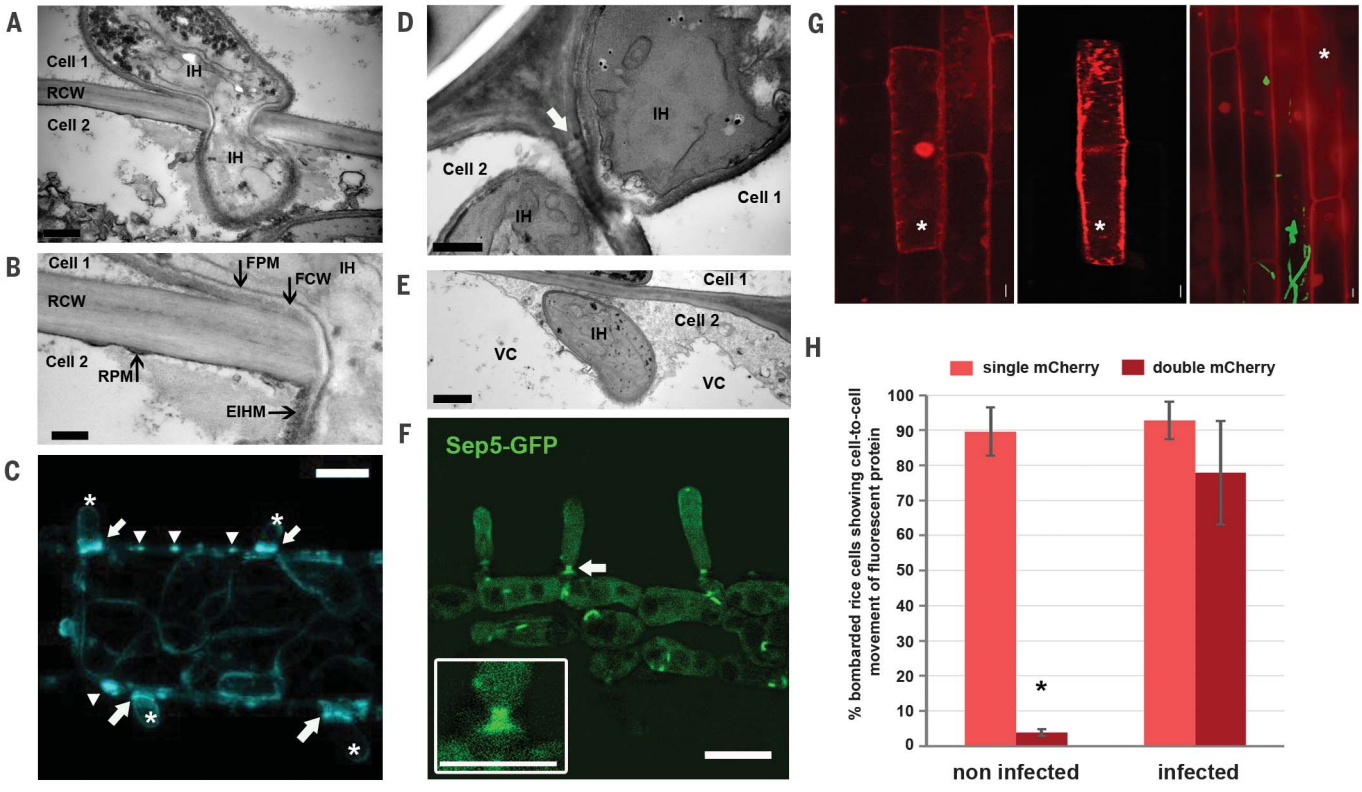

Fig. 1. Cell-to-cell invasion and plasmodesmal manipulation by *M. oryzae*. (**A**) Transmission electron micrograph of an invasive hypha (IH) traversing a rice cell wall (RCW) at 42 hpi. Scale bar, 0.5 μm. (**B**) High-magnification view of the crossing site. The rice plasma membrane (RPM), fungal plasma membrane (FPM), and fungal cell wall (FCW), and extrainvasive hyphal membrane (EIHM) are indicated. Scale bar, 20 nm. (**C**) Callose deposition in an infected rice cell at 34 hpi, shown by aniline blue staining. Arrowheads indicate plasmodesmal callose deposition. Arrows indicate callose collars that form around hyphae after they enter adjacent cells (asterisks). Scale bar, 5 μm. (**D**) Hyphae traversing the cell wall at a pit field (arrow). Scale bar, 0.5 μm. (**E**) Difference in host cytoplasmic contents between the first and second invaded cells (for a larger image, see fig. S1G). VC, vacuole. Scale bar, 1 μm. (**F**) Localization of a septin Sep5-GFP collar at rice cell crossing points (arrow and high-magnification inset) at 40 hpi. Scale bars, 10 μm (main panel); 5 μm (inset). (**G**) Diffusion of single and double mCherry fluorescent proteins in uninfected leaf tissue (left and middle panels, respectively) and in leaves infected with *M. oryzae* (right panel) at 24 hours (*9*). Asterisks indicate bombarded cells. Scale bars, 10 μm. (**H**) Percentages of bombarded cells showing diffusion of mCherry proteins in blast-infected and uninfected rice tissues (*P = 0.05; n = 100 cells; error bars indicate SE).

of BICs or the morphology of invasive hyphae (fig. S6A). In the presence of 1NA-PP1, hyphae of the *pmk1*^{AS} mutant still formed terminal swellings at host wall contact points (Fig. 2C) (*9*) but could not breach adjacent cells. Inhibition of Pmk1 also blocked rice cell invasion in a second rice cultivar, Mokoto, and in barley (fig. S6, B and C). Pmk1 inhibition was accompanied by rapid derepression of reactive oxygen species (ROS) generation, a key plant defense response, and increased ROS-dependent callose deposition (Fig. 2, D and E, and fig. S6). To confirm the role of Pmk1 in cell wall crossing, we performed live-cell imaging of a functional Pmk1-GFP protein, which showed expression of the protein during appressorium-dependent cuticle penetration (Fig. 2F) (*17*) but also upon contact of invasive hyphae with rice cell walls just before invasion of the neighboring cell (Fig. 2G and movie S4). *M. oryzae* has two additional MAPKs: Osm1, which is dispensable for virulence (*18*), and Mps1, which regulates cell integrity and is necessary for fungal infection (*19*). We therefore generated an analog-sensitive *mps1* (*mps1*^{AS}) mutant and found that selective inactivation of Mps1 enhanced host defenses (*20*) but did not block cell-to-cell invasion (fig. S7).

To investigate how Pmk1 regulates invasive growth, we performed RNA sequencing (RNA-seq) analysis to compare *M. oryzae* gene expression levels during infection with the *pmk1*^{AS} mutant in the presence and absence of 1NA-PP1. Using an adjusted P value of ≤0.05 for differential gene expression, we found 1457 fungal genes with altered expression during Pmk1 inhibition, accounting for 11.5% of total protein-encoding genes. Of these, 715 fungal genes were up-regulated and 742 were down-regulated (table S2). A subset of effector genes implicated in plant immunity suppression were positively regulated by Pmk1, including genes for Avr-Pita1 (*6*); Slp1, which suppresses chitin-triggered immunity (*21*); Avr-Pik; and several Bas effectors, including Bas2 and Bas3 effectors (*8*) that putatively function at cell wall crossing sites (Fig. 3A and fig. S8). We expressed Bas2-GFP and Bas3-GFP in the *pmk1*^{AS} mutant and found that they were not expressed in the presence of 1NA-PP1 (Fig. 3, B and C). We also generated a *pmk1*^{AS} strain expressing cytosolic GFP under control of the Bas3 promoter (Fig. 3, D to F). The addition of 1NA-PP1 inhibited GFP expression during appressorium-mediated infection (Fig. 3D) and during invasive growth (Fig 3, E and F). Localization of other fungal effectors was not affected by Pmk1 inactivation (fig. S8), and Pmk1 therefore affects expression of a subset of fungal effectors involved in suppression of host immunity.

To test whether suppression of host immunity, particularly at plasmodesmata, could explain the role of Pmk1 in cell invasion by *M. oryzae*, we suppressed host immune reactions simultaneously with Pmk1 inhibition. We found that chemical suppression of plant ROS or disruption of salicylic acid regulation did not reverse the effects of Pmk1 inactivation (fig. S9). To suppress host immunity completely, we therefore killed plant tissue by ethanol treatment before rehydration and inoculation with the *pmk1*^{AS} mutant. In the

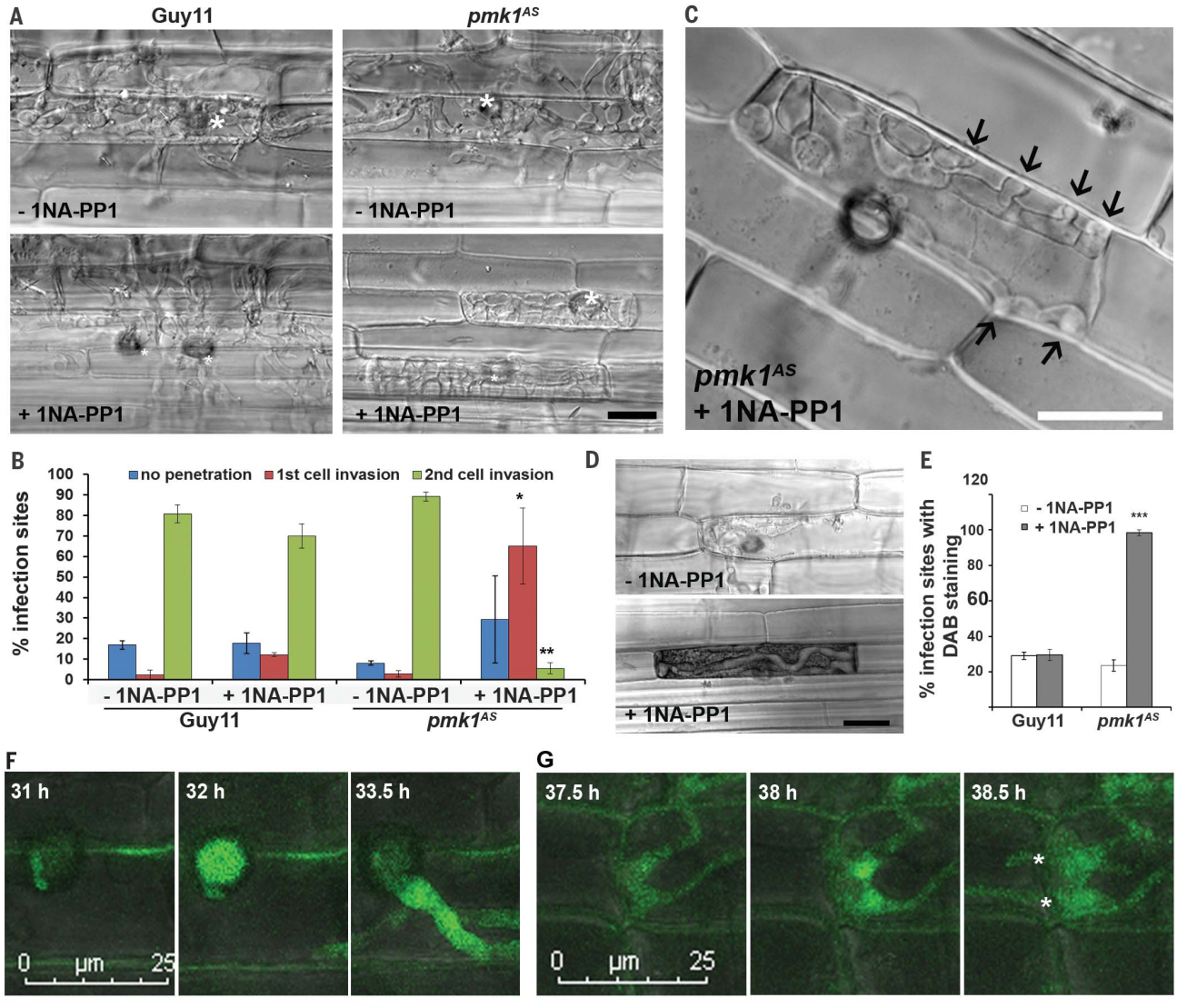

Fig. 2. Pmk1 MAPK-dependent regulation of cell-to-cell spread by *M. oryzae*. (**A** and **B**) Effect of Pmk1 inhibition on host colonization at 48 hpi. Infected rice tissues were treated with 5 µM 1NA-PP1 at 26 hpi. Asterisks indicate appressorium penetration sites. Error bars in (B) indicate SE. (**C**) Formation of swollen hyphae (arrows) by the *pmk1*^{AS} mutant upon contact with the host cell wall in the presence of 1NA-PP1, imaged at 40 hpi. (**D** and **E**) Induction of ROS production, shown by 3,3′-diaminobenzidine (DAB) staining, after the addition of 1NA-PP1 at 26 hpi. Images were taken at 48 hpi. n = 300 infection sites; $^{*}P < 0.05$, $^{**}P < 0.01$, $^{***}P < 0.001$, unpaired Student's t test. Error bars in (E) denote SE. Scale bars in (A), (C), and (D), 20 µm. (**F**) Transient accumulation of Pmk1-GFP in an appressorium during emergence of a penetration hypha. (**G**) Transient accumulation of Pmk1-GFP in hyphae at rice cell crossing points (asterisks).

presence of 1NA-PP1, the mutant still remained trapped in the first dead plant cell (Fig. 4A). We therefore hypothesized that Pmk1-dependent hyphal constriction must be critical for cell wall crossing at pit fields. This relationship would correspond with the role of Pmk1 in septin-dependent appressorium repolarization (fig. S5) (*3*, *13*). Consistent with this idea, RNA-seq analysis revealed several morphogenetic regulators down-regulated during Pmk1 inhibition. Genes for Chm1, a homolog of Cla4 p21-activated protein kinase that phosphorylates septins (*22*), and a putative F-actin cross-linking protein, alpha-actinin, for example, are among genes positively regulated by Pmk1 during plant infection (table S2).

We therefore investigated septin organization during Pmk1 inhibition. Sep5-GFP still accumulated at cell wall contact points but as a disorganized mass instead of the septin collars that normally form at cell wall crossing sites (Fig. 4, figs. S10 and S11, and movies S3 and S5). Finally, we investigated the ability of septin mutants to invade plant tissue. Septin mutants do not penetrate the rice cuticle efficiently because of the roles of septins in appressorium repolarization and the development of penetration hyphae (*3*). However, a small proportion of penetration events are successful. In these rare instances, the Δ*sep6* mutant, in particular, showed a reduction in its ability to spread between rice cells, consistent with a role for septins in cell invasion (fig. S12).

Taken together, our results demonstrate that the Pmk1 MAPK pathway controls plant tissue invasion by controlling the constriction of invasive hyphae to traverse pit fields in order to invade new rice cells while maintaining the cellular integrity of the host. To accomplish this feat, the MAPK also regulates expression of a battery of effectors to suppress plant immunity, thereby preventing plasmodesmal closure until the fungus has invaded neighboring cells. Plant tissue invasion by the blast fungus is therefore orchestrated, rapid, and necessary for the devastating consequences of the disease.

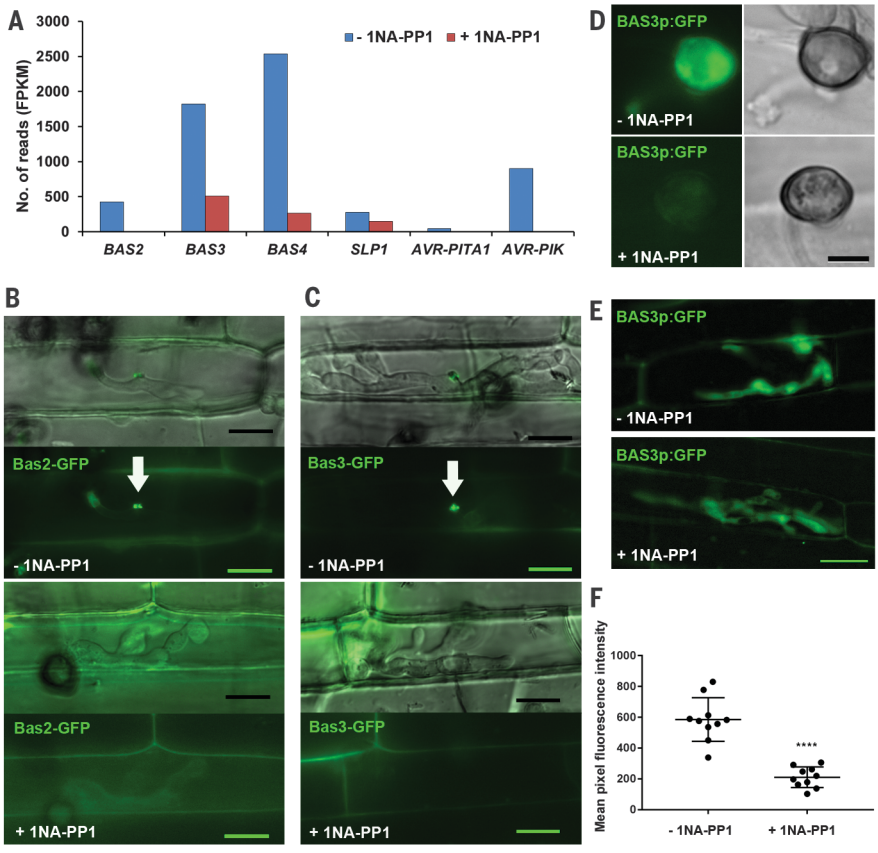

Fig. 3. Pmk1-dependent regulation of effector gene expression during biotrophic growth. (**A**) Bar chart showing relative expression levels [fragments per kilobase of transcript per million mapped reads (FPKM)] of known effector genes differentially regulated during Pmk1 inhibition in RNA-seq analysis. (**B** and **C**) Localization of Bas2-GFP and Bas3-GFP effectors in a *pmk1*^{AS} mutant with and without 1NA-PP1. BICs are indicated by arrows. Scale bars in (B), (C), and (E), 20 μm. (**D** to **F**) Expression of cytosolic GFP driven by the *BAS3* promoter (Bas3p:GFP) in a *pmk1*^{AS} mutant. (D) Strong GFP expression at 24 hpi in appressoria undergoing infection and lack of GFP expression in appressoria treated with 1NA-PP1 at 8 hpi. Scale bar, 10 μm. (E) GFP expression in *pmk1*^{AS} hyphae exposed to 1NA-PP1 at 26 hpi and imaged at 30 hpi. (F) Dot plot of Bas3p:GFP fluorescence in a *pmk1*^{AS} mutant treated with 5 μM 1NA-PP1 at 26 hpi or left untreated. Images were taken at 30 hpi, and background was subtracted before measurement of fluorescence levels. ****$P < 0.0001$, unpaired Student's *t* test; three biological replicates.

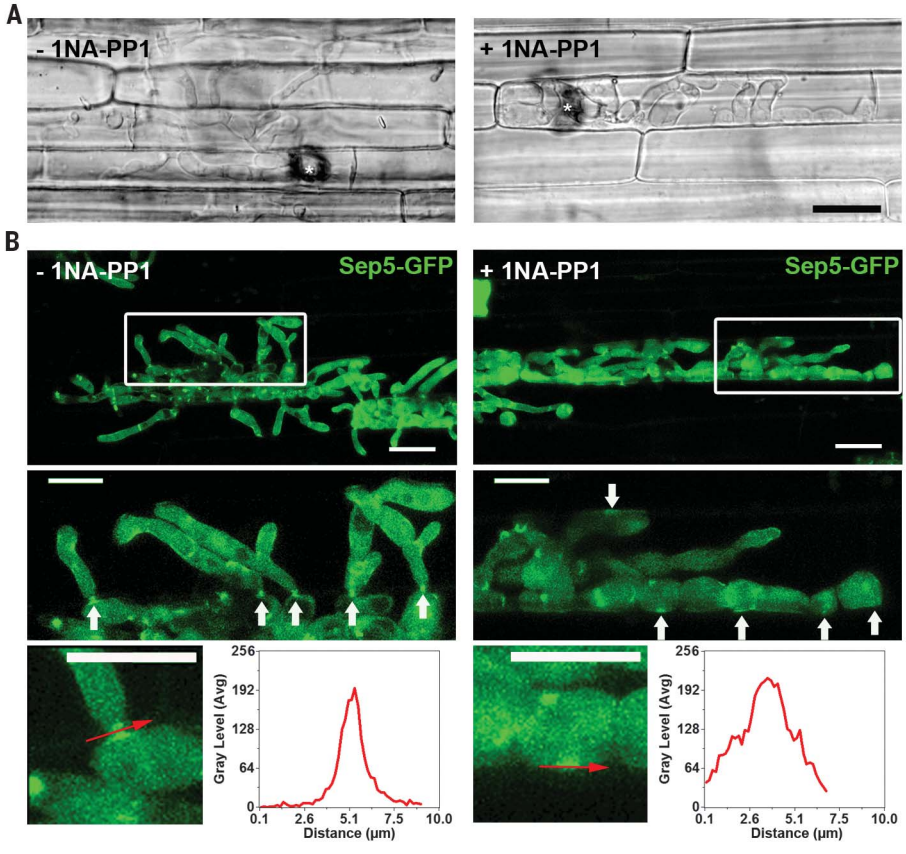

Fig. 4. Pmk1 controls septin-dependent morphogenesis of narrow invasive hyphae traversing cell walls. (**A**) Micrographs showing that the *pmk1*^{AS} mutant, growing in ethanol-killed rice tissue treated with 1NA-PP1 at 14 hpi, remained trapped inside initially invaded rice cells in all 200 infection sites examined at 48 hpi. Asterisks indicate appressorium penetration sites. Scale bar, 20 μm. (**B**) Confocal micrographs showing localization of Sep5-GFP in a *pmk1*^{AS} mutant at 42 hpi after the addition of 1NA-PP1 (5 μM) at 26 hpi or in the absence of 1NA-PP1. Arrows indicate accumulation of Sep5-GFP at rice cell contact points. Scale bars, 10 μm. Red arrows in high-magnification panels show line scans used to generate corresponding fluorescence intensity distribution graphs.

REFERENCES AND NOTES

1. R. A. Wilson, N. J. Talbot, *Nat. Rev. Microbiol.* **7**, 185–195 (2009).
2. Y. Inoue *et al*., *Science* **357**, 80–83 (2017).
3. Y. F. Dagdas *et al*., *Science* **336**, 1590–1595 (2012).
4. C. Veneault-Fourrey, M. Barooah, M. Egan, G. Wakley, N. J. Talbot, *Science* **312**, 580–583 (2006).
5. M. C. Giraldo *et al*., *Nat. Commun.* **4**, 1996 (2013).
6. C. H. Khang *et al*., *Plant Cell* **22**, 1388–1403 (2010).
7. S. Mochizuki, E. Minami, Y. Nishizawa, *Microbiologyopen* **4**, 952–966 (2015).
8. G. Mosquera, M. C. Giraldo, C. H. Khang, S. Coughlan, B. Valent, *Plant Cell* **21**, 1273–1290 (2009).
9. P. Kankanala, K. Czymmek, B. Valent, *Plant Cell* **19**, 706–724 (2007).
10. K. Jones, D. W. Kim, J. S. Park, C. H. Khang, *BMC Plant Biol.* **16**, 69 (2016).
11. C. Cheval, C. Faulkner, *New Phytol.* **217**, 62–67 (2018).
12. C. Faulkner *et al*., *Proc. Natl. Acad. Sci. U.S.A.* **110**, 9166–9170 (2013).
13. L. S. Ryder *et al*., *Proc. Natl. Acad. Sci. U.S.A.* **110**, 3179–3184 (2013).
14. W. Cui, J. Y. Lee, *Nat. Plants* **2**, 16034 (2016).
15. J.-R. Xu, J. E. Hamer, *Genes Dev.* **10**, 2696–2706 (1996).
16. A. C. Bishop *et al*., *Nature* **407**, 395–401 (2000).
17. K. S. Bruno, F. Tenjo, L. Li, J. E. Hamer, J.-R. Xu, *Eukaryot. Cell* **3**, 1525–1532 (2004).
18. K. P. Dixon, J.-R. Xu, N. Smirnoff, N. J. Talbot, *Plant Cell* **11**, 2045–2058 (1999).
19. J.-R. Xu, C. J. Staiger, J. E. Hamer, *Proc. Natl. Acad. Sci. U.S.A.* **95**, 12713–12718 (1998).
20. X. Zhang, W. Liu, Y. Li, G. Li, J. R. Xu, *Environ. Microbiol.* **19**, 4190–4204 (2017).
21. T. A. Mentlak *et al*., *Plant Cell* **24**, 322–335 (2012).
22. L. Li, C. Xue, K. Bruno, M. Nishimura, J.-R. Xu, *Mol. Plant-Microbe Interact.* **17**, 547–556 (2004).

ACKNOWLEDGMENTS

We thank S. Yoshida (RIKEN, Japan) for providing Nipponbare and NahG rice lines. **Funding:** This work was funded by a Halpin Scholarship for rice blast research to W.S., a European Research Council (ERC) Advanced Investigator Award to N.J.T. under the European Union's Seventh Framework Programme (FP7/2007-2013) and ERC grant no. 294702 GENBLAST, and Agriculture and Food Research Initiative Competitive grant no. 2012-67013-19291 to B.V. from the U.S. Department of Agriculture National Institute of Food and Agriculture. This is contribution number 18-174-J from the Kansas Agricultural Experiment Station. **Author contributions:** W.S., B.V., and N.J.T. conceived of the project. W.S., M.O.-R., and E.O.G. performed experimental work. D.M.S. provided bioinformatic data analysis. G.R.L. carried out laser confocal imaging. C.H. and A.C. performed ultrastructural analysis. W.S., M.O.-R., B.V., and N.J.T. wrote the paper with the assistance and input of all coauthors. **Competing interests:** The authors declare no competing interests. **Data and materials availability:** All data are available in the article or in the supplementary materials. Differential gene expression analysis data can be accessed at Gene Expression Omnibus (www.ncbi.nlm.nih.gov/geo/) under accession number GSE106845.

SUPPLEMENTARY MATERIALS

www.sciencemag.org/content/359/6382/1399/suppl/DC1
Materials and Methods
Figs. S1 to S13
Tables S1 and S2
References (*23*–*40*)
Movies S1 to S5

7 October 2017; accepted 24 January 2018
10.1126/science.aaq0892

CANCER

Lymph node metastases can invade local blood vessels, exit the node, and colonize distant organs in mice

Ethel R. Pereira,[1] Dmitriy Kedrin,[1,2] Giorgio Seano,[1] Olivia Gautier,[1,3] Eelco F. J. Meijer,[1] Dennis Jones,[1] Shan-Min Chin,[1] Shuji Kitahara,[1] Echoe M. Bouta,[1] Jonathan Chang,[4,5] Elizabeth Beech,[1] Han-Sin Jeong,[6] Michael C. Carroll,[5,7] Alphonse G. Taghian,[8] Timothy P. Padera[1]*

Lymph node metastases in cancer patients are associated with tumor aggressiveness, poorer prognoses, and the recommendation for systemic therapy. Whether cancer cells in lymph nodes can seed distant metastases has been a subject of considerable debate. We studied mice implanted with cancer cells (mammary carcinoma, squamous cell carcinoma, or melanoma) expressing the photoconvertible protein Dendra2. This technology allowed us to selectively photoconvert metastatic cells in the lymph node and trace their fate. We found that a fraction of these cells invaded lymph node blood vessels, entered the blood circulation, and colonized the lung. Thus, in mouse models, lymph node metastases can be a source of cancer cells for distant metastases. Whether this mode of dissemination occurs in cancer patients remains to be determined.

Solid tumor progression is characterized by metastasis to regional lymph nodes and dissemination to distant organs. The presence of lymph node disease in cancer patients correlates with a poorer prognosis and partially dictates the course of treatment (*1*–*5*). However, there is a robust ongoing debate about the role of lymph node metastasis in further progression of disease (*6*, *7*). Some experts contend that localized lymph node metastases are clinically inconsequential (*8*, *9*), whereas others contend that lymph node metastases have the potential to seed distant organs (*5*, *10*–*12*) and therefore should be treated to prevent distant metastasis (*13*, *14*). This debate has taken on new urgency with the recent completion of clinical trials that suggest that nodal dissection beyond the sentinel (first) lymph node does not provide therapeutic benefit to patients who have received adjuvant radiation therapy and systemic therapies (*15*–*19*). Other data show that radiation therapy of regional lymph nodes improves the outcome of patients with early stage breast cancer (*20*, *21*), suggesting that treatment of metastatic lymph nodes benefits a subgroup of patients (*22*, *23*).

In this study, we used mouse models to investigate whether cancer cells can exit the lymph node and disseminate to distant sites. We stably expressed the photoconvertible fluorescent protein Dendra2 (cytosolic localization) or Dendra2 fused to the nuclear protein histone H2B (Dendra2H2B nuclear localization) in 4T1 murine mammary cancer cells (a model of triple-negative breast cancer), B16F10 murine melanoma cells, and SCCVII murine squamous cell carcinoma cells. Dendra2 is a green-emitting fluorescent protein that can be converted to emit red light by exposure to 405-nm light (*24*). Expression of Dendra2 in these cell lines did not affect cell migration, proliferation rates, or in vivo tumor growth when compared with parental lines (fig. S1). We orthotopically implanted tumor cells into syngeneic mice and resected the primary tumor once it reached a volume of ~250 to 500 mm^3. Next, we used a 405-nm laser diode on 5 consecutive days to convert Dendra2H2B cancer cells from green to red fluorescence, restricting the light exposure to the metastatic lymph node (Fig. 1A). Tissue clearing of the resected primary tumor revealed that no cancer cells at the primary site underwent spontaneous photoconversion (fig. S2). The in vivo photoconversion efficiency in the lymph node was 70% for 4T1 cells, 62% for B16F10 cells, and 56% for SCCVII cells (fig. S3).

We next determined whether photoconverted circulating tumor cells (CTCs) appeared in the blood of animals that had undergone photoconversion of the lymph node. The presence of red fluorescent CTCs would show that these cells originated from lymph node metastases. We identified red photoconverted 4T1 CTCs and B16F10 CTCs (Fig. 1, B and C, and fig. S4, A and B) that disseminated from the lymph node. CTCs from 4T1-Dendra2 and 4T1-Dendra2H2B lymph node metastasis were grown in vitro to confirm viability. Both viable red (lymph node origin) and green fluorescent CTCs were observed after 1 day in culture. By day 7, only green colonies formed, as red fluorescence is lost as the photoconverted cells divide (fig. S4C). These data show that viable cancer cells from the lymph node have the potential to exit the node and survive in the blood. We did not detect photoconverted SCCVII CTCs (Fig. 1B and fig. S4D), although our methods could detect these cancer cells when photoconverted in vitro (fig. S5A) and in the lymph node of SCCVII tumor–bearing animals (fig. S5B).

To explore whether cancer cells in lymph nodes can seed distant organs, we analyzed the lungs of mice after photoconversion of their lymph node metastasis. Confocal microscopy revealed the presence of isolated photoconverted (red) cancer cells in the lungs of animals with 4T1 (Fig. 2, A and B) and B16F10 cancers (Fig. 2, C and D). Among the isolated cancer cells detected in the lung, 70% of 4T1 cells and 68% B16F10 cells were of lymph node origin (Fig. 2, B and D). We performed a spectral scan from 426 to 661 nm with a 5-nm bandwidth (fig. S6), which showed distinct signals for DAPI (4′,6-diamidino-2-phenylindole) (emission maximum: 450 nm), native Dendra2H2B (emission maximum: 507 nm), and photoconverted Dendra2H2B (emission maximum: 572 nm) (*24*) in lung sections, with no detectable signal at other wavelengths. These data demonstrate the specificity of our detection methods to identify lung metastasis of lymph node origin. We did not detect cancer cells in the lungs of SCCVII-bearing mice.

We next evaluated whether the primary tumor can also seed the lung directly without transiting the lymph node. By photoconverting 4T1-Dendra2H2B primary tumors only (fig. S7A), before their dissemination to the draining lymph node (fig. S7B), we detected photoconverted CTCs (fig. S7C) in whole blood from these animals, which could only have originated from the primary tumor. Next, we prophylactically excised the sentinel lymph nodes from BALB/c mice (fig. S8) before injecting 4T1-DendraH2B cancer cells into the mammary fat pad (MFP). Two weeks after primary tumor resection, we detected CTCs and lung metastases in the absence of lymph nodes. However, animals with intact lymph nodes had higher numbers of CTCs and lung metastases compared with animals with lymph nodes removed (fig. S8). Taken together, these data show that cancer cells from the primary site can directly enter the systemic circulation and seed the lung.

We then examined whether both routes of metastasis—transit via the lymph node or transit directly from the primary tumor—can contribute to distant metastatic lesions. To this end, we injected Dendra2-expressing (green fluorescent protein) 4T1 cancer cells directly in the axillary lymph node (fig. S9A). On the contralateral side, the lymph node was removed 1 week before injection of mCherry-expressing (red fluorescent protein) 4T1 cancer cells into the MFP (Fig. 2E and fig. S9B). Ten days after resecting both the tumor-bearing lymph node and the MFP tumor, we detected both red and green lung metastases

[2]Division of Gastroenterology, MGH and HMS, Boston, MA 02114, USA. [3]Department of Biological Engineering, Massachusetts Institute of Technology, Cambridge, MA 02142, USA. [4]Graduate Program in Immunology, Division of Medical Sciences, HMS, Boston, MA 02115, USA. [5]Program in Cellular and Molecular Medicine, Children's Hospital Boston and HMS, Boston, MA 02115, USA. [6]Department of Otorhinolaryngology and Head and Neck Cancer Center, Samsung Medical Center, Sungkyunkwan University School of Medicine, Seoul, South Korea. [7]Department of Pediatrics, Children's Hospital Boston and HMS, Boston, MA 02115 USA. [8]Department of Radiation Oncology, MGH and HMS, Boston, MA 02114, USA.
*Corresponding author. Email: tpadera@steele.mgh.harvard.edu

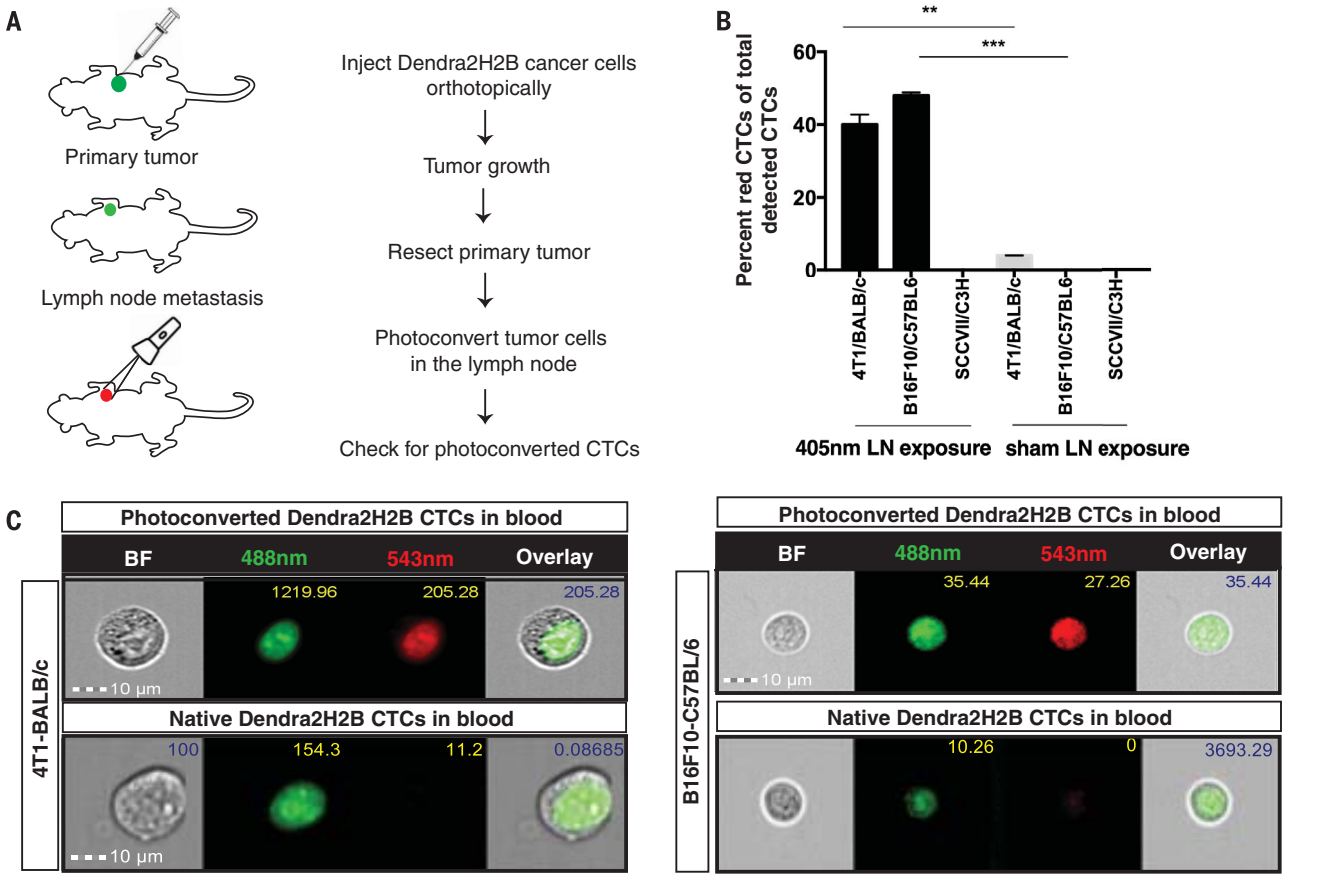

Fig. 1. Circulating tumor cells (CTCs) that transited through the lymph node are detected in mouse models. (**A**) Dendra2H2B-positive cancer cells were injected orthotopically into syngeneic recipients. Approximately 20 days later, the primary tumor was resected and tumor-draining lymph nodes were photoconverted using a 405-nm diode for 5 consecutive days. Blood was analyzed for the presence of green and red fluorescent CTCs using an Amnis Imagestream flow cytometer. (Photoconverted animals: 4T1 model, $n = 11$; B16F10 model, $n = 7$; SCCVII model, $n = 5$. Control animals: 4T1 model, $n = 5$; B16F10 model, $n = 7$; SCCVII, $n = 3$.) (**B**) Dendra2H2B-4T1 and Dendra2H2B-B16F10 cells but not Dendra2H2B-SCCVII cells photoconverted in the draining lymph node (LN) were detected in the blood. Data are represented as the percentage of red CTCs (photoconverted) among total detected CTCs. Green CTCs were detected in all three models. For 405-nm light exposure compared with sham exposure for individual cells lines, $^{**}P < 0.005$ and $^{***}P < 0.0005$. Error bars indicate SEM. (**C**) Representative images obtained by Imagestream flow cytometry of CTCs from 4T1/BALB/c and B16F10/C57BL/6 mouse models show positive photoconverted cancer cells verified by nuclear localization of Dendra2H2B. Numbers indicate fluorescence intensity. BF, bright field.

(Fig. 2F; H&E staining in fig. S9C). We measured a large variation in the ratio of green:red metastatic lung lesions across multiple animals (average ratio of eight green:five red metastatic lesions) (Fig. 2G). Despite this large variation, every animal had lung metastases that originated from both lymph node lesions and directly from the primary tumor.

Cancer cells could take two possible routes to exit the lymph node and spread systemically—through lymph node blood vessels or efferent lymph. We hypothesized that cancer cells can escape the lymph node by directly invading lymph node blood vessels. Immunohistochemical analysis of 4T1 tumor–draining lymph nodes revealed isolated cancer cells (cytokeratin positive) in close association with CD31-positive blood vessels, within high endothelial venules and breaching the vascular basement membrane (collagen IV positive) (Fig. 3A). In metastatic lymph nodes with only isolated cancer cells (fig. S10A), quantitative analysis showed that 23 ± 2% of isolated cancer cells were within 5 µm of a blood vessel, compared with only 11 ± 1% of cancer cells in a model of randomly distributed cells in the lymph node (Fig. 3, B and C, $P < 0.05$). Further, 6 ± 2% of the cancer cells were inside blood vessels (Fig. 3D and fig. S10B). A similar analysis performed in lymph nodes containing larger metastatic lesions (>200 µm in diameter, fig. S11A) did not show this tropism (fig. S11B, $P > 0.05$). As metastatic lesions grow, the surface area of the blood vessels becomes limiting, causing the distribution of cancer cells to revert to that of a random distribution. This phenotype is consistent with the lack of sprouting angiogenesis in lymph node metastases (*25*). In lymph nodes with large lesions, 1 ± 0.5% of cancer cells were found in blood vessels (Fig. 3D). A similar analysis did not show an association between cancer cells and lymphatic vessels in tumor-draining lymph nodes (fig. S12, $P > 0.05$).

We also analyzed lymph nodes with large metastatic lesions from 19 patients with head and neck cancer. Similar to large lesions in mouse lymph nodes, cancer cells in human lymph nodes did not demonstrate measurable tropism to blood vessels, owing to the limitation in vessel surface area. However, at the edge of the metastatic lesions, we found cancer cells that were closely associated with blood vessels (fig. S13). In addition, we detected isolated cancer cells inside blood vessels in 6 of the 19 patient samples (fig. S13), consistent with our preclinical data.

To confirm that metastatic cancer cells in a lymph node have an affinity for lymph node blood vessels, we used time-lapse multiphoton intravital microscopy to measure cancer cell migration in an optical lymph node window in mice (*25*). Dendra2-expressing metastatic cancer cells are first seen in the subcapsular sinus and later invade the cortex of the lymph node. There, they accumulate around rhodamine-dextran–labeled

blood vessels (Fig. 4, A to C, and fig. S14) or associate with lymph node conduits, which contain a fibrillar collagen core surrounded by fibroblastic reticular cells (FRCs) (Fig. 4D). Cancer cells can be observed in directed migration toward blood vessels as well as moving inside blood vessels (movies S1 to S3 and Fig. 4E). Time-lapse imaging of tumor-draining lymph nodes revealed that only a small fraction of cancer cells in the lesion are motile. Both 4T1 and SCCVII cells that were motile had an average speed of 7 μm/hour (Fig. 4F), similar to the speed of resident lymph node stromal cells such as FRCs, follicular dendritic cells, macrophages, and resident dendritic cells (*26*). However, a greater fraction of 4T1 cells were motile compared with SCCVII cells (Fig. 4G). Consistent with our observations in tissue sections (Fig. 3F), cancer cells create persistent associations with blood vessels (Fig. 4, B and C) as well as conduits (Fig. 4D). The conduit system is an interconnected collagen network formed by FRCs that creates pathways for dendritic cells to navigate through the lymph node to interact with naïve lymphocytes near high endothelial venules (*27*). We speculate that, similar to dendritic cells, cancer cells use the conduit system to aid in their migration to lymph node blood vessels.

The Dendra2 system has limitations. First, the photoconversion of the green Dendra2 protein to red fluorescence can be detected for only 5 to 6 days before the cells appear green again. Second, the photoconversion efficiency of Dendra2H2B in the lymph node was ~60 to 70% in our tumor models. Thus, in mice that underwent photoconversion of metastatic cancer cells in the lymph node, green-Dendra2H2B–expressing cancer cells in the blood or lungs could have multiple sources, including the primary tumor directly, unconverted cancer cells in the lymph node, or photoconverted cancer cells in the lymph node that lost their red fluorescence with cell division. These limitations prevent us from accurately assessing what percentage of distant metastases originates from lymph node metastases.

The absence of detectable photoconverted CTCs and lung metastasis in the SCCVII cancer model reflects the variability in the aggressiveness of cancer models in mice. We do not expect the selected mouse cell lines to represent the variability present in patient populations. Further, cancer cells alter their phenotype in response to local microenvironments as they spread to metastatic sites. We measured changes in the expression of chemokines—signaling molecules that regulate cell homing and migration—as cancer cells spread from the primary tumor to the lymph nodes and lungs (fig. S15). These data may provide clues as to how cancer cells can navigate from one metastatic site to another.

The route of cancer cell dissemination to distant sites in patients is complex and highly debated, in part because of limited clinical and experimental evidence. However, animal studies have linked large lymph node metastases to distant metastases (*28*). Further, studies using patient lymph node samples, human mammary carcinoma cells, and xenograft tumors in immunedeficient mice have shown that cancer cells can invade lymphatic vessels in the sentinel lymph node and spread to additional nodes (*29*). Several clinical studies have also shown a relationship between the number of involved axillary lymph nodes and a higher risk for distant recurrence in breast cancer patients (*13*, *30*, *31*). Genetic studies examining the clonal relationships between cancer cells in the primary site, lymph nodes, and distant organs have shown that distant metastases are more closely related to lymph node metastases than to primary tumors in a subset of mice and patients (*32*, *33*). Our mouse studies validate these data by directly showing

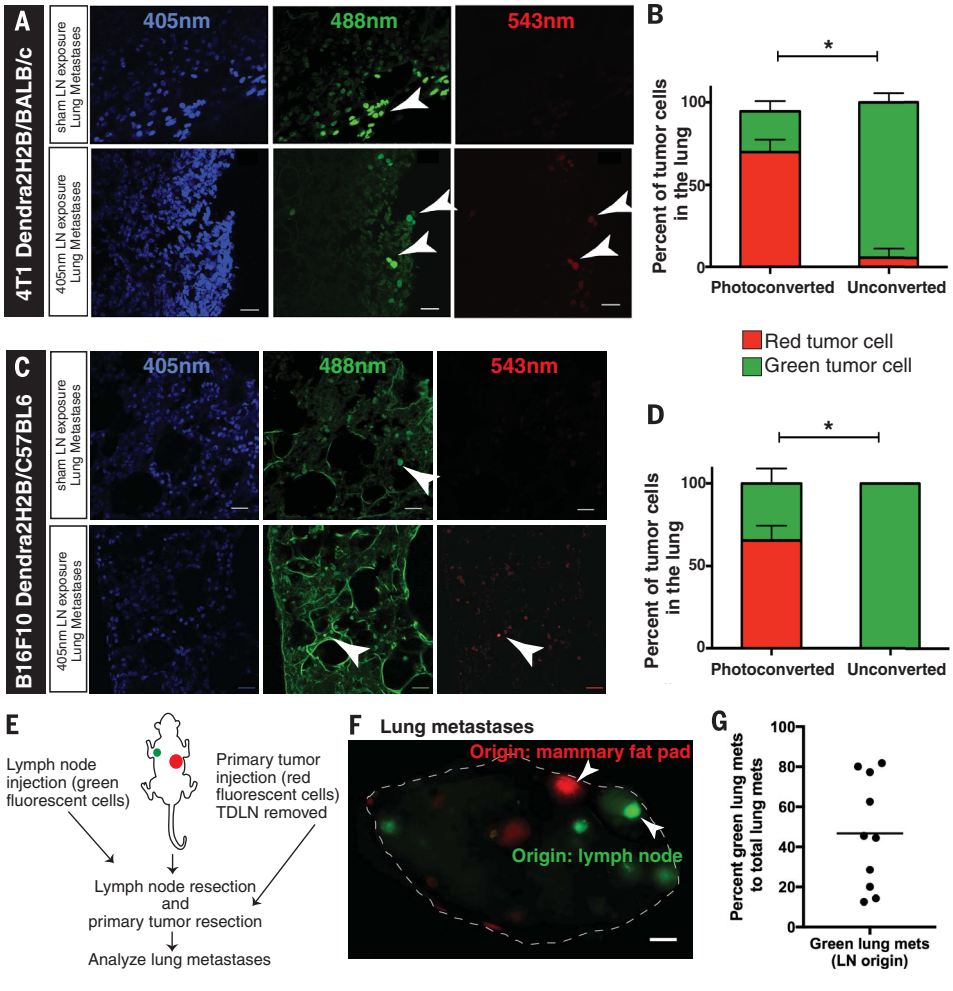

Fig. 2. Metastatic cancer cells in the lymph node can colonize the lung. (**A** and **C**) Sections (100-μm thickness) of fresh frozen lungs were obtained from Dendra2H2B-4T1 and Dendra2H2B-B16F10 tumor-bearing mice that either had their lymph nodes photoconverted with a 405-nm diode or had no photoconversion. The top panels are representative images of micrometastatic cancer cells (arrowheads) in the lung from control animals (no photoconversion), whereas the bottom panels show photoconverted isolated cancer cells that have colonized the lung via the lymph node. Scale bars, 20 μm. (**B** and **D**) Percentage of cancer cells (green, not photoconverted; red, photoconverted) detected in the lungs of Dendra2H2B-4T1 (n = 8) and Dendra2H2B-B16F10 (n = 8) tumor-bearing mice. *P < 0.05 when we compared 405-nm light exposure (photoconverted) to sham light exposure (unconverted) for individual cells lines. Error bars indicate SEM. (**E**) Schematic of experiment to determine whether cancer cells injected directly in the lymph node and in the mammary fat pad (MFP) can both form large metastases in the lungs. TDLN, tumor-draining lymph node. (**F**) Image of a lung with red lesions (originating from the MFP) and green lesions (originating from the lymph node) marked by arrowheads. Scale bar, 1 mm. (**G**) Lung metastases are represented as the percentage of metastatic lesions (mets) of lymph node origin (green) among total macroscopic lesions (red and green) (n = 10 animals). As assessed by a one-sample Student's t test, metastatic lung lesions were shown to have originated from both lymph node and MFP tumors (P < 0.001).

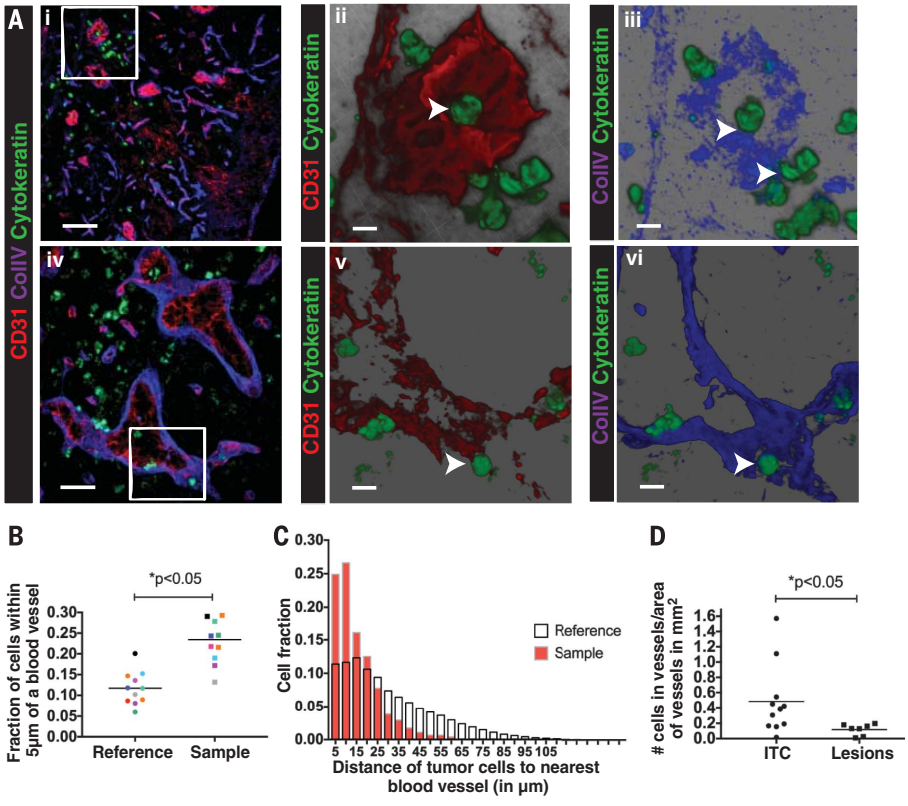

Fig. 3. Cancer cells in the lymph node associate with blood vessels and invade the vascular basement membrane. (**A**) (i and iv) Immunofluorescence staining of metastatic lymph nodes with isolated 4T1 cancer cells (anti-cytokeratin, green), blood vessels (anti-CD31, red), and basement membrane (anti-collagen IV, blue) shows cancer cells associating with blood vessels (ii and v, arrowheads) and the vascular basement membrane (iii and vi, arrowheads). A cancer cell is observed inside a blood vessel (ii and iii) (arrowhead). Scale bars, 50 μm (i); 20 μm (iv); 10 μm (ii, iii, v, and vi). (ii) and (iii) represent zoomed-in views of the boxed area in (i); (v) and (vi) represent zoomed-in views of the boxed area in (iv). (**B**) Quantification of the fraction of cancer cells within 5 μm of a blood vessel (sample) in a lymph node compared with a theoretical random distribution (reference) of the same number of cells in the same lymph node shows cancer cell association with lymph node blood vessels. $n = 11$ individual lymph nodes $^*P < 0.05$. (**C**) Representative histogram of the fraction of cancer cells at varying distances from the nearest blood vessel in a given lymph node with isolated cancer cells (sample) compared with the reference distribution for that lymph node (reference). The measured distribution shows an association of cancer cells with blood vessels in the lymph node. (**D**) Quantification of the fraction of cancer cells inside a blood vessel in lymph nodes containing macro-metastatic lesions (lesions) or isolated tumor cells (ITC).

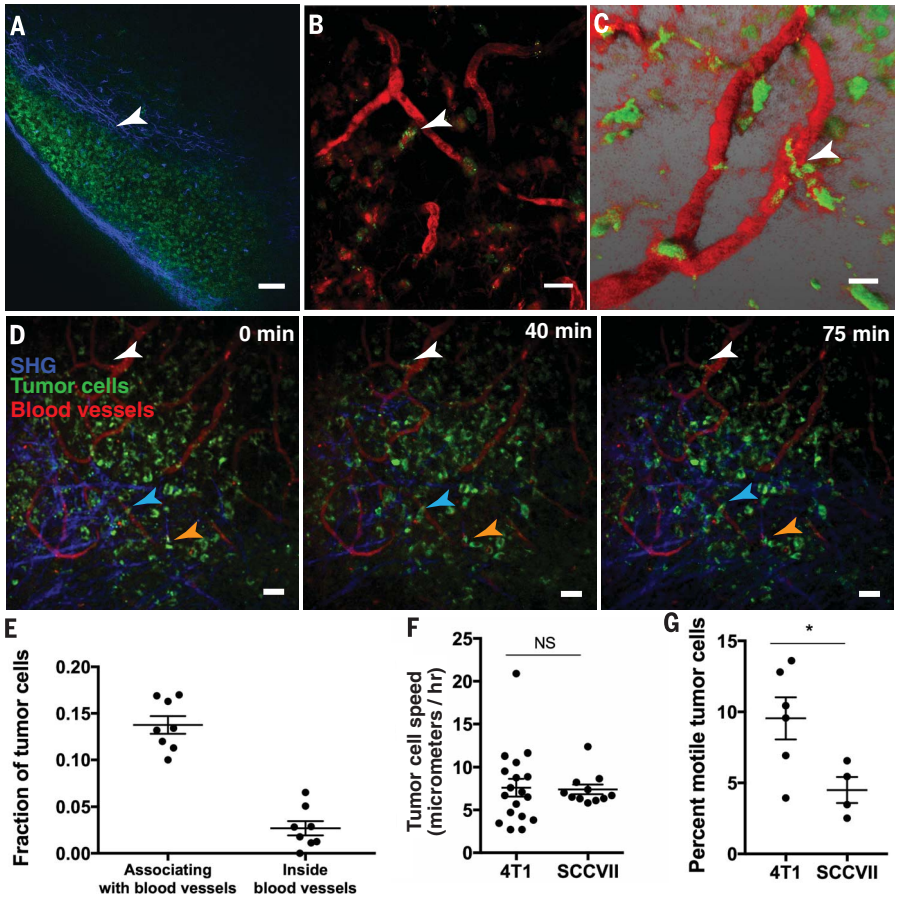

Fig. 4. Time-lapse intravital imaging of lymph node metastasis shows slow cancer cell migration toward blood vessels. (**A**) 4T1-Dendra2–expressing cancer cells (green fluorescence) form a large colony in the subcapsular sinus of the draining lymph node (arrowhead). Scale bar, 60 μm. (**B** and **C**) Cancer cells (green) that invaded the lymph node cortex wrapped around blood vessels (arrowheads), which were labeled by intravenous injection of rhodamine-dextran (red). Images were obtained by multiphoton microscopy at a depth of 80 to 110 μm below the surface of the lymph node. Scale bars, 20 μm. (**D**) Time-lapse intravital imaging of cancer cells (green) in association with blood vessels (red) and collagen fibers [blue, detected by second harmonic generation (SHG)] over the course of 75 min shows slow movement (arrowheads) of some cancer cells toward blood vessels. Images were obtained every 2 min, with a 50-μm z-stack. Scale bar, 50 μm. See also supplementary movies. (**E**) Quantification of the fraction of 4T1 tumor cells per field that associate with blood vessels or were inside blood vessels, analyzed by intravital microscopy in a tumor-draining lymph node. (**F**) Quantification of the speed of individual cancer cells in 4T1 and SCCVII lymph node metastases. (**G**) Quantification of the percentage of motile tumor cells in the image field over 75 min in 4T1 and SCCVII lymph node metastases. Quantification for (E) to (G) was performed on four to six individual mice. NS, not significant; $^*P < 0.05$.

that lymph node metastases can be a source of cancer cells for distant metastases. Our data are similar to results obtained independently by Brown *et al.*, using different methodologies in mouse models (*34*). Additionally, we have revealed that lymph node metastases can disseminate by invading lymph node blood vessels rather than by transiting through efferent lymphatic vessels. Further studies are needed to determine whether dissemination of cancer cells from lymph nodes is a feature of human cancer and, if so, whether it should be a factor in treatment decisions.

REFERENCES AND NOTES

1. I. Jatoi, S. G. Hilsenbeck, G. M. Clark, C. K. Osborne, *J. Clin. Oncol.* **17**, 2334–2340 (1999).
2. K. Kawada, M. M. Taketo, *Cancer Res.* **71**, 1214–1218 (2011).
3. R. L. Ferris, M. T. Lotze, S. P. Leong, D. S. Hoon, D. L. Morton, *Clin. Exp. Metastasis* **29**, 729–736 (2012).
4. M. A. Saksena, A. Saokar, M. G. Harisinghani, *Eur. J. Radiol.* **58**, 367–374 (2006).
5. H. Starz, B.-R. Balda, K.-U. Krämer, H. Büchels, H. Wang, *Cancer* **91**, 2110–2121 (2001).
6. S. D. Nathanson, R. Shah, K. Rosso, *Semin. Cell Dev. Biol.* **38**, 106–116 (2015).
7. E. R. Pereira, D. Jones, K. Jung, T. P. Padera, *Semin. Cell Dev. Biol.* **38**, 98–105 (2015).
8. B. Cady, *Ann. Surg. Oncol.* **14**, 1790–1800 (2007).
9. B. Fisher *et al.*, *N. Engl. J. Med.* **347**, 567–575 (2002).
10. W. S. Halsted, *Ann. Surg.* **46**, 1–19 (1907).
11. N. Cascinelli, A. Morabito, M. Santinami, R. M. MacKie, F. Belli, *Lancet* **351**, 793–796 (1998).
12. S. D. Nathanson, D. Kwon, A. Kapke, S. H. Alford, D. Chitale, *Ann. Surg. Oncol.* **16**, 3396–3405 (2009).
13. Early Breast Cancer Trialists' Collaborative Group (EBCTCG), *Lancet* **366**, 2087–2106 (2005).
14. D. L. Morton *et al.*, *N. Engl. J. Med.* **370**, 599–609 (2014).
15. A. E. Giuliano *et al.*, *JAMA* **305**, 569–575 (2011).
16. V. Galimberti *et al.*, *Lancet Oncol.* **14**, 297–305 (2013).
17. M. Donker *et al.*, *Lancet Oncol.* **15**, 1303–1310 (2014).
18. R. Jagsi *et al.*, *J. Clin. Oncol.* **32**, 3600–3606 (2014).
19. M. B. Faries *et al.*, *N. Engl. J. Med.* **376**, 2211–2222 (2017).
20. P. M. Poortmans *et al.*, *N. Engl. J. Med.* **373**, 317–327 (2015).
21. T. J. Whelan *et al.*, *N. Engl. J. Med.* **373**, 307–316 (2015).
22. B. H. Ly, N. P. Nguyen, V. Vinh-Hung, E. Rapiti, G. Vlastos, *Breast Cancer Res. Treat.* **119**, 537–545 (2010).
23. R. S. Punglia, M. Morrow, E. P. Winer, J. R. Harris, *N. Engl. J. Med.* **356**, 2399–2405 (2007).
24. N. G. Gurskaya *et al.*, *Nat. Biotechnol.* **24**, 461–465 (2006).
25. H. S. Jeong *et al.*, *J. Natl. Cancer Inst.* **107**, djv155 (2015).
26. J. V. Stein, S. F Gonzalez, *J. Allergy Clin. Immunol.* **139**, 12–20 (2017).
27. J. E. Chang, S. J. Turley, *Trends Immunol.* **36**, 30–39 (2015).
28. G. Crile Jr., W. Isbister, S. D. Deodhar, *Cancer* **28**, 657 (1971).
29. D. Kerjaschki *et al.*, *J. Clin. Invest.* **121**, 2000–2012 (2011).
30. J. Ragaz *et al.*, *N. Engl. J. Med.* **337**, 956–962 (1997).
31. M. Overgaard *et al.*, *N. Engl. J. Med.* **337**, 949–955 (1997).
32. D. G. McFadden *et al.*, *Cell* **156**, 1298–1311 (2014).
33. K. Naxerova *et al.*, *Science* **357**, 55–60 (2017).
34. M. Brown *et al.*, *Science* **359**, 1408–1411 (2018).

ACKNOWLEDGMENTS

We thank R. K. Jain for critical discussion, S. Mordecai for assistance with imaging experiments, and K. Piatkevich for assistance with laser diodes. **Funding:** This work was supported by NIH grants DP20D008780, R01CA214913, and R01HL128168 (T.P.P.); National Cancer Institute (NCI) Federal Share/MGH Proton Beam Income-C06CA059267 (T.P.P.); MGH Executive Committee on Research Interim Support Funding (T.P.P.); NIH grant T32 DK007191 (D.K.); Susan G. Komen Foundation Fellowship PDF14301739 (G.S.); a United Negro College Fund–Merck Science Initiative Postdoctoral Fellowship (D.J.); a Burroughs Wellcome Postdoctoral Enrichment Program Award (D.J.); NIH NCI grant F32CA183465 (D.J.); Korean Ministry of Education, Science, and Technology grant NRF-2012R1A1A2040866 (H.-S.J.); Samsung Biomedical Research Institute grant GL1B22912 (H.-S.J.); and NIH grant P01CA080124 (T.P.P.). We thank M. Vangel and Harvard Catalyst, the NIH (award UL1 TR001102), and Harvard University for assistance with biostatistical methods and financial contributions. **Author contributions:** E.R.P., D.K., and T.P.P. conceived and designed experiments. E.R.P., D.K., G.S., O.G., E.F.J.M., D.J., S.-M.C., S.K., E.M.B., and E.B. performed experiments. E.R.P., G.S., O.G., and T.P.P. analyzed data. E.R.P., D.K., G.S., D.J., J.C., H.-S.J., M.C.C., A.G.T., and T.P.P. discussed results and strategy. T.P.P. supervised the study. E.R.P. and T.P.P. wrote the manuscript, which was revised and approved by all authors. **Competing interests:** The authors declare no competing financial interests. **Data and materials availability:** All data are available in the main paper or the supplementary materials.

SUPPLEMENTARY MATERIALS

www.sciencemag.org/content/359/6382/1403/suppl/DC1
Materials and Methods
Figs. S1 to S15
References (*35*–*39*)
Movies S1 to S3

8 November 2016; resubmitted 14 April 2017
Resubmitted 5 October 2017
Accepted 24 January 2018
10.1126/science.aal3622

CANCER

Lymph node blood vessels provide exit routes for metastatic tumor cell dissemination in mice

M. Brown,[1,2]* F. P. Assen,[2] A. Leithner,[2] J. Abe,[3] H. Schachner,[1] G. Asfour,[1] Z. Bago-Horvath,[1] J. V. Stein,[3] P. Uhrin,[4] M. Sixt,[2]*† D. Kerjaschki[1]*†

During metastasis, malignant cells escape the primary tumor, intravasate lymphatic vessels, and reach draining sentinel lymph nodes before they colonize distant organs via the blood circulation. Although lymph node metastasis in cancer patients correlates with poor prognosis, evidence is lacking as to whether and how tumor cells enter the bloodstream via lymph nodes. To investigate this question, we delivered carcinoma cells into the lymph nodes of mice by microinfusing the cells into afferent lymphatic vessels. We found that tumor cells rapidly infiltrated the lymph node parenchyma, invaded blood vessels, and seeded lung metastases without involvement of the thoracic duct. These results suggest that the lymph node blood vessels can serve as an exit route for systemic dissemination of cancer cells in experimental mouse models. Whether this form of tumor cell spreading occurs in cancer patients remains to be determined.

Lymph nodes (LNs) are central trafficking hubs for recirculating immune cells (*1*). Conceivably, tumor cells could use this gateway function of LNs for metastatic colonization of peripheral organs (*2*). Although this route of tumor dissemination is supported by correlative evidence from mouse models (*3*–*5*) and patients (*6*–*17*), a causal link between LN colonization (*18*–*21*) and peripheral metastasis has not been established (*22*). A scenario in which LNs act as gateways to systemic dissemination raises the question of whether tumor cells reach the blood circulation via efferent lymphatic vessels, via LNs of higher echelons and the thoracic duct, or directly via the LN blood vasculature.

To investigate this question, we used intralymphatic microinfusion (*23*) to directly deposit defined numbers of murine 4T1 mammary carcinoma cells into the subcapsular sinus of popliteal LNs of mice (fig. S1A). These experimental LN metastases (ELMs) allow precise analysis of the earliest steps in the development of LN and successive pulmonary metastases in the absence of a primary tumor. Microinfusion was carefully adjusted to preserve the delicate microarchitecture of the LN. It did not affect the physiological solute filter function of the LN stromal backbone (fig. S1, B and C), and it did not alter the conventional migratory paths of infused leukocytes (fig. S6, B and C) (*1*). Infused particles did not leak into the downstream medial iliac LN or into the lung (fig. S1, D and E).

[1]Clinical Institute of Pathology, Medical University of Vienna, 1090 Vienna, Austria. [2]Institute of Science and Technology Austria (IST Austria), 3400 Klosterneuburg, Austria. [3]Theodor Kocher Institute, University of Bern, 3012 Bern, Switzerland. [4]Institute of Vascular Biology, Medical University of Vienna, 1090 Vienna, Austria.
*These authors contributed equally to this work.
†Corresponding author. Email: dontscho.kerjaschki@meduniwien.ac.at (D.K.); michael.sixt@ist.ac.at (M.S.)

LNs harvested immediately after intralymphatic infusion with 4T1 tumor cells revealed that these cells initially accumulated in the subcapsular sinus (Fig. 1A and fig. S1F). Within 1 day, tumor cells crossed the floor of the subcapsular sinus, and during the following 3 days, they progressed along the LN stromal network toward the center of the LN (Fig. 1 and fig. S1G). A comparison with tumor-bearing sentinel LN samples from human breast cancer patients (fig. S1H) shows that the histological picture of ELMs closely resembles human pathology. Invasiveness of mammary carcinoma has been linked to the expression of basal cell marker molecules (*24*), such as p63 and cytokeratin 14 (CK14). Because tumor cells arriving in the avascular subcapsular sinus need rapid access to the parenchymal blood supply for survival, we hypothesized that upon intralymphatic infusion the tumor cells would show early up-regulation of invasion markers. Indeed, 2 days after infusion, CK14 expression in the 4T1 tumor cells was substantially increased in comparison with expression in orthotopically injected or cultured 4T1 cells (fig. S1, I and J). At 3 days after infusion, when tumor cells had infiltrated the deep LN parenchyma, the average CK14 levels had renormalized and the remaining CK14-expressing cells preferentially localized to the invasive margins of the ELM (fig. S1, K and L). Together, these data indicate that ELMs are a valid model of LN metastasis.

Invading 4T1 tumor cells were found in close proximity and in direct contact with blood vessels 2 days after infusion (Fig. 2A and movie S1). On day 3, the cells had wrapped around (movie S2) and intravasated (Fig. 2, B to D, and fig. S2, A to C) the blood vessel lumen. This association between tumor cells and blood vessels was not due to local induction of angiogenesis, as we found similar vessel densities within and outside infiltrated areas (fig. S2D). The LN blood vasculature is characterized by special postcapillary segments termed "high endothelial venules" (HEVs), which serve as entry ports for incoming lymphocytes (*1*). Two- and three-dimensional morphometrical analyses of ELM specimens showed that upon their progression toward the LN center, tumor cells gradually became associated with HEVs and frequently localized in their lumen (Fig. 2, C to E; fig. S2, E and F; and movies S3 to S6). These data indicate that HEVs are the main exit route by which tumor cells gain access to the blood circulation. Similar tumor cell–blood vessel associations and intravasations were observed in samples of LN micrometastases from human breast cancer patients (fig. S2G). Furthermore, in ex vivo adhesion assays (fig. S2H) in which 4T1 cells were incubated on slices of native mouse LNs, we likewise observed colocalization of tumor cells and blood vessels (fig. S2I).

To explore whether the associations between tumor cells and LN blood vessels correlate with the formation of systemic metastasis, we intralymphatically infused mice with mCherry- and luciferase-expressing (mCherry$^+$ luciferase$^+$) 4T1 cells and then performed whole-animal in vivo bioluminescence imaging. Genetic labeling with fluorescent proteins and firefly luciferase did not alter tumor cell proliferation or migration (fig. S3). As late as 35 days after intralymphatic infusion with the tumor cells, the lung was the only organ showing macrometastasis (Fig. 3A and fig. S4A). This metastatic seeding pattern was similar to that seen when 4T1 tumor cells were orthotopically injected into syngeneic mice (fig. S4B) and to that seen when MDA-MB-231 human mammary carcinoma cells were intralymphatically infused into immunodeficient mice (fig. S4C). Bioluminescence imaging of isolated lungs (Fig. 3B and fig. S4D) showed luciferase-expressing multifocal metastases 11 and 21 days after intralymphatic infusion with 4T1 tumor cells, and microscopic examination revealed tumor cell clusters as early as 6 and 11 days after infusion (fig. S4, E and F). These data demonstrate that ELMs rapidly disseminate to peripheral tissues.

To determine the earliest time point at which tumor cells colonized the lungs, we intralymphatically infused luciferase$^+$ mCherry$^+$ 4T1 cells into LNs and removed the LNs after 2 or 3 days (Fig. 3C and fig. S4G). The 2-day versus 3-day treatment groups were examined 11 days after infusion. In the 3-day cohort, 33.3% of the mice displayed lung metastases, whereas none were detected in the 2-day cohort (Fig. 3D and fig. S4H). These results supported our finding that tumor cells invaded LN blood vessels 3 days after intralymphatic infusion (Fig. 2, B to E, and fig. S2, A to F). Accordingly, using flow cytometry (FC), we detected circulating tumor cells in the blood as early as 3 days after intralymphatic infusion with fluorescent 4T1 cells (Fig. 3, E and F).

These results were at odds with the conventional view that tumor spreading from LNs occurs via passage through efferent lymphatic vessels, LNs of higher echelons, the thoracic duct, and the subclavian vein (*25*). Hence, we used quantitative

FC to determine the tumor cell seeding kinetics of mCherry$^+$ 4T1 ELMs into lungs versus into medial iliac LNs, which drain the ELM-bearing popliteal LN (Fig. 3G and fig. S5, A to C). We found that tumor cell numbers in medial iliac LNs did not predict lung metastatic burden (fig. S5C). At 3 days after infusion, when metastatic tumor cells were detected in the lungs of 80% of all infused mice, medial iliac LNs were invariably free of tumor cells. All medial iliac LNs became colonized only after 28 days (fig. S5D). ELMs with the mCherry-expressing mouse colon carcinoma cell line CT26 revealed similar results (fig. S5, E to H): 12 days after infusion, CT26 cells had disseminated into the lungs in 83%

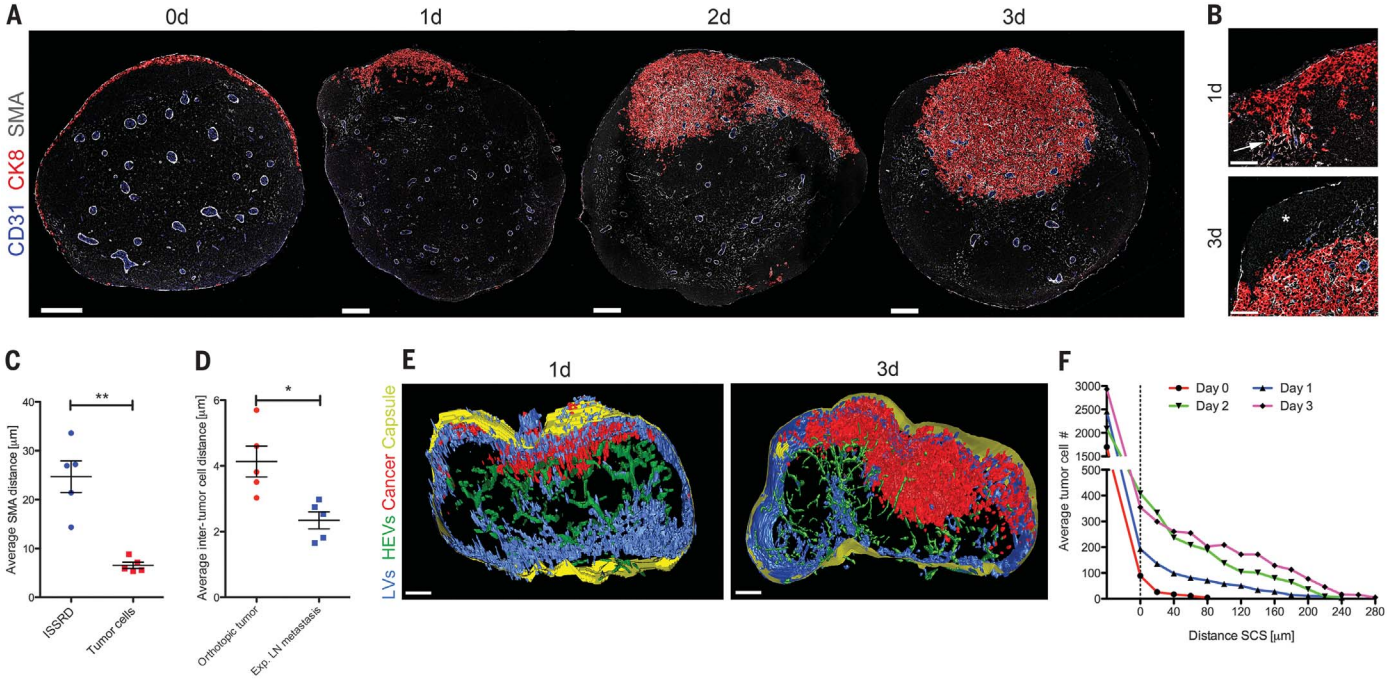

Fig. 1. Intralymphatically infused 4T1 mammary carcinoma cells invade the LNs. (**A**) Immunofluorescence of 4T1 ELMs 0, 1, 2, and 3 days after intralymphatic infusion. Red, cytokeratin 8 (CK8); blue, CD31; gray, smooth muscle actin (SMA). Scale bars, 200 µm. n = 5 ELMs. d, day. (**B**) Zoom-in of images from (A) for 1 day (top) and 3 days (bottom) after intralymphatic infusion showing the SMA$^+$ fibroblastic reticular cell network (arrow) and B cell follicles (asterisk). Scale bars, 100 µm. (**C**) Distances (means ± SEM) of tumor cells and in silico–simulated equally distributed isosurfaces (ISSRD) from the SMA$^+$ fibroblastic reticular cell network in sections of 4T1 ELMs 3 days after infusion. n = 5 ELMs (paired, two-tailed t test). (**D**) Distances (means ± SEM) between tumor cells of 4T1 tumors 3 days after orthotopic transplantation of tumor spheroids or intralymphatic infusion of tumor cell suspensions. n = 5 experimental tumor samples (unpaired, two-tailed t test). Significance: $^*P \le 0.05$; $^{**}P \le 0.01$. (**E**) Representative segmentations of 200-µm sections in light sheet fluorescence microscopy images showing LNs at 1 and 3 days after infusion with mCherry$^+$ 4T1 tumor cells. Red, mCherry$^+$ tumor cells; yellow, autofluorescent capsule; green, peripheral node adressin (PNAd)–positive HEVs; cyan, Prox1$^+$ LN sinuses. Scale bars, 200 µm. n = 5 sections. (**F**) Average 4T1 tumor cell numbers at the indicated distances from the subcapsular sinus (SCS) 0, 1, 2, and 3 days after intralymphatic infusion. Dotted line, sinus border or floor. n = 5 ELMs.

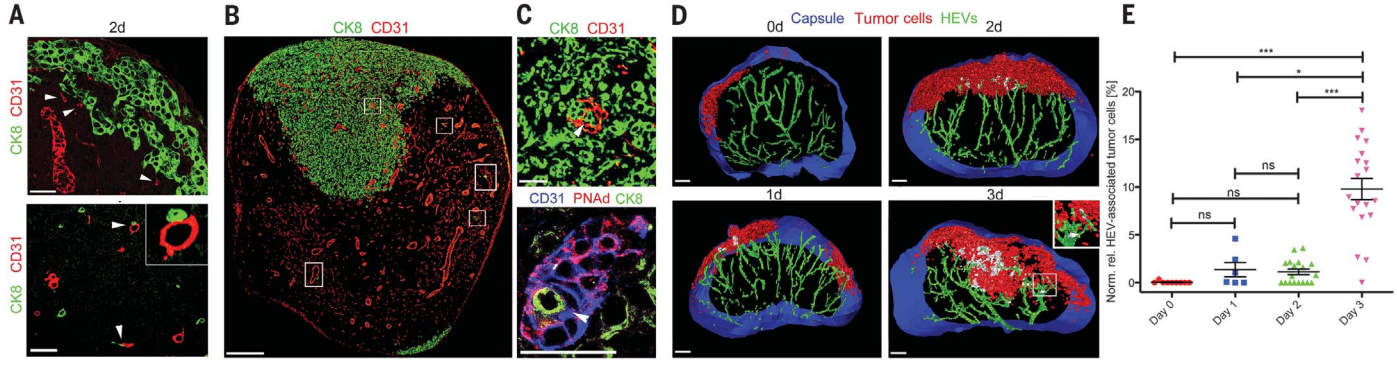

Fig. 2. 4T1 Tumor cells associate with and intravasate LN blood vessels. (**A**) Immunofluorescence 2 days after intralymphatic infusion with 4T1 tumor cells. Arrowheads indicate CD31$^+$ blood vessels. The inset is a zoom-in showing tumor cell–blood vessel interaction. Scale bars, 50 µm. n = 5 ELMs. (**B**) Image of 4T1 ELMs 3 days after infusion. Scale bar, 300 µm. n = 5 ELMs. (**C**) Zoom-in and serial section of a representative boxed area of (B). (Top) Tumor cell (arrowhead) in blood vessel lumen. (Bottom) Tumor cell (arrowhead) in HEV lumen. Scale bars, 50 µm. (**D**) Representative segmentations of 200-µm sections in light sheet fluorescence microscopy images showing 4T1 ELMs 0, 1, 2, and 3 days after infusion. Red, mCherry$^+$ tumor cells; blue, autofluorescent capsule; green, PNAd$^+$ HEVs. Tumor cell–HEV interactions are marked in white. Scale bars, 100 µm. n = 5 ELMs. (**E**) Tumor cell associations with HEVs [means ± SEM, normalized relative (norm. rel.) to tumor cell density] 0, 1, 2, and 3 days after infusion. Significance: $^*P \le 0.05$; $^{***}P \le 0.001$; ns, $P > 0.05$ ($n \ge 6$ ELMs; Kruskal-Wallis test).

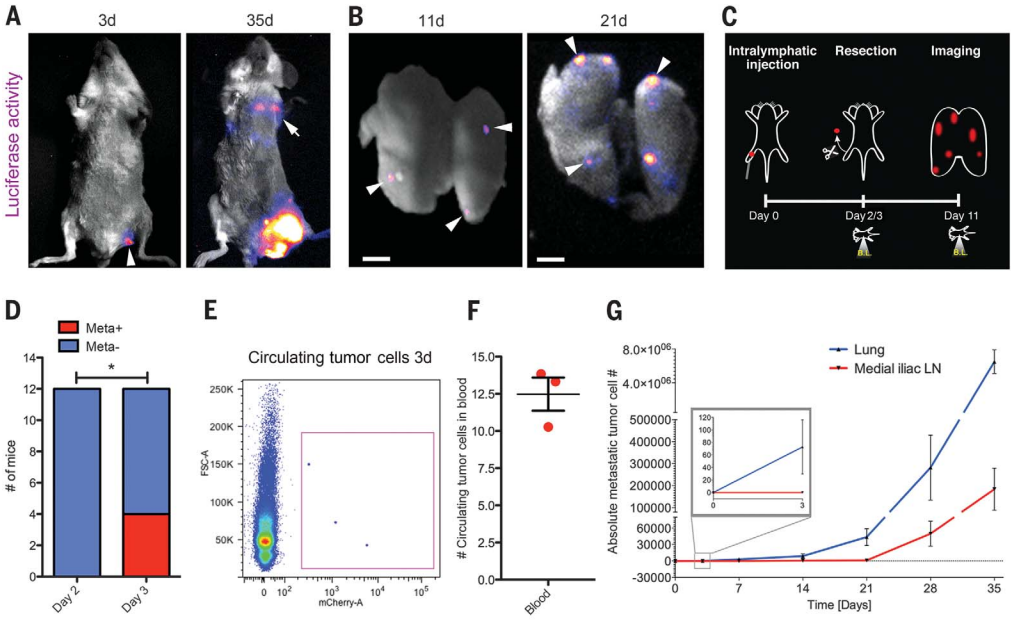

Fig. 3. ELMs seed lung metastases independently of the thoracic duct. (**A** and **B**) Bioluminescence after intralymphatic infusion with mCherry$^+$ luciferase$^+$ 4T1 tumor cells. (A) Popliteal fossa (arrowhead) and lung (arrow) 3 and 35 days after infusion. n = 12 mice. (B) Lung metastases (arrowheads) 11 and 21 days after infusion. Scale bars, 4 mm. n = 5 mice. (**C**) Experimental design. At 0 days, mCherry$^+$ luciferase$^+$ 4T1 tumor cells were infused (red). At 2 and 3 days, in vivo bioluminescence confirmed tumor growth, and ELMs were resected thereafter. At 11 days, lungs analyzed by in vivo bioluminescence were harvested for ex vivo analysis. (**D**) Quantitation of metastasis-positive (Meta$^+$) and metastasis-negative (Meta$^-$) lungs of mice with ELMs represented in (C). n = 12 mice (*$P \leq$ 0.05; two-sided, chi-square test). (**E**) FC analysis of circulating mCherry$^+$ 4T1 tumor cells pooled from five mice 3 days after infusion. x axis, mCherry fluorescence intensity; y axis, forward scatter (FSC). n = 3 pooled samples. (**F**) Average absolute circulating tumor cell numbers ± SEM in FC analyses 3 days after infusion with mCherry$^+$ 4T1 tumor cells. Blood was pooled from five mice per experiment, and values were normalized to those for control mice. n = 3 pooled samples. (**G**) Kinetics of average absolute mCherry$^+$ 4T1 tumor cell numbers ± SEM in FC analyses of medial iliac LNs and lungs over the 35-day time course after infusion. Tumor cell numbers were normalized to those for control mice. $n \geq 5$ mice.

of the mice, whereas only 17% of mice showed evidence of tumor cells in medial iliac LNs. Together, these results indicate that early peripheral dissemination of ELMs is unlikely to occur via efferent lymphatics. To experimentally prevent passage via the efferent lymphatics, we surgically ligated the efferent lymphatic vessel before intralymphatic infusion with mCherry$^+$ luciferase$^+$ 4T1 tumor cells (fig. S6D). Complete blockade of the efferent lymphatic vessel was confirmed by the inability of an intralymphatically injected dye to reach the downstream medial iliac LN (fig. S6A), as well as the inability of intralymphatically injected T cells to recirculate into the spleen (fig. S6, B and C). We found that lymphatic ligation did not compromise the ability of 4T1 tumor cells to seed lung metastasis within 3 days after infusion (fig. S6, E and F). On the basis of these results, we conclude that in our experimental mouse model, LN blood vessels are a gateway for the early transit of nodal tumor cells into the systemic circulation.

Our experimental setup establishes the contribution of an ELM to peripheral metastasis in the absence of a primary tumor. However, there is substantial evidence that the metastatic process is preceded by adaptations both within the tumor and within the host microenvironment (*8*, *9*, *20*, *22*, *26*), which are both bypassed in the ELM model. To model the premetastatic conditions in the host, we implanted mice with a peripheral tumor by inoculating unlabeled 4T1 tumor cells into the lateral tarsal zone above the ankle (fig. S7A). After 8 days of priming, ELMs were induced by intralymphatic infusion with mCherry$^+$ luciferase$^+$ 4T1 tumor cells (fig. S7, B and C). These experiments revealed that ELMs in LNs that were previously primed by a peripheral tumor seeded lung metastasis at a frequency similar to that for ELMs in naïve LNs (fig. S7, D and E). Under primed conditions, metastatic dissemination was equally independent of the thoracic duct passage as under unprimed conditions (fig. S7, D and E). To mimic possible adaptations of the tumor cells (*27*, *28*), we allowed orthotopically induced mCherry$^+$ luciferase$^+$ 4T1 tumors to colonize draining LNs. We recovered tumor cells from these LNs, briefly recultured them, and reinfused them into popliteal LNs of new host animals (fig. S7F). Under these conditions, 83.3% of infused animals developed lung metastases, and this was again independent of the thoracic duct passage (fig. S7, G and H). Collectively, these results demonstrate that the direct metastatic dissemination via the LN blood vasculature is not artificially induced by intralymphatic injection of naïve tumor cells into unprimed LN environments.

We have established a mouse model of sentinel LN metastasis that allows the analysis of early metastatic pathways via the LN. We discovered that early tumor cell attachment to and invasion into the LN blood vasculature coincided with the appearance of circulating tumor cells and the successful metastatic colonization of the lung. Our experimental model revealed that LN blood vessels are effective gateways from lymphatics into the systemic circulation and that this pathway may be more efficient than direct metastatic dissemination from the primary tumor (fig. S8). Our data are similar to results obtained independently by Pereira *et al.* using different methodologies with mouse models (*29*). Though our investigations in a reductionist mouse model support the view that LNs are active hubs for systemic tumor cell spreading, future clinical and experimental studies are required to determine whether these findings are relevant to human cancer.

REFERENCES AND NOTES

1. J.-P. Girard, C. Moussion, R. Förster, *Nat. Rev. Immunol.* **12**, 762–773 (2012).
2. S. Hellman, *J. Clin. Oncol.* **12**, 2229–2234 (1994).
3. N. Roberts *et al.*, *Cancer Res.* **66**, 2650–2657 (2006).
4. J. B. Burton *et al.*, *Cancer Res.* **68**, 7828–7837 (2008).
5. Z. Chen *et al.*, *Cancer Res.* **65**, 9004–9011 (2005).
6. S. D. Nathanson, D. Kwon, A. Kapke, S. H. Alford, D. Chitale, *Ann. Surg. Oncol.* **16**, 3396–3405 (2009).
7. I. Jatoi, S. G. Hilsenbeck, G. M. Clark, C. K. Osborne, *J. Clin. Oncol.* **17**, 2334–2340 (1999).
8. S. Podgrabinska, M. Skobe, *Microvasc. Res.* **95**, 46–52 (2014).
9. K. Alitalo, *Nat. Med.* **17**, 1371–1380 (2011).
10. R. A. Mohammed *et al.*, *Am. J. Surg. Pathol.* **31**, 1825–1833 (2007).
11. J. Ragaz *et al.*, *N. Engl. J. Med.* **337**, 956–962 (1997).
12. Early Breast Cancer Trialists' Collaborative Group (EBCTCG), *Lancet* **366**, 2087–2106 (2005).
13. M. Overgaard *et al.*, *N. Engl. J. Med.* **337**, 949–955 (1997).
14. EBCTCG, *Lancet* **378**, 1707–1716 (2011).
15. T. J. Whelan *et al.*, *N. Engl. J. Med.* **373**, 307–316 (2015).
16. P. M. Poortmans *et al.*, *N. Engl. J. Med.* **373**, 317–327 (2015).
17. K. Naxerova *et al.*, *Science* **357**, 55–60 (2017).
18. K. Kawada, M. M. Taketo, *Cancer Res.* **71**, 1214–1218 (2011).
19. C. L. Chaffer, R. A. Weinberg, *Science* **331**, 1559–1564 (2011).
20. S. D. Nathanson, R. Shah, K. Rosso, *Semin. Cell Dev. Biol.* **38**, 106–116 (2015).
21. R. R. Turner, D. W. Ollila, D. L. Krasne, A. E. Giuliano, *Ann. Surg.* **226**, 271–278 (1997).
22. A. Alitalo, M. Detmar, *Oncogene* **31**, 4499–4508 (2012).
23. A. Braun *et al.*, *Nat. Immunol.* **12**, 879–887 (2011).
24. K. J. Cheung, E. Gabrielson, Z. Werb, A. J. Ewald, *Cell* **155**, 1639–1651 (2013).

25. J. I. Burn, A. L. Watne, G. E. Moore, *Br. J. Cancer* **16**, 608–615 (1962).
26. G. G. Van den Eynden *et al*., *Clin. Cancer Res.* **13**, 5391–5397 (2007).
27. S. Das *et al*., *J. Exp. Med.* **210**, 1509–1528 (2013).
28. A. Müller *et al*., *Nature* **410**, 50–56 (2001).
29. E. R. Pereira *et al*., *Science* **359**, 1403–1407 (2018).

ACKNOWLEDGMENTS

We thank C. Moussion for establishing the intralymphatic injection at IST Austria and for providing anti-PNAd hybridoma supernatant, R. Förster and A. Braun for sharing the intralymphatic injection technology, K. Vaahtomeri for the lentiviral constructs, M. Hons for establishing in vivo multiphoton imaging, the Sixt lab for intellectual input, M. Schunn for help with the design of the in vivo experiments, F. Langer for technical assistance with the in vivo experiments, the bioimaging facility of IST Austria for support, and R. Efferl for providing the CT26 cell line. **Funding:** M.B. was supported by the Cell Communication in Health and Disease graduate study program of the Austrian Science Fund (FWF) and the Medical University of Vienna. M.S. was supported by the European Research Council (grant ERC GA 281556) and an FWF START award. **Author contributions:** M.B., D.K., and M.S. conceived of the project and wrote the manuscript. M.B. was involved in planning and performing all experiments. F.P.A. performed the dextran, the LN priming, and the polymerase chain reaction (PCR) array profiling experiments and prepared manuscript figures. A.L. performed the leukocyte recirculation and PCR array profiling experiments. Z.B.-H. provided tissue samples. H.S. and G.A. performed the embedding, sectioning, and immunostaining of tissues. J.A. and J.V.S. performed the light sheet microscopy imaging. P.U. helped design the in vivo experiments. **Competing interests:** None declared. **Data and materials availability:** All data needed to evaluate the conclusions in the paper are present in the paper and/or the supplementary materials.

SUPPLEMENTARY MATERIALS

www.sciencemag.org/content/359/6382/1408/suppl/DC1
Materials and Methods
Figs. S1 to S8
References (*30, 31*)
Movies S1 to S6

8 November 2016; resubmitted 17 April 2017
Resubmitted 19 October 2017
Accepted 2 February 2018
10.1126/science.aal3662

BIOCHEMISTRY

The biosynthesis of methanobactin

Grace E. Kenney,[1] Laura M. K. Dassama,[1] Maria-Eirini Pandelia,[2] Anthony S. Gizzi,[3] Ryan J. Martinie,[4] Peng Gao,[1] Caroline J. DeHart,[1] Luis F. Schachner,[1] Owen S. Skinner,[1] Soo Y. Ro,[1] Xiao Zhu,[1] Monica Sadek,[1] Paul M. Thomas,[1] Steven C. Almo,[3] J. Martin Bollinger Jr.,[4] Carsten Krebs,[4] Neil L. Kelleher,[1] Amy C. Rosenzweig[1]*

Metal homeostasis poses a major challenge to microbes, which must acquire scarce elements for core metabolic processes. Methanobactin, an extensively modified copper-chelating peptide, was one of the earliest natural products shown to enable microbial acquisition of a metal other than iron. We describe the core biosynthetic machinery responsible for the characteristic posttranslational modifications that grant methanobactin its specificity and affinity for copper. A heterodimer comprising MbnB, a DUF692 family iron enzyme, and MbnC, a protein from a previously unknown family, performs a dioxygen-dependent four-electron oxidation of the precursor peptide (MbnA) to install an oxazolone and an adjacent thioamide, the characteristic methanobactin bidentate copper ligands. MbnB and MbnC homologs are encoded together and separately in many bacterial genomes, suggesting functions beyond their roles in methanobactin biosynthesis.

Metals are necessary for many biological processes, and strategies to facilitate their acquisition have evolved across the domains of life. Metal scarcity presents a particular challenge, whether due to low environmental levels of soluble metals or metal-limiting conditions imposed by other organisms (*1*, *2*). Iron acquisition, particularly by pathogenic bacteria in environments where iron is sequestered by the host, is the canonical example of high-affinity metal uptake in low-metal environments (*3*). Instead of relying on passive import of scarce Fe(II), bacteria secrete natural products known as siderophores to bind Fe(III) sequestered in insoluble iron oxides or in host proteins; the Fe(III)-siderophore complex is then imported, and the iron is made available to the organism. In addition, some of these compounds play additional roles in metal regulation and protection from toxicity of metals other than iron (*4*). There is increasing evidence for the existence of similar processes for other metals. Staphylopine, recently discovered in *Staphylococcus aureus*, is involved in the import of a range of divalent metals (*5*), and nickelophores [ranging from simple amino acids (*6*) to more complex organic molecules (*7*)] are thought to be present in both *S. aureus* and *Helicobacter pylori*. Yersiniabactin has been shown to bind copper as well as iron (*8*). Similarly, despite iron-responsive regulation, delftibactin binds gold (*9*), and further reexamination of other siderophores suggests that many have roles as non-iron metallophores (*10*). Some of the first identified non-iron metallophores belong to the family of copper-binding compounds known as methanobactins (Mbns) (*11*).

Mbns were initially discovered in obligate methanotrophs (*12*), which oxidize their sole carbon source, methane, using the copper-dependent particulate methane monooxygenase or, when starved for copper, the iron-dependent soluble methane monooxygenase. Under copper-limiting conditions, methanotrophs also produce and secrete Mbns, peptidic compounds that chelate Cu(I) directly or Cu(II) via a reductive process with an unknown mechanism, resulting in Cu(I)Mbn. The high affinity and specificity of Mbns for Cu(I) is conferred by a pair of bidentate ligands, each comprising a nitrogen heterocycle (most commonly an oxazolone ring) and an adjacent thioamide or enethiol, which chelate the metal in a distorted tetrahedral geometry (Fig. 1A and fig. S1) (*11*).

Operons encoding the biosynthetic machinery for Mbns, first identified and shown to be copper-regulated in the methanotroph *Methylosinus* (*Ms.*) *trichosporium* OB3b (*13*, *14*), are present in a range of methanotrophic and nonmethanotrophic bacteria (Fig. 1, A and B) (*11*, *15*). The gene encoding the precursor peptide (MbnA) was recognized because the predicted C-terminal amino acid sequence corresponds to the peptidic Mbn backbone (*13*). Disruption of this gene abolishes Mbn production (*16*), providing evidence that Mbns are ribosomally produced, posttranslationally modified natural products (RiPPs), a class that also includes microcins, lasso peptides, lanthipeptides, thiopeptides, and pyrroloquinoline quinone (*15*, *17*). Like the precursor peptides in most other RiPP families, MbnAs consist of an N-terminal leader peptide, which is cleaved in the final natural product, and a C-terminal core peptide, to which posttranslational modifications are directed (Fig. 1C).

The locations of oxazolone rings and their neighboring thioamide groups in the peptidic backbones of mature Mbns indicate that these groups are installed at cysteine residues (*15*). Bioinformatic analysis of all MbnA sequences reveals that the modified cysteines are part of conserved motifs, wherein the cysteine is followed by a small, typically hydrophobic residue (usually glycine or alanine, but occasionally serine) and then by a larger, more frequently hydrophilic residue (primarily serine and threonine) (Fig. 1C). In *Ms. trichosporium* OB3b MbnA, there are two modification sites, at Cys^{21} and Cys^{27} (residue numbering from the full-length peptide). Notably, Mbn operons lack genes associated with oxazolone or thioamide biosynthesis, indicating that the pathway(s) for their generation in Mbns must be biochemically distinct from nonenzymatic oxazolone biosynthesis in jadomycins (*18*) and the unrelated microbial enzymatic thioamide formation pathways for closthioamide, thioviridamide, and methyl coenzyme M reductase (*19*–*21*).

Mbn operons, which vary in the composition and arrangement of their genes, have been divided into five major groups on the basis of their content as well as sequence-based phylogenetic analyses of three core components present in all operons (Fig. 1B and fig. S2). Also present are genes encoding proteins with predicted or, in some cases, experimentally established roles in regulation, transport, and secondary posttranslational modifications (Fig. 1B and fig. S2) (*15*). Of particular interest are two genes encoding uncharacterized proteins designated MbnB and MbnC. These proteins are encoded within every Mbn operon identified to date, along with the precursor peptide MbnA, and we previously proposed (*15*) that they are responsible for the posttranslational modifications of MbnA that form the copper-binding ligands of Mbns. For the structurally characterized Mbns (and most predicted Mbns), there are two heterocycle-thioamide moieties in the final compound (fig. S1) (*13*, *22*–*24*). The second heterocycle is uniformly an oxazolone; the identity of the first varies, but it is predicted that all originate from oxazolone precursors (*15*). Formation of each oxazolone-thioamide moiety requires a net four-electron oxidation. The responsible enzymes would thus be expected to contain a redox cofactor.

MbnBs are members of the uncharacterized DUF692 subfamily (Fig. 2A). Although these proteins are distantly related to characterized members of the TIM barrel family 15, including divalent metal-dependent enzymes such as xylose isomerase and endonuclease IV (*25*), no DUF692 family member has been functionally characterized, despite their presence in a wide range of Gram-positive and Gram-negative bacteria. An unpublished crystal structure (PDB: 3BWW) of one family member from *Haemophilus* (*Hs.*) *somnus* 129Pt revealed a diiron cluster at the center of the TIM barrel fold, with ligands corresponding to two of the three metal-binding sites observed in endonuclease IV enzymes. Two of the three ligands required for the third endonuclease IV metal binding site are present in the sequence of the *Hs. somnus* 129Pt protein but were disordered in the structure. The metal-binding residues observed in the *Hs. somnus* 129Pt structure are strictly conserved throughout the DUF692 family, including MbnBs, and a plausible structure for *Ms. trichosporium* OB3b MbnB was generated

[1]Department of Molecular Biosciences and Department of Chemistry, Northwestern University, Evanston, IL 60208, USA. [2]Department of Biochemistry, Brandeis University, Waltham, MA 02453, USA. [3]Department of Biochemistry, Albert Einstein College of Medicine, Bronx, NY 10461, USA. [4]Department of Chemistry and Department of Biochemistry and Molecular Biology, The Pennsylvania State University, University Park, PA 16802, USA.
*Corresponding author. Email: amyr@northwestern.edu

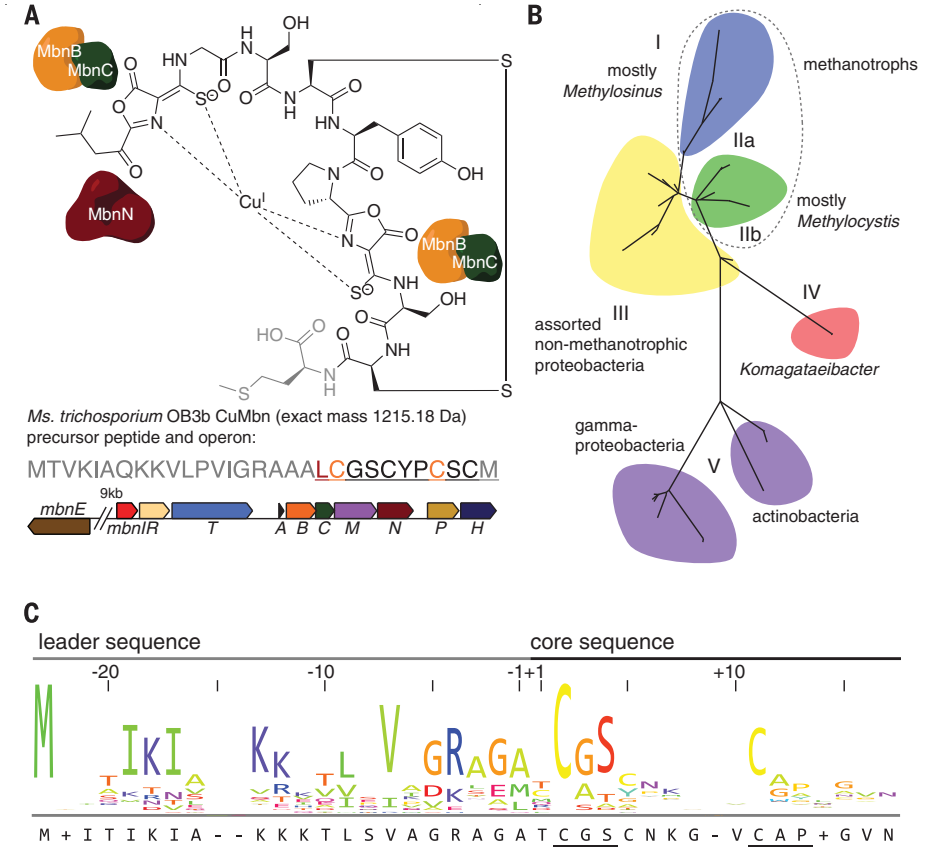

Fig. 1. Mbn structure, operon organization, phylogeny, and precursor peptide sequence. (**A**) Structure of CuMbn from *Ms. trichosporium* OB3b (top); sequence of the MbnA precursor peptide (middle) and Mbn operon (bottom) from that species. The operon includes genes related to import (the periplasmic binding protein MbnE and the TonB-dependent transporter MbnT), export (the MATE multidrug exporter MbnM), regulation (the sigma/anti-sigma factor pair MbnIR), biosynthesis (the precursor peptide MbnA, the hypothetical proteins MbnB and MbnC, and the aminotransferase MbnN), and two genes of unknown function (MbnP and MbnH). Color coding of the genes in the operon indicates previously proposed roles: MbnB (orange) and MbnC (green) are responsible for modifying the two orange cysteines in the peptide to form oxazolone-thioamide pairs in the final natural product, whereas MbnN (dark red) is responsible for a transamination reaction at the leucine (dark red) in the peptide and the final natural product. The final methionine, depicted in gray, is sometimes missing from the compound. (**B**) Phylogenetic tree for Mbn operons. All Mbn operons contain *mbnA*, *mbnB*, and *mbnC* genes, and phylogenetic analyses of all three genes support the subgroups illustrated here. (**C**) MbnA sequence logo, illustrating the leader and core peptide sequences and the conserved cysteine modification motifs. Amino acid abbreviations: A, Ala; C, Cys; D, Asp; E, Glu; F, Phe; G, Gly; H, His; I, Ile; K, Lys; L, Leu; M, Met; N, Asn; P, Pro; Q, Gln; R, Arg; S, Ser; T, Thr; V, Val; W, Trp; Y, Tyr.

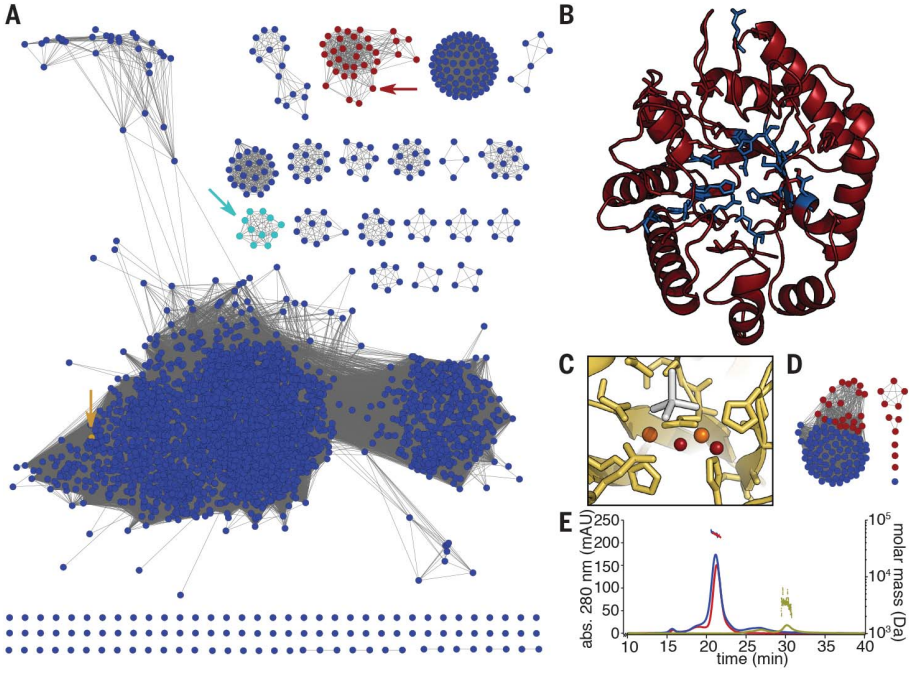

Fig. 2. Bioinformatic and biochemical analyses of the MbnBC heterodimer. (**A**) Sequence similarity network for the DUF692 family. MbnBs are depicted in red, MbnXs (found only in the fifth Mbn subgroup) are in teal, and the structurally characterized *Hs. somnus* 129Pt protein sequence (PDB: 3BWW) is in yellow. Arrows indicate the location of the relevant nodes. (**B**) The predicted structure of *Ms. trichosporium* OB3b MbnB (red), as modeled against 3BWW using iTasser (RMSD, 4.2 ± 2.8 Å). Residues in blue are strictly conserved in MbnBs. (**C**) Diiron site as observed in the 3BWW structure (yellow). All amino acids coordinating the two irons (orange) are strictly conserved in MbnBs. Two water molecules (red) are also present in the coordination sphere in the crystal structure, along with a cacodylate molecule (gray) from the crystallization buffer. (**D**) Sequence similarity network for the broader MbnC family. Red circles, MbnCs; blue circles, related non-MbnC genes found exclusively in *Pseudomonas* species. (**E**) SEC-MALS analysis of MbnA (yellow; 3 kDa predicted, 3 kDa observed), MbnBC (red; 58 kDa predicted, 55 kDa observed), and MbnABC (blue; 61 kDa predicted, 58 kDa observed) indicates that MbnB and MbnC form a heterodimeric complex that can bind MbnA.

by modeling its sequence onto the experimentally determined structure of the *Hs. somnus* 129Pt protein, even though MbnBs constitute a distinct subfamily within the DUF692 family (Fig. 2, B and C). Less is known about MbnC. Four years after the initial bioinformatics study, this predicted protein still has no identifiable domains, and members of this family are found only in Mbn operons or separate from *mbnB* in *Pseudomonas* species (Fig. 2D). Neither MbnB nor MbnC contains a RiPP precursor protein recognition element, which is present in leader peptide–dependent modifying enzymes from many RiPP families (*26*).

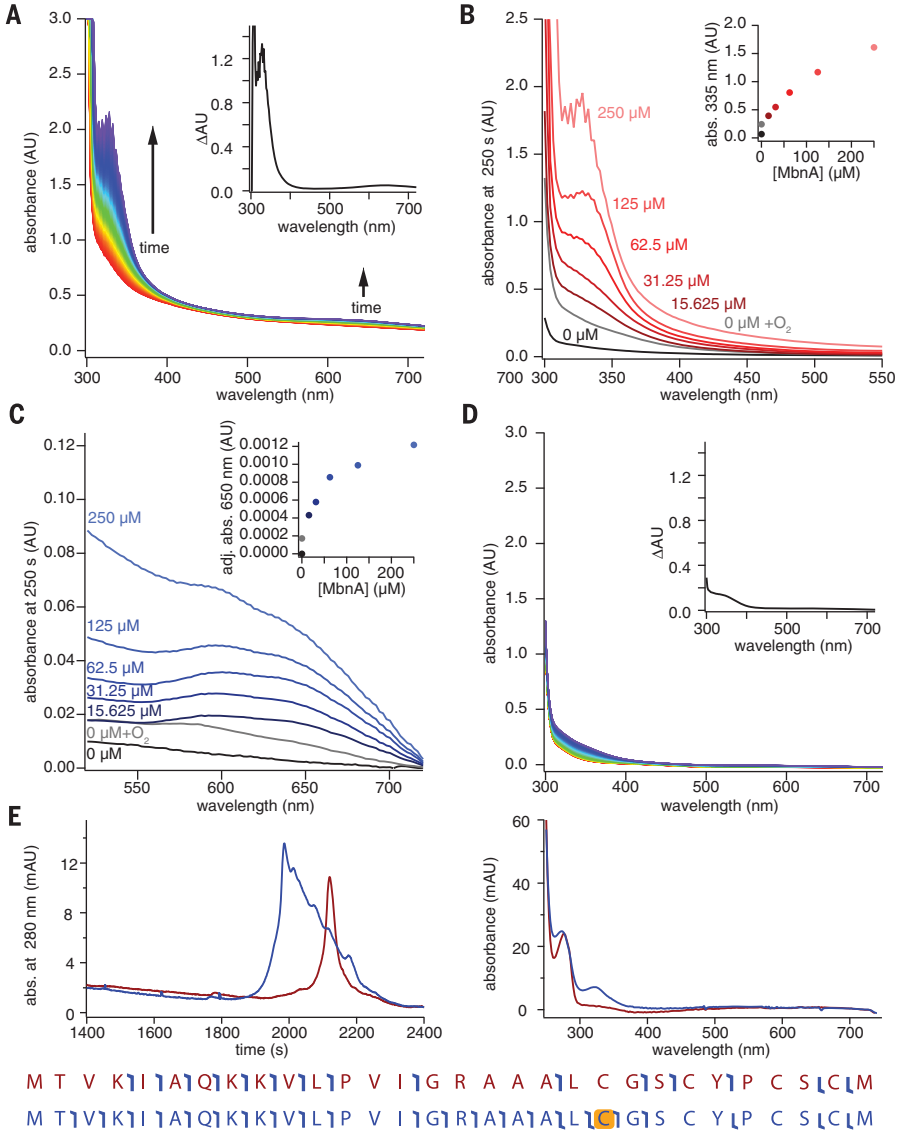

Fig. 3. Modification of *Ms. trichosporium* OB3b MbnA by MbnBC. (**A**) Reaction of 100 μM anaerobic MbnBC with 125 μM MbnA and 900 μM O_2 over a period of 250 s; two prominent features are observed at 335 and 650 nm. Inset shows a difference spectrum between the final (250 s) and initial (0 s) time points. (**B**) UV-vis absorption spectra of the feature at 335 nm with different concentrations of MbnA. Inset shows the absorbance at 335 nm at different concentrations of MbnA. (**C**) UV-vis absorption spectra of the feature at 650 nm at different concentrations of MbnA; inset shows absorbance at 650 nm adjusted via a dropline correction using values at 640 and 660 nm. (**D**) Reaction of 100 μM anaerobically prepared MbnBC containing 140 μM Fe with 900 μM O_2 over a period of 250 s reveals the formation of a broad spectral feature between 300 and 400 nm. Inset shows a difference spectrum between the final (250 s) and initial (0 s) time points. (**E**) LC-UV-MS-MS shows that the retention time (left chromatogram) of the modified peptide (blue) changes relative to the unmodified peptide (red), that the absorption spectrum of the modified peptide maintains the 335-nm feature (right spectrum), and that the presence of the 335-nm feature is associated with a mass shift of −4 Da that can be assigned to the first of the two modifiable cysteines (yellow highlight, bottom). Angled blue "flags" in the peptide sequence maps indicate the location of fragment ions observed during tandem MS.

Separate heterologous overexpression of either MbnB or MbnC from several species failed to yield soluble protein. However, simultaneous coexpression of MbnB and MbnC from a single vector (*27*) yielded soluble, stable heterodimeric complexes (MbnBC; 58.2 kDa for the *Ms. trichosporium* OB3b proteins with intact affinity tags) that could be purified via affinity and size exclusion chromatographies (Fig. 2E and fig. S3). Consistent with the proposed role of MbnBC in Mbn biosynthesis, addition of MbnA resulted in the formation of a heterotrimeric MbnA-MbnBC complex, detectable by size exclusion chromatography with multiangle light scattering (SEC-MALS) (Fig. 2E) as well as denaturing and native polyacrylamide gel electrophoresis (fig. S3). Moreover, purified MbnBC complexes from six different species (table S1 and fig. S4) contained iron, potentially satisfying the expected requirement for a redox cofactor.

Supplementation with 200 to 500 μM ferrous ammonium sulfate during expression increased the iron loading, and in our model construct of MbnBC from *Ms. trichosporium* OB3b, purified protein samples contained 1.3 ± 0.2 iron atoms per heterodimer (table S1). ^{57}Fe-Mössbauer spectra of MbnBC are complex, but for aerobically purified protein from three species, a mixture of exchange-coupled di- and trinuclear clusters was observed in addition to smaller amount(s) of unidentified species (fig. S5 and supplementary materials). Native top-down mass spectrometry (nTDMS) of MbnBC from six species showed that, as anticipated, all the iron was associated with the MbnB subunit (figs. S6 and S7). A notable subset of the population appeared to have as many as three iron ions per MbnB subunit, indicating that a fraction of the MbnB protein remained in the metal-free (apo) state, which was also observed by native mass spectrometry (figs. S6 and S7). The heterogeneity implied by the noninteger iron stoichiometry and observed by both Mössbauer spectroscopy and nTDMS implied that only a fraction of the purified MbnBC complexes were in the active state. Reduced Fe(II) is commonly required to initiate the oxidation of aliphatic carbon centers (*28*, *29*), and less than 5% of the total iron in aerobically purified MbnBC was in this form. Purification of MbnBC under O_2-free conditions resulted in a variable increase in Fe(II) levels at the expense of diminished iron loading.

Both aerobically and anaerobically produced MbnBC react with MbnA in the presence of O_2, without the addition of external reductant, to yield a product characterized by a sharp absorption feature at 335 nm and a broad feature at 650 nm (Fig. 3A and fig. S8). Despite its decreased iron content, the anaerobically produced MbnBC was more active, consistent with the involvement of an Fe(II) species in the active form of the cofactor. In the presence of excess O_2, the 335-nm feature increased in intensity with increasing quantities of substrate (Fig. 3B and fig. S8), whereas the intensity of the 650-nm feature was limited by MbnBC concentration (Fig. 3C and fig. S8). This latter feature likely reflects a charge-transfer transition associated with the complex of MbnA with

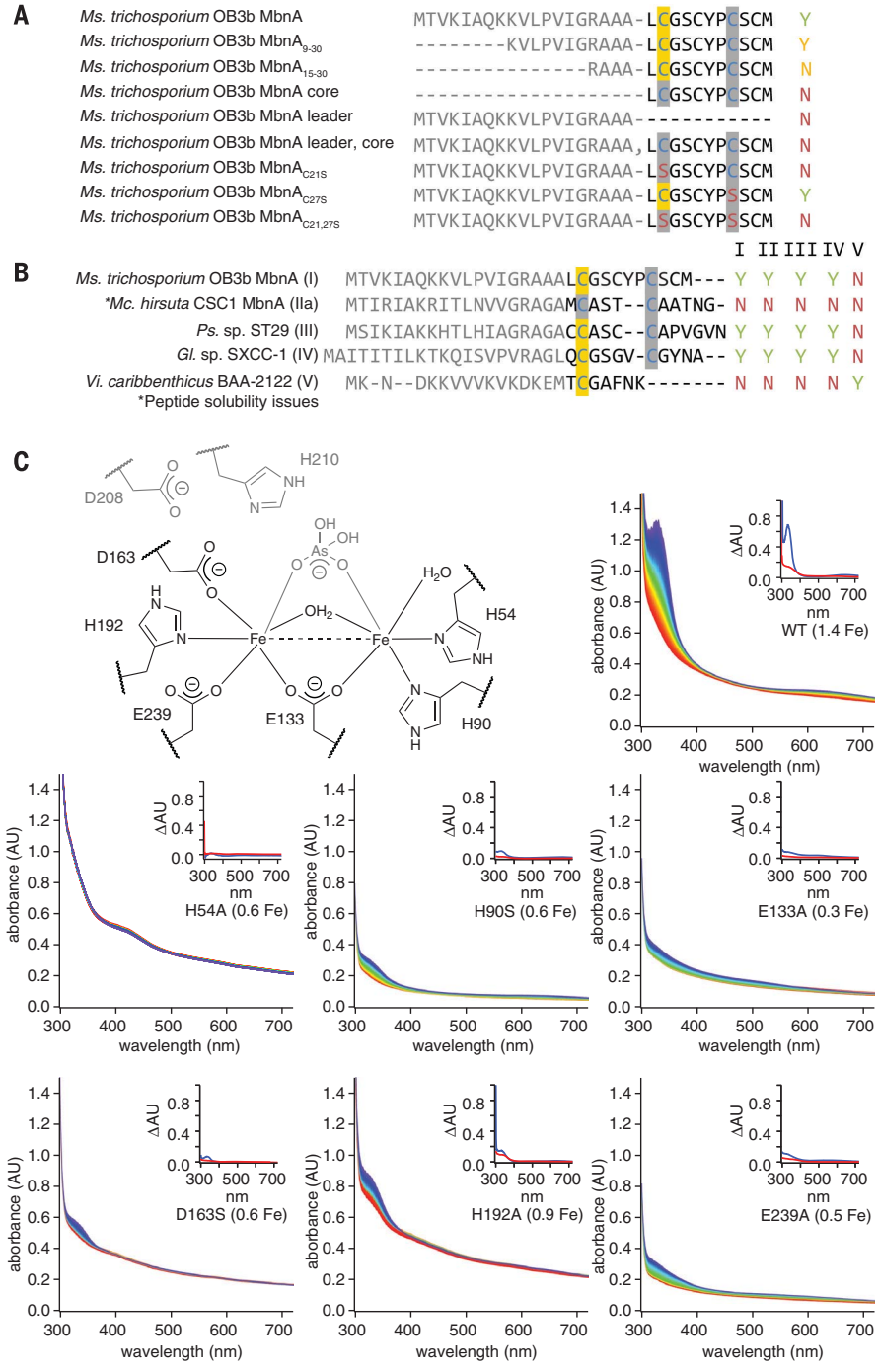

Fig. 4. Correlation of MbnBC activity with proposed diiron active site ligands and MbnA sequence. (**A**) Summary of activity observed via UV-vis absorption spectroscopy and LC-MS for 125 μM *Ms. trichosporium* OB3b MbnA variants with 100 μM *Ms. trichosporium* OB3b MbnBC and excess O_2. Yes (Y) indicates that modification is observed; No (N) indicates no modification. Modified cysteines localized via tandem MS are highlighted in yellow. (**B**) Summary of activity observed via UV-vis absorption spectroscopy and LC-MS for 125 μM MbnA substrate peptides and 100 μM MbnBC enzyme complexes from the different Mbn operon families in the presence of excess (~900 μM) O_2. (**C**) Stopped-flow UV-vis absorption spectra over a period of 250 s for reactions between 125 μM MbnA, excess (~900 μM) O_2, and 100 μM wild-type *Ms. trichosporium* OB3b MbnBC or one of six enzyme variants with alanine mutations in predicted active-site residues (the diiron site from the *Hs. somnus* 129Pt structure, labeled with *Ms. trichosporium* OB3b residue numbers, is provided for reference). Spectra are colored in rainbow order according to time, with the earliest spectra in red and the latest spectra in blue. Iron content per heterodimer is included in each label. Insets depict difference spectra for the enzyme in the presence of oxygen (red) or oxygen and the MbnA substrate peptide (blue).

the MbnBC iron cofactor. When MbnA was omitted from the reaction, a broader, weaker feature with a wavelength of maximum absorption (λ_{max}) of 340 nm developed more slowly (Fig. 3D and fig. S9). This feature resembles those arising from oxo-to-ferric charge-transfer transitions in non-heme dinuclear Fe enzymes (*30*) and likely derives from a species generated by unproductive oxidation of the Fe(II) in the MbnBC cofactor in the absence of substrate. Similarly, incubation of MbnA with MbnBC in the absence of O_2 did not yield the intense 335-nm feature, consistent with a role for O_2 in production of the chromophore. Minor spectral changes observed under these conditions likely reflect low levels of residual O_2 in the deoxygenated reaction buffers.

Analysis of MbnA before and after exposure to MbnBC and O_2 by coupled liquid chromatography, ultraviolet-visible (UV-vis) absorption spectroscopy, and tandem mass spectrometry (LC-UV-MS-MS) showed that the 335-nm feature is associated with MbnA and correlates with a mass shift of –4.031 Da localized to Cys^{21}, which is the position of the N-terminal oxazolone ring (Oxa_A) in the final natural product (Fig. 3E and fig. S10). This mass shift matches that predicted for the installation of a single oxazolone-thioamide group. In support of this assignment, addition of 100 to 500 mM HCl resulted in the decay of the 335-nm feature in modified MbnA, as expected if the modification is indeed an oxazolone-thioamide group (fig. S11) (*13*, *24*). Although species with mass shifts of –2 and –6 Da could also be detected in many reactions, fragmentation analyses indicated that these species corresponded to intramolecular disulfide formation between unmodified cysteines and modification together with intramolecular disulfide bond formation, respectively. Consistent with modification of Cys^{21}, a $Cys^{21} \rightarrow$ Ser substitution eradicated peptide modification as observed via UV-vis spectroscopy and mass spectrometry, whereas a $Cys^{27} \rightarrow$ Ser substitution had no effect (Fig. 4A and figs. S12 and S13). MbnBC additionally did not modify the core peptide alone, nor did it react with the leader and core peptides added in trans, and even the truncation of the leader peptide resulted in diminished activity (Fig. 4A and figs. S12 and S13).

Despite this marked sensitivity to the presence of valid leader peptides and modification sites, MbnBCs are otherwise promiscuous. MbnBCs from Mbn groups I to IV were all capable of modifying heterologous MbnA groups I to IV, despite the substantial differences in leader and core peptide sequences. MbnA from group V has the most divergent sequence (*11*), and the MbnBC from this group could interact only with the group V MbnA (Fig. 4B and fig. S14). All observed MbnA modifications were associated with the same mass shift of –4 Da observed in the *Ms. trichosporium* MbnABC system (fig. S15), indicating that a detailed analysis of this system can be generalized to the larger MbnBC family.

Although the mass shift and acid hydrolysis data are consistent with a single oxazolone-thioamide moiety in modified MbnA, the 335-nm absorption feature differs from the 392-nm feature of Oxa_A in mature Mbns. This discrepancy is

attributable to structural differences between the modified MbnA product and mature Mbn. In mature Mbn, the leader peptide is cleaved and the N-terminal primary amine is converted to a carbonyl group by the pyridoxal-5′-phosphate (PLP)–dependent aminotransferase MbnN (*15*). This modification extends the conjugation of the oxazolone ring, accounting for the bathochromic shift in the spectral feature; Oxa_B moieties in all Mbns lack such extended conjugation, and their absorption features fall within the 325- to 345-nm range (*13*, *23*, *24*, *31*). Consistent with this explanation, disruption of *mbnN* in *Ms. trichosporium* OB3b resulted in accumulation of a previously unknown copper-binding compound that exhibited a single major spectral feature with λ_{max} of 332 nm and a mass shift of +1 Da with respect to CuMbn, reflecting the presence of the N-terminal primary amine in place of the carbonyl group (fig. S16).

The formation of this oxazolone-thioamide moiety is dependent on the presence of the iron cofactor. Mutagenesis of the proposed iron ligands in *Ms. trichosporium* OB3b MbnB (fig. S17) diminished or eradicated both iron incorporation and modification of MbnA (Fig. 4C). Native mass spectrometry confirmed that diminished iron loading of MbnBC measured by inductively coupled plasma optical emission spectrometry (ICP-OES) correlated with reduced metal binding by MbnB (fig. S18 and table S1). Activity could also be eliminated in the wild-type enzyme by removal of the iron or complete oxidation with excess H_2O_2 before reaction with MbnA and O_2 (fig. S19). The clear requirements for reduced iron and O_2 (and no other reductants or cofactors) suggest that MbnBC is an oxidase that activates O_2 for cleavage of the three aliphatic C–H bonds on C_α and C_β of the first modifiable cysteine of MbnA to promote the cyclization/migration reaction necessary to complete the biosynthesis of the oxazolone-thioamide group.

The observed conversion of Cys^{21} to an oxazolone-thioamide appears to be an O_2-dependent four-electron oxidation involving multiple aliphatic carbons; such reactions are mediated by several mononuclear (*32*, *33*) and dinuclear (*34*, *35*) iron enzymes. A hallmark of all these enzymes is the ability to extract all necessary electrons from the substrate, allowing them to mediate multiple turnovers in the absence of a cosubstrate. By contrast, related iron enzymes that promote two-electron oxidations uniformly require reducing cosubstrates (*29*, *36*). Because MbnBC performed multiple turnovers in reactions lacking an obvious reductant (figs. S8, S9, and S20), it may mediate a single four-electron oxidation rather than two sequential two-electron oxidations. As the MbnA or O_2 concentration increased, the transition from the single-turnover regime (characterized by a single-exponential kinetic phase in development of the 335-nm feature) to the multiple-turnover regime (characterized by multiphasic kinetics) was observed at an MbnA concentration markedly lower than the total iron present in the anaerobically prepared proteins (figs. S8 and S9); this finding is potentially consistent with an active cofactor that contains more than one iron ion. The presence of a multinuclear iron (Fe_2 or Fe_3) cluster is consistent with the nTDMS analysis and the observation by Mössbauer spectroscopy of multinuclear iron species in aerobically purified MbnBC. Moreover, examination of the metal centers in xylose isomerase, endonuclease IV, and the *Hs. somnus* 129Pt DUF692 protein—the closest structurally characterized relatives of MbnB—suggests that a dinuclear or perhaps even trinuclear cluster is distinctly possible (fig. S21). By analogy to other nonheme iron enzymes that mediate four-electron oxidations, MbnA processing could be initiated by abstraction of a hydrogen atom from the C_β of the first modifiable cysteine by a superoxo(di/tri)iron(III) intermediate (fig. S22).

How MbnBC proceeds to the second modification site remains unclear, as does the mechanism of leader peptide loss (fig. S23). The enzyme complex may require leader peptide cleavage to install the C-terminal oxazolone-thioamide group, although neither modification site in the core peptide can be modified without the leader (Fig. 4A and figs. S12 and S13). The only genes found in all Mbn operons are *mbnA*, *mbnB*, and *mbnC*. Mbn operons encode no proteases, and MbnA leader peptides lack known protease recognition motifs at the cleavage location. It may be that a protease not encoded in the operon is required. Alternatively, the missing protease could be MbnC, for which neither a role nor a cofactor requirement has been established. However, addition of a wide range of potential cofactors as well as lysate from Mbn-producing *Ms. trichosporium* OB3b cells to MbnABC reactions in vitro failed to enable leader peptide cleavage (figs. S24 and S25). In addition, coexpression of MbnBC from *Vibrio caribbenthicus* BAA-2122 with C-terminally His_6-tagged MbnA from the same species resulted in the same mass shift and UV-visible spectral features observed in vitro (fig. S26). This may indicate that the protease, a cofactor, or a cosubstrate for the protease is absent or incorrectly assembled during heterologous expression. Additional work will be necessary to fully reconstruct the biosynthetic pathway in heterologous expression systems or in vitro.

The involvement of a metalloenzyme in oxazolone and thioamide biosynthesis is unprecedented, and both components of the MbnBC complex belong to previously uncharacterized protein families. Similar to RiPP systems such as the cyanobactins and lantibiotics (*37*, *38*), the promiscuity of the Mbn biosynthetic system suggests that it might be amenable to engineering efforts, which could facilitate the development of natural and non-natural Mbns as drugs for Wilson disease and other disorders involving copper accumulation (*39*–*41*). Furthermore, the new understanding of these enzymes sets the stage for elucidating the biosynthesis and function of the Mbn-like natural products from nonmethanotrophic bacteria.

REFERENCES AND NOTES

1. A. Butler, *Science* **281**, 207–210 (1998).
2. L. D. Palmer, E. P. Skaar, *Annu. Rev. Genet.* **50**, 67–91 (2016).
3. M. Nairz, A. Schroll, T. Sonnweber, G. Weiss, *Cell. Microbiol.* **12**, 1691–1702 (2010).
4. M. Miethke, M. A. Marahiel, *Microbiol. Mol. Biol. Rev.* **71**, 413–451 (2007).
5. G. Ghssein *et al.*, *Science* **352**, 1105–1109 (2016).
6. P. T. Chivers, E. L. Benanti, V. Heil-Chapdelaine, J. S. Iwig, J. L. Rowe, *Metallomics* **4**, 1043–1050 (2012).
7. M. V. Cherrier, C. Cavazza, C. Bochot, D. Lemaire, J. C. Fontecilla-Camps, *Biochemistry* **47**, 9937–9943 (2008).
8. K. S. Chaturvedi, C. S. Hung, J. R. Crowley, A. E. Stapleton, J. P. Henderson, *Nat. Chem. Biol.* **8**, 731–736 (2012).
9. C. W. Johnston *et al.*, *Nat. Chem. Biol.* **9**, 241–243 (2013).
10. T. C. Johnstone, E. M. Nolan, *Dalton Trans.* **44**, 6320–6339 (2015).
11. L. M. K. Dassama, G. E. Kenney, A. C. Rosenzweig, *Metallomics* **9**, 7–20 (2017).
12. H. J. Kim *et al.*, *Science* **305**, 1612–1615 (2004).
13. B. D. Krentz *et al.*, *Biochemistry* **49**, 10117–10130 (2010).
14. G. E. Kenney, M. Sadek, A. C. Rosenzweig, *Metallomics* **8**, 931–940 (2016).
15. G. E. Kenney, A. C. Rosenzweig, *BMC Biol.* **11**, 17 (2013).
16. J. D. Semrau *et al.*, *Environ. Microbiol.* **15**, 3077–3086 (2013).
17. P. G. Arnison *et al.*, *Nat. Prod. Rep.* **30**, 108–160 (2013).
18. U. Rix *et al.*, *J. Am. Chem. Soc.* **126**, 4496–4497 (2004).
19. S. Behnken, C. Hertweck, *Appl. Microbiol. Biotechnol.* **96**, 61–67 (2012).
20. M. Izawa, T. Kawasaki, Y. Hayakawa, *Appl. Environ. Microbiol.* **79**, 7110–7113 (2013).
21. D. D. Nayak, N. Mahanta, D. A. Mitchell, W. W. Metcalf, *eLife* **6**, e29218 (2017).
22. L. A. Behling *et al.*, *J. Am. Chem. Soc.* **130**, 12604–12605 (2008).
23. A. El Ghazouani *et al.*, *Proc. Natl. Acad. Sci. U.S.A.* **109**, 8400–8404 (2012).
24. G. E. Kenney *et al.*, *J. Am. Chem. Soc.* **138**, 11124–11127 (2016).
25. N. Nagano, C. A. Orengo, J. M. Thornton, *J. Mol. Biol.* **321**, 741–765 (2002).
26. B. J. Burkhart, G. A. Hudson, K. L. Dunbar, D. A. Mitchell, *Nat. Chem. Biol.* **11**, 564–570 (2015).
27. N. H. Tolia, L. Joshua-Tor, *Nat. Methods* **3**, 55–64 (2006).
28. B. J. Wallar, J. D. Lipscomb, *Chem. Rev.* **96**, 2625–2658 (1996).
29. M. Costas, M. P. Mehn, M. P. Jensen, L. Que Jr., *Chem. Rev.* **104**, 939–986 (2004).
30. C. A. Brown, G. J. Remar, R. L. Musselman, E. I. Solomon, *Inorg. Chem.* **34**, 688–717 (1995).
31. H. J. Kim, N. Galeva, C. K. Larive, M. Alterman, D. W. Graham, *Biochemistry* **44**, 5140–5148 (2005).
32. E. Tamanaha *et al.*, *J. Am. Chem. Soc.* **138**, 8862–8874 (2016).
33. S. C. Peck *et al.*, *J. Am. Chem. Soc.* **139**, 2045–2052 (2017).
34. G. Xing *et al.*, *Proc. Natl. Acad. Sci. U.S.A.* **103**, 6130–6135 (2006).
35. B. Wörsdörfer *et al.*, *Proc. Natl. Acad. Sci. U.S.A.* **110**, 18874–18879 (2013).
36. A. Trehoux, J.-P. Mahy, F. Avenier, *Coord. Chem. Rev.* **322**, 142–158 (2016).
37. D. Sardar, Z. Lin, E. W. Schmidt, *Chem. Biol.* **22**, 907–916 (2015).
38. A. J. van Heel, D. Mu, M. Montalbán-López, D. Hendriks, O. P. Kuipers, *ACS Synth. Biol.* **2**, 397–404 (2013).
39. A. Ala, A. P. Walker, K. Ashkan, J. S. Dooley, M. L. Schilsky, *Lancet* **369**, 397–408 (2007).
40. K. H. Summer *et al.*, *J. Trace Elem. Med. Biol.* **25**, 36–41 (2011).
41. J. Lichtmannegger *et al.*, *J. Clin. Invest.* **126**, 2721–2735 (2016).

ACKNOWLEDGMENTS

Supported by NIH grants GM118035 (A.C.R.), R01AT009143 (N.L.K.), U54-GM094662, U54 GM093342, P01 GM118303 (S.C.A.), R00GM111978 (M.-E.P.), and F32GM110934 (L.M.K.D.), as well as NSF grants MCB0842366 (A.C.R.) and MCB1330784 (J.M.B. and C.K.) and the Price Foundation (S.C.A.). G.E.K. was supported by American Heart Association grant 14PRE20460104. L.M.K.D. was additionally funded by a Postdoctoral Enrichment Program grant from the Burroughs Wellcome Fund. L.F.S. was supported by NIH grant T32GM105538 and a Howard Hughes Medical Institute Gilliam Fellowship. O.S.S. was supported by NSF GRFP grant 2014171659 and R.J.M. under NSF grant DGE1255832. At Northwestern University, the Quantitative Bio-element Imaging Center is supported by NASA Ames Research Center grant NNA06CB93G, the Proteomics Center for Excellence is supported by National Resource for Translational and Developmental Proteomics under NIH grant P41 GM108569 and National Cancer Institute (NCI) grant CCSG P30 CA060553, the Integrated

Molecular Structure Education and Research Center is supported by Northwestern University and the State of Illinois, the International Institute for Nanotechnology, and the Soft and Hybrid Nanotechnology Experimental (SHyNE) Resource (NSF grant NNCI-1542205), and the Keck Biophysics Facility is supported in part by NCI Cancer Center Support Grant CA060553. Some work was performed at the Albert Einstein Anaerobic Structural and Functional Genomics Resource. All authors declare no conflicts of interest. All data are presented in the supplementary materials.

SUPPLEMENTARY MATERIALS

www.sciencemag.org/content/359/6382/1411/suppl/DC1
Materials and Methods
Supplementary Text
Figs. S1 to S28
Tables S1 to S3
Data Files S1 to S7
References (*42*–*64*)

12 September 2017; accepted 7 February 2018
10.1126/science.aap9437

CELL BIOLOGY

Locally translated mTOR controls axonal local translation in nerve injury

Marco Terenzio,[1] Sandip Koley,[1] Nitzan Samra,[1] Ida Rishal,[1] Qian Zhao,[2]* Pabitra K. Sahoo,[3] Anatoly Urisman,[2] Letizia Marvaldi,[1] Juan A. Oses-Prieto,[2] Craig Forester,[4] Cynthia Gomes,[3]† Ashley L. Kalinski,[3]‡ Agostina Di Pizio,[1] Ella Doron-Mandel,[1] Rotem Ben-Tov Perry,[1] Indrek Koppel,[1] Jeffery L. Twiss,[3,5] Alma L. Burlingame,[2] Mike Fainzilber[1]§

How is protein synthesis initiated locally in neurons? We found that mTOR (mechanistic target of rapamycin) was activated and then up-regulated in injured axons, owing to local translation of mTOR messenger RNA (mRNA). This mRNA was transported into axons by the cell size–regulating RNA-binding protein nucleolin. Furthermore, mTOR controlled local translation in injured axons. This included regulation of its own translation and that of retrograde injury signaling molecules such as importin β1 and STAT3 (signal transducer and activator of transcription 3). Deletion of the mTOR 3′ untranslated region (3′UTR) in mice reduced mTOR in axons and decreased local translation after nerve injury. Both pharmacological inhibition of mTOR in axons and deletion of the mTOR 3′UTR decreased proprioceptive neuronal survival after nerve injury. Thus, mRNA localization enables spatiotemporal control of mTOR pathways regulating local translation and long-range intracellular signaling.

Local translation enables spatiotemporal specificity in cell functions (*1*, *2*) such as the neuronal response to axon injury (*3*, *4*) or regrowth of injured axons (*5*, *6*). However, apart from a requirement for intra-axonal calcium (*7*), the mechanisms that regulate local protein synthesis in axons are largely unknown. mTOR, the mechanistic target of rapamycin, is a central regulator of translation (*8*), neuronal regeneration (*9*–*12*), and protein synthesis in neurons (*13*–*16*). We examined mTOR signaling in the sciatic nerve (SN) versus in dorsal root ganglia (DRG) after axonal injury and found differential phosphorylation of mTOR and associated signaling components (Fig. 1, A and B, and table S1). This suggested a specific role for mTOR in the early injury response in axons. We verified mTOR serine 2448 (S2448) phosphorylation (*17*) in axons by immunostaining, observing significant elevation within axons at 3 hours after injury, with a return to baseline at 12 hours (Fig. 1, C and D). We also observed that phosphorylation levels of EiF4b (S406), Akt (S473), S6 kinase (S6K; threonine 389), and ribosomal protein S6 (S240 and S244), all well-known effectors and regulators of mTOR signaling, increased rapidly after injury (Fig. 1E). Typically, Eif4b is activated in response to mTORC1, whereas Akt plays a role in both mTORC1 and mTORC2 signaling (*8*, *18*); hence, both mTOR complexes are activated locally by axonal injury.

We used the mTOR inhibitor torin-1 (fig. S1, A to C) to examine functions of local mTOR activation in nerve injury. Injection of torin-1 at the injury site before a conditioning SN lesion (*19*) reduced the subsequent lesion-induced axon outgrowth in culture (fig. S1, D and E). Neuron numbers recovered from torin-1–treated animals were also reduced (fig. S1F), so we examined the effects of torin-1 injection into the SN on proprioceptive neuron survival in DRG in vivo. Injecting torin-1 into the nerve concomitantly with injury reduced proprioceptive neuron numbers in the corresponding DRG (Fig. 1, F and G), supporting a role for axonal mTOR activation in neuronal injury response and survival. Examination of SN mTOR expression revealed unexpectedly low levels of mTOR protein in axons before injury. Axonal mTOR was markedly elevated in the vicinity of the lesion site up to 9 hours post-injury, which was followed by a decline back to baseline levels (Fig. 2A and fig. S2A). Up-regulation of mTOR in injured axons was further confirmed by immunoelectron microscopy on SN sections (fig. S2B).

The time frame of mTOR elevation in axons suggested that it might be synthesized locally. We examined this possibility by biotinylation of nascent synthesized proteins tagged with the puromycin derivative *O*-propargyl-puromycin (OPP) (*20*). We performed OPP incubation in rat nerve segments ex vivo, followed by axoplasm extraction (*21*), biotinylation, and precipitation with streptavidin (SA). Immunoblots of SA precipitates revealed robust de novo synthesis of mTOR, similar to that of importin β1, a well-established locally synthesized protein (*4*) (Fig. 2B). Immunostaining on mouse SN segments incubated ex vivo with the translation inhibitor cycloheximide indicated inhibition of axonal mTOR up-regulation (fig. S2, C and D), and fluorescent in situ hybridization (FISH) showed robust granular signals for mTOR mRNA in axons (fig. S2E). Direct visualization of de novo synthesized mTOR by puromycin labeling combined with a proximity ligation assay revealed robust signals for de novo synthesis of mTOR in sensory axons in culture (fig. S3, A to C). mTOR axonal up-regulation in nerve segments ex vivo and in culture was torin-1–sensitive (Fig. 2, C and D, and fig. S3, A to C), indicating that it is controlled by mTOR itself. Last, mTOR up-regulation after injury was mirrored by a decrease in axonal PTEN (fig. S3, D and E), a functional mTOR antagonist.

A complex comprising the RNA-binding protein (RBP) nucleolin and the kinesin motor Kif5A traffics importin β1 mRNA to axons (*22*). We tested for mTOR mRNA association with this complex by quantitative reverse transcription polymerase chain reaction (PCR) on immunoprecipitates of nucleolin or Kif5A from SN axoplasm. mTOR mRNA was robustly coprecipitated with both nucleolin and Kif5A (Fig. 2E and fig. S4, A and B). Furthermore, we observed significant colocalization of mTOR mRNA with nucleolin protein by combining FISH with immunostaining on sensory axons (Fig. 2, F and G). Last, restriction of nucleolin to neuronal somata by pretreatment of neuronal cultures with the DNA aptamer AS1411 (*22*) reduced mTOR mRNA in axons while increasing it in cell bodies (Fig. 2H and fig. S4, C and D), confirming that mTOR mRNA is transported to axons by the RBP nucleolin.

To assess the overall impact of mTOR on local translation in axons, we carried out puromycin labeling on SN segments preincubated with anisomycin, a general protein synthesis inhibitor, or with torin-1. We quantified puromycin incorporation into axonal proteins by immunostaining (Fig. 3, A and B) and capillary immunoelectrophoresis of axoplasm (Fig. 3, C and D). Torin-1 effectively inhibited axonal protein synthesis to a similar degree as anisomycin (Fig. 3, B and D). We then used OPP to characterize the ensemble of de novo synthesized proteins in axon injury by mass spectrometry (MS). SN segments were preincubated ex vivo with vehicle, anisomycin, or torin-1 and then pulsed with OPP before axoplasm extraction and biotinylation (fig. S5A). The efficiency of the reactions was assessed by immunoblotting with SA–horseradish peroxidase (HRP) (Fig. 3E). A cohort of ~550 proteins was identified after affinity purification and MS, of which 234 were affected equivalently by anisomycin or torin-1 pretreatments (Fig. 3F, fig. S5B, and table S2). Almost 80% of the torin-1–sensitive candidates were shared with the largest

[1]Department of Biomolecular Sciences, Weizmann Institute of Science, Rehovot 76100, Israel. [2]Department of Pharmaceutical Chemistry, University of California, San Francisco, CA 94158, USA. [3]Department of Biological Sciences, University of South Carolina, Columbia, SC 29208, USA. [4]Division of Pediatric Allergy, Immunology and Bone Marrow Transplantation, University of California, San Francisco, CA 94158, USA. [5]Department of Neurobiology and Anatomy, Drexel University College of Medicine, Philadelphia, PA 19129, USA.
*Present address: Department of Applied Biology and Chemical Technology, Hong Kong Polytechnic University, Hong Kong. †Present address: Department of Anatomical Sciences and Neurobiology, University of Louisville, KY 40202, USA. ‡Present address: Department of Cell and Developmental Biology, University of Michigan Medical School, 109 Zina Pitcher Place, Ann Arbor, MI 48188, USA.
§Corresponding author. Email: mike.fainzilber@weizmann.ac.il

known translatome data set of mTOR-regulated survival-promoting mRNAs (*23*, *24*) (fig. S5C). The mTOR-dependent axonally synthesized proteins included many known axonal injury response proteins (*25*) (table S2), leading us to test the effect of torin-1 on injury-induced axonal up-regulation of STAT3 (signal transducer and activator of transcription 3; Fig. 3, G and H), importin β1 (fig. S5, D and E), and vimentin (fig. S5, F and G). Locally translated STAT3 is phosphorylated in sensory axons as a retrograde survival signal (*26*), so we also tested the effect of torin-1 on phospho-STAT3 (Fig. 3, G and H). Torin-1 effectively inhibited the localized axonal elevation of all the tested injury-signaling proteins, indicating that local translation for retrograde injury signaling is controlled by mTOR in sensory axons.

The findings above suggest that axonal localization of mTOR mRNA enables subcellular regulation of axonal protein synthesis. Localization motifs are often located in the 3′ untranslated regions (3′UTRs) of axonal mRNAs (*27*), and axonal localization was previously reported for the mTOR 3′UTR (*15*). We sequenced 3′RACE (rapid amplification of cDNA ends) PCR products and identified a single major mTOR 3′UTR sequence, as expected from genome annotation. The mTOR 3′UTR effectively localized green fluorescent protein mRNA to axons in transfected neurons (fig. S6, A and B). We then removed most of the 3′UTR sequence from the mTOR locus by using CRISPR-Cas9 gene editing (fig. S6C and table S3), without affecting the open reading frame or other elements of the gene. We verified that the segment targeted for deletion had axon-localizing capacity (mTOR 3′UTR 54 to 789), whereas segments predicted to be retained in the mutant mouse lacked axon-localizing capacity (mTOR 3′UTR 1 to 69 and 774 to 825; fig. S6, A and B). mTOR 3′UTR–null mice were viable, and 3′RACE analyses of homozygous null DRG neurons confirmed the deletion (fig. S6D).

FISH analyses of SN sections revealed a significant reduction in axonal mTOR mRNA levels in vivo in the SN of mTOR 3′UTR–null mice (Fig. 4, A and B, and fig. S6E), with no significant changes in stability or half-life of mTOR mRNA or protein (fig. S7). Ex vivo incubation of mTOR 3′UTR–null SN segments showed a large reduction in injury-induced mTOR protein up-regulation compared with the wild type (Fig. 4, C and D). Cultures of 3′UTR-null neurons revealed little or no change in mTOR protein levels in the soma, whereas mTOR protein levels in the growth cones and axon tips were significantly reduced (fig. S8, A and B). These subcellular effects on mTOR protein up-regulation were mirrored in mTOR downstream signaling, with no change in phospho-S6 levels in the somata of 3′UTR-null neurons, in contrast to a marked deficit in phospho-S6 up-regulation in injured axons from the mutant mice (fig. S8, C and D).

We then examined effects of the mTOR 3′UTR deletion on axonal protein synthesis and on the mTOR-dependent injury response in lesioned DRG neurons. Puromycinylation experiments in

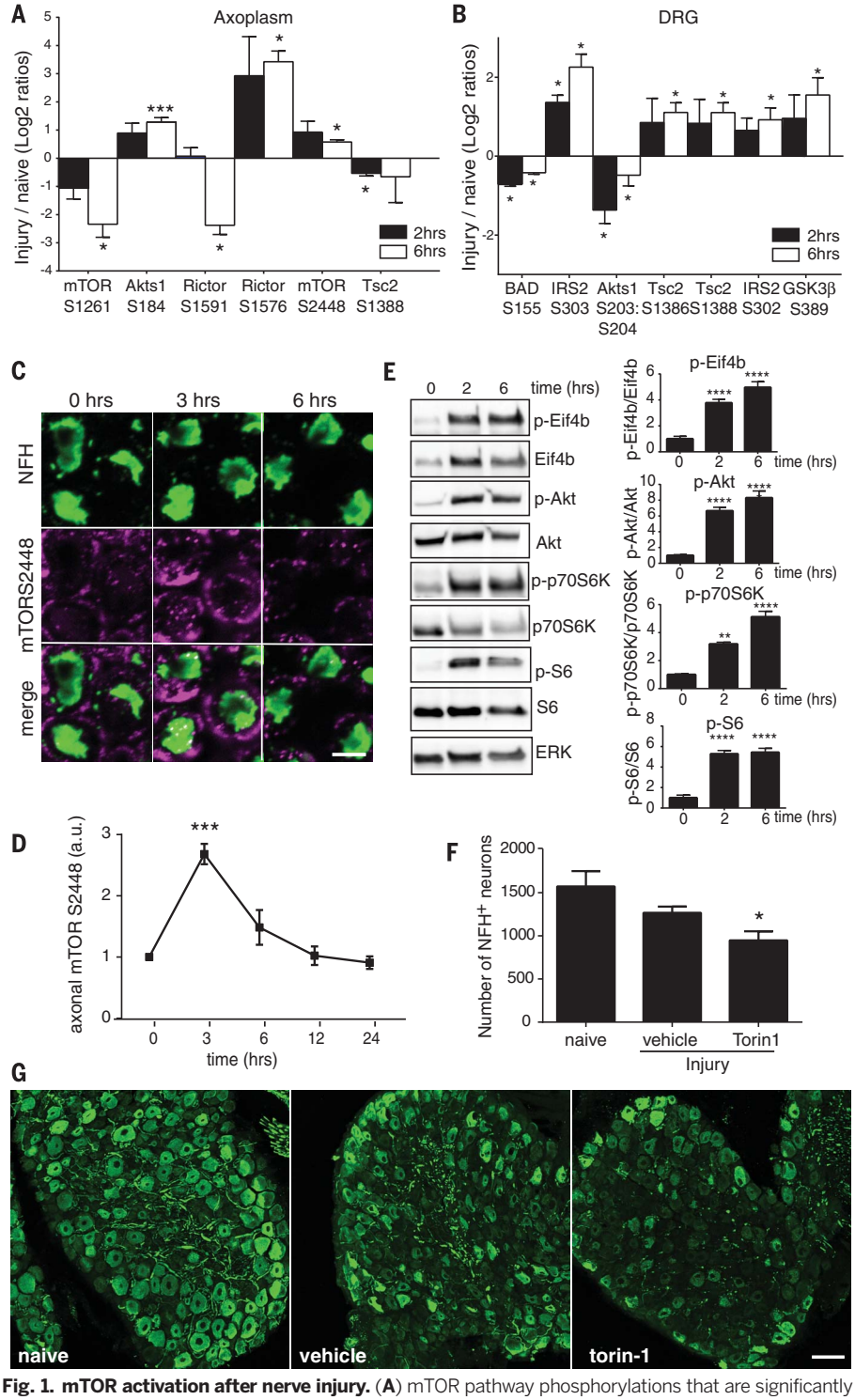

Fig. 1. mTOR activation after nerve injury. (**A**) mTOR pathway phosphorylations that are significantly regulated by SN injury ($n = 3$; means ± SEM; $^*P < 0.05$, $^{***}P < 0.001$; t test). (**B**) As in (A), for L4/L5 DRG ($n = 3$; means ± SEM; $^*P < 0.05$; t test). (**C**) SN sections stained for the axonal marker NFH (green) and mTOR S2448 (magenta), naive versus 3 and 6 hours after injury. Scale bar, 5 μm. (**D**) Axonal mTOR S2448 over time after injury, normalized to naive conditions [$n = 3$; means ± SEM; $^{***}P < 0.001$; one-way analysis of variance (ANOVA) with Bonferroni's post-test]. a.u., arbitrary units. (**E**) Immunoblots of phospho-EIF4b, -Akt, -S6K, and -S6 and the corresponding total proteins in SN axoplasm over time after injury. Quantifications are shown on the right ($n = 4$; means ± SEM; $^{**}P < 0.01$, $^{****}P < 0.0001$; one-way ANOVA with Bonferroni's post-test). (**F** and **G**) SNs were injected with vehicle or torin-1 before injury, and L4 DRG were harvested 7 days later, serially sectioned at 20-μm intervals, and stained for NFH (green) to allow counting of proprioceptive neurons. Quantifications of NFH-positive neuron numbers per DRG are shown in (F) ($n = 7$; means ± SEM; $^*P < 0.05$; t test); representative images are in (G) (scale bar, 50 μm).

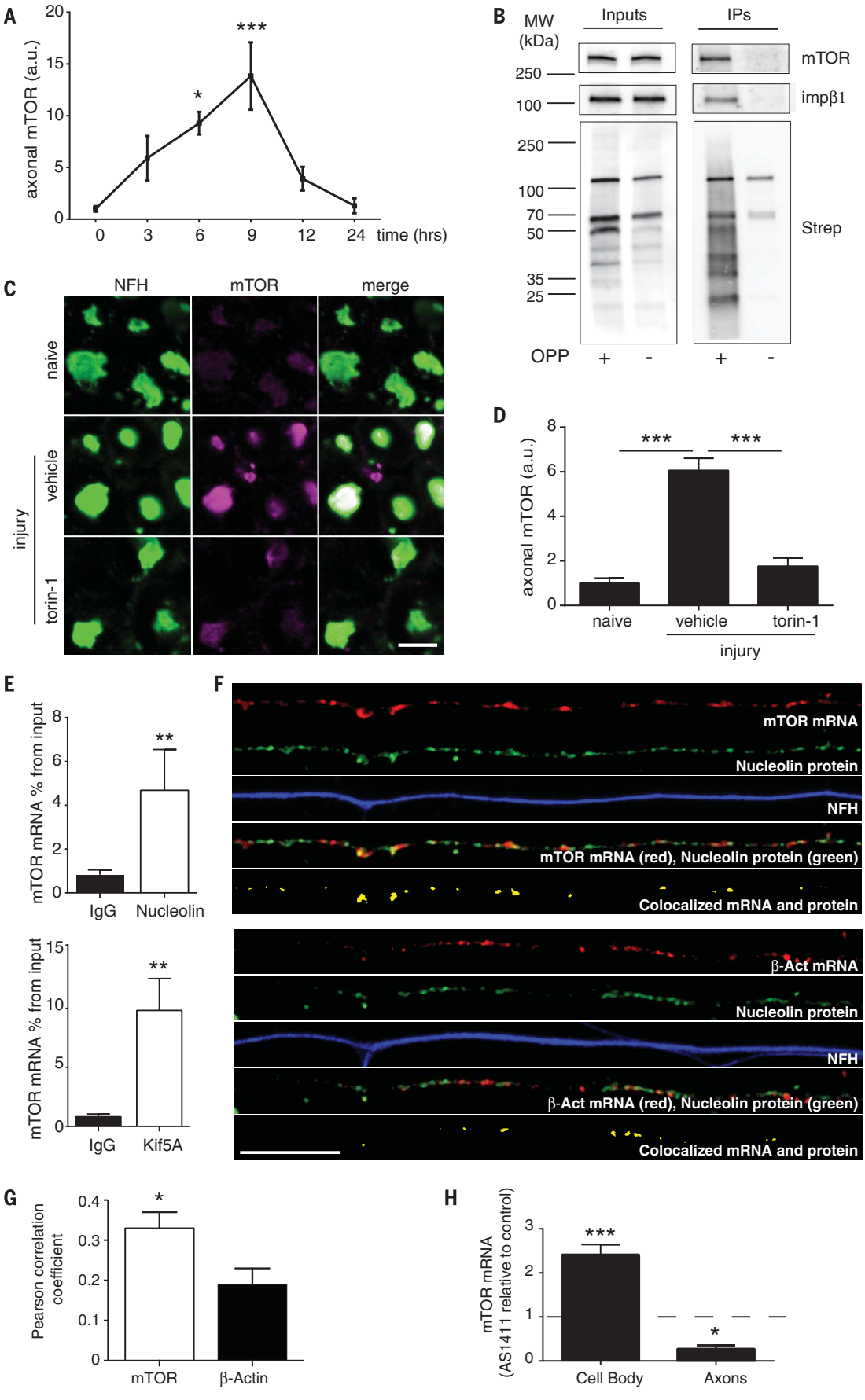

Fig. 2. mTOR is locally translated after SN injury. (**A**) mTOR regulation over time after injury at the SN lesion site ($n = 5$; means ± SEM; $^{*}P < 0.05$, $^{***}P < 0.001$; one-way ANOVA with Bonferroni's post-test). (**B**) Immunoblots reveal newly synthesized mTOR and importin β1 (Impβ1) from OPP-treated rat SNs, confirming their local translation after injury. IPs, immunoprecipitates; Strep, streptavidin. (**C**) Torin-1 (4 μM) effects on mTOR up-regulation in sections from SN 4 hours ex vivo, stained for NFH (green) and mTOR (magenta). Scale bar, 5 μm. (**D**) Quantification of axonal mTOR from (C) ($n = 6$; means ± SEM; $^{***}P < 0.001$; one-way ANOVA with Bonferroni's post-test). (**E**) Quantification of mTOR transcript levels after pulldown for Kif5A or nucleolin in axoplasm (percent from input; $n = 6$; means ± SEM; $^{**}P < 0.01$; ratio paired t test). IgG, immunoglobulin G. (**F**) Representative epifluorescent images for colocalization of endogenous mTOR or β-actin transcripts, visualized by in situ hybridization (red), and nucleolin protein, visualized by immunostaining (green). Axons were visualized by neurofilament immunostaining (blue). Scale bar, 10 μm. (**G**) Pearson's correlation coefficient for mTOR mRNA colocalization with nucleolin (0.33 ± 0.04; $n = 24$) differs significantly from that for β-actin mRNA colocalization with nucleolin (0.19 ± 0.04; $n = 20$). $^{*}P < 0.05$; t test. (**H**) Quantification of relative mTOR transcript levels in cell bodies and axons of neurons treated with AS1411 versus control aptamer, plotted as the fold change over control aptamer. 18S RNA served as an internal control ($n = 3$; means ± SEM; $^{*}P < 0.05$, $^{***}P < 0.001$; unpaired two-sample t test).

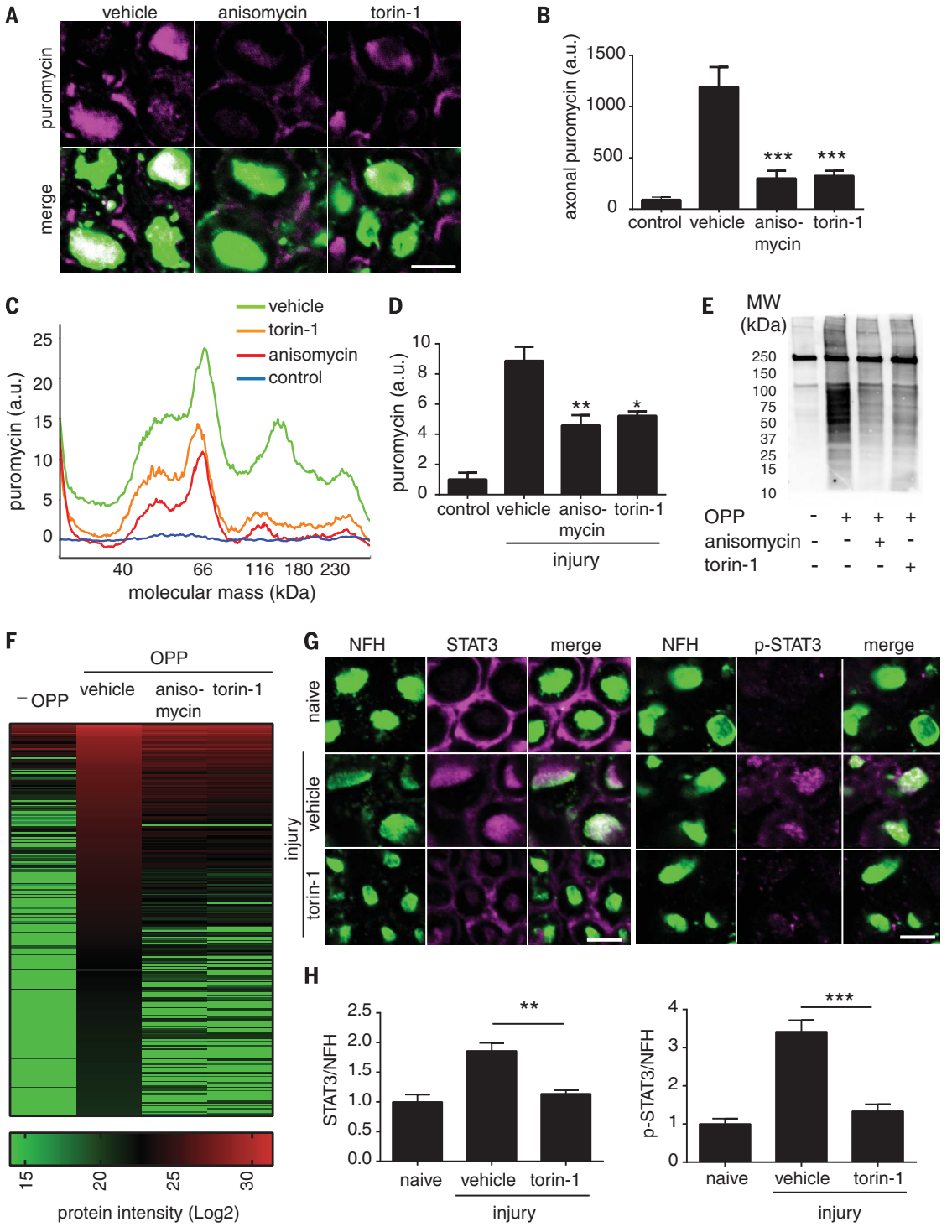

Fig. 3. mTOR regulates axonal local translation after SN injury. (**A**) SN segments 2 hours ex vivo with anisomycin (200 μg/ml), torin-1 (4 μM), or vehicle, followed by 1 hour with puromycin (100 μg/ml), sectioned and stained for NFH (green) and puromycin (magenta). Scale bar, 5 μm. (**B**) Quantification of axonal puromycin in the experiment described in (A) (n = 5; means ± SEM; ***P < 0.001; one-way ANOVA with Bonferroni's post-test). (**C**) Representative runs of puromycinylated proteins in SN axoplasm from the experiment described in (A), analyzed by capillary immunoelectrophoresis. (**D**) Quantification of (C) (n = 4; means ± SEM; *P < 0.05, **P < 0.01; ANOVA with Bonferroni's post-test). (**E**) SA-HRP immunoblots of OPP-biotin–labeled axoplasm samples before MS. (**F**) Heat map of OPP-biotin–labeled protein candidates identified by MS. (**G**) SN segments 4 hours ex vivo with torin-1 (4 μM) or vehicle (dimethyl sulfoxide), sectioned and stained for NFH (green) and STAT3 or phospho-STAT3 (both magenta). Scale bars, 5 μm. (**H**) Quantification of axonal STAT3 and phospho-STAT3 for the experiment described in (G) (n = 4; means ± SEM; **P < 0.01, ***P < 0.001; one-way ANOVA with Bonferroni's post-test).

SN segments ex vivo showed a clear reduction in puromycin incorporation in mTOR 3′UTR–null axons (Fig. 4, E and F, and fig. S9, A to D). SN injury in mutant mice led to reductions in L4 DRG proprioceptive neuron numbers 7 days later, to a similar degree as we previously observed for torin-1 injection concomitant with injury (Fig. 4I and fig. S9E). We tested whether the observed effects were indeed due to the loss of mTOR up-regulation in injured axons by injecting recombinant mTOR protein into the nerve concomitantly with injury. Exogenously supplied mTOR protein restored both local axonal translation (Fig. 4, G and H) and neuronal survival (Fig. 4I and fig. S9E) in the mutant mice. Thus, removal of the mTOR 3′UTR reduces axonal localization of mTOR mRNA and attenuates local elevation of mTOR protein in injured axons. Subcellular reduction in axonal mTOR affects overall local protein synthesis in injured axons and reduces the survival of lesioned neurons.

Maintenance of a latent and silent axonal pool of mTOR in mRNA form enables rapid and local up-regulation of protein synthesis upon need. The linkage of mTOR mRNA transport to nucleolin likely explains nucleolin regulation of subcellular protein synthesis in cell size regulation (*22*). Regulation of mTOR pathways through mRNA localization may have impacts on many aspects of

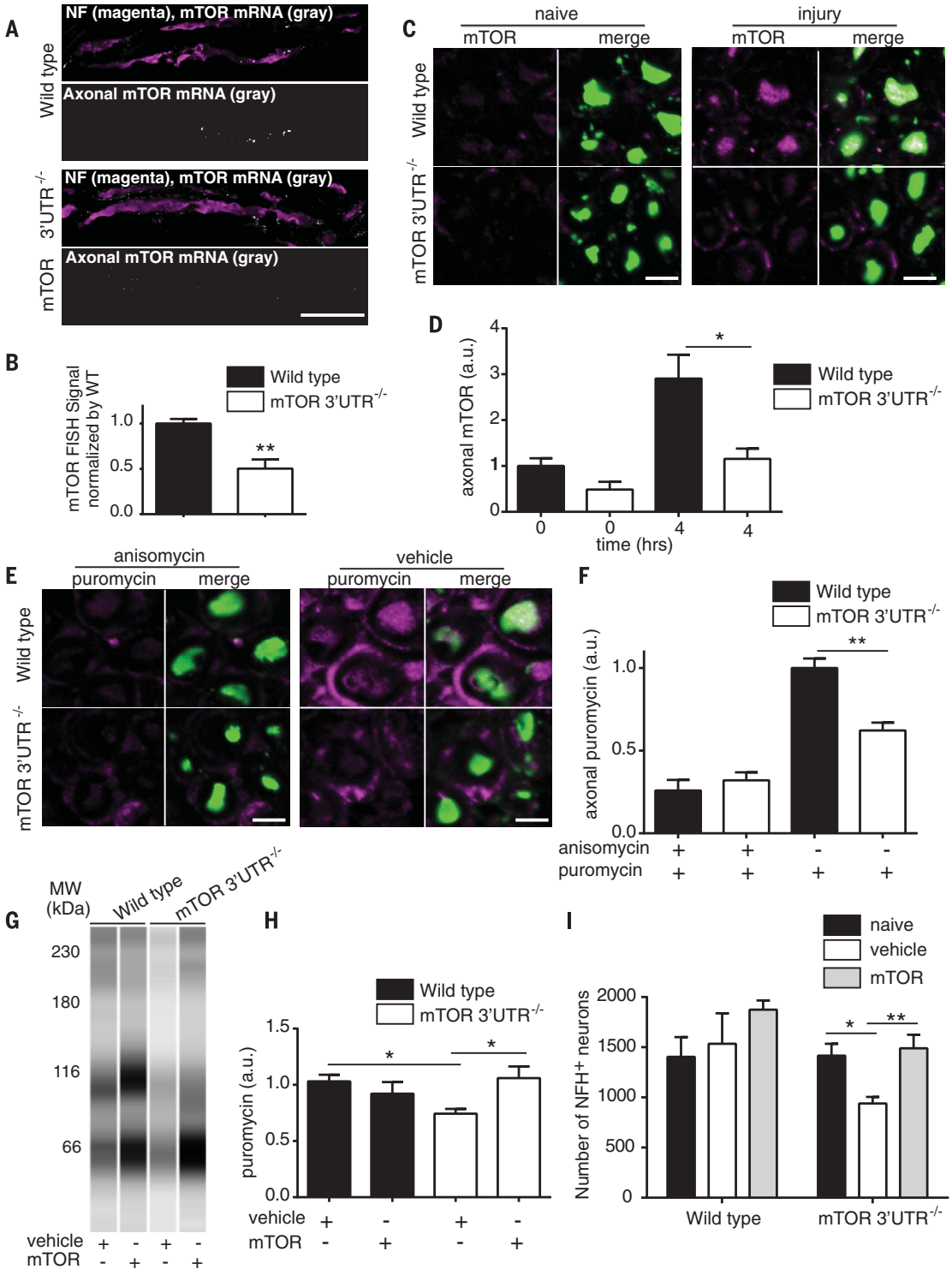

Fig. 4. Effects of mTOR 3′UTR deletion. (**A**) Representative, exposure-matched confocal images of FISH (Stellaris) for mTOR mRNA and neurofilament (NF) immunostaining from SN sections of wild-type and mTOR 3′UTR$^{-/-}$ mice. Upper panels show single optical planes for merged NFH and mTOR channels. Lower panels show single optical planes of mTOR mRNA pixels that overlap with NFH and were projected to a separate channel as "axon only" mTOR signals. Scale bar, 10 μm. (**B**) Quantification of (A) reveals a ~50% reduction in axonal mTOR in the 3′UTR$^{-/-}$ mice (n = 4; means ± SEM; $^{**}P < 0.01$; unpaired t test). WT, wild type. (**C**) SN segments from the indicated genotypes 4 hours ex vivo, sectioned and stained for NFH (green) and mTOR (magenta). Scale bars, 5 μm. (**D**) Quantification of (C) (n = 3; means ± SEM; $^{*}P < 0.05$; one-way ANOVA with Bonferroni's post-test). (**E**) SN segments from the indicated genotypes 2 hours ex vivo with anisomycin (200 μg/ml) or vehicle, followed by 1 hour with puromycin (100 μg/ml), then sectioned and stained as indicated. Scale bars, 5 μm. (**F**) Quantification of (E) (n = 3; means ± SEM; $^{**}P < 0.01$; one-way ANOVA with Bonferroni's post-test). (**G**) SN segments from wild-type and mTOR 3′UTR$^{-/-}$ mice not injected, injected with vehicle, or injected with 350 ng of mTOR protein were incubated in DMEM 2 hours ex vivo, followed by 1 hour of puromycin (100 μg/ml) treatment. A representative pseudoblot of puromycinylated proteins in SN axoplasm analyzed by capillary immunoelectrophoresis is shown. (**H**) Quantification of (G) (n = 4; means ± SEM; $^{*}P < 0.05$; one-way ANOVA with Bonferroni's post-test). (**I**) SNs from wild-type and mTOR 3′UTR$^{-/-}$ mice were injected with either vehicle or 350 ng of mTOR protein concomitantly with crush injury. L4 DRGs connected to the injured SN were harvested 7 days after injury, serially sectioned at 20-μm intervals, and stained for the proprioceptive marker NFH. Naive L4 DRG were also processed as a reference. Shown are the number of NFH-positive neurons per DRG (n = 4; means ± SEM; $^{*}P < 0.05$, $^{**}P < 0.01$; one-way ANOVA with Tukey's post-test).

neuronal physiology apart from injury, because localized changes in mTOR activity affect diverse processes, including viral latency (*28*), autophagy (*29*), and synaptic plasticity (*30*). Intracellular localization of mTOR at the protein level is well established in non-neuronal cells (*31*–*33*). mTOR localization at the RNA level provides an additional mode of spatiotemporal regulation of its pathways, with potentially broad physiological implications.

REFERENCES AND NOTES

1. V. Rangaraju, S. tom Dieck, E. M. Schuman, *EMBO Rep.* **18**, 693–711 (2017).
2. M. Terenzio, G. Schiavo, M. Fainzilber, *Neuron* **96**, 667–679 (2017).
3. S. Hanz *et al.*, *Neuron* **40**, 1095–1104 (2003).
4. R. B.-T. Perry *et al.*, *Neuron* **75**, 294–305 (2012).

5. J. Q. Zheng *et al*., *J. Neurosci.* **21**, 9291–9303 (2001).
6. C. J. Donnelly *et al*., *EMBO J.* **30**, 4665–4677 (2011).
7. D. Yudin *et al*., *Neuron* **59**, 241–252 (2008).
8. B. D. Fonseca *et al*., *Semin. Cell Dev. Biol.* **36**, 102–112 (2014).
9. K. K. Park *et al*., *Science* **322**, 963–966 (2008).
10. N. Abe, S. H. Borson, M. J. Gambello, F. Wang, V. Cavalli, *J. Biol. Chem.* **285**, 28034–28043 (2010).
11. X. Duan *et al*., *Neuron* **85**, 1244–1256 (2015).
12. W. Chen *et al*., *eNeuro* **3**, ENEURO.0358-16.2016 (2016).
13. K. F. Raab-Graham, P. C. Haddick, Y. N. Jan, L. Y. Jan, *Science* **314**, 144–148 (2006).
14. N. M. Sosanya *et al*., *J. Cell Biol.* **202**, 53–69 (2013).
15. M. J. Kye *et al*., *Hum. Mol. Genet.* **23**, 6318–6331 (2014).
16. N. G. Gracias, N. J. Shirkey-Son, U. Hengst, *Nat. Commun.* **5**, 3506 (2014).
17. O. Meyuhas, *Int. Rev. Cell Mol. Biol.* **320**, 41–73 (2015).
18. R. A. Saxton, D. M. Sabatini, *Cell* **168**, 960–976 (2017).
19. D. S. Smith, J. H. Skene, *J. Neurosci.* **17**, 646–658 (1997).
20. C. M. Forester *et al*., *Proc. Natl. Acad. Sci. U.S.A.* **115**, 2353–2358 (2018).
21. I. Rishal *et al*., *Dev. Neurobiol.* **70**, 126–133 (2010).
22. R. B. Perry *et al*., *Cell Rep.* **16**, 1664–1676 (2016).
23. V. Gandin *et al*., *Genome Res.* **26**, 636–648 (2016).
24. O. Meyuhas, T. Kahan, *Biochim. Biophys. Acta* **1849**, 801–811 (2015).
25. I. Rishal, M. Fainzilber, *Nat. Rev. Neurosci.* **15**, 32–42 (2014).
26. K. Ben-Yaakov *et al*., *EMBO J.* **31**, 1350–1363 (2012).
27. C. Andreassi, A. Riccio, *Trends Cell Biol.* **19**, 465–474 (2009).
28. M. Kobayashi, A. C. Wilson, M. V. Chao, I. Mohr, *Genes Dev.* **26**, 1527–1532 (2012).
29. D. Ebrahimi-Fakhari *et al*., *Cell Rep.* **17**, 1053–1070 (2016).
30. T. J. Younts *et al*., *Neuron* **92**, 479–492 (2016).
31. C. Betz, M. N. Hall, *J. Cell Biol.* **203**, 563–574 (2013).
32. Y. Sancak *et al*., *Cell* **141**, 290–303 (2010).
33. M. Ebner, B. Sinkovics, M. Szczygieł, D. W. Ribeiro, I. Yudushkin, *J. Cell Biol.* **216**, 343–353 (2017).

ACKNOWLEDGMENTS

We thank D. Gordon, N. Korem, A. Lin, N. Okladnikov, and E. Kanevskaya for excellent assistance; V. Kiss and V. Shinder for professional microscopy support; S. Ben-Dor for help with guide RNA design; R. Haffner-Krausz for mouse genome editing; and R. Rotkopf for statistical consultations. **Funding:** This work was supported by funding from the European Research Council (Neurogrowth, to M.F.), the Dr. Miriam and Sheldon G. Adelson Medical Research Foundation (to M.F., J.L.T., and A.L.B.), the Minerva Foundation (to M.F.), the Israel Science Foundation (1284/13 to M.F.), the Department of Defense Congressionally Mandated Research Program (W81XWH-2013-1-308 OR120042 to J.L.T. and M.F.), the National Institutes of Health (R01-NS041596 to J.L.T. and GM103481 to A.L.B.), and the Company of Biologists (*Journal of Cell Science* travel grants to I.K. and N.S.). M.T. was supported by a Koshland senior postdoctoral fellowship. M.F. is the incumbent of the Chaya Professorial Chair in Molecular Neuroscience at the Weizmann Institute of Science. J.L.T. is the incumbent of the SmartState Chair in Childhood Neurotherapeutics at the University of South Carolina. **Author contributions:** M.F. and M.T. designed the study. M.T., S.K., N.S., I.R., Q.Z., P.K.S., A.U., L.M., J.A.O.-P., C.G., A.L.K., A.D.P., R.B.-T.P., E.D.-M., and I.K. performed experiments and data analyses. Q.Z., C.F., A.U., and J.A.O.-P. carried out MS analyses. P.K.S., C.G., and A.L.K. conducted FISH analyses. I.R. performed electron microscopy. M.F., J.L.T., and A.L.B. supervised research. M.F. and M.T. wrote the initial manuscript draft. All authors revised the manuscript and approved the final version. **Competing interests:** None declared. **Data and materials availability:** All data needed to evaluate the conclusions of the paper are present in the paper and/or the supplementary materials.

SUPPLEMENTARY MATERIALS

www.sciencemag.org/content/359/6382/1416/suppl/DC1
Materials and Methods
Figs. S1 to S9
Tables S1 to S3
References (*34*–*51*)

5 March 2017; resubmitted 13 December 2017
Accepted 30 January 2018
10.1126/science.aan1053

Millipore®
Filtration, Separation
& Preparation

REFINED WITH YOU IN MIND

Stericup® Quick Release Filtration Systems

Work With Ease. Filter With Confidence.

Stericup® Quick Release Filtration Systems streamline your workflow with ergonomic design updates and safeguard your results with the proven performance of Millipore® membranes.

1. Quarter-Turn Quick Release Funnel Removal
2. Frosted Writing Surface
3. Lighter Color for Legibility
4. Click-Seal Confidence Cap

Explore New Features
SigmaAldrich.com/stericupquickrelease

The life science business of Merck KGaA, Darmstadt, Germany operates as MilliporeSigma in the U.S. and Canada.

MilliporeSigma

Quantum Laser Rangefinder

Smaller, Lighter, Farther, Smarter

Exclusive techniques for extremely weak light detection enable the emitted light and received light to share the same path of the telescope.

- 12m-3km range, 0.1m accuracy
- 32mm object lens, 8x magnification
- Height, speed, and angle measurement
- OLED display, blue tooth

Our final goal is to develop single-photon laser rangefinders. Meanwhile we are studying particle teleportation, especially in superconductivity and superfluidity (Y. Wei, Phys. Rev. E **93** (2016), 066103). Cooperation is welcome. We believe that the time for quantum technique is coming soon. Within 5 years from now, anyone who wins a Noble Prize in Quantum Physics may come to our company to obtain a reward of the same amount.

Wanjun Zhang
Inventor & President

Let quantum serve you.

DYX International Inc.

One World Trade Center

www.dyxint.com

info@dyxint.com

Yuchuan Wei
Chief Scientist & CEO

INAUGURAL AACR INTERNATIONAL MEETING

ADVANCES IN MALIGNANT LYMPHOMA:

MAXIMIZING THE BASIC-TRANSLATIONAL INTERFACE FOR CLINICAL APPLICATION

In Cooperation with the International Conference on Malignant Lymphoma (ICML)

June 22-26, 2018
Boston Marriott Copley Place | Boston, MA

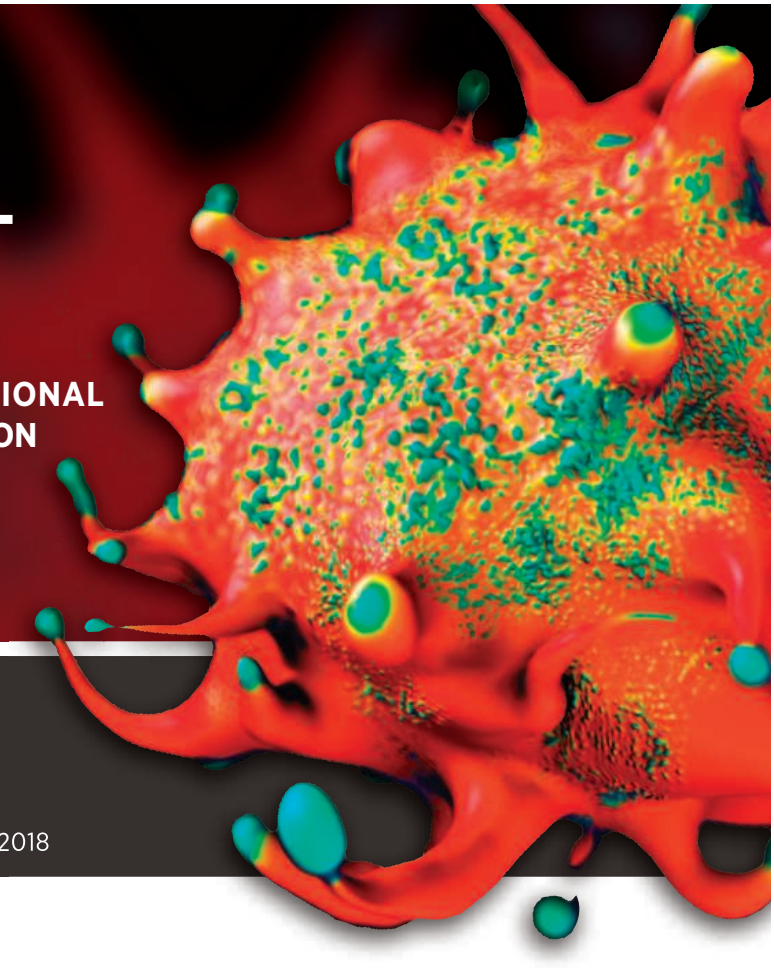

Abstract Submission and Clinical Trials Placeholder Deadline: Friday, April 6, 2018

Deadline to Submit Final Placeholder Clinical Trials Data: Friday, May 4, 2018

Advance Registration Deadline: Friday, May 11, 2018

SCIENTIFIC COMMITTEE CHAIR

Ari M. Melnick, MD
Gebroe Family Professor of Hematology/Oncology
Departments of Medicine and Pharmacology
Weill Cornell Medical College, New York, NY

ABOUT THIS MEETING

We invite you to register and submit an abstract for the Inaugural AACR International Meeting: Advances in Malignant Lymphoma: Maximizing the Basic-Translational Interface for Clinical Application, which is being held in cooperation with the International Conference on Malignant Lymphoma (ICML).

This must-attend program will provide a unique forum for interactive discussion and brainstorming among basic scientists, translational researchers, clinical investigators, hematologists, radiotherapists, pediatric oncologists, pathologists; and computational and systems biologists, and patient-advocates about how recent advances and emerging areas of lymphoma research hold enormous potential for transforming clinical care.

The AACR is the first and largest professional organization in the world dedicated to conquering all cancers, both solid tumors and blood cancers, and this inaugural lymphoma meeting serves as the launching point for an increased focus on lymphoma and related lymphoid malignancy programs presented by the AACR.

Continuing Medical Education (CME) Activity–*AMA PRA Category 1 Credits™*

Learn more and register at
AACR.org/Lymphoma18

#AACRLYMP18

AACR American Association for Cancer Research®
FINDING CURES TOGETHER®

Enzo

Step Up Your Game

CYTO-ID® Autophagy 2.0 Kit

Visit Us at AACR, Booth #1048

Why Transfect…When You Can Simply Detect?

Rapidly Quantify Autophagy Without Transfection

CYTO-ID Autophagy Detection Kits are the simplest, most specific fluorescent assays for quantifying autophagy in live cells. The CYTO-ID Kits include a unique cell-permeable dye that selectively stains pre-autophagosomes, autophagosomes, and autolysosomes, with minimal staining of lysosomes.

No Transfection Needed – Our cell-permeable dye detects autophagosomes and autolysosomes in 100% of cells without transfection or selection

Rapid Staining – Eliminates need for time and effort-consuming transfection efficiency validation

Study Intact Pathways – Monitor autophagy in homogeneous cell populations without overexpressing LC3

Low Background – Minimize non-specific staining seen with MDC and other dye-based methods

Fully Quantitative – Quantify changes in autophagy by flow cytometry and microscopic imaging platforms

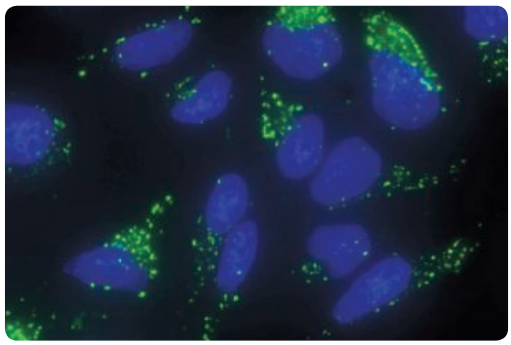

Autophagic vesicles stained with CYTO-ID Autophagy Dye in HeLa cells induced by starvation.

Microscopy | Flow Cytometry | Microplate Reader

scientists ***enabling*** scientists™

www.enzolifesciences.com/autophagy

Student E-poster Competition Winners

The 2018 Student E-poster Competition took place at the AAAS Annual Meeting in Austin on February 17-18. The winners' work displayed originality and understanding that set them apart from their peers. The 2019 AAAS Annual Meeting poster entry site will open in July 2018.

BRAIN AND BEHAVIOR

Winner: Christopher Tokita, Princeton University
Towards Complex Societies: Division of Labor Helps Early Social Groups Succeed

Honorable Mention: Gabriella Cabrera-Brown, Arizona State University
Abrupt Nicotine Reduction Increases Essential Value of Nicotine and Exacerbates Reinstated Nicotine Seeking

CELLULAR AND MOLECULAR BIOLOGY

Winner: Melody Tan, Rice University
Optical Imaging for Improved Oral Cancer Diagnosis at the Point of Care

Honorable Mention: Kimberley Kissoon, University of Houston, Downtown
Density-Dependent Colony Expansion of Socially Motile Myxococcus Xanthus Cells is Driven by Exopolysaccharides

Honorable Mention: Oluwaseun Adegbite, University of California, Irvine
Widespread Blatem-1b Locus within Flexible Multidrug Resistance Region in an Environmental Escherichia Coli

DEVELOPMENTAL BIOLOGY, PHYSIOLOGY AND IMMUNOLOGY

Winner: Caitlin Short, University of Wisconsin, Madison
Growth Cone Invadosome Formation and Function in Axon Growth and Guidance

Honorable Mention: Edward van Opstal, Vanderbilt University
The Genetic Basis of Host Suppression of a Maternally Transmitted Bacterium

Honorable Mention: Emily Bryant, University of California, Irvine
A Multiresistance Region Including Extended Spectrum B-Lactamase Antibiotic Resistance Genes in an Escherichia Coli Collected from an Aquatic Environment

EDUCATION

Winner: Ally Huang, Massachusetts Institute of Technology
Synthetic Biology Educational Kits Based on Cell-Free, Freeze-Dried Biomolecular Components

Honorable Mention: Michael McClellan, Massachusetts Institute of Technology
Investigating Meteorological and Anthropogenic Effects on Urban Air Quality

ENVIRONMENT AND ECOLOGY

Winner: Jennifer Schlauch, The University of Texas at Austin
Microbial Communities Associated with the Social Paper Wasp Polistes Exclamans (Hymenoptera: Vespidae)

Honorable Mention: Danial Nasr Azadani, Texas A&M University-Corpus Christi
A Novel Bacteriophage for a Promising Viable Alternative in the Fight Against Antibiotic-Resistant Bacteria

MEDICINE AND PUBLIC HEALTH

Winner: Vasiliki Rahimzadeh, McGill University
Teaching the Blockchain to Facilitate Learning Primary Healthcare Systems

Honorable Mention: Norah Ashoura, The University of Texas at Austin
The Force Awakens: Illuminating the Role of Kynurenine in Cancer Progression and Treatment

Honorable Mention: Glenn Guardamondo, University of California, Irvine
Poly(Lactide-Co-Glycolide) and the Innate Immune Response Following a Spinal Cord Injury Drives Human Neural Stem Cell Fate

PHYSICAL SCIENCES

Winner: Yujin Cho, The University of Texas at Austin
Study of Nonlinear Optical Properties of Indium Selenide Using Second Harmonic Generation Microscopy

Honorable Mention: Jia Hui Li, Columbia University
High-Performance Porphyrin-Based Dye-Sensitized Solar Cells with Iodine and Cobalt Redox Shuttles

Honorable Mention: Samantha M. Powell, University of Oklahoma
Formation of Myoglobin-Nitroso Adducts from Amine- and Nitro-Containing Drugs

SCIENCE AND SOCIETY

Winner: Rachel Damiani, University of Florida
Relating to Researchers: How Citizen Scientists Invest in Learning the Language of Science

Honorable Mention: Victor Rodriguez, University of Central Florida
A Look at Nanomedicine Clinical Trials in Comparison to Disability-Adjusted Life Year (DALY)

Honorable Mention: Alexis Darby, Arizona State University
Tuberculosis in Arizona: An Examination of its Effects on Communities, Infrastructure, and Health from 1890 to 2010

SOCIAL SCIENCES

Winner: Charlotte Till, Arizona State University
Environmental Perceptions and Their Place within Migration Decision Frameworks: Analysis from At-Risk Locations Along the US Gulf Coast

Honorable Mention: Cyrus Hester, Arizona State University
Economic, Climatic, and Geographic Drivers of Urban Water Demand in Arizona, 1991 –2011

TECHNOLOGY, ENGINEERING AND MATH

Winner: Rileigh Bandy, The University of Texas at Austin
Investigating Global Optimization Methodology

Honorable Mention: Sam Aminfard, The University of Texas at Austin
Multi-Layered Spatial Methodology for Assessing the Technical and Economic Viability of Using Renewable Energy to Power Brackish Groundwater Desalination

Waseda University pushes forward with global academic network

Innovative programs and prioritized funding have propelled Waseda University to record highs in world university rankings, underscoring the university's reputation for openness, dynamism, and diversity.

Japan's top-notch university in sport sciences promotes healthier lifestyles

—Health Promotion: The Joy of Sports and Exercise

Waseda University has played a leading role promoting Japanese sports since its founding. The university produced Japan's first Olympic gold medalist in 1928. This legacy is carried on by student athletes and alumni, such as internationally known swimmers Ippei Watanabe and Natsumi Hoshi; and figure skaters Yuzuru Hanyu and Shizuka Arakawa. Notably, 24 of these athletes competed at the Rio 2016 Olympic and Paralympic Games, bringing home six medals. "Our athletes are now training for the 2020 Tokyo Games," says **Toshimasa Yanai, head of the Health Promotion: The Joy of Sports and Exercise Unit.**

Waseda's global presence in sports is not limited to competition. Based on statistics published by the 2017 Quacquarelli Symonds (QS) World University Rankings, the university ranked 1st in Japan and 19th in the world in sports-related subjects including health and sport sciences.

"Japan faces challenges in terms of physical and mental well-being issues, for example, inactivity among children and the increasing number of elderly people who require nursing care," explains Yanai. "The goal of our unit is to promote healthier lifestyles by establishing a global center in education and research for the field of health and sport sciences."


Toshimasa Yanai

On an academic level, the unit is trying to achieve this through its newly established, English-based Master's course focusing on health and exercise sciences, and sport management, scheduled to start in September 2018. Yanai says that Waseda is not only looking for highly motivated students for the program, but is also recruiting international staff to teach and conduct research for the program.

"Most of the faculty members of this unit studied abroad for their doctorates," adds Yanai. "We want to use their experience to play a greater global role in sport sciences, and investigate ways to help solve various health-related issues that affect people of all ages."

Health Promotion: The Joy of Sports and Exercise Unit
www.waseda.jp/inst/sgu/en/unit/health-promotion

For reconciliation and sustainable development in East Asia

—Global Asia Studies

"World leaders and academics have resolved major conflicts in Southeast Asia and Africa, but there are hardly any such initiatives in East Asia," says **Naoyuki Umemori, head of the Global Asia Studies Unit.** "The goal of this unit is to establish interdisciplinary approaches on reconciliation and sustainable development in East Asia, and disseminate our results globally."


Naoyuki Umemori (left) and Kazuo Kuroda (right)

But why is Waseda University leading such activities? "Waseda was founded in 1882 by Shigenobu Okuma, a Japanese politician and former prime minister," explains **Kazuo Kuroda, deputy faculty of the unit.** "Good citizenship and making contributions to peace and prosperity in Asia were central to his vision for the university. Through this unit, we are implementing our tradition of promoting peace and harmony in 21st-century East Asia."

The unit offers courses taught by experts with backgrounds including history, economic development, media studies, and international law. Because attaining reconciliation in East Asia is a challenging and multifaceted task requiring intricate management skills as well as genuine support and understanding from participating institutes overseas, Umemori and Kuroda have established partnerships with institutes including Korea University, Nanyang Technological University, National Taiwan University, Peking University, the Harvard-Yenching Institute, and the Université libre de Bruxelles.

"There is increasing, genuine interest in this area of research," says Kuroda. "We will undertake the development of individuals contributing to resolve various problems facing the world today, [who are] rooted in the university's long-standing tradition and experience."

Global Asia Studies Unit
www.waseda.jp/inst/sgu/en/unit/global-asia-studies

Light
your way.

Get the full picture with trusted tumor immune response results from our in-house validated antibodies.

When it comes to your tumor immune response research, blind spots are unacceptable. Independent testing has demonstrated that 75% of antibodies in today's market are non-specific or simply do not work at all.* But at Bethyl, we've manufactured and validated every antibody we make on site to ensure target specificity and sensitivity. All to guarantee our antibodies will function as designed in your assay 100% of the time. More than 10,000 independent citations over the past 15 years have proven that, at Bethyl, we put a lot in every drop.

See our data at bethyl.com/immuno-oncology

**Weller, MG, Analytical Chemistry Insights:11, 21-27 (2016).*

Antibodies shown: Rabbit anti-PD-L1 (red, A700-020) & Lamin-A/C (green, A303-430A) in FFPE lung.

BETHYL
LABORATORIES, INC

Really Good Antibodies

eppendorf

The Next Benchmark

The new refrigerated Centrifuge 5910 R

The Centrifuge 5910 R sets the next benchmark in versatility, capacity and user convenience.

Its main swing-bucket rotor holds both conical tubes and plates – no need to change rotor buckets or adapters. This improves handling and saves time.

> Max. capacity: 4 x 750 mL or 36 x 50 mL conical
> Excellent rotor versatility
> Modern operating system with outstanding functionality
> Advanced temperature management that keeps your samples safe

www.eppendorf.com/next-benchmark

eppendorf & Science

PRIZE FOR NEURO BIOLOGY

2017 Winner
Flavio Donato, Ph.D.
Kavli Institute
Norwegian University of
Science and Technology

For research on how neural networks mature during development to represent space in the brain

Application Deadline
June 15, 2018

Call for Entries

Eppendorf & Science Prize for Neurobiology
The annual Eppendorf & Science Prize for Neurobiology is an international award which honors young scientists for their outstanding contributions to neurobiological research based on methods of molecular and cell biology. The winner and finalists are selected by a committee of independent scientists, chaired by *Science's* Senior Editor, Dr. Peter Stern. To be eligible, you must be 35 years of age or younger.

As the Grand Prize Winner, you could be next to receive
> Prize money of US$25,000
> Publication of your work in *Science*
> Full support to attend the Prize Ceremony held in conjunction with the Annual Meeting of the Society for Neuroscience in the USA
> 10-year AAAS membership and online subscription to *Science*
> Complimentary products worth US$1,000 from Eppendorf
> An invitation to visit Eppendorf in Hamburg, Germany

It's easy to apply! Learn more at:

www.eppendorf.com/prize

eppendorf Science AAAS

CURIOUS2018
FUTURE INSIGHT CONFERENCE

July 16-18 2018
Darmstadt, Germany

More than 30 top speakers
including five Nobel Laureates
Bruce Beutler · Fraser Stoddart · Harald zur Hausen · Jean-Marie Lehn · Joachim Frank

Healthy Lives
New breakthrough therapies and diagnostics

Material & Solutions
Chemistry and beyond

Bright Future
New ways of working and collaborating

Life Reimagined
Synthetic biology and beyond

Vibrant Digital
The power of in-silico

Apply now
Join the invite-only conference and apply now for a free ticket, deadline May 1st 2018, at **curious2018.com**

Sponsored by Merck KGaA, Darmstadt, Germany
at the occasion of the 350th anniversary

Merck KGaA
Darmstadt, Germany

R&D SYSTEMS
a bio-techne brand

GMP-Grade Growth Factors

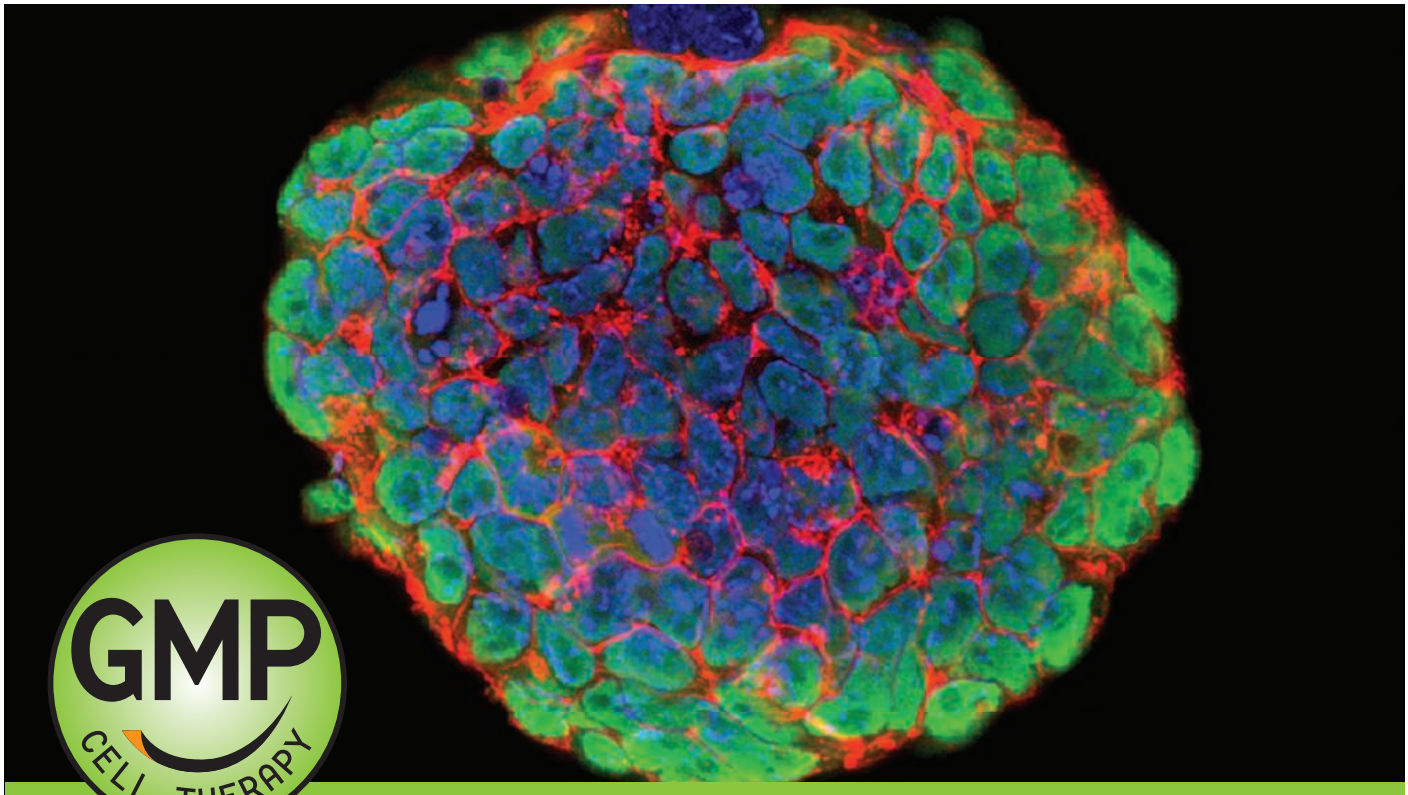

Dedicated to Consistent Proteins

The Widest Selection for

- Cell Manufacturing
- Immunotherapy
- Regenerative Medicine
- Stem Cell Therapy

Learn more | rndsystems.com/gmp

bio-techne®

Global bio-techne.com info@bio-techne.com TEL +1 612 379 2956 **North America** TEL 800 343 7475
Europe | Middle East | Africa TEL +44 (0)1235 529449 **China** info.cn@bio-techne.com TEL +86 (21) 52380373

Science Robotics | AAAS

The First Journal of Interdisciplinary Robotics Research

UPCOMING SPECIAL ISSUES IN 2018

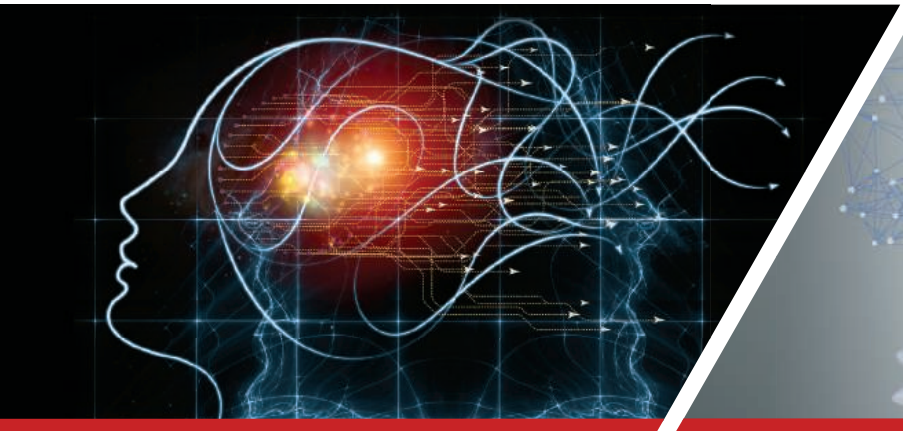

Social Robotics: Summer 2018

Learning—Beyond Imitation: Fall 2018

Submit Your Article for Publication in *Science Robotics*:

- Rapid review, scoop protection, and no article page limits.
- Exposure to an international audience, including 11,000 science journalists.
- Supportive and knowledgeable editorial staff.
- Promotion on the *Science Robotics* website and the potential for accompanying commentary or podcasts.
- AAAS social media and media relations support.

Learn more at **robotics.sciencemag.org**.
Send pre-submission inquiries to **sciroboteditors@aaas.org**.

Forensic DNA Grade Products

Human DNA contamination is one of the main concerns in forensic DNA analysis. Eppendorf Forensic DNA Grade products comply with the stringent requirements of the recently released ISO 18385, which specifies manufacturing requirements for products used in forensic DNA laboratories, to further minimize contamination risks. Eppendorf confirms compliance for every production lot and provides lot-specific certificates. Highly automated production lines and strict access controls are only two production conditions for Eppendorf Forensic DNA Grade consumables. Individually blistered packaging or mini-batches in resealable bags effectively protect against contamination and ensure error-free handling. The comprehensive approach of this product line assures excellent purity and performance levels. Forensic DNA Grade products from Eppendorf encompass DNA extraction, sample processing, and PCR setup as well as sample storage.

Eppendorf
For info: 800-645-3050
www.eppendorf.com/us-en

Flow Cytometer

The BD Accuri C6 Plus personal flow cytometer is a powerful benchtop tool for a variety of research applications from cancer biology to water testing, and from CRISPR/Cas to cell counting. BD Accuri products have been widely recognized with more than 7,500 citations. This easy-to-use, lightweight cell analyzer will help you advance your research quickly while staying within your budget. Its compact footprint and transportable weight make it a valuable tool for both novice and experienced researchers who want a cytometer that is readily available when and where they need it. The system features an intuitive software interface, software templates, and reagent kits that guide users new to flow cytometry through workflows for popular applications.

BD Biosciences
For info: 877-232-8995
www.bdbiosciences.com/us/instruments/s/accuric6

Entry-Level Flow Chemistry Systems

Available in a choice of configurations, the Uniqsis FlowLab range is an affordable flow chemistry system ideal for use in research, education, and for those wishing to try flow chemistry without the associated costs of a fully automatic system. The FlowLab system comprises two high-pressure pumps, a HotCoil coil reactor station, and the FlowLab system control computer. It can be controlled remotely by Wi-Fi, allowing the control computer to be conveniently operated outside the fume hood. FlowLab Cold includes the Polar Bear Plus Flow cryogenic module, which provides cooling down to –40°C without the need for liquid nitrogen or solid carbon dioxide (dry ice). FlowLab application software is highly intuitive and provides real-time control of the system. Programs can be designed and saved reactions run automatically, including priming and washing. FlowLab also automatically detects any modules that have been added to the system.

Uniqsis
For info: +44-(0)-845-864-7747
www.uniqsis.com/paproductsdetail.aspx?id=flowlab

Synthetic sgRNA

CRISPR application requires two key functional elements: target-specific guide RNA (gRNA) and the CAS9 enzyme. Scientists have created gRNA using multiple methods, such as transfection of gRNA-expression plasmids, in vitro transcription, or the annealing of short CRISPR RNA (crRNA) oligos with a transactivating crRNA (tracrRNA) scaffold. Recently, synthetic single-guide RNA (sgRNA) has been recognized as the preferred way for highly efficient and accurate editing. Origene's synthetic sgRNA is a pure 100-mer RNA oligo that contains the target gRNA sequence and the tracrRNA scaffold in a single entity. Our 100-mer sgRNA saves time by using a one-step protocol. It is more efficient (60%–80%) and consistent than in vitro–transcribed gRNAs, and is also cost-effective, being highly scalable for large numbers of experiments.

Origene
For info: 888-267-4436
www.origene.com/crispr-cas9/sgrna

Parallel Synthesizer

The DrySyn Octo 8-position parallel synthesizer is a convenient, entry-level product for chemists wishing to conduct synthetic reactions under an inert atmosphere with temperature control, reflux, and powerful magnetic stirring. It accommodates low-cost, consumable reaction tubes, each with a working volume of 5 mL–6 mL. The large surface area of these glass reaction tubes allows the DrySyn Octo to be used for air-cooled, gentle reflux reactions. Up to three units can be employed together on any standard magnetic hotplate stirrer, using a DrySyn MULTI baseplate. In this Octo-Plus configuration, users can perform 24 parallel reactions in a very small space. Gas-tight closure on each tube connection enables the instrument to carry out reactions under inert atmospheres. Additions or reaction sampling can be made under inert conditions using a syringe. The unit uses inexpensive stoppers that are easily replaceable and consumable.

Asynt
For info: +44-(0)-1638-781-709
www.asynt.com/product/drysyn-octo-reaction-station

Stain-Free Gels

Spend less time assessing proteins and more time discovering. Stain-free gels from Bio-Rad provide visual confirmation of protein purity and yield in minutes instead of hours, by combining the speed of stain-free gel chemistry with the high throughput of multidimensional chromatography on our NGC chromatography system. Researchers can use stain-free gels to quickly assess protein purity and molecular weight in as little as 25 minutes, identify which fractions to pool, and optimize chromatography runs.

Bio-Rad
For info: 510-724-7000
www.bio-rad.com

Electronically submit your new product description or product literature information! Go to www.sciencemag.org/about/new-products-section for more information.

Newly offered instrumentation, apparatus, and laboratory materials of interest to researchers in all disciplines in academic, industrial, and governmental organizations are featured in this space. Emphasis is given to purpose, chief characteristics, and availability of products and materials. Endorsement by *Science* or AAAS of any products or materials mentioned is not implied. Additional information may be obtained from the manufacturer or supplier.

want new technologies?

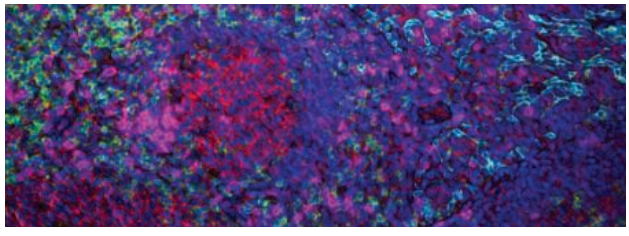

antibodies
apoptosis
biomarkers
cancer
cytometry
data
diseases
DNA
epigenetics
genomics
immunotherapies
medicine
microbiomics
microfluidics
microscopy
neuroscience
proteomics
sequencing
toxicology
transcriptomics

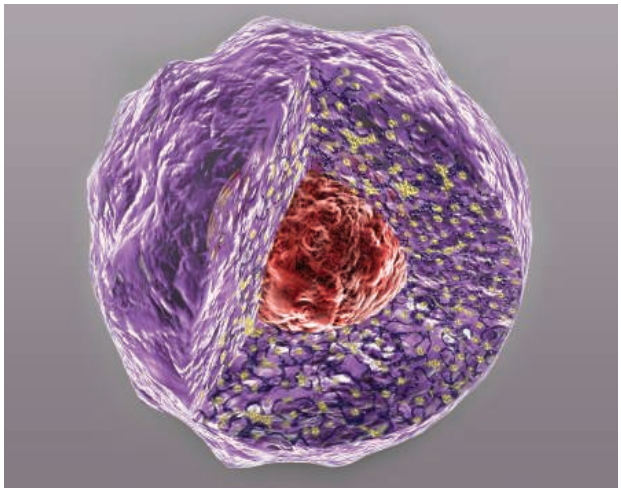

watch our webinars

Learn about the latest break-throughs, new technologies, and ground-breaking research in a variety of fields. Our expert speakers explain their quality research to you and answer questions submitted by live viewers.

VIEW NOW!
webinar.sciencemag.org

Science
AAAS

Brought to you by the *Science*/AAAS Custom Publishing Office

@SciMagWebinars

Everything in one place for your gene-based research?

Brilliant!

cDNA Clones · Lentivirus · CRISPR · Antibodies · Proteins · RNAi · Tissues

OriGene Technologies.

Supporting your path to discovery

We are committed to providing you with high quality products and services. With over 2 million off-the-shelf products, we are here to support your gene-based research and scientific discoveries.

Shop now at www.origene.com

ORIGENE

Science Careers

SCIENCE CAREERS ADVERTISING

For full advertising details, go to ScienceCareers.org and click For Employers, or call one of our representatives.

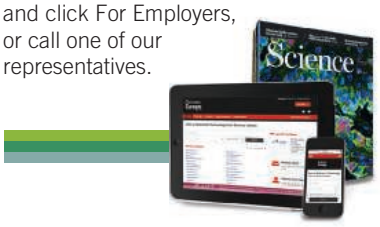

AMERICAS

+1 202 326-6577
+1 202 326-6578
advertise@sciencecareers.org

EUROPE, INDIA, AUSTRALIA, NEW ZEALAND, REST OF WORLD

+44 (0) 1223 326527
advertise@sciencecareers.org

CHINA, KOREA, SINGAPORE, TAIWAN, THAILAND

+86 131 4114 0012
advertise@sciencecareers.org

JAPAN

+81 3-6459-4174
advertise@sciencecareers.org

CUSTOMER SERVICE

AMERICAS

+1 202 326-6577

REST OF WORLD

+44 (0) 1223 326528

advertise@sciencecareers.org

All ads submitted for publication must comply with applicable U.S. and non-U.S. laws. *Science* reserves the right to refuse any advertisement at its sole discretion for any reason, including without limitation for offensive language or inappropriate content, and all advertising is subject to publisher approval. *Science* encourages our readers to alert us to any ads that they feel may be discriminatory or offensive.

ScienceCareers
FROM THE JOURNAL SCIENCE AAAS

ScienceCareers.org

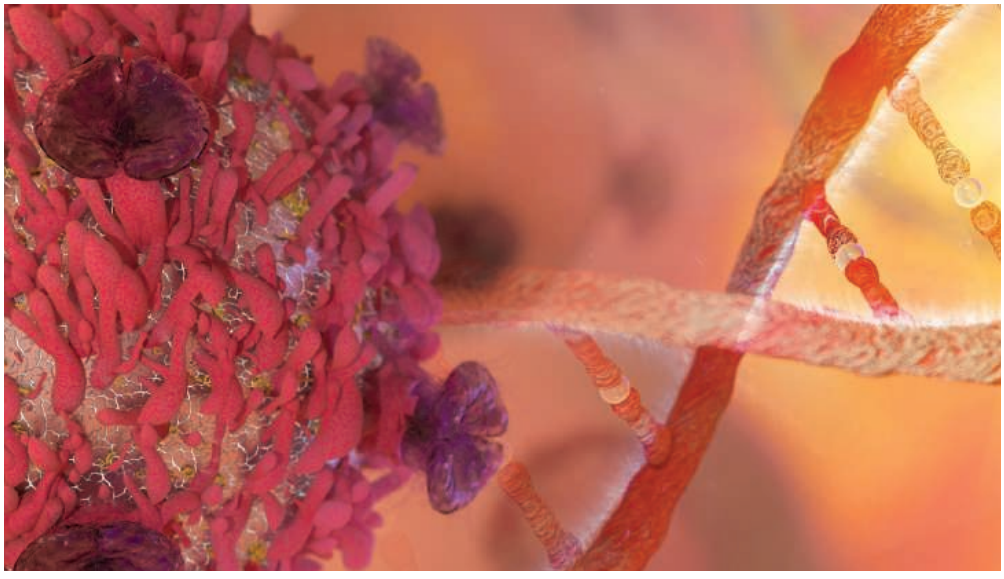

Timothy Chan

Cancer genomics and immunotherapy: Opportunities at the intersection

Clinical progress in cancer immunotherapy is driving career, collaboration, and leadership opportunities. Along with that progress comes a need for people with many different skills. Academic institutions, research hospitals, and life science companies large and small are seeking scientists who are fluent, or at least conversant, in fields such as genetics, oncology, immunology—and especially informatics. **By Chris Tachibana**

Eye-catching cancer immunotherapy headlines arrived in 2017 with nearly every season. In the spring, the U.S. Food and Drug Administration approved an antibody that is the first cancer therapy based on a tumor genetic biomarker instead of a location in the body. Summer and fall brought approval of chimeric antigen receptor (CAR) T-cell therapies for forms of leukemia and lymphoma. These attention-getting stories about cancer immunotherapy underline the vast career opportunities in academic, clinical, and industry research for those entering this field.

We're at a scientific crossroads, says physician-scientist **Timothy Chan,** director of the Immunogenomics and Precision Oncology Platform at Memorial Sloan Kettering Cancer Center in New York City. "Only a few years ago, cancer genomics and immunology were separate fields," he says. "That's changed with evidence that immunotherapy can work, and with the realization that cancer genomes and mutations influence how well it works." The result is the reinvigorated, integrated field of precision immuno-oncology. "It's one of the most fast-paced, active areas in cancer research," Chan says, "because it's at the intersection of fields, where breakthroughs happen."

Immuno-oncology is data-driven, creating a high demand for informaticians, says Professor **Zemin Zhang,** a principal investigator at the Beijing Advanced Innovation Center for Genomics, College of Life Sciences, Peking University. Since they often have many collaborators from diverse fields, Zhang says, "Bioinformaticians are in the best position to connect fields for truly novel findings."

Current landscape and new directions

Recent immunotherapy approvals are in two areas. Immune checkpoint blockade therapies use antibodies to counter the defensive tactics of tumor cells. CAR T cells target and kill cancer cells via bioengineered T-cell receptors. Much current research in immuno-oncology focuses on improving these treatments, for example, by finding new immunotherapy targets and identifying biomarkers that predict a patient's response.

We have a lot to learn about improving therapeutic effectiveness, Chan says: "Immunotherapy isn't magic. It's just another family of cancer therapies with rules that are still relatively undefined." In addition, since combination therapy that includes multiple immunotherapies and traditional chemotherapy and radiation looks clinically promising, researchers are working to develop new immunotherapy options based on completely novel strategies.

Chan's laboratory uses genomic analyses to identify neoantigens—novel peptides found only in tumors that arise from mutations accumulated by cancerous cells. According to Chan, neoantigens have two advantages: First, they look very foreign to the immune system and second, they don't appear in normal cells. The foreignness of neoantigens means therapies based on them could induce strong, specific antitumor responses. These responses should target only tumors and not normal tissues, resulting in low toxicity. Another focus in Chan's group is personalized vaccines that are based on neoantigens identified by sequencing a patient's tumor. cont.>

PHOTOS: (FROM LEFT) © CI PHOTOS/SHUTTERSTOCK.COM; MEMORIAL SLOAN KETTERING CANCER CENTER

Upcoming features

Faculty: Alternative funding resources—September 14 ■ Faculty: Moving a lab to another country—October 5 ■ Top employers survey—October 26


DISCOVER
SOMETHING
COURAGEOUS.
For 125 years, Merck has tackled the most serious health threats of their generations. Some have retreated. Others have become footnotes of history. Because we've been relentless about going to the unexplored places. Daring boldly on behalf of the world's people. That's science at its very best.
Join Merck, and discover something courageous. In you.
We have scientific opportunities at numerous sites in many therapeutic areas.
merck.com/careers
INVENTING FOR LIFE
MERCK
Merck is proud to embrace diversity in all its manifestations | EOE M/F/D/V

JOIN A GLOBAL FORCE IN CANCER RESEARCH

At **Cancer Research UK**, we bring together the world's best scientists and help you to tackle the biggest problems in cancer. We fund global research teams and partner with organisations around the world. Find out more about how we can work together.

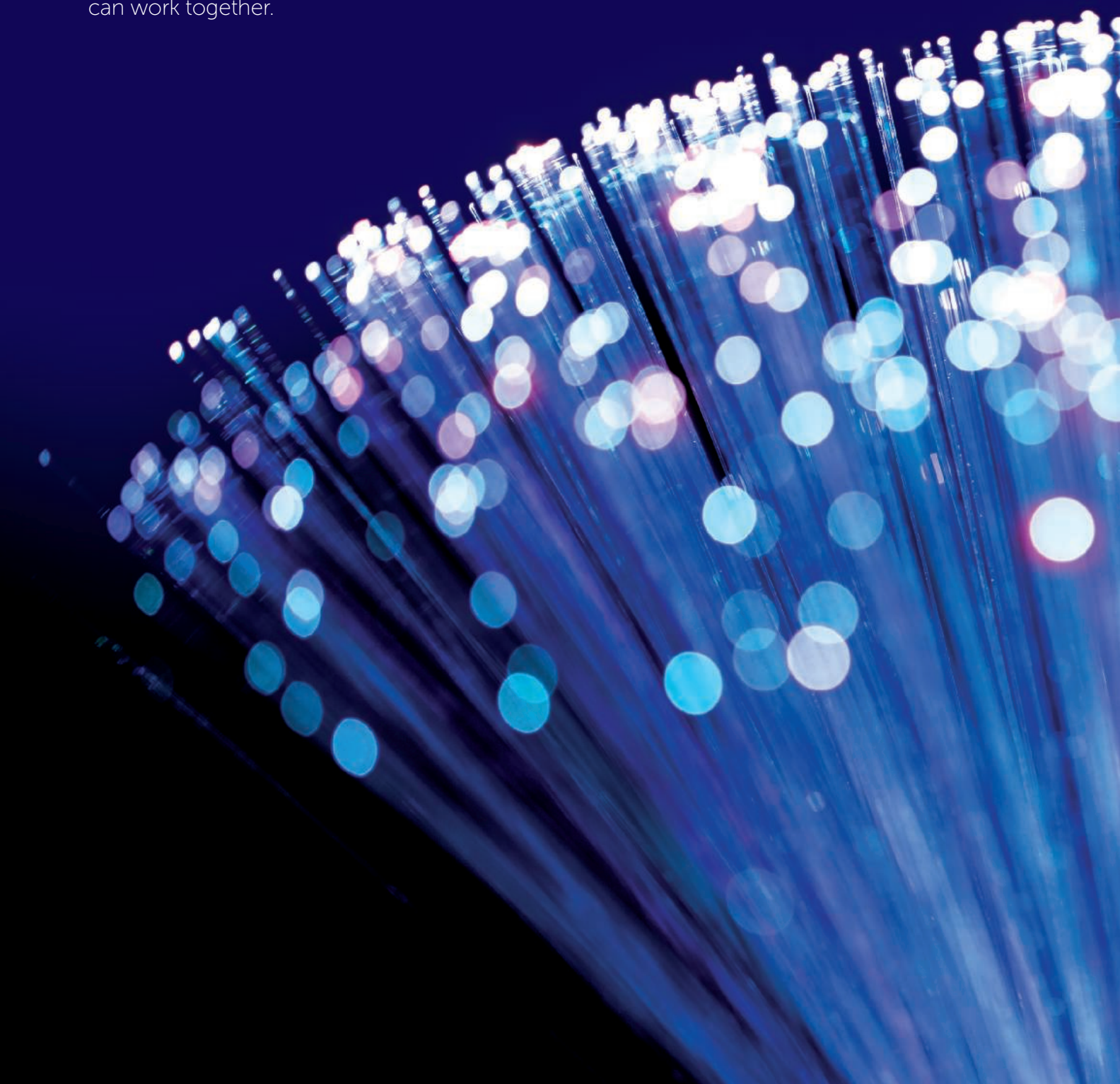

EXPLORE GREAT IDEAS WITH COLLABORATIVE SCIENCE AWARDS

Are you looking for freedom to take your research in new directions?

We invest in innovative ideas that advance our understanding of cancer and benefit patients. Here are some of the opportunities open to you outside of the UK:

Our $25m Grand Challenge is an ambitious international award aiming to solve cancer's toughest questions. We're looking for big, innovative ideas from multidisciplinary teams across the world. If you think you have what it takes to tackle a grand challenge, we want to hear from you. The next round will open in spring 2019.

Our $6.25m Catalyst Award brings together surveillance, early diagnosis, prevention, and clinical researchers on big-impact population research projects. PIs and co-investigators can apply from anywhere in the world. Expressions of interest re-open in August 2018.

In early detection research we're inviting researchers not currently working in cancer to apply your expertise to open up new frontiers in how early cancers and precancerous states are detected. The Fulbright Cancer Research UK Scholar Awards allow US researchers to pursue early detection cancer research in the UK.

Explore funding opportunities at cruk.org/science

ACCELERATE YOUR CAREER

Have you considered the UK?

From PhD to PI, we support researchers at every stage, and offer more than just funding for exceptional individuals from around the world.

Our research institutes and centres offer postdocs and students excellent training, working alongside outstanding people, as part of a powerful research network.

For the brightest scientists and physician scientists, our flexible fellowships offer a package of funding and personal support to develop your independent research group.

And for established researchers, our research institutes have tenure-track group leader positions supported by generous start-up packages.

Learn more at cruk.org/leaders-of-tomorrow

CANCER RESEARCH UK

"Targeted vaccines have a lot of promise," Chan says, "and could be used in combination with immune checkpoint inhibitors."

More precise application of immunotherapies and the development of new approaches requires knowing the detailed immune landscape of individual patients and tumors. Zhang's group is moving beyond bulk sequencing of tumor samples and is now conducting genomics on single cells. Tumor tissue is a diverse mix of cell types and states, so Zhang and others are characterizing the individual genomes, expression patterns, and mutational status of thousands of cells from a single tumor. By comparing the results to cells from paired normal tissue, researchers get a detailed molecular picture of the tumor environment, including the types and activity levels of T cells that are critical to the immunotherapy response. "Single-cell analysis is helping us find new genomic patterns and biomarkers that tell us the functional status of T cells associated with tumors," Zhang says. "This type of analysis is one of the most exciting developments in biomedicine. It will drive the study of cancer immunotherapy in the future."

Zhang's work aligns with what **Liselotte Brix** hears from cancer genomicists about leading-edge research in the field. Brix is chief scientific officer and cofounder of Immudex, a small company headquartered in Denmark that supplies reagents and tools for disease-specific T-cell research and diagnostics. "Researchers are using newer technologies to look directly into tumors," she says, "to make sure immunotherapies induce a response that works in the tumor." She says demand is high for biomarkers backed by clinical evidence, to determine which patients will likely respond to therapeutics and also to monitor treatment progress. To make their work more efficient, scientists are interested in developing multiplexed assays and clinical tests that provide information on several factors at once, such as T-cell type, specificity, and activation level. "The idea," she says, "is taking biomarkers from being merely tools for research to becoming a way to make immunotherapy more personalized."

Cancer genomics overall is becoming more translational, and is moving toward "bringing results to patients," says **Jean Claude Zenklusen.** He directs The Cancer Genome Atlas (TCGA), an initiative of the U.S. National Cancer Institute (NCI) and the U.S. National Human Genome Research Institute. For example, TCGA, with genomic data on 33 tumor types taken from samples from 11,000 patients, is finishing 2018 by publishing a series of papers and holding a symposium. Future resources from the NCI Center for Cancer Genomics (CCG), which oversees TCGA and other activities, will support more translationally focused research, including databases with genomic information on clinical samples linked to outcomes of their patient donors. CCG is also developing cell lines that are cultured to represent tumor behavior in vivo, and computational methods that will help researchers understand tumor behavior and apply the resulting data to diagnoses, treatments, and cures.

Catherine Sabatos-Peyton, Novartis Institutes for BioMedical Research

> Sabatos-Peyton recommends preparing for an industry career by "learning good basic research and scientific interrogation skills."

TCGA data, which has been the foundation of many immuno-oncology hypotheses and discoveries, will still be available for research. "TCGA is a valid model for a genomics resource," Zenklusen says, "but by no means juices the whole fruit." CCG will be 'squeezing' more clinically meaningful information out of cancer genomics, to understand at the molecular level how genes and mutations drive cancer and determine response to treatment. CCG will also continue its collaboration with the International Cancer Genome Consortium, Zenklusen says. Even small projects with other countries contribute important information on how genetic backgrounds and cultural factors such as diet affect cancer development, he adds. Global cancer genomics research also helps us understand geographical hotspots for certain tumor types.

Developing skills and finding a niche

Early career scientists have opportunities in basic and clinical research and in both small and large industries, Zenklusen says. Researchers who want to participate in large-scale projects like CCG initiatives should look at government and academic laboratories. To use genomics resources to benefit patients, consider research hospitals that do clinical trials, he advises; to turn discoveries into diagnostic tools and medicines, look for opportunities in the life science industry.

Catherine Sabatos-Peyton endorses an industry career for the rewards of seeing scientific discoveries translate into clinical practice. She studied T cells, including the role of a checkpoint inhibitor, for her Ph.D. and postdoctoral projects and at a startup company that was acquired by Novartis. She is now a director in Exploratory Immuno-Oncology at the Novartis Institutes for BioMedical Research (NIBR), where she relies on her basic research background. Her team works on new immune-modulating therapies. Their approach is to make a detailed exploration of tumors. "We're interrogating the tumor microenvironment," she says, "by looking at suppressive cues as well as cells and secreted proteins that protect tumors from the immune response."

NIBR is similar to an academic setting, Sabatos-Peyton says, because scientists do in-depth, foundational research on a topic, for example the validity of a potential therapeutic target. But sometimes, they also have the privilege of seeing a therapy they worked on go to clinical trials or even to patients.

When hiring, Sabatos-Peyton looks for scientists with deep knowledge in their field and an ability to apply that knowledge to translational research. Novartis uses a collaborative model with teams of people from many disciplines—including genetics, immunology, informatics, and chemistry—so Sabatos-Peyton recommends preparing for an industry career by "learning good basic research and scientific interrogation skills." Early career scientists can get industry experience through the NIBR postdoctoral program. The goals are the same as an academic postdoc, she explains: "To publish and establish an independent body of work." NIBR cont.>

PHOTO: NOVARTIS


Ph.D. students and postdocs in the Zemin Zhang lab

PHOTO: PEKING UNIVERSITY STAFF

Featured participants

Center for Cancer Genomics
www.cancer.gov/about-nci/organization/ccg

Immudex
www.immudex.com

Immunogenomics and Precision Oncology Platform, Memorial Sloan Kettering Cancer Center
www.mskcc.org/research-areas/programs-centers/immunogenomics-and-precision-oncology-platform

Novartis Institutes for BioMedical Research
www.novartis.com/our-science/novartis-institutes-biomedical-research

Peking University
english.pku.edu.cn

The Cancer Genome Atlas
cancergenome.nih.gov

U.S. National Cancer Institute
www.cancer.gova

postdocs either continue in industry or return to academia, she says. For established immuno-oncology researchers, academic–industry partnerships are an opportunity to move findings closer to clinical applications.

Sabatos-Peyton says immuno-oncology will offer career opportunities for years to come. "The clinical success is exciting," she says, "but still limited. We have so much more biology to understand when it comes to immunotherapy and patient response at a molecular level."

For all scientists, Zenklusen recommends getting solid, basic science training. Don't specialize too early, he cautions, because science is constantly changing thanks to emerging new technologies, discoveries, and even research fields. Adaptability is a strength, as Zenklusen's own career shows. He trained as a chemist, but says, "Whatever techniques I learned 20 years ago are prehistoric." The most important factor in education is a reliable scientific foundation that can be applied to any field, he says: "Generalists can move from one area to another."

Zenklusen was not the only expert to promote flexibility through moving between different fields. Zhang says multifunctional team members who can take samples from wet-lab assays to dry-lab data analysis are increasingly valued for their varied skill sets. "The next wave of researchers," he says, "is versed in two languages, biological and computational." Zenklusen agrees. "You don't have to be an expert in every facet of cancer genomics," he says, "but you need to be conversant."

Scientists in small companies need to be exceptionally versatile, Brix says. Immudex researchers must understand not only the scientific details about the products they are developing, but also the process of bringing those products to market, including manufacturing, marketing, and costs. "Industry needs creative scientists who can overcome challenges throughout the development process," she says.

At a small company, people wear many hats, Brix notes: "One moment I'm talking with scientists about new research and the next, I'm working on marketing, sales, or regulatory issues." Scientists at big companies don't usually worry about these issues because specialists or entire departments handle these matters. However, Brix says, "At a small company, you have more direct influence on the products that reach the market"—although you also might have to take out the garbage, she jokes.

For young scientists interested in industry, Brix suggests a student internship or part-time job at a small company. "It's a good way to find out if you're comfortable with the constantly changing environment," she says. If you want to run your own company, she says, "Just start. You need money and protection for your idea and a business development plan. If you need to, find a partner who can help with those areas."

Preparing for the future: Embrace new technologies and data

Regardless of career path, one thing is certain: New technologies will continue to bring more and different types of data to cancer genomics and immunotherapy. "Being able to deal with a lot of data is critical," Chan emphasizes. Students and postdocs should use their training time to get wide-ranging experience with large-scale data. "In translational work," he says, "the more tools and experiences you can add during training, the better." Get familiar with data-analysis methods, he advises, and with best practices such as how to normalize data properly. Scientists who are no longer trainees can learn genomic analyses on the job by trying out the tools of the trade, interacting with colleagues (e.g., in genomics core facilities), and taking short courses and workshops.

Scientists who anticipate technological advances and think about how to apply the data they generate are positioned for a career of discoveries, Zhang says. "As an informatics person, I'm banking on new technologies coming along that will generate tons of data." Being able to quickly process and add new data to existing information positions a scientist to see patterns, similarities, and differences in a way that advances the field. "Our best projects combine data from different technologies," he says.

Zhang has noticed a keen interest in people with dual experience in biology and informatics. He often gets calls from recruiters looking for bioinformaticians. "They call from everywhere," he says, "big pharma, small startups, clinical labs, and research teams. Researchers with biology and computational expertise are in high demand, and in a position to take leadership roles," he says. "If you go for an informatics career, you have a bright future ahead of you."

Chris Tachibana is a science writer based in Seattle, USA, and Copenhagen, Denmark.

POSTDOC AND YOUNG INVESTIGATOR **OPPORTUNITIES**

SÃO PAULO
Brazil

The São Paulo Research Foundation (FAPESP), one of the leading Brazilian agencies dedicated to the support of research, has ongoing programs and support mechanisms to bring researchers from abroad to excellence centers in São Paulo.

MORE INFORMATION

YOUNG INVESTIGATOR AWARDS
www.fapesp.br/yia

POSTDOC
www.fapesp.br/en/postdoc

FAPESP
SÃO PAULO
RESEARCH FOUNDATION

WWW.FAPESP.BR/EN

FOCUS ON CANCER RESEARCH

Penn Dental Medicine

FACULTY POSITION
UNIVERSITY OF PENNSYLVANIA

The Microbiology Department in the School of Dental Medicine is seeking an outstanding scientist for a tenure-track/tenured position at the Assistant, Associate or Professor level. The position is for basic and translational work in Head and Neck Cancers. Research areas of interest include virology, immunology and tumorigenic mechanisms. The appointment requires a strong record of research productivity, extramural funding and excellence in teaching. The candidate is expected to teach modern aspects of cancer biology and immunology to dental students, establish a vigorous research program that will enhance interactions with world-renowned cancer research faculty at UPENN and be involved in graduate student training.

The candidate must be a PhD., DMD or MD. Applicants should apply online at: **http://facultysearches.provost.upenn.edu/postings/1082** and include a curriculum vitae with publications and a statement of research interests.

The University of Pennsylvania is an Affirmative Action/Equal Opportunity Employer. All qualified applicants will receive consideration for employment and will not be discriminated against on the basis of race, color, religion, sex, sexual orientation, gender identity, creed, national or ethnic origin, citizenship status, age, disability, veteran status, or any other characteristic protected by law. Minorities/Women/Individuals with disabilities/Protected Veterans are encouraged to apply

POSITIONS OPEN

Director Position

Institute of Molecular Biology
Academia Sinica, Taiwan

Academia Sinica, Taiwan, invites applications and nominations for the position of Director of Institute of Molecular Biology (IMB). The initial appointment is for a period of three years (renewable for a second term), and will also carry the title of Research Fellow.

As the pre-eminent academic institution in Taiwan, Academia Sinica is devoted to basic and applied research in mathematics and physical sciences, life sciences, and humanities and social sciences. IMB, consisting of 36 laboratories, engages in research leading to the better understanding of biological processes at the molecular and cellular level. Current efforts focus on the study of protein complexes, gene expression and transmission, signal transduction and organismic development, with special interests in the problems of neuroscience, chromosome organization, immunology and plant biology. IMB is well funded and equipped with modern research facilities. It maintains a high research standard with an excellent publication record. For details about Academia Sinica and IMB, please consult the website: http://www.sinica.edu.tw

Interested candidates should have a PhD or equivalent degree, with outstanding research accomplishments and demonstrated leadership experience. Besides conducting a vigorous research program, the successful candidate is expected to build on the existing strengths of the institution, develop new research thrusts, promote basic biological sciences and provide intellectual leadership in relevant basic and applied life sciences in Taiwan.

Applications and nominations, including complete curriculum vitae, a publication list, and three letters of recommendation, should be submitted to **Director Search Committee, Institute of Molecular Biology, Academia Sinica, 128 Academia Road, Section 2, Nankang, Taipei 115, Taiwan** or by Email to: **mwang@gate.sinica.edu.tw**. Screening of applications/nominations will begin immediately, and will continue until the position is filled.

POSITIONS OPEN

Columbia University
Vagelos College of Physicians and Surgeons

Assistant Professor – Research Scholar

The Vagelos College of Physicians and Surgeons is seeking one or more outstanding scientists in the Biomedical Sciences for appointment at the inaugural College of Physicians and Surgeons Research Scholar. These assistant professor positions are limited to MD, PhD, or MD-PhD researchers who have, in general, 4 years or less of post-doctoral fellowship and who have demonstrated exceptional ability, creativity and productivity as reflected in first or senior authored publications in leading scientific journals. Applicants who do not meet these criteria should not apply.

There is no limitation regarding the field of research. Appropriate departmental affiliation will be decided after selection. Adequate start-up funds, space, and mentorship will be provided. Priority will be given to applicants outside Columbia University.

Applicants should provide 3 names of references and a proposed plan for their work over the next five years with the application.

To apply please visit: https://academicjobs.columbia.edu/applicants/Central?quickFind=66057 or search by requisition number 0008603.

Columbia University is an Equal Opportunity/Affirmative Action employer Race/Gender/ Disability/Veteran.

RECRUITING TALENTS AT HOME AND ABROAD IN SOUTHEAST UNIVERSITY

Southeast University (SEU) is one of the national key universities administered directly under the Central Government and the Ministry of Education of China. It is also one of the universities of Project 211 and Program 985 that is financed by the Central Government to build as a world-class university, and has become a comprehensive and research-oriented university featuring the coordinated development of such multi-disciplines as science, engineering, medicine, literature, law, philosophy, education, economics, management, art, etc., with engineering as its focus.

In 2017, Southeast University was selected as a Class A first-class university building university with a total of 11 top-level disciplines including: Materials Science and Engineering, Electronic Science and Engineering, Information Science and Engineering, Control Science and Engineering , Computer Science and Engineering, Architecture, Civil Engineering, Transportation Engineering, Biological Science and Medical Engineering, Landscape Architecture, Art Theory, etc., occupying the 8th place in terms of the number. In the fourth round of discipline evaluation organized by the degree and postgraduate education development centers of the Ministry of Education, there are 5 A+ disciplines, which are Architecture, Civil Engineering, Transportation Engineering, Biological Science and Medical Engineering, Art Theory. The number of A + disciplines tied the country's 8th place. According to the latest published ESI discipline rankings, the 11 disciplines of Engineering Science, Computer Science,Materials Science, Mathematics, Physics, Chemistry, Clinical Medicine, Biology and Biochemistry, Pharmacology & Toxicology, Neuroscience and Behavioral Science, Social Science rank among the first 1% of global ESI database, with Engineering Science ranking 32th and Computer Science ranking 35th, both of which ranking among the first 1‰ of global ESI database . In USNews2017 engineering college rankings of the world, SEU ranked 7th in mainland of China, 23 of the world.

Southeast University is now facing a long and open recruitment of high-level talent and full-time teachers at home and abroad, warmly welcomes the outstanding talents at home and abroad!

1. Chang Jiang Scholars Program for Distinguished Professor

Requirement:

1) Applicants specialized in natural sciences, engineering and technical should be less than 45 years old, applicants specialized in humanities and social sciences should be no more than 55 years old.
2) Applicants should be associate professor or higher position in high-level university overseas.
3) Continuous work in school for 5 years.

Treatment:

1) Position: directly hired as a senior two posts;
2) Salary: the term of employment is 5 years, during which annual salary is ¥700,000;
3) Research funding: the school provides ¥200-300 million research funding;
4) Housing: After applying for full-time employment, applicants who meet the requirements of the state and the school may offer a set of preferential purchase of qualified personnel;
5) Others: provide sufficient office lab space, giving priority to the establishment of scientific research team, and doctoral or master enrollment targets should be policy-oriented. Assist in spouses' job and children's enrollment.

2. 1000 Plan Program for Young Talent

Requirement:

1)Applicants specialized in natural sciences or engineering technology should be less than 40 years old.
2)Applicants should have obtained PhD degrees at well-known universities at home and abroad, and have over 3 years of continuous overseas scientific research work experience.
3) Applicants need to return to work full time.
4) Outstanding overseas doctor of excellence can break through the working life.

Treatment:

In addition to the ¥500,000(duty-free) and ¥100-300 million research funds provided by the nation, the school also provides:
1) Position: directly hired as a senior four posts;
2) Salary: The first employment period of 3 years, annual salary of ¥500,000;
3) Research funding: for natural sciences or engineering technology and medical, schools provide ¥100-200 million discipline construction funds; Priority is given to supporting the declaration of other talents projects (the research funding of "High level innovation and entrepreneurial talent introduction program in Jiangsu" for team is ¥300 million, for person is ¥50-100 million, the research funding of "Jiangsu distinguished professor" is ¥50-100 million, the project funding of "Jiangsu 333 program" is ¥3-100 million)
4) Housing: in line with national and school policies, preferential purchase of talent special approval room;
5) Others: Provide sufficient office lab space, giving priority to the establishment of scientific research team, and doctoral or master enrollment targets should be policy-oriented. Assist in spouses' job and children's enrollment.

3.full-time teachers

Requirement:

Applicants should be outstanding doctoral or post-doctoral in well-known universities or research institutes overseas, and in line with the Southeast University job requirements of the academic level, with excellent teaching, research and social services.

Treatment:

The school provides accommodation fees, research start-up fees, monetization housing subsidies.

APPLICATION METHOD

Applicants should log in to the school webpage and prepare detailed CVs, full texts of academic reps (more than 5), references and evaluations of others, future work plans and other materials, and send them by e-mail to the applicant's college e-mail address and copy School E-mail (about full-time teachers, please send the material directly to the colleges).

Detailed resumes include: educational background, work experience, part-time academic positions, research projects presided over or participated in, representative achievements, catalogs of important works, citations of citations, and contact details. Please specify the type of candidates in the mail.

About Chang Jiang Scholars Program for Distinguished Professor, 1000 Plan Program for Young Talent, please contact: Southeast University Talent Service Office

Contact: Teacher Liu, Teacher Yin, Teacher Liao
Tel: + 86-25-83793301,
+ 86-25-52090253,
+ 86-25-52090251
E-mail: rcb@pub.seu.edu.cn
Fax: + 86-25-83793301
Website:
http://rsc.seu.edu.cn/2016/0613/c3575a161483/page.htm

About full-time teachers, please contact: Personnel Office of Southeast University Human Resource Department

Contact: Teacher Wang, Teacher Yang, Teacher Li, Teacher Sun
Tel: + 86-25-83792753,
+ 86-25-52090259,
+ 86-25-52090260
Address: Human Resource Department, Southeast University, 2 Sipailou Rd, Nanjing, China, 210096

The long-term effective recruitment information
more information please pay attention to WeChat public number：gh_762600e12fb4

By **Irini Topalidou**

The freedom of choice

A postdoc friend recently called me to discuss his career options. He didn't want to run his own lab, he said. Instead, he wanted to become a research scientist, mainly working at the bench—like me. I sensed that his mind was already made up, but he needed validation about pursuing a path that is not generally thought of as a professional success. Our conversation got me thinking about my own decision to become a research scientist—and about other career choices I made that went against the norm.

When I was a high school student in my home country of Greece, good students were expected to become doctors, and my biology teacher insisted that I apply to medical school. But the idea of being a doctor did not excite me, and I pursued "basic" biology instead. In this case and the ones to follow, I couldn't guarantee at the time that I was making the right decisions. But I knew that, because they were based on my personal preferences, they would be harder to regret.

Years later, as I was wrapping up my Ph.D. after having spent countless hours centrifuging yeast, I couldn't wait to work with a new model organism. When an older, successful collaborator told me, "The model system doesn't matter; what matters is the scientific question that you want to answer," I was ashamed to admit to myself that I didn't feel the same way. Almost any scientific question can trigger my curiosity, and I didn't want to spend long hours with some experimental model that didn't interest me.

Around that time, I took a course on model organisms and fell in love with the tiny roundworm *C. elegans*. Their simplicity and short life cycle were a good match for my impatience: A daily feeling of discovery helps calm my existential angst. But the worm wouldn't take me high on the scientific ladder, my colleagues told me. I was advised to go to a mouse lab and do more hardcore science. I valued the input, but I couldn't discount my own feelings. So, somewhat insecure in my decision, I followed my intuition and spent the next 8 years happily probing these humble creatures.

As the years went by, I knew that I needed to move on, which typically would mean opening my own lab. But I found myself doing anything possible to delay this transition. My gut feeling was that I wouldn't be happy as a principal investigator (PI) supervising other people's experiments. Or was I simply a coward, afraid of the unknown? I put off making a decision by taking a research scientist position in the lab of a new PI so that I could see the job up close, with all its benefits and struggles. My decision again disappointed my scientific advisers and even some of my friends. I was hesitant and anxious about it myself. But I was unable to follow advice that didn't resonate with me.

"I was unable to follow advice that didn't resonate with me."

My experiences over the next 5 years reinforced my decision not to pursue PI positions. I realized that I like being the person who not only thinks of scientific questions, but also performs the experiments. I don't want to miss the eureka moments at the lab bench, even if the discovery is as insignificant as a new transgenic worm. I need this daily feeling of personal accomplishment that I get from being an experimentalist.

But quite wrongly, research (or staff) scientist positions in academia are associated with lack of ambition or scientific drive. This view needs to change, and more positions need to be created for the increasing number of qualified scientists who are not interested in opening their own labs or who do not secure the few faculty positions available. And scientists like me, who are not interested in becoming PIs, should be confident in our decisions and advocate for the research scientist position to be recognized as a valid professional choice. When there is a mismatch between what society considers successful and our own definitions of success, we need to hold fast to our beliefs and follow our own road to personal satisfaction. ■

Irini Topalidou is a research scientist in the Department of Biochemistry at the University of Washington in Seattle. Send your career story to SciCareerEditor@aaas.org.